



NASA CR-72

C 1

NASA CONTRACTOR  
REPORT

NASA CR-723

DERIVATION OF A METEOROLOGICAL BODY OF  
DATA COVERING THE NORTHERN HEMISPHERE  
IN THE LONGITUDE REGION BETWEEN  
60°W AND 160°W FROM MARCH 1964  
THROUGH FEBRUARY 1965

*by Roy E. Peterson, John Schuetz, William E. Shenk,  
and Wen Tang*

*Prepared by*  
HONEYWELL INC.  
Minneapolis, Minn.  
*for Langley Research Center*



DERIVATION OF A METEOROLOGICAL BODY OF DATA  
COVERING THE NORTHERN HEMISPHERE IN THE  
LONGITUDE REGION BETWEEN  $60^{\circ}$  W AND  $160^{\circ}$  W  
FROM MARCH 1964 THROUGH FEBRUARY 1965

By

Roy E. Peterson, Honeywell Inc.  
John Schuetz, Honeywell Inc.  
William E. Shenk, GCA Corp.  
Wen Tang, GCA Corp.

Distribution of this report is provided in the interest of  
information exchange. Responsibility for the contents  
resides in the author or organization that prepared it.

Prepared under Contract No. NAS 1-6010 by  
HONEYWELL INC.  
Minneapolis, Minn.

for Langley Research Center

NATIONAL AERONAUTICS AND SPACE ADMINISTRATION

---

For sale by the Clearinghouse for Federal Scientific and Technical Information  
Springfield, Virginia 22151 - Price \$3.25



## FOREWORD

This report documents the first phase of An Analytical and Conceptual Design Study for an Earth Coverage Infrared Horizon Definition study performed under National Aeronautics and Space Administration Contract NAS 1-6010 for Langley Research Center.

This study provides for delineation of the experimental data required to define the infrared horizon on a global basis and for all time periods. Once defined, a number of flight techniques are evaluated to collect the experimental data required. The study includes assessment of the factors which affect the infrared horizon through statistical examination of a large body of meteorological information and the development of a state-of-the-art infrared horizon simulation.

The contractual effort was divided into numerous subtasks which are listed as follows:

Infrared Horizon Definition - A State-of-the-Art Report

Derivation of a Meteorological Body of Data Covering the Northern Hemisphere in the Longitude Region Between 60° W and 160° W from March 1964 through February 1965

The Synthesis of 15 $\mu$  Infrared Horizon Radiance Profiles from Meteorological Data Inputs

The Analysis of 15 $\mu$  Infrared Horizon Radiance Profile Variations Over a Range of Meteorological, Geographical, and Seasonal Conditions

Derivation and Statistical Comparison of Various Analytical Techniques Which Define the Location of Reference Horizons in the Earth's Horizon Radiance Profile

The 15 $\mu$  Infrared Horizon Radiance Profile Temporal, Spatial, and Statistical Sampling Requirements for a Global Measurement Program

Evaluation of Several Mission Approaches for Use in Defining Experimentally the Earth's 15 $\mu$  Infrared Horizon

Evaluation of the Apollo Applications Program Missions for Use in an Earth Coverage Horizon Measurement Program in the 15 $\mu$  Infrared Spectral Region

Computer Program for Synthesis of 15 $\mu$  Infrared Horizon Radiance Profiles

Compilation of Computer Programs for a Horizon Definition Study

Compilation of Atmospheric Profiles and Synthesized  $15\mu$  Infrared Horizon Radiance Profiles Covering the Northern Hemisphere in the Longitude Region Between  $60^\circ$  W and  $160^\circ$  W from March 1964 through February 1965 - Part I

Compilation of Atmospheric Profiles and Synthesized  $15\mu$  Infrared Horizon Radiance Profiles Covering the Northern Hemisphere in the Longitude Region Between  $60^\circ$  W and  $160^\circ$  W from March 1964 through February 1965 - Part II

Horizon Definition Study Summary - Part I

Honeywell Inc., Systems and Research Division, performed this study program under the technical direction of Mr. L. G. Larson. The program was conducted during the period 28 March 1966 through 10 October 1966.

The study results from the first five subtasks listed previously are of considerable interest and warrant wide distribution to the scientific community. It is anticipated that the results of the last eight subtasks are of limited interest to the general scientific community; therefore, distribution is provided to U. S. Government Agencies only.

Acknowledgement is extended to GCA Corporation and Barnes Engineering Company for their contributions on atmospheric physics/meteorology and locator identification respectively. The contributions on profile synthesis by Dr. J. C. Gille of Florida State University and on statistical analysis by Dr. J. H. Parks, Jr. of the University of Minnesota are also gratefully acknowledged.

Gratitude is extended to NASA/Langley Research Center for their technical guidance, under the program technical direction of Mr. L. Keafer and direct assistance from Messrs. J. Dodgen, R. Davis, and H. Curfman, as well as the many people within their organization.

# CONTENTS

	Page
SUMMARY	1
INTRODUCTION	3
Sounding Profiles	4
Carbon Dioxide Variability	6
High Cloud Characteristics and Frequency of Occurrence	6
Profile Identifier Classification Scheme	6
TEMPERATURE AND PRESSURE PROFILES	7
Objectives	7
Availability of Basic Data	7
Real-Time Data	7
Climatological Data	9
Analytical Techniques	11
Horizontal Interpolation from Analyzed Charts	11
Vertical Interpolation of Temperature and Pressure-Height Data	15
Derivation of Horizontal Temperature Gradients from Wind Data	17
Vertical Extrapolation of Temperature and Pressure	18
Selection of Profile Study Cases	20
Synoptic Cases	23
Space Cross Sections	25
Time Cross Sections	25
Stratospheric Warming Time Series	27
Climatological Cases	33
Auxiliary Data	33
Determination of Temperature/Pressure Profiles	39
Synoptic Cases	39
Space Cross Sections	47
Time Cross Sections	47
Stratospheric Warming Time Series	69
Climatological Cases	72
Profile Data Coding and Conversion	75
Formats Used	75
Computer Checking Operation	75
Conversion of Data to Local Time	81
Conversion of Temperature Profile Data	81
Accuracy of Temperature/Pressure Profiles	85
Observation Errors	85
Errors in Analysis	92
Errors in Data Handling and Tabulation	103
Overall Uncertainties in Derived Profile Data	103
VARIABILITY OF CARBON DIOXIDE CONCENTRATION	105

18	Cape Kennedy Time Height Cross Section From 8-17 February 1966	68
19	White Sands Missile Range Time Height Cross Section of Temperature (°C) From 7-9 February 1964	70
20	Time Cross Section at Fort Churchill During March, 1965	71
21	Location of the 50 Interpolated Climatological Soundings for Each Season	73
22	Temperature and Pressure Profiles Taken From the Body of Synoptic Case Data for 8 April 1964, 33.75°N, 75°W	86
23	Isotherm Analysis at 42 km on 9 December 1964 for Case 1	94
24	Isotherm Analysis at 42 km on 9 December 1964 for Case 2	95
25	Isotherm Analysis at 42 km on 9 December 1964 for Case 3	97
26	Temperature Analysis Error: Case 1 and 2	98
27	Temperature Analysis Error: Case 1 and 3	99
28	Cape Kennedy Time Height Cross Section	101
29	Difference Between Analyst A and Analyst B for Isotherm Analysis at 42 km on 9 December 1964	102
30	Chart Showing the Three Confidence Zones for the Estimate of Temperature From the MRN Measurements	104
31	Average Daily Variation of CO <sub>2</sub> Concentration at Different Heights Above Vegetation	107
32	Diurnal Variation of Atmospheric CO <sub>2</sub> at Mauna Loa Observatory in Hawaii	108
33	Diurnal Variation of Atmospheric CO <sub>2</sub> at Mauna Loa Observatory in Hawaii	109
34	Annual Average Diurnal Course of Atmospheric CO <sub>2</sub> at Mauna Loa Observatory	110
35	Year Variation of Daily Maximums and Minimums of the CO <sub>2</sub> Concentration 18 Meters Above a Crop Field	112

36	Daily Average Concentration of Atmospheric CO <sub>2</sub> at Mauna Loa Observatory for 1963	113
37	Monthly Average Concentration of Atmospheric CO <sub>2</sub> at Mauna Loa Observatory versus Time	114
38	CO <sub>2</sub> Concentration at 700 mb Level Near Hawaii	115
39	Concentration of Atmospheric CO <sub>2</sub> at 500 mb Level and Latitudes Between 40 and 60°N and Between 70 and 85°N as Functions of the Month of the Year	116
40	Concentration of Atmospheric CO <sub>2</sub> at 500 mb Level and Latitudes Between 25 and 30°N and Between 35 and 41°N as Functions of the Month of the Year	117
41	Annual Average Concentration of Atmospheric CO <sub>2</sub> as a Function of Latitude at the Surface, at 700 mb and at 500 mb	118
42	Estimated Mean CO <sub>2</sub> Concentration and Average Deviation of CO <sub>2</sub> Concentration as a Function of Height	124
43	Percentage Frequency of 6/10 Through 10/10 Cloud Cover - Greater Than 9 km, January	128
44	Percentage Frequency of 6/10 Through 10/10 Cloud Cover - Greater Than 9 km, July	129
45	Pictorial Presentation NIMBUS II MRIR Orbit 59	131
46	Brush Record of Channel 2 and 3 of Nimbus II on 19 May 1966 at 1639 GMT	132
47	Mean Temperature Profiles at Latitudes 20°N and 75°N and Longitude 90°W, January	135
48	Fifteen Micron CO <sub>2</sub> Horizon Profiles Spectral Interval 615 - 715 cm <sup>-1</sup> , at Latitudes 20°N and 75°N and Longi- tude 90°W, January	136
49	Average Weighting Function for Zero Tangent Height in the 615-715 cm <sup>-1</sup> Spectral Range	137
50	Mean Temperature Profiles at Latitudes 20°N and 75°N and Longitude 90°W, July	139

51	Fifteen Micron CO <sub>2</sub> Horizon Profiles Spectral Interval 615-715 cm <sup>-1</sup> , at Latitudes 20°N and 75°N and Longitude 90°W, July	140
52	Temperature Profiles at Latitudes 20°N and 75°N, January and July	141
53	Fifteen Micron CO <sub>2</sub> Horizon Profile Spectral Interval 615-715 cm <sup>-1</sup> , at Latitudes 20°N and 75°N, January	142
54	Temperature Sensitivity of Horizon Radiance Profiles	143
55	CO <sub>2</sub> Concentration Effect, ± 10 Percent	145
56	CO <sub>2</sub> Concentration Effect, ± 20 Percent	146
57	Cloud Effects on the 15 Micron Horizon Profile, 615-715 cm <sup>-1</sup> , 20°N, January	148
58	Percentage Deviation from No-Cloud Effect Radiance Level as a Function of Nadir Angle, 20°N, January	149
59	Comparison of 16 km-Cloud and No-Cloud Radiance Profiles, 20°N, January	150
60	Typical Temperature Distribution with Height	154
61	Mean Temperature in January at 60°N, and 60°W	156
62	Temperature Profile at Fort Churchill on 9 February 1965 1200 GMT	157
63	Temperature Profile at Fort Churchill on 12 December 1964, 1200 GMT	158

## TABLES

Table		Page
1	Information Sources for the Climatological Data	12
2	Heights of Pressure Levels in a Standard Atmosphere	15
3	Rocket Sounding Data - Synoptic Cases	24
4	Rocket Sounding Data -- Space Cross Section	26
5	Rocket Sounding Data -- Time Cross Section 3-Day Resolution	28
6	Periods Covered by the 12-Hour Resolution Time Cross Section	30
7	Rocket Sounding Data -- Time Cross Sections 12-Hour Resolution	31
8	Rocket Sounding Data -- Time Cross Section 4-Hour Resolution	32
9	Rocket Sounding Data -- Stratospheric Warming Time Series - 24-Hour Resolution	34
10	Auxiliary Rocketsonde Observations -- MRN	36
11	Auxiliary Rocketsonde Observations -- USNS Croatan	37
12	Auxiliary Rocketsonde Observations -- Used in Developing Extrapolation Procedure	38
13	Latitude and Longitude of Synoptic Grid Points	41
14	Latitude and Longitude of Space Cross Section Interpolation Points	48
15	Latitude and Longitude of Climatological Grid Points	74
16	Temperature Profile Identification Format	76
17	Correction Factors for Conversion to Local Time	82
18	Errors in Radiosonde Temperature and Pressure Data	87
19	Pressure Height Errors of Radiosonde	88

20	Errors in M/R Temperature and Density Data	90
21	Stations Used for Study Cases of Analytical Error	93
22	Smoothed Average Values of the CO <sub>2</sub> Concentration ppm, by Latitude and Month	120
23	Monthly Average Concentration of Atmospheric Carbon Dioxide at Little America in 1960 Through 1963	121
24	Measurements of CO <sub>2</sub> Concentration in Scandinavia From 0 to 3 km	122
25	Primary Identifiers	152
26	Reserve Identifiers	160

DERIVATION OF A METEOROLOGICAL  
BODY OF DATA COVERING THE NORTHERN  
HEMISPHERE IN THE LONGITUDE REGION  
BETWEEN 60°W AND 160°W FROM  
MARCH 1964 THROUGH FEBRUARY 1965

By Roy E. Peterson, Honeywell Inc.  
John Schuetz, Honeywell Inc.  
William E. Shenk, GCA Corp.  
Wen Tang, GCA Corp.

SUMMARY

Identification and analysis has been made of implicit factors between 0-90 km which may cause significant change in the magnitude and shape of the Earth's horizon radiance profile in the 15 micron carbon dioxide absorption band. The implicit factors considered include: (1) horizontal and vertical variability of temperature and pressure, (2) seasonal, synoptic, interdiurnal and diurnal variability of temperature and pressure, (3) variability of CO<sub>2</sub> concentration, (4) variability of high cloud occurrence, and (5) miscellaneous factors such as topological features.

Major emphasis was placed on the study of spatial and temporal variability of temperature since the preliminary results of radiance profile sensitivity analyses indicated that temperature effects were more important than CO<sub>2</sub> variability or cloud effects. The study of temperature variability was based, therefore, upon the development of an extensive series of interpolated profiles which were representative of several different space and time scales. The availability of rocketsonde data covering the 30-60 km layer limited the choice of study cases to the North American region covered by the Meteorological Rocket Network. Sounding data from 0-30 km were available from radiosonde observations; between 60-90 km, extrapolation techniques based upon infrequent high level rocket observations were used to obtain temperature estimates.

A primary set of 1039 interpolated sounding profiles was determined for the following basic categories of temperature (and pressure) variability: (1) large-scale synoptic variability at 56 grid points over North America, sampled at eight representative times in a one-year period, (2) small-scale spatial variability at 100-km intervals along a 5600-km long space cross section, sampled at two representative times, (3) small-scale temporal variability at three different locations, sampled at time resolutions of 3 days, 12 hours and 4 hours, (4) temporal variability at a northern latitude station during a select case of true stratospheric warming, sampled throughout a 27-day period, and (5) large-scale climatological variability at 50 grid points over North America, determined from seasonal statistics. In addition, a set of 46 auxiliary profiles was developed for different locations and/or time periods not covered by the primary set.

An error analysis was made to determine the uncertainties in the interpolated profile temperatures. This analysis indicated that the temperatures, for the worst case where extensive interpolation is used, are accurate to within  $\pm 2-3^{\circ}\text{C}$ . between 0-30 km,  $\pm 5-10^{\circ}\text{C}$ . between 30-60 km, and  $\pm 20-30^{\circ}\text{C}$ . between 60-90 km. The uncertainty in interpolated temperatures strongly depends upon the altitude, the season of the year, and the extensiveness and quality of the data coverage.

## INTRODUCTION

Knowledge of the infrared characteristics of the Earth's horizon is essential in the design of space vehicle guidance and control systems which employ the horizon to establish an attitude reference or to make distance measurements. This knowledge can be gained only by a comprehensive measurement program which would determine the radiative properties of the Earth's horizon, as viewed from space, over the appropriate range of geographic, seasonal, and temporal conditions, and which would produce sufficient data to establish an acceptable level of statistical confidence. The effectiveness of this measurement program is predicated upon the program being designed to collect data of the type and in the quantity needed to augment significantly our present knowledge. A primary objective of the Horizon Definition Study is to examine rigorously the present knowledge and theories of the Earth's radiance characteristics and to delineate an effective measurement program which would produce data suitable for use in the design and application of instruments which employ the Earth's infrared horizon.

The above objective can be stated more specifically as one which involves the determination of the type and amount of data necessary to adequately define the Earth's horizon profile in the 15 micron carbon dioxide absorption band and to specify its functional variability both in time and space. In general, an infrared horizon profile depends upon the vertical distributions of temperature and various absorbing constituents. One of the reasons for choosing a carbon dioxide band for horizon definition is that the carbon dioxide mixing ratio in the atmosphere is relatively constant compared to other possible gaseous absorbers, such as water vapor or ozone. Thus, the time and space variability of the radiance profile due to variations in atmospheric carbon dioxide can be expected to be minimal. Another reason for choosing the 15 micron carbon dioxide band is that this is a rather strong absorption band. Thus, the outgoing radiation in this band will originate mainly from relatively high levels in the atmosphere, rather than at the surface or in the troposphere. This reduces the effects of large variations in surface temperature and, more importantly, the effects of tropospheric cloudiness on the outgoing radiation.

The specific objectives of the study to be described in this report include the following:

- (1) Identification and analysis of implicit factors which may cause significant change in the magnitude and shape of the Earth's horizon

radiance profile in the 15 micron carbon dioxide absorption band. The implicit factors to be considered include:

- (a) Spatial variability of temperature and pressure in the horizontal and vertical.
  - (b) Temporal variability of temperature and pressure on a seasonal, synoptic, interdiurnal, and diurnal basis.
  - (c) Variability of CO<sub>2</sub> concentration.
  - (d) Variability of high cloud occurrence.
  - (e) Miscellaneous factors such as the global distribution of topological features affecting the observed radiance profile.
- (2) Determination of meteorological data sources and suitable techniques for data analysis, interpolation, extrapolation, error estimation, tabulation, and storage.
  - (3) Generation of an organized, indexed body of empirical meteorological data.
  - (4) Development of a profile classification scheme based upon significant features of the vertical temperature distribution, associated meteorological parameters, and circumstantial factors such as location, date/time, and topography.

Before a definite commitment could be made to the selection of a particular body of basic data and specific methods of generating required inputs for the mathematical model, preliminary studies were performed to obtain an indication of which implicit factors were more significant and, therefore, more deserving of concentrated attention. It became obvious from these preliminary studies that the spatial and temporal variability in the temperature (and pressure) profile produced the most important effects upon the behavior of the horizon radiance profile. Major attention was focused, therefore, upon the procurement of data and the development of analytical techniques for generating a representative body of sounding profiles covering the range of 0-90 km. Nevertheless, the problems of CO<sub>2</sub> variability and high cloud occurrence also received considerable attention since it was necessary to determine on a quantitative basis the upper limits of their effects upon the radiance profiles.

### Sounding Profiles

The ideal approach to the generation of a representative body of synthesized temperature/pressure profiles would be to sample selectively from an extensive

source of complete and accurate basic data available on a global basis over a period of several years. Ideally, these basic data would have been taken at sufficiently close intervals in time and space that all the scales of temperature variability could have been rigorously examined in terms of the associated variance in the horizon profiles. Unfortunately, this ideal data base does not exist at this time.

Radiosonde data between 0-30 km are regularly available at 12-hour intervals over relatively dense observational networks in North America and Eurasia, but truly global data coverage is not available. Rocketsonde data between 30-60 km are available at 2-3 day intervals from a mere handful of 23 stations over North America; many of these stations do not report regularly, the rocketsonde data coverage is even less global than the radiosonde data coverage. From 60-90 km, extrapolation techniques based upon a sporadic scattering of actual data observations must necessarily be used.

In view of the above limitations in basic data coverage, the choice of representative study cases for the determination of sounding profiles was necessarily constrained. Nevertheless, by careful selection of cases and by the use of a variety of analytical techniques, it was possible to sample a large number of atmospheric profiles representative of several different time and space scales, with sufficient resolution to satisfy the requirements of the radiance profile study.

The sounding profile study cases which were selected include the following basic categories:

- (1) Large-scale synoptic variability over North America and surrounding oceans-sampled at eight representative times within a one-year period.
- (2) Small-scale spatial variability along a cross-section from the British West Indies to the Southwestern United States - sampled at two representative times.
- (3) Small-scale temporal variability at three locations in the Southern United States and Northern Canada - sampled at select periods when 3-day, 12-hour and 4-hour time resolutions could be obtained.
- (4) Temporal variability at a northern-latitude station during a select case of true stratospheric warming-sampled throughout a 27-day period.
- (5) Large-scale climatological variability over North America and surrounding oceans-determined from seasonal statistics.

The total of 1039 sounding profiles interpolated from these study cases represents, by far, the largest collection of synthesized profiles ever assembled for horizon radiance studies. Attention was also directed toward the estimation of resultant errors in the interpolated profiles. The component errors which were analyzed include those in the reported data, errors of grid-point

interpolation from analyzed charts, errors of subjective interpretation of data, extrapolation errors, and tabulation errors.

### Carbon Dioxide Variability

Available observations of carbon dioxide variations were reviewed in terms of diurnal variations, monthly and yearly variations, latitude variations and variations with height in the atmosphere. Based upon these various observations a standard vertical profile of carbon dioxide concentration was developed for the 0-90 km altitude interval; this standard profile includes curves showing the mean and the average deviation of CO<sub>2</sub> concentration. These results provided an important input for calculating the effects of CO<sub>2</sub> variability upon the horizon radiance profiles.

### High Cloud Characteristics and Frequency of Occurrence

Since clouds are opaque in the infrared and block radiation from the lower atmosphere, it is necessary to determine their characteristics and frequencies of occurrence. A study was made of available information related to high clouds, emphasizing clouds whose tops extend above 9-10 km. On the basis of radar cloud studies, climatological analyses of high cloud frequency, and radiometric measurements from meteorological satellites, it was possible to determine, in a preliminary manner, the geographical and seasonal distribution of high clouds and to relate their occurrence to large-scale atmospheric circulation features such as the summer monsoon and the intertropical convergence zone.

### Profile Identifier Classification Scheme

Another important element in this study was the development of a profile classification scheme based upon select identifiers. Each sounding profile embodies within it a large variety of information relating to (1) significant features of the vertical temperature distribution (for example, temperature and height of the tropopause), (2) associated meteorological conditions (for example, the large-scale atmospheric circulation regime within which the specific profile condition occurs), and (3) various circumstantial factors such as location, date/time, and topography (which help explain why certain profile characteristics happen to occur). The profile classification scheme developed in this study thus provides a simple quantified basis for describing each profile in terms of the many implicit factors related to profile variability.

# TEMPERATURE AND PRESSURE PROFILES

## OBJECTIVES

The meteorological study cases were selected to provide inputs for the mathematical model in the form of temperature and pressure profiles representative of the spatial and temporal variations which occur in the atmosphere on a climatological, synoptic, and local basis. These profiles were required to extend from the surface to 90 km. At tangent heights above 90 km, the amount of radiant energy received by a  $15\mu$  carbon dioxide detector is quite small; in addition, at higher levels direct measurements of temperature are very rarely obtained and extrapolated estimates rapidly diminish in reliability.

Another basic study objective was to identify the various sources of atmospheric sounding data within the 0-90 km altitude range, to establish suitable techniques for analyzing the basic data, and to estimate the overall resultant error in the derived profiles.

## AVAILABILITY OF BASIC DATA

### Real-Time Data

Real-time data represent individual sounding observations made at specific stations. The sources and availability of these data can be best described in terms of three discrete altitude ranges:

#### (1) 0-30 km

In this altitude range, radiosonde observations provide temperature and pressure-height data at regularly scheduled 12-hour intervals from a world-wide network of stations. The distribution of radiosonde stations in the Northern Hemisphere is shown in Figure 1 (the Southern Hemisphere station distribution is considerably less dense). It is obvious from this figure that relatively dense radiosonde coverage is obtainable only over North America and Eurasia. This fact, together with the fact that sounding data above 30 km are only obtainable over North America on a systematic basis, necessarily led to the choice of this region as the only one where concentrated studies of atmospheric profiles from 0-90 km could be performed.

All radiosonde information used in this study was gathered in the form of microfilmed copies of constant pressure charts obtained from the National Weather Records Center at Asheville, North Carolina. These constant pressure charts covered the 850, 700, 500, 300, 200, 100, 50, 30, and 10 mb levels (in addition, surface charts were obtained from this same source to determine surface-boundary values of temperature and pressure-height).

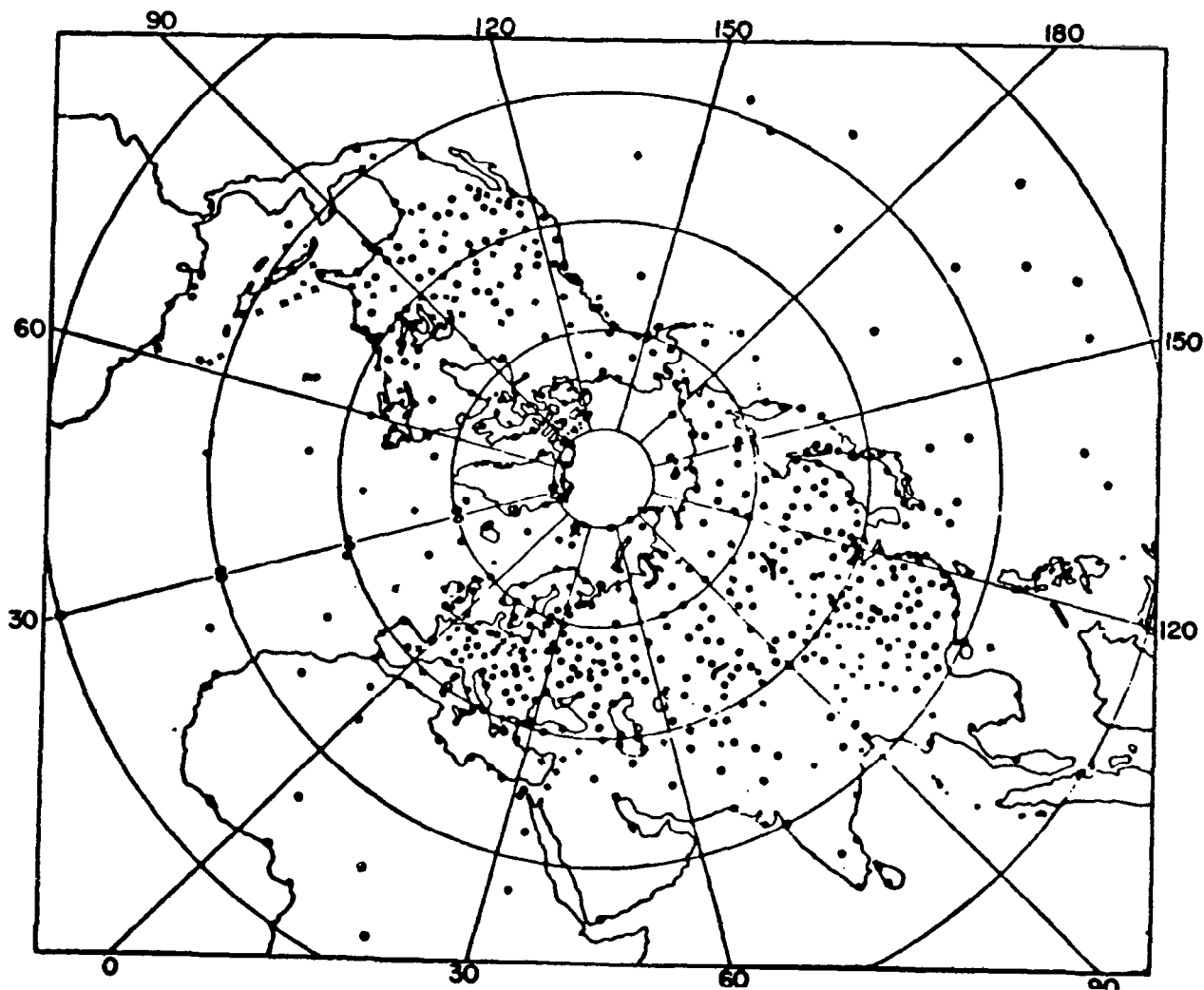


Figure 1. Location of Aerological Stations Regularly Reporting Observations

(2) 30-60 km

Temperature and pressure data in the 30-60 km layer were obtained from sounding observations conducted by the Meteorological Rocket Network (MRN). Analyzed constant height charts were not available; thus, the basic MRN data had to be plotted and analyzed as a part of this study.

The rocketsonde data were obtained from a series of publications entitled "Data Report of the Meteorological Rocket Network Firings", which is published monthly. The rocket data tables are prepared under the direction of the U.S. Army Electronics Research and Development Activity at White Sands Missile Range, New Mexico.

Figure 2 shows the locations of the 23 stations that are participating members of MRN. The station density, it should be noted, is roughly an order of magnitude less than that of the radiosonde network; in addition, the MRN observational schedule is considerably more irregular, with soundings carried out at typical intervals of 2-3 days but with occasional gaps of up to several weeks between observations. Furthermore, not all MRN stations regularly report temperature, but may only report wind data. For example, the Ft. Greely and Wallops Island Stations rarely report temperature. Rocketsonde wind information can be used, however, to help derive estimates of temperature by means of the thermal wind equation. This estimation technique, which will be described at length in this section, permits the calculation of horizontal temperature gradients from wind data; the integrated analysis of estimated gradients with actual temperature reports at surrounding stations permits more accurate analysis of the temperature field to be made than would be otherwise possible. Thus, the successful application of relatively sparse rocketsonde data clearly depends upon the resourceful use of all available temperature and wind information.

(3) 60-90 km

Meteorological data coverage above 60 km is extremely sparse. Occasional MRN observations do extend to 65-70 km however, special rocket measurements covering the entire 60-90 km layer are but infrequently made. It is necessary, therefore, to use extrapolation techniques based upon the few coincident observations of temperature within the 30-60 and 60-90 km range to estimate the temperature profile in the higher layer. This section will describe the temperature extrapolation technique developed on the basis of 30 atmospheric soundings where coincident measurements of the 50 and 80 km temperature were available.

### Climatological Data

A large number of climatological information sources were surveyed in order to obtain seasonal data regarding temperature means and standard deviations

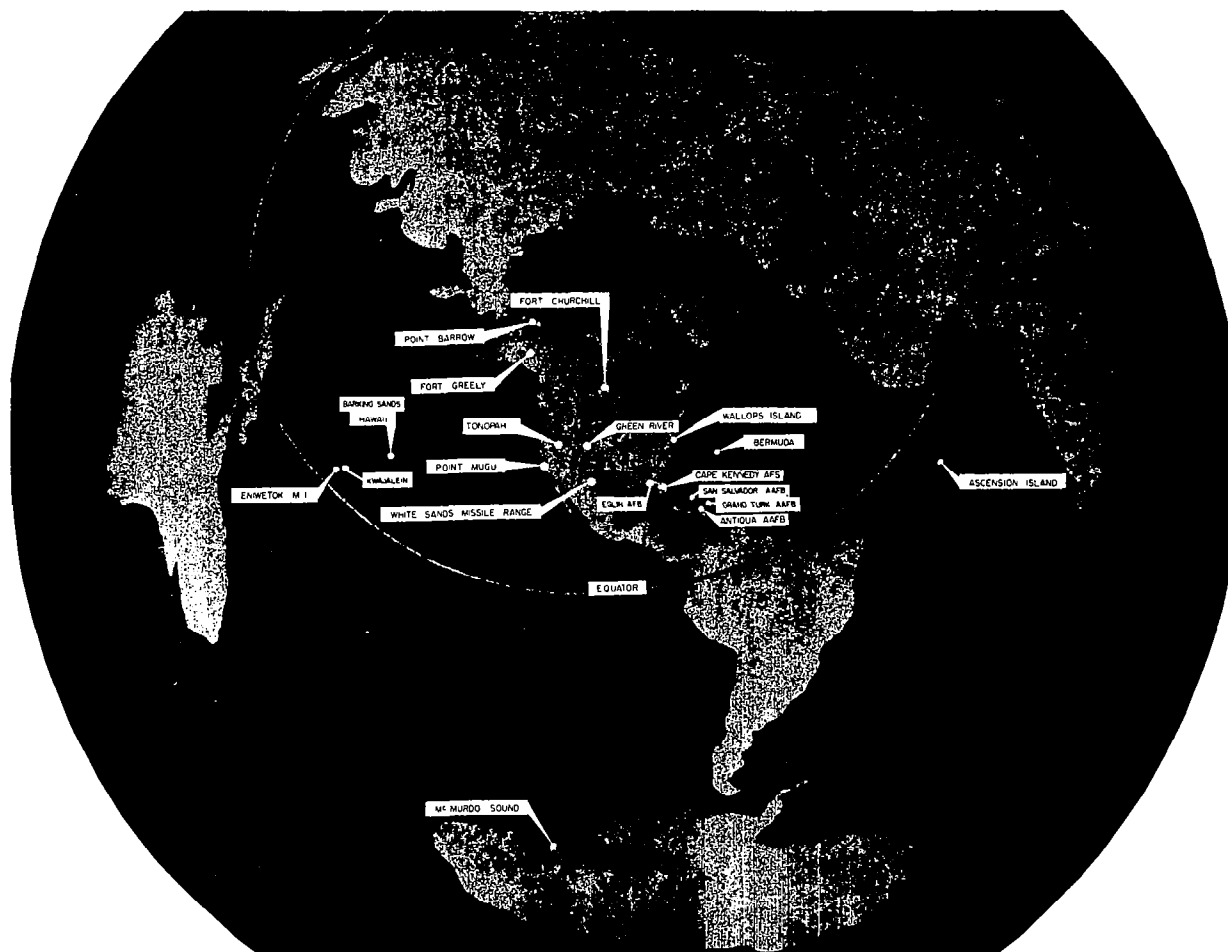


Figure 2. Meteorological Rocket Network (MRN)

within the required 0-90 km altitude range. Table 1 lists the various types of climatological information which are available, the supplying agency and specific references to the individuals or groups who published the information.

The preceding comments regarding real-time data coverage also apply to the climatological data which are derived from the basic observations. Thus, the resolution and reliability of temperature statistics markedly decrease above the 30 km level of highest radiosonde data coverage and become speculative above the 60 km level of highest rocketsonde coverage.

Further discussion of available climatological data and their specific applications to this study will be presented in this section.

### ANALYTICAL TECHNIQUES

Since upper air sounding observations do not, as a rule, provide data for the specific locations, altitudes and times which are required for a particular study application, a variety of analytical techniques have been developed to interpolate and extrapolate the required values from the observed data. The analytical techniques which have been used in this study are described below.

#### Horizontal Interpolation from Analyzed Charts

Real-time data. -- The conventional method of deriving values of meteorological parameters at grid points which do not coincide with the reporting stations is to (1) plot the observed values on constant level (pressure or height) charts, (2) draw isopleths at selected values, and (3) interpolate values at the desired grid points from the isopleths. Automated methods for performing this interpolation process have been developed, but in cases where the data are sparse the subjective interpretation of a skilled analyst is highly desirable.

In this study, the horizontal interpolation of temperature at levels between 0-30 km was performed on analyzed charts for the pressure levels listed in Table 2. (This table also includes the corresponding heights of these pressure levels for a standard atmosphere.) In addition, the heights of each constant pressure level were interpolated from the height-contour analysis at each required grid point. Figure 3 presents a typical analysis performed at the 200 mb level, where the plotted radiosonde values of temperature, pressure-height and wind have been analyzed on a collective basis.

Horizontal interpolation of temperature at levels in the 30-60 km range was carried out on constant level charts analyzed from reported MRN rocket-sonde data. These charts were drawn at 3 km intervals (that is, 30, 33, 36, . . . , 60 km) over the required altitude range. Figure 4 illustrates an isotherm analysis performed at 42 km. The scarcity of data at this level, relative to that previously shown at 200 mb in Figure 3, is quite obvious. The importance of each station report is equally obvious. For example, in

TABLE 1.- INFORMATION SOURCES FOR THE CLIMATOLOGICAL DATA

Level	Climatological information	Agency	Reference
Surface	$\bar{T}, \bar{P}$	ESSA	James O'Connor (1966)
850 mb	$\bar{T}, \sigma_T$	USAF ( $\bar{T}$ ) USWB ( $\sigma_T$ )	3rd Weather Wing (1962) ( $\bar{T}$ ) B. Ratner (1958) ( $\sigma_T$ )
700 mb	$\bar{T}, \sigma_T$	USAF ( $\bar{T}$ ) BMO ( $\sigma_T$ )	3rd Weather Wing (1962) ( $\bar{T}$ ) N. Goldie, et al., (1958) ( $\sigma_T$ )
500 mb	$\bar{T}, \bar{h}, \sigma_T$	USAF ( $\bar{T}$ ), USN ( $\bar{h}$ ) BMO ( $\sigma_T$ )	$\bar{T}$ and $\sigma_T$ same as 700 mb R. A. Bryson, et al. (1958)
400 mb	$\bar{T}, \sigma_T$	Same as 700 mb	Same as 700 mb
300 mb	$\bar{T}, \sigma_T$	Same as 700 mb	Same as 700 mb
200 mb	$\bar{T}, \sigma_T$	Same as 700 mb	Same as 700 mb
100 mb	$\bar{T}, \sigma_T$	Same as 700 mb	Same as 700 mb
50 mb	$\bar{T}$	USAF	3rd Weather Wing (1962)
25 mb	$\bar{T}$	USAF	Muench and Borden (1962)
$\Delta 30-52$ km	$\bar{T}, \sigma_T$	USAF	Quiroz, Lambert, and Dutton (1963)
* (48, 51 km)	$\bar{T}$	USAF	Cole and Kantor (1963)
**54-90 km (January, July-20°, 30°, 45°, 60°)	$\bar{T}$	USAF	Cole and Kantor (1963)
54-90 km **(April, Oct. 30°, 60°)	$\bar{T}$	USAF	Kantor and Cole (1965)

Legend:

$\bar{T}$  = Mean temperature

$\bar{P}$  = Mean sea level pressure

$\sigma_T$  = Temperature standard deviation

$\bar{h}$  = Mean 500 mb height

ESSA = Environmental Science Services Administration

USAF = United States Air Force

USWB = United States Weather Bureau

USN = United States Navy

BMO = British Meteorological Office

$\Delta$  - Mean temperatures and standard deviations approximately every 3 km.

\* - Mean temperature data were supplied at these levels only in the summer session at 20°, 30°, 45°, and 60°N when the 49 and 52 km level mean temperatures were missing from the Quiroz, et al.,(1963) data.

\*\* , - Mean temperatures every 3 km. Also, note that mean temperatures were available only for the months and latitudes indicated in parentheses.

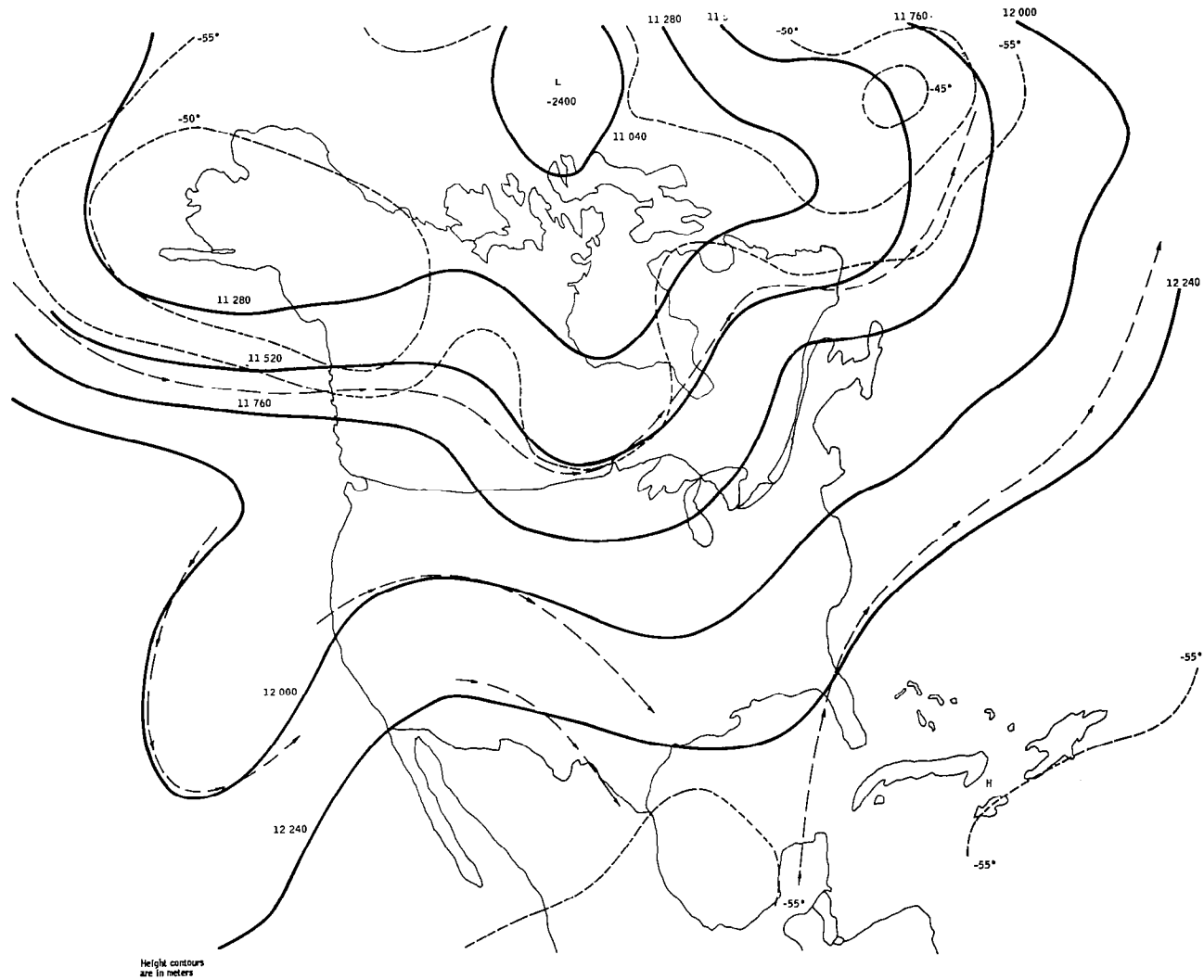


Figure 3. Analysis at 200 mb for 28 October 1964

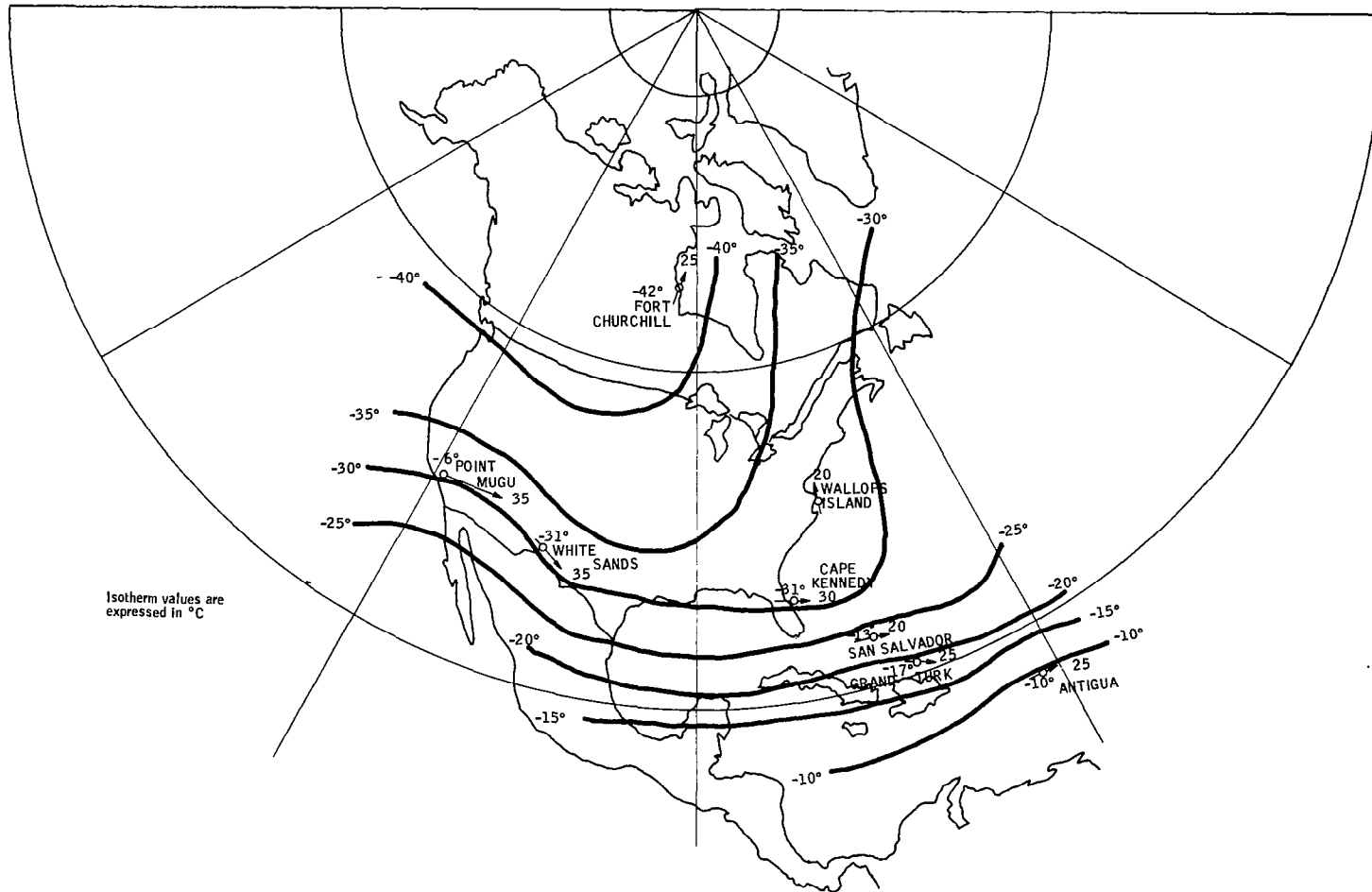


Figure 4. Isotherm Analysis at 42 km on 9 December 1964 Using All Available Data

TABLE 2.- HEIGHTS OF PRESSURE LEVELS IN  
A STANDARD ATMOSPHERE

Pressure, mb	Height, km
850	1.457
700	3.012
500	5.574
300	9.164
200	11.784
100	16.180
50	20.576
30	23.849
10	31.055

Figure 4, the missing temperature report at Wallops Island produces a significant data gap. It is possible, however, by use of the thermal wind technique to be described in this section, to estimate the horizontal temperature gradient at Wallops Island from the reported wind profile and, thus, make a better estimate of the isotherm pattern than would otherwise be possible.

Climatological data. -- The interpolation procedure followed for the climatological data was quite similar to the methods for the real-time information. Mean temperature data from the surface to 25 mb were interpolated directly from analyzed charts and tables. Between 30-52 km mean temperature and standard deviation charts were plotted and analyzed using MRN information prepared by Quiroz, Lambert and Dutton (ref. 3). Then the interpolation was performed in the same fashion as with the real-time data. There were no thermal winds to assist in the analysis of the climatological data. Also, there were fewer data points per chart. Thus, the climatological data in this layer must be considered as speculative.

#### Vertical Interpolation of Temperature and Pressure-Height Data

In order to compute the vertical temperature profiles at the required altitude levels (which did not necessarily correspond to the height levels reported by the radiosonde and rocketsonde observations), it was necessary to interpolate between data at reported levels. Therefore, a computer program was developed to convert the original temperature-height profiles at reported levels to profiles which included interpolated data at all specified altitudes between 0-90 km.

In addition to the interpolation computations, this program checked the original temperature-height profile for missing points, and if points were missing, it

computed these points by interpolation between the two adjacent points or by extrapolation from the two nearest points. Extrapolation was used only when the end points in the original profile were missing.

#### (1) 0-30 km Interpolation

For this lower altitude range of radiosonde data coverage, the surface temperature and surface altitude, and the temperatures, pressures, and heights ( $T_i$ ,  $P_i$ ,  $Z_i$ ) are specified in the computer program for the mandatory levels (that is, 850, 700, 500, 300, 200, 100, 50, 30, and 10 mb). Mandatory levels are always included in radiosonde observations to the highest pressure level which the sounding data permit.

By means of the computer program, additional temperatures and heights are linearly interpolated between any two original temperatures and heights, and additional pressures are computed by means of the hydrostatic equation. Thus, if  $n$  additional points ( $t_j$ ,  $z_j$ ,  $p_j$ ) are desired between two original points,  $T_{i-1}$ ,  $P_{i-1}$ ,  $Z_{i-1}$  and  $T_i$ ,  $P_i$ ,  $Z_i$ , these points are computed from the following equations:

$$z_j = Z_{i-1} + \frac{j}{(n+1)} (Z_i - Z_{i-1}), \quad (1)$$

$$t_j = T_{i-1} + \left( \frac{T_i - T_{i-1}}{Z_i - Z_{i-1}} \right) (z_j - Z_{i-1}), \quad (2)$$

and

$$P_j = P_{i-1} \exp \left[ -\frac{1}{R} \sum_{\ell=1}^j \left( \frac{g}{T} \right)_{\ell} (z_{\ell} - z_{\ell-1}) \right], \quad (3)$$

where  $R$  is the gas constant for dry air

$$(R = 2.87 \times 10^6 \text{ cm}^2/\text{sec}^2\text{deg}),$$

$$\left( \frac{g}{T} \right)_{\ell} = \frac{1}{2} \left( \frac{g_{\ell-1}}{t_{\ell-1}} + \frac{g_{\ell}}{t_{\ell}} \right),$$

$g_{\ell}$  (cm/sec<sup>2</sup>) is the acceleration due to gravity at  $z_{\ell}$  km,

$$g_l = \frac{3.987487 \times 10^{10}}{(R_e + z_l)^2}$$

where  $R_e$  is the radius of the Earth (km).

## (2) 30-90 km Interpolation

In the 30-90 km height range, the additional temperatures are computed in a manner similar to that used between 0-30 km. The hydrostatic equation, Equation (3), is used to compute the additional pressure values, where the base pressure is the lowest pressure in the original profile (generally 10 mb).

### Derivation of Horizontal Temperature Gradients From Wind Data

In the analysis of MRN temperature data on constant height charts for levels between 30-60 km, the analysis of the thermal field would be at times quite difficult if only the plotted temperature values were considered. Fortunately, it is possible to use available rocket wind data, and by means of the thermal winds equation, to estimate the horizontal temperature gradient in the vicinity of the wind-reporting station. In view of the relatively sparse MRN station density, such estimates are of considerable value in extending the isotherm analysis to areas not covered by data from the temperature-reporting stations.

The thermal wind is the vector difference between the geostrophic wind at two levels (ref. 4). Therefore, observed wind differences will be equal to the thermal wind only when the wind field is geostrophic, i.e., when friction and accelerations are unimportant. Between 30 and 60 km the geostrophic limitations are not considered to be of great importance.

The expression for the thermal wind is as follows:

$$\vec{V}_{\text{thermal}} \times \vec{k} = \frac{R}{f} \left( \log_e \frac{p}{p'} \right) \left( \frac{\partial \vec{T}}{\partial n} \right)$$

where

$\vec{V}_{\text{thermal}}$  = the thermal wind

$\vec{k}$  = the unit vector along the vertical axis

$R$  = the gas constant for dry air

$f$  = the Coriolis parameter

$p, p'$  = the pressures at the bottom and top of the layer, respectively

$\frac{\partial T}{\partial \hat{n}}$  = the horizontal temperature gradient, normal

$\hat{n} = \frac{\vec{V} \times \vec{k}}{|\vec{V}|}$

The thermal wind is parallel to the isotherms with warm air to the right of the thermal wind facing downwind. Also, the strength of the thermal wind is proportional to the magnitude of the temperature gradient, and, with the aid of the thermal wind, temperature analysis can be improved significantly. Thus, even though an MRN station report contains only wind information, this report is still of great value since the strength and direction of the computed thermal wind give information on the spacing and direction of the isotherms.

In this study, the vertical wind shears were computed every 3 km with the temperature centered in each layer.

#### Vertical Extrapolation of Temperature and Pressure

Temperature extrapolation. -- As noted earlier, temperature measurements above the 60 km level are relatively rare. Such measurements are beyond the present capability of the MRN network on a routine basis; an occasional sounding does go higher than the 60 km level but almost never beyond 65 km. A logical solution to the lack of data above 60 km is to extrapolate from data at lower levels to the higher levels with the use of statistical relationships developed from all of the available information at the higher levels. Since the 30-60 km region provides an adequate base of observed temperature data, it seems logical to use the temperatures in this layer to extrapolate above 60 km.

Kantor and Cole (ref. 5) noticed an inverse relationship between stratopause (50 km) temperatures and those near the mesopause (80 km). This held regardless of season and latitude. When the 50 km temperature was colder than the 50 km temperature of the 1962 Standard Atmosphere, the 80 km temperature appeared to be warmer than the 1962 Standard Atmosphere temperature at that height.

To derive a statistical relationship for use in this study, thirty atmospheric soundings were obtained (ref. 6) where both 50 and 80 km temperatures were measured. These soundings were made over North America. A scatter diagram (Figure 5) was prepared showing the difference between (1) the observed 50 km temperature and the corresponding standard atmosphere temperature as the predictor and (2) the 80 km difference from standard atmosphere temperature as the predictand. Separate linear correlation

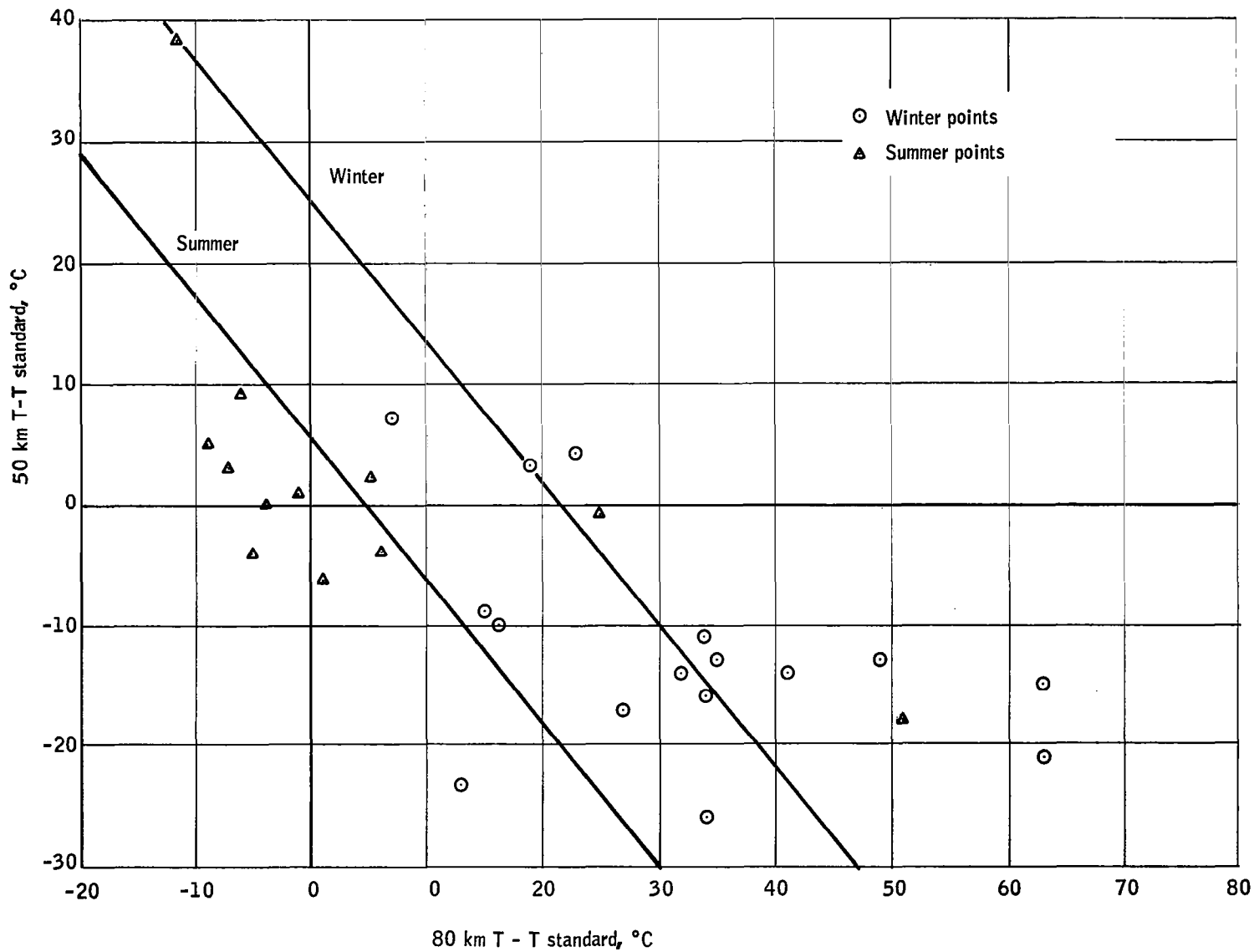


Figure 5. Scatter Diagram Showing the Temperature Combinations Used to Develop the Extrapolation Technique

coefficients and regression lines were computed for summer (May-October) and winter (November-April). The linear correlation coefficients were 0.62 for summer (14 points) and 0.47 for winter (16 points).

Figures 6 and 7 show the set of curves which were used with 50 km and estimated 80 km temperatures to obtain temperature values from 63 to 90 km for summer and winter, respectively. In preparing these charts, the 1962 Standard Atmosphere was plotted first. Then, the 50 km and predicted 80 km temperatures were plotted. These two temperatures were corrected by a non-linear curve based upon the general shape of the standard atmosphere curve. Above 80 km, isothermal conditions were assumed.

With the above set of curves and a knowledge of the 50 km temperature, the temperature could be estimated above this level to 90 km. In nearly all cases, real temperature data were available to heights above 50 km. Whenever this situation occurred, the highest point of real data was used to estimate the temperatures to 66 km and the 50 km temperature was used for the higher levels. The 66 km level was chosen because the constructed curves cross one another generally at about this level for both summer and winter. Thus, estimation of the high level temperature was based on a combination of the 50 km temperature and the highest point of real data.

Pressure extrapolation. -- In the 30-90 km region, the hydrostatic equation is used to compute the pressures at specified heights, using as the base pressure the lowest pressure of the original profile (generally 10 mb). The hydrostatic equation, Equation (3), relates the vertical change in pressure for a corresponding change in altitude to the mean temperature in the intervening layer, and is readily computed from the measured (or extrapolated) temperature profile.

### SELECTION OF PROFILE STUDY CASES

The profile study cases were selected in order to provide a representative sampling of profile variability over several different time and space scales. Basic data limitations, especially those which apply above 30 km, serve to constrain the choice of profile study cases to those where adequate data coverage (in terms of coincident observations at more than one station) or time resolution (in terms of unbroken series of observations at a particular station) permit a relatively complete and reliable analysis. As already indicated, a considerable analytical burden must be borne in terms of data interpolation and extrapolation. Great care was exercised, therefore, in the selection of the profile cases to include only those cases where the data were adequate to satisfy specified sets of objectives.

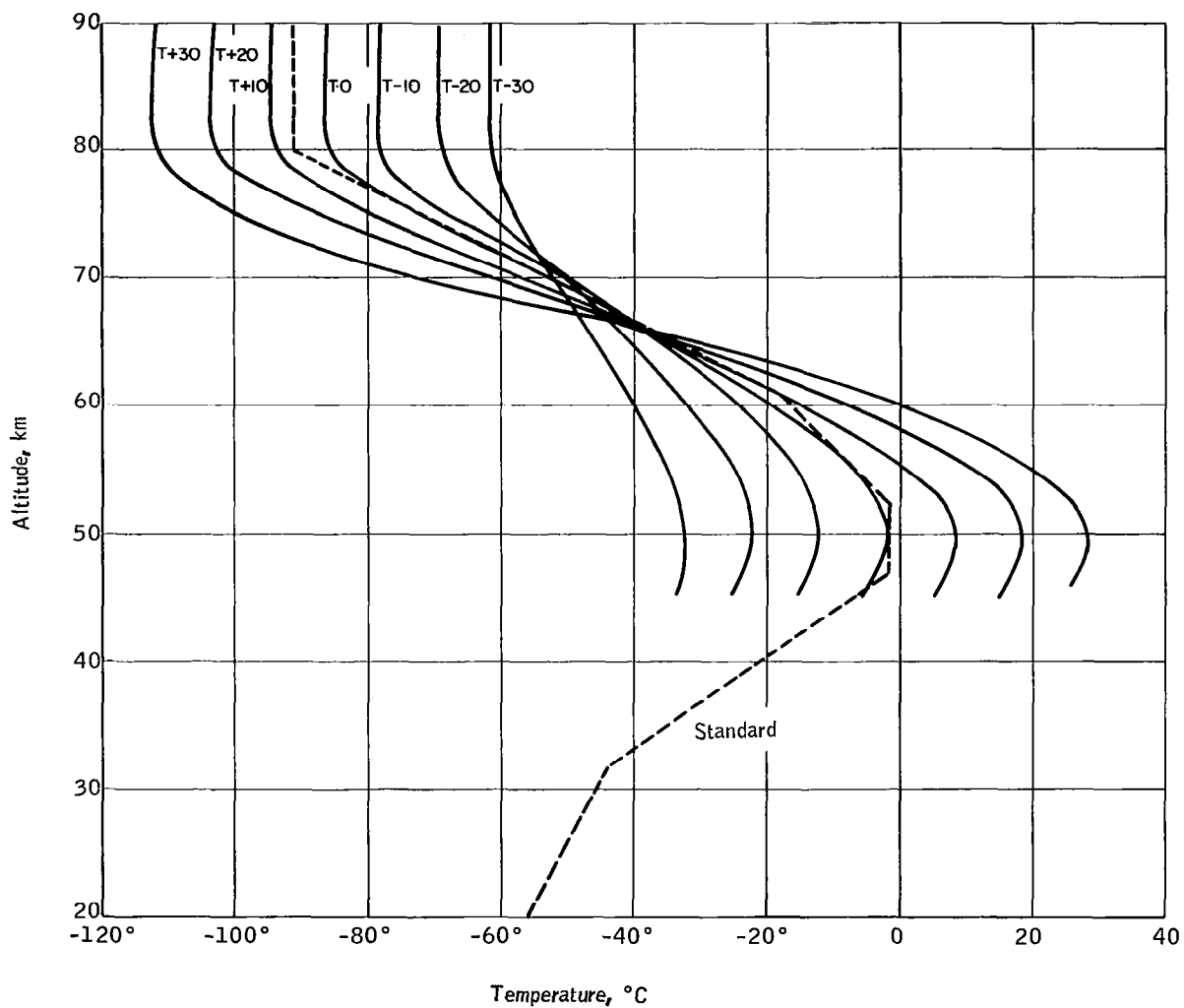


Figure 6. Family of Curves Used to Estimate the Temperatures Above the Highest Level of Reported Rocket Data for Summer

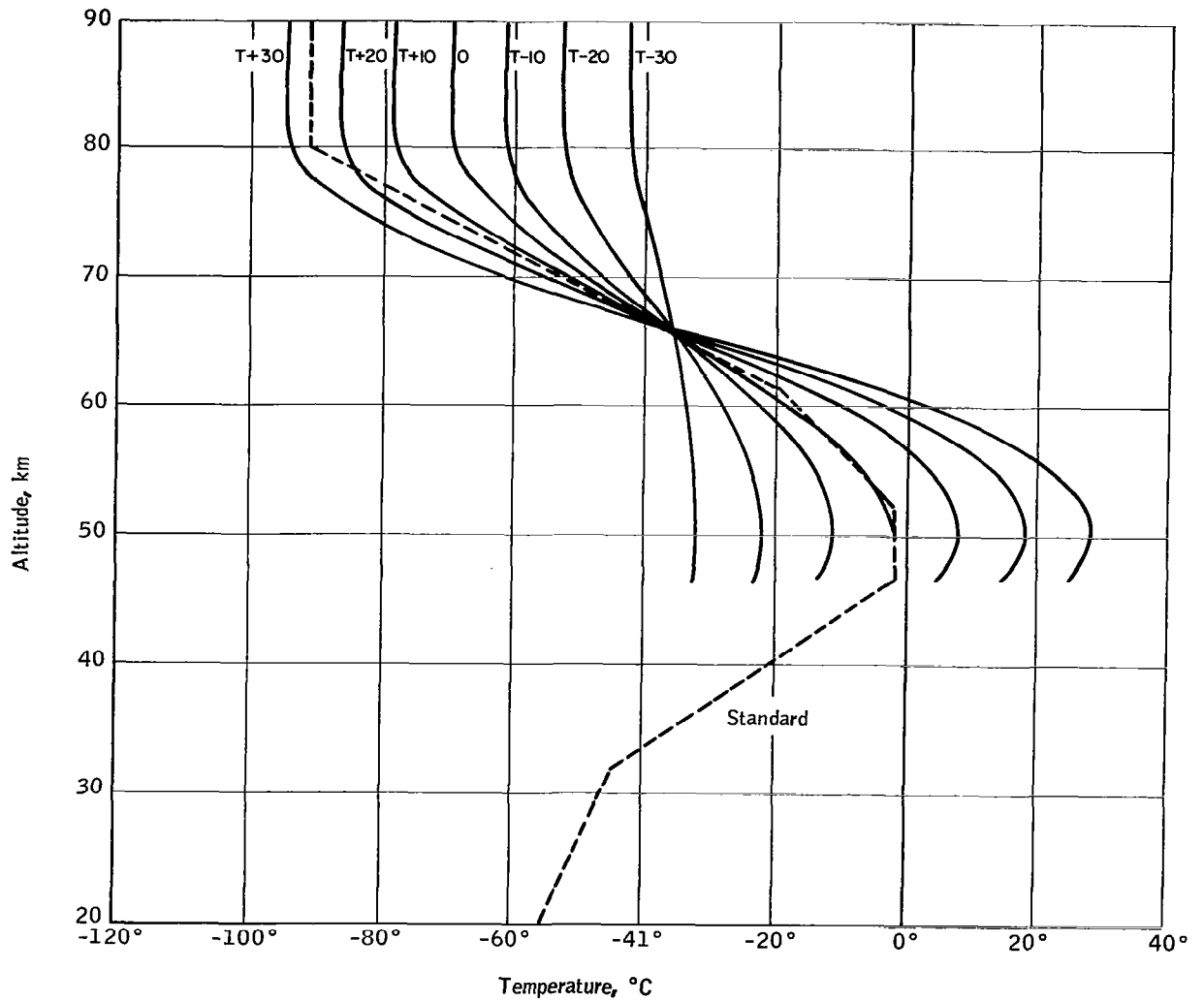


Figure 7. Family of Curves Used to Estimate the Temperatures Above the Highest Level of Reported Rocket Data for Winter

The profile study cases which were selected fall within the following general categories:

- (1) Large-scale synoptic variability over North America and surrounding oceans - sampled at eight representative times within a one-year period.
- (2) Small-scale spatial variability along a 5600-km cross section from Antigua, B.W.I. to White Sands Missile Range - sampled at two representative times.
- (3) Small-scale temporal variability at White Sands, Cape Kennedy and Fort Churchill, Canada - sampled during select periods when 3-day, 12-hour or 4-hour time resolution could be obtained from the reported MRN data.
- (4) Temporal variability at one station (Ft. Churchill) during a select case of stratospheric warming - sampled at various times during a 27-day period.
- (5) Large-scale climatological variability over North America and surrounding oceans - determined from the seasonal statistics for winter, spring, summer and autumn.
- (6) Miscellaneous estimates of synoptic climatological and local variability - obtainable as an auxiliary body of data for stations and/or times other than those used in items (1) - (5) above.

The sets of temperature and pressure profiles derived for the above cases, thus, provide a representative sampling of atmospheric variability to be used as the basis for analyzing the concomitant variability in the radiance profiles.

#### Synoptic Cases

Eight synoptic study cases were selected at representative intervals within a 12-month period where good temperature data coverage was available for the MRN stations in North America and surrounding oceans and where a representative variety of synoptic situations were included. The specific dates covered by these cases are 8 April, 3 June, 12 August, 21 October, 13 November, 9 December 1964, and 30 January and 10 February 1965.

Table 3 lists, for each synoptic case, the MRN station locations, the date and time of the available sounding data, and the maximum height of the temperature trace. It may be noted that the temperature data coverage for each synoptic case ranged from a minimum of three to eight stations, and was available, on the average, for six MRN stations.

The radiosonde data for each synoptic case were available for the regularly scheduled 1200 GMT observation time. As shown in Table 3, the rocket sounding observations were not taken on a "same-time" (or truly synoptic)

Table 3.- Rocket Sounding Data - Synoptic Cases

Location	Date	Time (GMT)	Maximum height of the temp. trace, km	Location	Date	Time (GMT)	Maximum height of the temp. trace, km
	April 8, 1964				June 3, 1964		
C. Kennedy	4/8/64	1800	47	Ft. Greely	6/3/64	2015	63
Ft. Greely	4/8/64	2000	62	Pt. Mugu	6/3/64	1810	44
WSMR	4/8/64	1700	65	WSMR	6/3/64	1800	65
				Ft. Churchill	6/3/64	1900	47
	August 12, 1964				October 21, 1964		
Antigua	8/15/64	0511	49	Antigua	10/21/64	1920	61
C. Kennedy	8/12/64	1600	58	C. Kennedy	10/23/64	1043	64
Ft. Churchill	8/12/64	0316	65	Grand Turk	10/19/64	1700	61
Wallops Is.	8/12/64	0226	40	Ft. Churchill	10/21/64	1845	59
Pt. Mugu	8/12/64	1715	56	Pt. Mugu	10/21/64	1730	56
				WSMR	10/21/64	2100	57
	November 13, 1964				December 9, 1964		
Antigua	11/13/64	1731	56	Antigua	12/9/64	0413	54
C. Kennedy	11/12/64	1530	55	C. Kennedy	12/9/64	0306	53
Grand Turk	11/11/64	1800	53	Grand Turk	12/9/64	0300	52
Ft. Churchill	11/13/64	1807	44	S. Salvador	12/9/64	0315	55
Ft. Greely	11/12/64	2000	50	Ft. Churchill	12/9/64	1900	55
WSMR	11/13/64	1905	65	Pt. Mugu	12/9/64	2352	58
				WSMR	12/9/64	1545	54
	January 20, 1965				February 10, 1965		
Antigua	1/20/65	1821	50	Antigua	2/10/65	1815	51
C. Kennedy	1/20/65	1600	62	C. Kennedy	2/10/65	1600	51
Grand Turk	1/20/65	1800	55	Grand Turk	2/10/65	1930	51
Ft. Churchill	1/20/65	1502	56	Ft. Churchill	2/10/65	1800	55
Ft. Greely	1/20/65	2000	52	Pt. Mugu	2/9/65	0000	53
Pt. Mugu	1/20/65	1805	47	W. Geirnish	2/11/65	2115	65
W. Geirnish	1/20/65	1948	70	WSMR	2/11/65	1830	42
WSMR	1/20/65	2340	46				

basis; in fact, some rocketsonde data were necessarily used in the analysis even though they were as much as two days removed in time from the assigned observation time. A later section will discuss the use which was made of such data in performing the analysis of the synoptic cases.

### Space Cross Sections

The general criteria for selecting the space cross section study cases were (1) that the reporting stations along the cross-sectional axis must provide a complete, nearly simultaneous set of observations to permit the reliable determination of small-scale spatial variability, and (2) that data be available for the same set of stations for sampling two contrasting situations in early autumn and mid-winter, representative of minimum and maximum spatial variability along the cross-sectional axis.

The relatively low density of MRN stations, Figure 2, does not provide much leeway in choosing a line of closely spaced stations for analyzing the spatial variability in temperature and pressure profiles. Thus, examination of available rocketsonde stations and data led to the choice of a line of four stations extending from White Sands Missile Range (WSMR) to Antigua, British West Indies. The two specific cases selected for space cross section analysis were for 1200 GMT on 28 October 1964 and 24 February 1965.

Table 4 lists the rocketsonde observations which were used for the two space cross section cases: the MRN station location, the date and time of the available sounding data, and the maximum height of the temperature trace. In both cases, all four stations reported temperature data; in each case, the observations were all taken on the same day, with no more than a 7.5-hour difference in rocket sounding times from the 1200 GMT radiosonde observation time.

### Time Cross Sections

The analysis of time cross sections derived from a series of observations at an individual station represents an important technique for studying the small-scale temporal variability of atmospheric profiles. An examination of the MRN sounding data indicated that a body of cases could be selected from which the temporal variability at individual stations could be studied in terms of three basic scales of time resolution: (1) 3-day (2) 12-hour, and (3) 4-hour. (The term resolution, as applied here, refers to the average frequency of a series of MRN observations).

Three-day resolution. -- Two extensive series of rocketsonde data were selected for the preparation of time cross sections with three-day resolution at Cape Kennedy, Florida and Fort Churchill in Central Canada. The Cape Kennedy cross section covered the desired one-year period, extending from 1 March 1964 to 27 February 1965. The Fort Churchill cross section was necessarily limited to a shorter period from 1 October 1964 to 13 February 1965, due to rocket data limitations.

TABLE 4.- ROCKET SOUNDING DATA -- SPACE CROSS SECTION

Location	Date	Time (GMT)	Maximum height of the temp. trace, km
	<u>October 28, 1964</u>		
Antigua	10/28/64	0435	59
Grand Turk	10/28/64	0435	50
Cape Kennedy	10/28/64	0435	37
WSMR	10/28/64	1515	61
	<u>February 24, 1965</u>		
Antigua	2/24/65	1435	51
Grand Turk	2/24/65	1630	51
Cape Kennedy	2/24/65	1430	61
WSMR	2/24/65	1800	63

The rocketsonde data used in deriving these cross sections are presented in Table 5. It may be noted that there are occasional gaps in the rocket data series which cover periods of four weeks (that is, Cape Kennedy - 5/28/64 to 6/24/64). On the average, however, the observational frequency at both stations can be regarded as excellent for consecutive series of rocketsonde data.

Radiosonde data at 1200 GMT were used to analyze the 0-30 km layer on both cross sections. Whenever radiosonde temperature and pressure heights were not reported at Cape Kennedy, sounding data from Tampa, Florida were used; no significant error was introduced by this data substitution since the two stations are sufficiently close and within a sufficiently homogeneous climatic zone to justify this approach.

Twelve-hour resolution. -- Four series of rocketsonde data were selected which provided an adequate basis for preparing time cross sections with 12-hour resolution. Three were selected from Cape Kennedy data and the remaining series from WSMR data. Table 6 lists the locations and the periods covered by the time cross sections. It may be noted that sounding times of 0000 GMT and 1200 GMT are used to take full advantage of radiosonde data coverage available at 12-hour intervals. It was necessary to limit the periods covered by the four time cross sections to 7.5, 7.5, 3.5 and 9.5 days, due to the lack of rocket data with sufficient time resolution. These periods are all below the two-week minimum which had been desired. The list of rocket sounding observations presented in Table 7 indicates, however, that the data which were selected for this study did provide relatively good coverage in the 30-60 km layer.

In the case of the radiosonde data, it was frequently necessary to substitute the Tampa sounding whenever the Cape Kennedy sounding was missing; this substitution, as noted earlier in this section, introduces a negligible error. Similarly, El Paso, Texas radiosonde data were used with the White Sands rocketsonde data; again, this non-coincidence of observing points was judged to produce negligible error.

Four-hour resolution. -- The four-hour resolution cross section study was conducted using WSMR rocketsonde and radiosonde data extending over the period from 0000 GMT February 7, 1964 to 2000 GMT February 9, 1964. This three-day period was the only interval which could be selected where the time resolution of the rocket data was sufficient on a four-hour basis. Table 8 lists the rocketsonde observations used in the analysis.

### Stratospheric Warming Time Series

One of the most striking phenomena that occur in the stratosphere almost every winter or spring is a period of sudden warming that generally occurs within a few days. The changes in temperature can be quite dramatic and generally amount to several tens of degrees. Since this phenomenon occurs in a very critical region for the horizon radiance study and since the changes in temperature can be great, a special time cross section was prepared at Fort Churchill, Canada. This high latitude station comes under the influence

TABLE 5.- ROCKET SOUNDING DATA -- TIME CROSS  
SECTION 3-DAY RESOLUTION

Date	Time (GMT)	Maximum height of the temp. trace, km	Date	Time	Maximum height of the temp. trace, km
Cape Kennedy, March 1964 - February, 1965					
3/11/64	1645	58	7/23/64	1539	56
3/18/64	1500	64	7/29/64	1700	49
3/19/64	1015	55	8/5/64	1604	52
3/22/64	1015	55	8/12/64	1600	58
3/24/64	1100	51	9/15/64	1200	58
3/31/64	0435	59	9/18/64	1900	49
4/1/64	1500	57	9/23/64	1600	58
4/1/64	2220	59	9/24/64	1800	56
4/8/64	0310	47	9/25/64	1600	50
4/8/64	1800	47	9/28/64	1500	42
4/10/64	1635	58	9/29/64	2230	41
4/14/64	1630	56	9/30/64	1600	42
4/20/64	1700	53	10/6/64	1545	62
4/22/64	1629	54	10/9/64	1600	39
4/24/64	1635	58	10/12/64	1600	51
4/24/64	2215	64	10/23/64	1043	64
5/6/64	1600	64	10/26/64	0215	42
5/13/64	1530	64	10/28/64	0435	37
5/15/64	1600	56	10/29/64	1846	46
5/19/64	1600	49	10/30/64	1617	45
5/21/64	1400	55	11/4/64	2049	52
5/22/64	1600	46	11/6/64	1610	53
5/23/64	1200	41	11/10/64	1800	45
5/25/64	0830	55	11/12/64	1530	55
5/25/64	2359	49	11/16/64	1600	33
5/26/64	0045	42	11/20/64	2230	57
5/26/64	1630	59	11/30/64	1600	53
5/27/64	1419	50	12/2/64	1730	43
5/28/64	0001	52	12/6/64	0200	58
5/28/64	2100	55	12/7/64	0200	55
6/24/64	1600	54	12/7/64	1115	62
7/17/64	1934	59	12/7/64	1705	55
7/19/64	1115	49	12/8/64	0200	58
7/19/64	1307	64	12/8/64	2300	55
7/20/64	1110	58	12/9/64	0306	53
7/22/64	0900	62	12/9/64	1835	50
7/22/64	1639	55	12/10/64	1800	40

TABLE 5.- ROCKET SOUNDING DATA -- TIME CROSS  
SECTION 3-DAY RESOLUTION- Concluded

Date	Time (GMT)	Maximum height of the temp. trace, km	Date	Time (GMT)	Maximum height of the temp. trace, km
Cape Kennedy, March, 1964 - February, 1965 (Contd.)					
12/10/64	2115	34	2/9/65	1700	50
12/15/64	1945	57	2/10/65	1500	50
12/18/64	1600	57	2/10/65	1600	51
12/21/64	1600	60	2/10/65	1700	48
5/2 12/23/64	1800	65	2/11/65	1830	47
5/2 12/28/64	1600	56	2/11/65	1930	56
5/2 12/30/64	1600	62	2/12/65	1600	48
5/2 1/6/65	1609	57	2/12/65	1700	49
5/2 1/14/65	1707	57	2/12/65	1800	50
5/2 1/18/65	1600	61	2/13/65	1911	64
5/2 1/19/65	1515	59	2/14/65	1424	62
5/2 1/19/65	1715	36	2/15/65	1330	52
5/2 1/20/65	1500	62	2/15/65	2344	54
5/2 1/20/65	1600	62	2/16/65	1634	46
1/20/65	1715	57	2/17/65	1500	57
1/22/65	1600	53	2/20/65	1200	56
1/25/65	1600	58	2/21/65	1200	43
1/29/65	0230	55	2/22/65	1202	58
12/ 1/29/65	1600	34	2/23/65	1100	51
12/ 2/1/65	1600	62	2/24/65	1430	61
12/ 2/8/65	1600	51			
Fort Churchill, October, 1964 - February, 1965					
12/ 10/7/64	1955	56	12/21/64	1828	64
12/ 10/9/64	1808	46	12/23/64	1800	65
12/ 10/16/64	1800	60	1/6/65	1800	60
12/ 10/21/64	1845	59	1/8/65	1800	55
11/13/64	1807	44	1/13/65	1730	49
11/16/64	1903	59	1/15/65	1930	54
11/25/64	2037	55	1/20/65	1502	56
11/27/64	2030	62	1/27/65	2115	65
11/30/64	2011	57	2/5/65	1800	60
12/4/64	1900	56	2/8/65	2000	45
12/9/64	1900	55	2/8/65	2100	62
12/11/64	1800	64	2/10/65	1800	55
12/14/64	2030	62	2/12/65	1800	59
12/16/64	1800	65			

TABLE 6.- PERIODS COVERED BY THE 12-HOUR  
RESOLUTION TIME CROSS SECTION

Location	Beginning	End
Cape Kennedy, Florida	0000 GMT 5/21/64	1200 GMT 5/28/64
WSMR, New Mexico	0000 GMT 11/18/64	1200 GMT 11/25/64
Cape Kennedy, Florida	0000 GMT 12/7/64	1200 GMT 12/10/64
Cape Kennedy, Florida	0000 GMT 2/8/65	1200 GMT 2/17/65

TABLE 7.- ROCKET SOUNDING DATA -- TIME CROSS-  
SECTIONS 12-HOUR RESOLUTION

Date	Time	Maximum height of the temp. trace, km	Date	Time	Maximum height of the temp. trace, km
Cape Kennedy(12 Hour)			WSMR (12 Hour)		
5/21/64	1400	55	11/18/64	1540	64
5/22/64	1600	46	11/19/64	1615	65
5/23/64	1200	41	11/19/64	2310	60
5/25/64	0830	55	11/20/64	2000	65
5/25/64	2359	49	11/21/64	2100	65
5/26/64	0045	42	11/21/64	2300	65
5/26/64	1630	59	11/22/64	1100	65
5/27/64	1419	50	11/22/64	1300	65
5/28/64	0001	52	11/24/64	1515	65
5/28/64	2100	55	11/24/64	1900	63
			11/25/64	1615	65
Cape Kennedy (12 Hour)			Cape Kennedy (12 Hour)		
12/7/64	0200	55	2/8/65	1600	51
12/7/64	1115	62	2/9/65	1700	50
12/7/64	1705	55	2/10/65	1500	50
12/8/64	0200	58	2/10/65	1600	51
12/8/64	2300	55	2/10/65	1700	48
12/9/64	0306	53	2/11/65	1830	47
12/9/64	1835	50	2/11/65	1930	56
12/10/64	1800	40	2/12/65	1600	48
12/10/64	2115	34	2/12/65	1700	49
			2/12/65	1800	50
			2/13/65	1911	64
			2/14/65	1424	62
			2/15/65	1330	52
			2/15/65	2344	54
			2/16/65	1634	46
			2/17/65	1500	57

TABLE 8.- ROCKET SOUNDING DATA -- TIME CROSS  
SECTION 4-HOUR RESOLUTION

Date	Time (GMT)	Maximum height of the temp. trace, km
	WSMR (4 Hour)	
2/7/64	1100	61
2/7/64	1700	61
2/7/64	1900	65
2/7/64	2105	56
2/7/64	2300	65
2/7/64	2305	56
2/8/64	0100	59
2/8/64	0300	58
2/8/64	0522	54
2/8/64	2300	61
2/8/64	1100	61

of the strong polar vortex which is the dominant meteorological feature of the fall and winter seasons. When the polar vortex begins to break down, generally in late winter, Fort Churchill usually experiences a period of warm stratospheric temperatures. March 1965 was no exception with the most intense warming occurring late in the month.

A time cross section at Fort Churchill was prepared, therefore, for the month of March 1965, on a 24-hour time resolution basis. The available rocket sounding data for this station are listed in Table 9. Above 10 mb the soundings were interpolated from the plotted and analyzed rocket data, while at or below 10 mb most of the data are from actual radiosonde runs as found in the Northern Hemisphere Data Tabulations. In cases where the radiosonde observations did not reach the 10 mb level, the temperatures and heights were estimated from analyzed maps obtained on microfilm from NWRC, Asheville.

### Climatological Cases

The objective in this study phase was to assemble and analyze a coherent body of climatological information from which a series of seasonal temperature and pressure profiles could be derived over the 0-90 km altitude range. Table 1 listed the various types of climatological information that are currently available with which to achieve this objective.

Climatological data coverage above 30 km is relatively sparse compared to that at lower levels. The key climatological inputs for this study are (1) the mean temperatures and standard deviations of temperature in the 30-52 km layer computed at approximate 3 km intervals for several North American rocket stations (ref. 3), and (2) mean temperatures in the 54-90 km layer computed at 3 km intervals for various latitudes in the mid-season months of January, April, July and October (ref. 5, ref. 7).

The selection of climatological cases was necessarily confined to North America and the surrounding oceans (an area similar to that used for the synoptic cases) where MRN temperature data provided an acceptable body of climatological statistics for use in profile determination.

### Auxiliary Data

In order to achieve the primary objectives of this study, the choice of synoptic and cross section cases was necessarily concentrated upon those stations and operational periods where relatively dense and continuous rocket data coverage were available from the MRN. However, this network only covers approximately one-fourth of the Northern Hemisphere; in addition, all study cases (aside from the climatological cases) were based upon rocketsonde data taken during the period March 1964 to March 1965. An effort was made, therefore, to determine the extent to which rocketsonde data were available for other geographical areas and other time periods for use in estimating the overall representativeness of the profile data body. For this purpose, an auxiliary data body was developed which included (1) data from MRN stations at times and/or locations other than those used in the primary data body, (2) data from

TABLE 9.- ROCKET SOUNDING DATA -- STRATOSPHERIC  
WARMING TIME SERIES - 24-HOUR RESOLUTION

Date	Time (GMT)	Maximum height of the temp. trace, km
Fort Churchill, March, 1965		
3/3/65	1834	60
3/10/65	2206	65
3/17/65	2230	66
3/19/65	2255	59
3/23/65	2126	66
3/24/65	2300	55
3/25/65	2000	52
3/26/65	1800	67
3/29/65	1800	64
3/30/65	1830	56

ship rocket observations in the Atlantic Ocean, and (3) older rocketsonde data used in developing the 50-80 km temperature extrapolation technique.

Table 10 lists the locations and dates of the auxiliary rocketsonde observations obtained from various MRN stations. Of special importance are the 18 soundings from McMurdo, Antarctica over a 14-month period, since there are no climatological summaries available for rocket soundings from Antarctica or any other area of the Southern Hemisphere.

Table 11 lists the locations and dates of the auxiliary rocketsonde observations obtained from the USNS Croatan, which made periodic firings at various locations in the Atlantic Ocean during the period from late February to mid-April 1965. This data is especially valuable since 14 of the 15 soundings are in the Southern Hemisphere, ranging in latitude from the mid-latitudes to the tropics.

Table 12 lists rocketsonde observations used in the development of the 50-80 km extrapolation procedure. The special importance of these data is that they extend to 80 km or above, whereas none of the ordinary MRN rocket observations attain this altitude. In addition, these data extend back to 1957 and, thus, cover time periods prior to that of the primary data body. It should be pointed out that a large number of these special rocket observations were taken during the International Geophysical Year (extending from July 1, 1957 to December 31, 1958), which represented a period of maximum solar activity associated with the 11-year solar cycle. The rocket data for this period may reflect, therefore, the effects produced upon upper-air thermal conditions by maximum solar activity. However, to a large extent such effects are counter-balanced by the inclusion into the extrapolation procedure development of data for 1962 and 1963, which represent years of relatively low solar activity in the solar cycle.

TABLE 10.7 AUXILIARY ROCKETSONDE OBSERVATIONS -- MRN

Place	Date	Place	Date
Barking Sands (Hawaii)	3/4/65	McMurdo (Antarctica)	11/7/62
	7/29/65		11/28/62
	12/9/65		12/5/62
	12/16/65		12/12/62
Kwajalein (Marshall Islands)			12/21/62
			1/9/63
			1/16/63
	6/18/63		5/16/63
	6/20/63		7/29/63
	11/9/63		9/17/63
McMurdo (Antarctica)	1/23/64	9/18/63	
	3/13/64	9/27/63	
	7/21/62	6/24/64	
	8/16/62		
	9/11/62		
	9/27/62		
Thule (Greenland)	10/3/62	7/17/64	
	10/18/62	8/12/64	

TABLE 11.- AUXILIARY ROCKETSONDE OBSERVATIONS --  
USNS CROATAN

Location	Date
37.5° N. - 75.2° W.	2/20/65
12.6° S. - 78.0° W.	3/16/65
12.5° S. - 77.6° W.	3/18/65
12.5° S. - 78.1° W.	3/21/65
11.3° S. - 78.2° W.	3/24/65
14.1° S. - 77.6° W.	3/27/65
12.2° S. - 78.1° W.	4/2/65
14.3° S. - 77.5° W.	4/3/65
0.5° S. - 75.0° W.	4/5/65
47.0° S. - 77.4° W.	4/10/65
48.4° S. - 77.4° W.	4/11/65
52.1° S. - 77.5° W.	4/11/65
59.0° S. - 77.6° W.	4/13/65
59.5° S. - 77.5° W.	4/14/65
52.3° S. - 78.1° W.	4/15/65

TABLE 12.7 AUXILIARY ROCKETSONDE OBSERVATIONS -- USED  
IN DEVELOPING EXTRAPOLATION PROCEDURE

Location	Date	Time (GMT)
Fort Churchill	7/22/57	0047
	7/24/57	0012
	8/20/57	2340
	8/25/57	1306
	12/15/57	2345
	1/27/58	1212
	12/4/62	2111
	12/6/62	2232
	3/9/63	2321
Wallops Island	11/26/63	1800

## DETERMINATION OF TEMPERATURE/PRESSURE PROFILES

### Synoptic Cases

For each of the eight synoptic cases defined earlier in this section, interpolated profiles were determined at 56 grid points spaced over North America and the surrounding oceans (a total of 448 profiles). Figure 8 shows the grid point distribution used for the synoptic cases; it may be noted that each point has been assigned a reference number. Table 13 lists the latitude and longitude for each synoptic grid point.

The actual determination of the synoptic profiles was performed by using the rocketsonde and radiosonde data and the various analytical techniques described earlier in this section. Thus, at and below the 10 mb level (approximately 30 km), the interpolated temperature values at each grid point for each synoptic case were obtained from the isotherm analysis on surface pressure charts and the constant pressure charts for 850, 700, 500, 300, 200, 100, 50, 30, and 10 mb. Between 30-60 km, the temperature values were interpolated from the isotherm analysis on constant level charts drawn at 3 km intervals throughout this layer. Above 60 km, temperature values were extrapolated by the technique discussed earlier in this section.

The pressure profiles were derived as follows: (1) at 10 mb and below, the height values at each grid point for each mandatory pressure level were interpolated from the analyzed constant pressure charts, and (2) above 10 mb, the pressure values for each 3 km interval from 30-90 km were derived from the temperature profile by using the hydrostatic equation.

The synoptic temperature and pressure profile data for each grid point were then tabulated on IBM punch cards, using the format to be presented in this section.

To illustrate more specifically the synoptic variability of the temperature field at levels within the region of rocketsonde data coverage, Figures 9-13 present a series of analyzed charts at the 36, 39, 42, 45, and 48 km levels for the 9 December 1964 synoptic case. This case featured better-than-average MRN data coverage, with 7 MRN stations reporting temperature to a level of at least 52 km.

It may be noted from the isotherm analysis on the above charts that the middle part of the North American continent was relatively cold at all levels and that it was relatively warm off both coasts. The warmth off the East Coast is especially pronounced at 42 and 45 km (Figures 11 and 12); the isotherms are oriented in a north-south direction with warmer temperatures on the ocean-ward side. The southerly thermal wind at Wallops Island, Virginia (where actual temperature sounding data were unavailable) clearly supports the isotherm analysis; this feature clearly demonstrates the usefulness of the thermal wind techniques. At 48 km, a relatively cool pool of air over the Southeastern United States, as outlined by the  $-10^{\circ}\text{C}$  isotherm, has been analyzed on the basis of the easterly thermal wind at Wallops Island, which served to indicate colder air to the south.

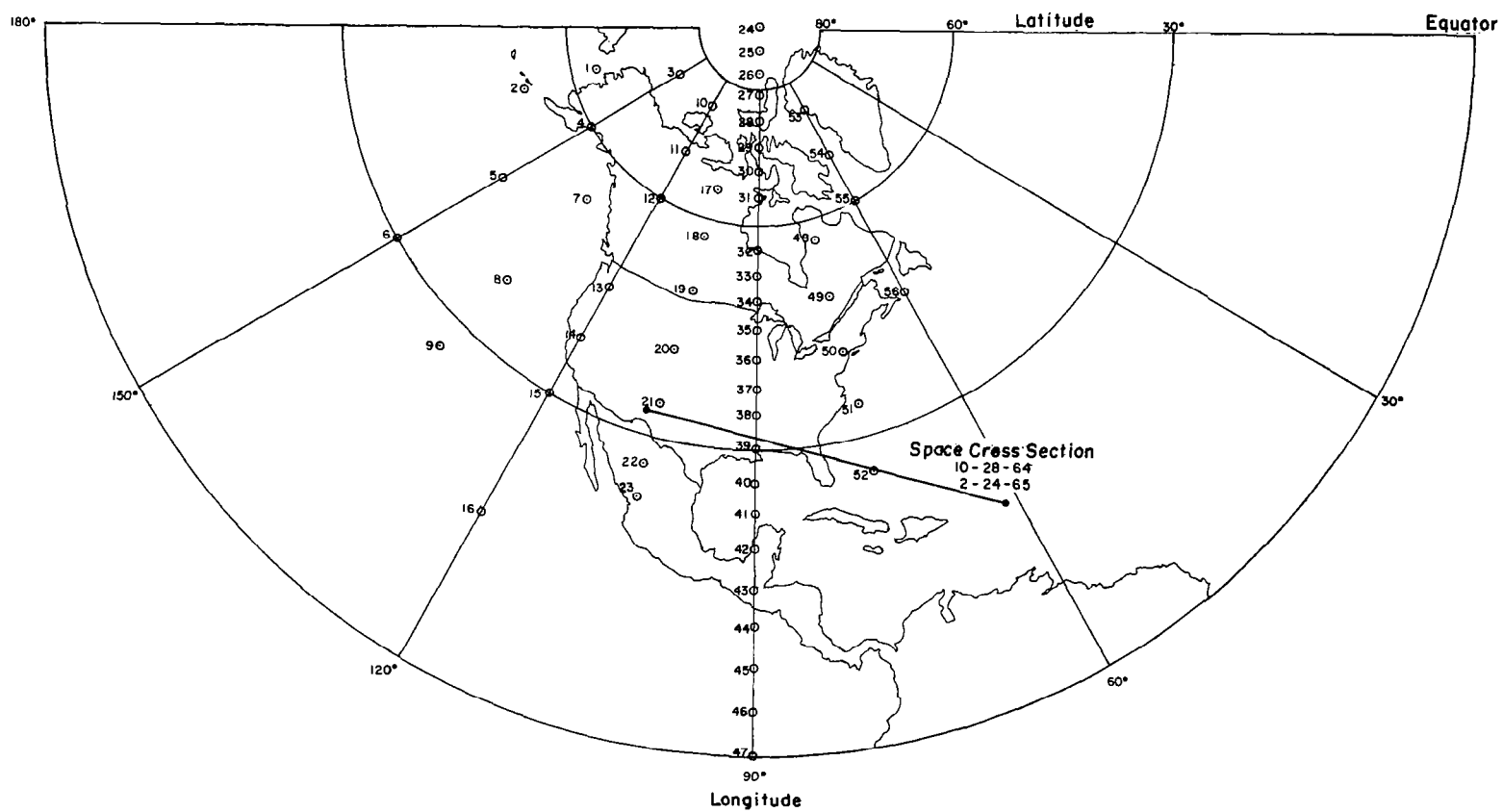


Figure 8. Location of the 56 Interpolated Soundings for Each Synoptic Case

TABLE 13.- LATITUDE AND LONGITUDE OF SYNOPTIC  
GRID POINTS

Grid point reference number	Latitude, °N	Longitude, °W	Grid point reference number	Latitude, °N	Longitude, °W
1	63.75	165	29	71.25	90
2	52.5	165	30	67.5	90
3	75	150	31	63.75	90
4	60	150	32	56.25	90
5	45	150	33	52.5	90
6	30	150	34	48.75	90
7	52.5	135	35	45	90
8	37.5	135	36	41.25	90
9	26.25	135	37	37.5	90
10	75	120	38	33.75	90
11	67.5	120	39	30	90
12	60	120	40	26.25	90
13	45	120	41	22.5	90
14	37.5	120	42	18.75	90
15	30	120	43	15	90
16	15	120	44	11.25	90
17	63.75	105	45	7.5	90
18	56.75	105	46	3.75	90
19	48.75	105	47	0	90
20	41.25	105	48	56.25	75
21	33.75	105	49	48.75	75
22	26.25	105	50	41.25	75
23	22.5	105	51	33.75	75
24	90	—	52	26.25	75
25	86.25	90	53	75	60
26	82.5	90	54	67.5	60
27	78.75	90	55	60	60
28	75	90	56	45	60

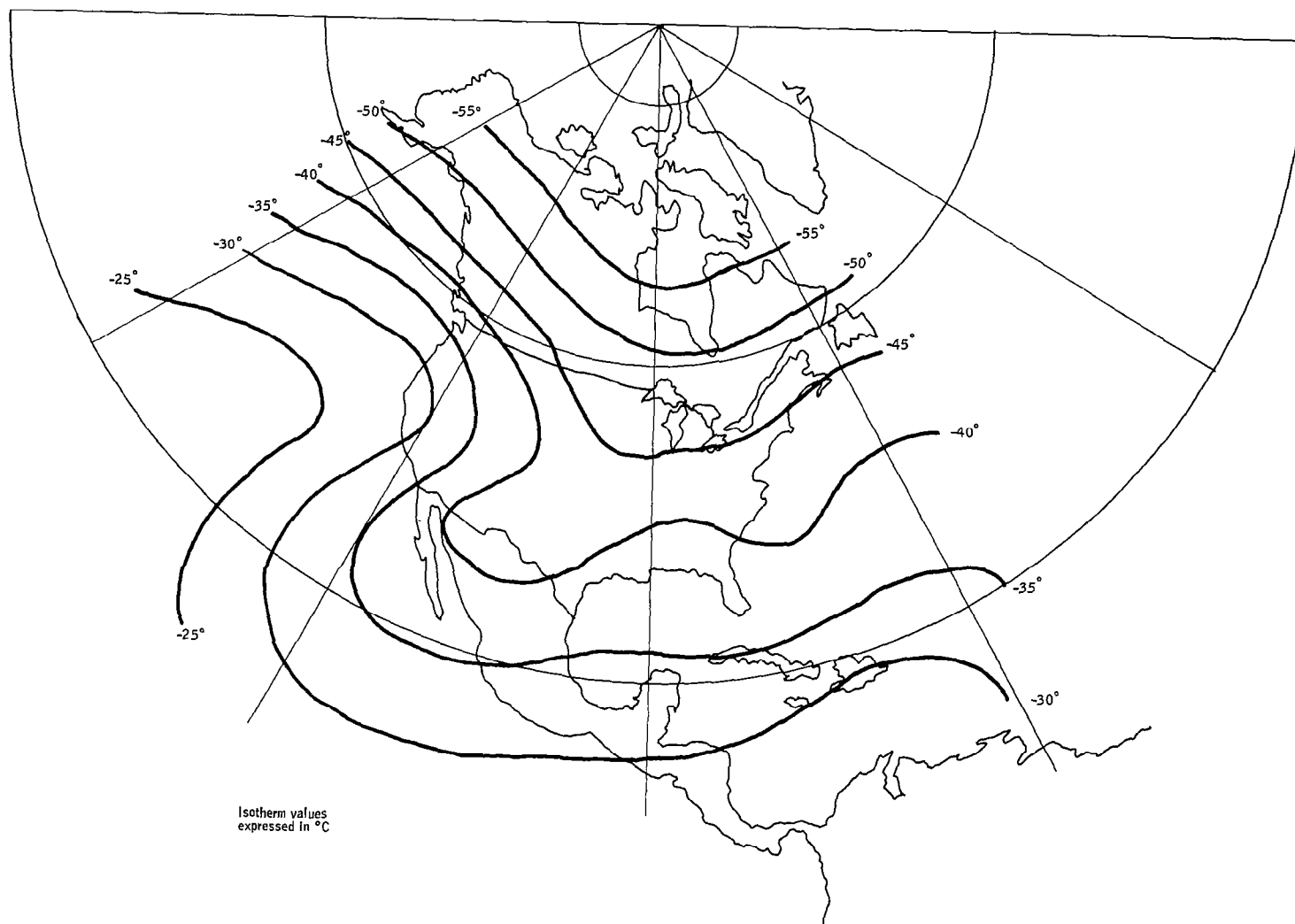


Figure 9. Isotherm Analysis at 36 km on 9 December 1964

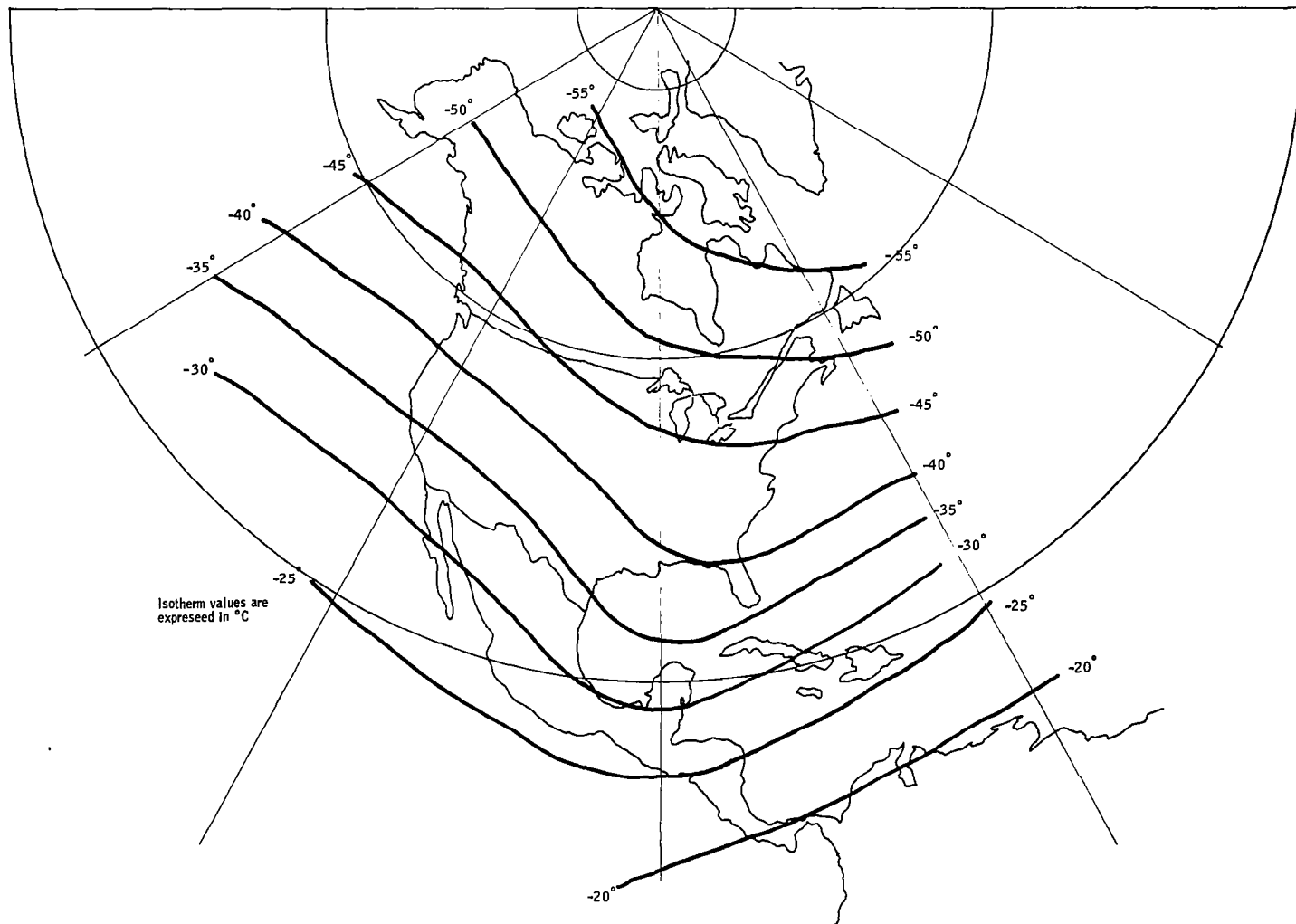


Figure 10. Isotherm Analysis at 39 km on 9 December 1964

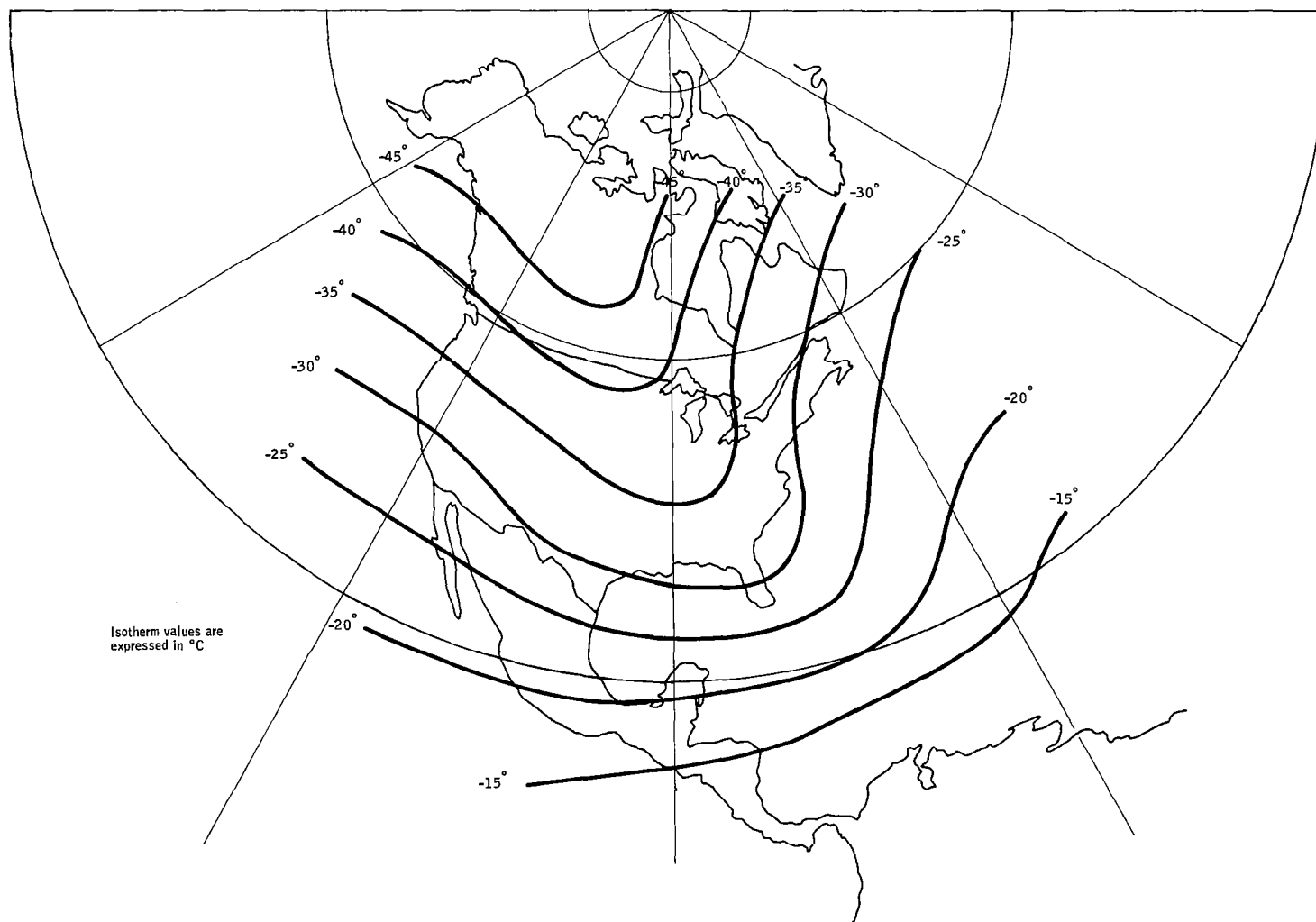


Figure 11. Isotherm Analysis at 42 km on 9 December 1964

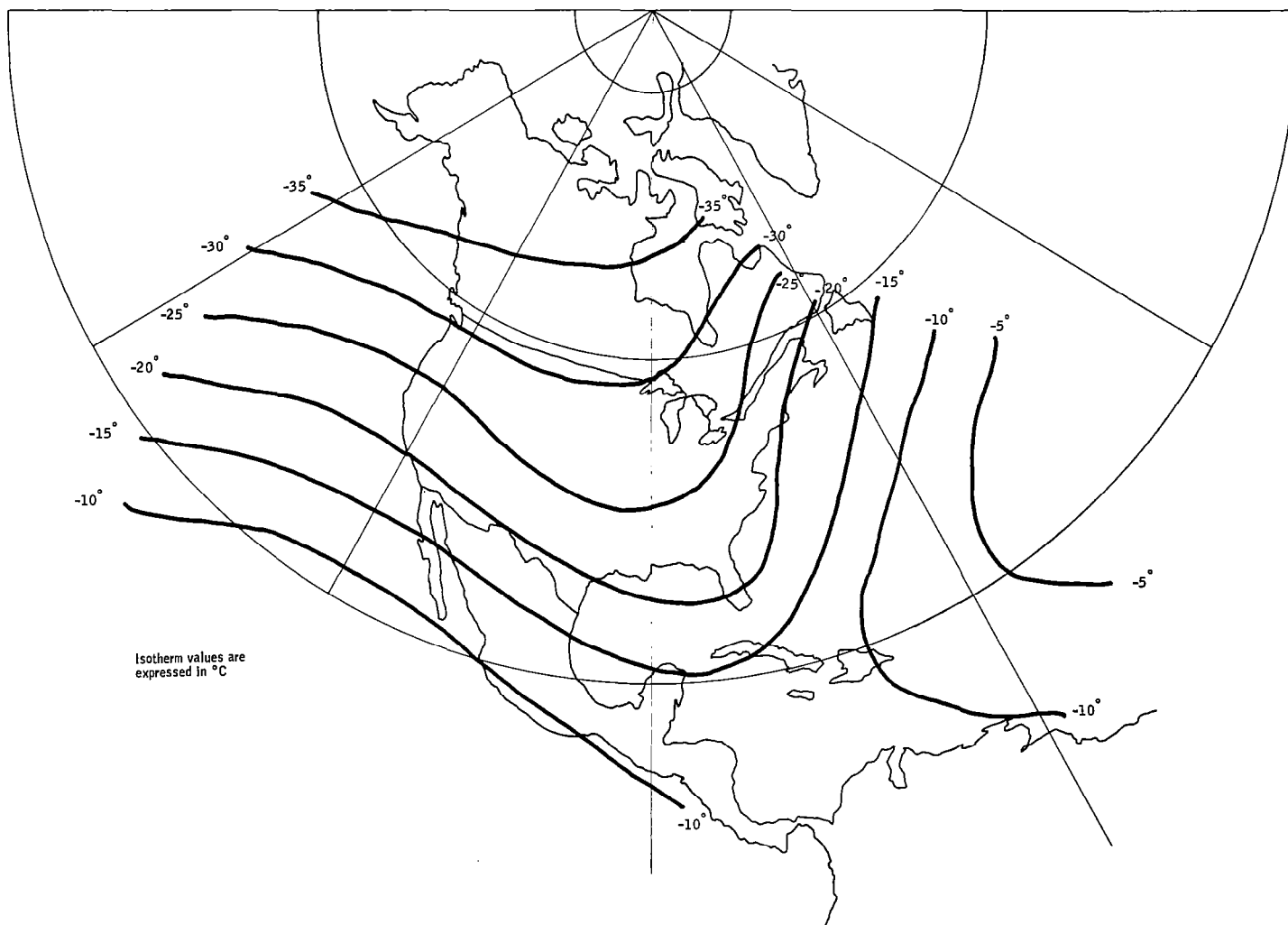


Figure 12. Isotherm Analysis at 45 km on 9 December 1964

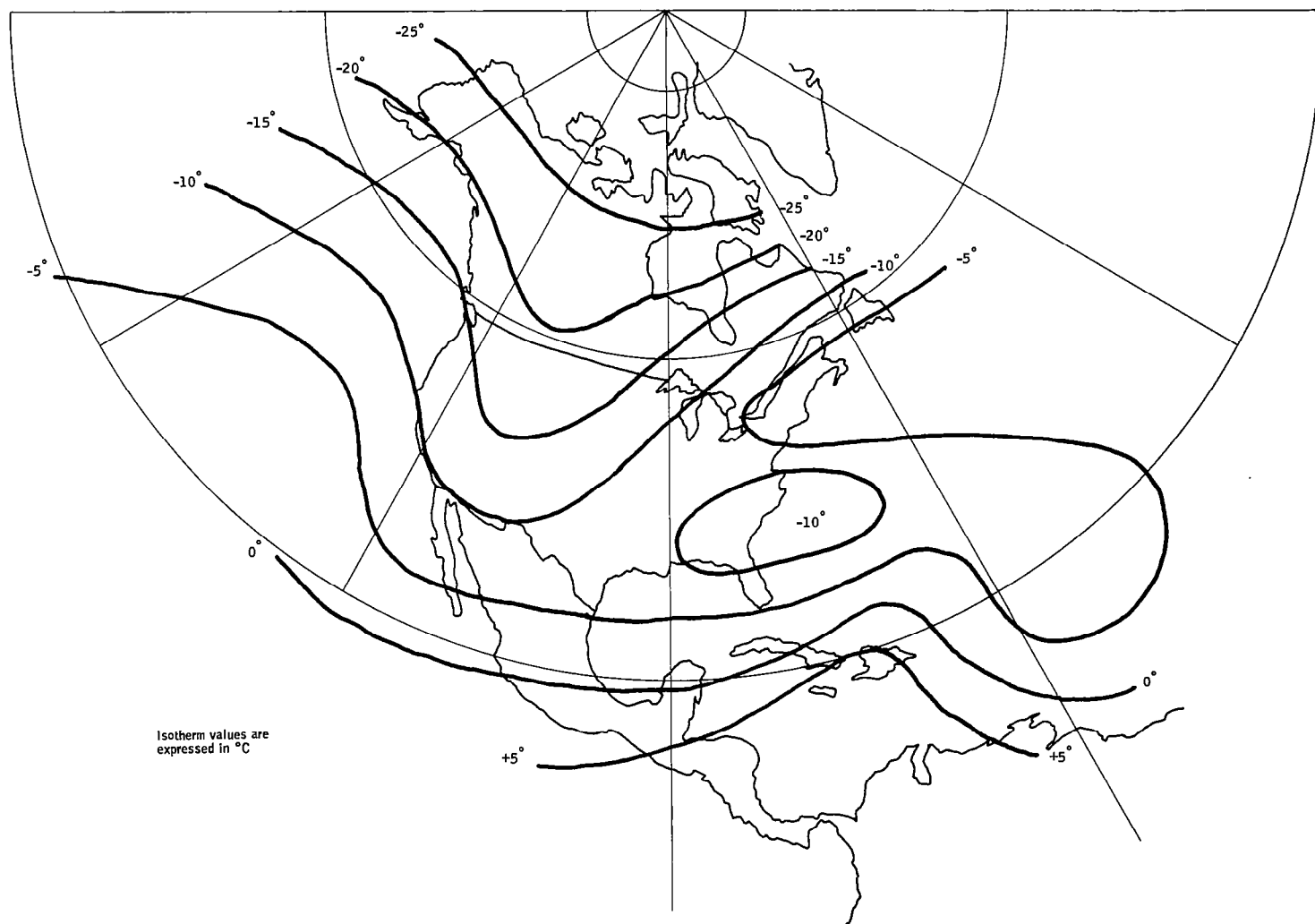


Figure 13. Isotherm Analysis at 48 km on 9 December 1964

This feature, together with the presence of a westerly thermal wind at Cape Kennedy, Florida (hereby indicating colder air to the north) provides strong support to the analysis of the cold pool of stratospheric air. Again, the importance of the thermal wind technique as an analytical tool is clearly demonstrated.

### Space Cross Sections

The two space cross section cases, the selection of which was previously discussed in this section, extended along a 5600 km line from White Sands to Antigua. (This space section line is shown on Figure 8). Points were selected at 100 km intervals along this line for the determination of interpolated profiles. Table 14 lists the latitude and longitude for each space cross-section interpolation point.

All of the required sounding data at 10 mb and below were interpolated from analyzed constant pressure charts at the various mandatory levels. The rocketsonde data at 30 km and above were plotted and analyzed for each case on a vertical cross-section chart and the sounding data were interpolated at each of the 57 points along the cross-section line. The vertical interpolation interval used for the sounding data between 30-60 km was 2.5 km; this interval, which differs from the 3 km interval used in the synoptic cases, was chosen due to a convenient 2.5 km vertical scale present on the cross-section charts.

Figure 14 presents the space cross section analysis which was used in one of the cases for interpolating the temperature profile values between 30-60 km. The temperatures are plotted in degrees centigrade and are analyzed every 10 degrees. It may be noted that the inherent spatial resolution associated with the spacing of data reporting stations considerably exceeds the 100 km interpolation interval which was used in determining the individual sounding profiles. This point is particularly true in the case of the Cape Kennedy-White Sands portion of the profile where a distance of some 2700 km separates the two stations. By way of justifying the approach which was used, it should be pointed out that the skilled analysis by meteorologists with an understanding of the spatial variability developed from long experience can enhance the effective resolution obtainable from a given body of upper air sounding data. As may be noted by examining Figure 14, the analysis has produced isotherm patterns which represent far more than mere linear interpolation; thus, the spatial variability, although perhaps not entirely real for this particular case, is nevertheless representative of the variability which it was the intention of these cases to provide for the select body of profile data.

The temperature and pressure profile data for the space cross section points were tabulated on IBM punch cards. A total of 57 points were determined for each of the two selected cases, for an overall total of 114 points.

### Time Cross Sections

The time cross section cases, as noted earlier in this section, were selected in terms of three different time resolutions: (1) 3-day, (2) 12-hour, and (3)

TABLE 14.- LATITUDE AND LONGITUDE OF SPACE CROSS  
SECTION INTERPOLATION POINTS

Point reference number	Latitude, °N	Longitude, °W	Point reference number	Latitude, °N	Longitude, °W
1	32.4	106.5	29	28.8	80.5
2	32.4	105.5	30	28.5	79.7
3	32.4	104.5	31	28.2	78.9
4	32.4	103.6	32	27.9	78.1
5	32.4	102.6	33	27.5	77.4
6	32.4	101.6	34	27.1	76.7
7	32.4	100.7	35	26.8	75.9
8	32.3	99.7	36	26.4	75.2
9	32.2	98.7	37	26.0	74.4
10	32.1	97.8	38	25.6	73.7
11	32.0	96.8	39	25.2	73.0
12	31.9	95.8	40	24.7	72.3
13	31.8	94.9	41	24.3	71.6
14	31.6	93.9	42	23.9	70.9
15	31.5	92.9	43	23.5	70.2
16	31.4	92.0	44	23.1	69.6
17	31.2	91.1	45	22.7	68.9
18	31.0	90.2	46	22.3	68.3
19	30.9	89.3	47	21.8	67.7
20	30.7	88.4	48	21.3	67.1
21	30.5	87.5	49	20.8	66.5
22	30.3	86.6	50	20.4	65.9
23	30.1	85.7	51	19.9	65.3
24	29.9	84.9	52	19.5	64.7
25	29.7	84.0	53	19.0	64.1
26	29.5	83.1	54	18.6	63.5
27	29.2	82.2	55	18.1	62.9
28	29.0	81.4	56	17.7	62.3
			57	17.2	61.8

24 February 1965

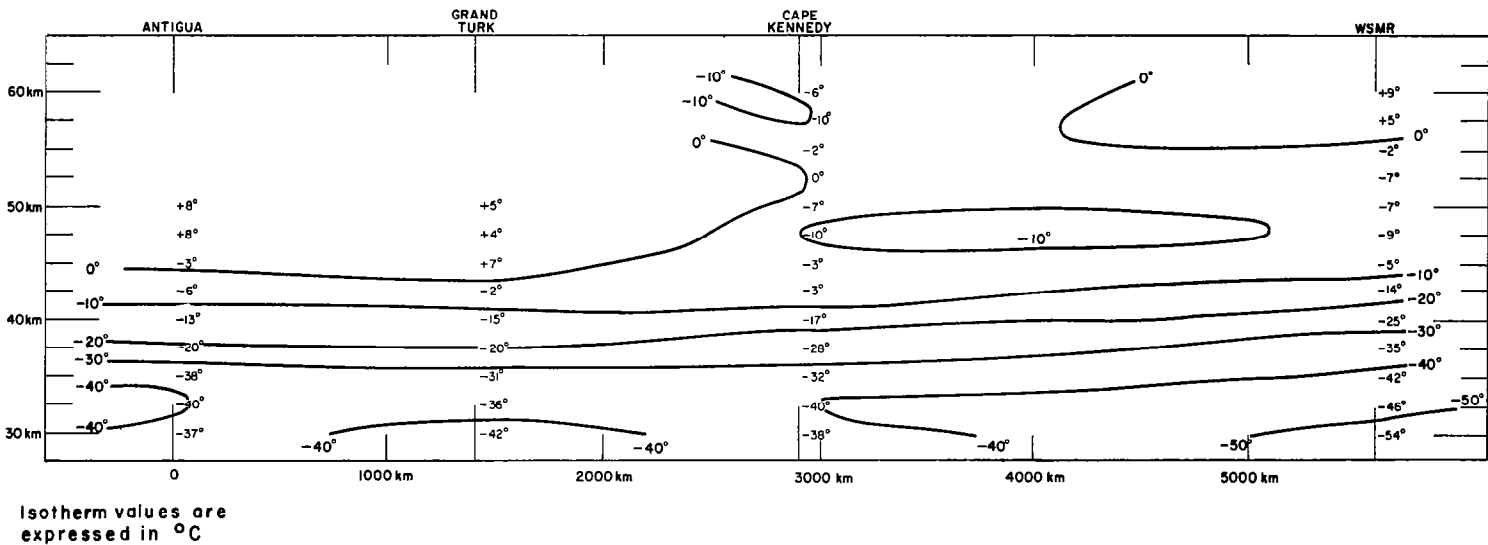


Figure 14. Space Cross Section From Antigua, B.W.I. to White Sands Missile Range, New Mexico at 1200 GMT on 24 February 1965

4-hour. The number of sounding profiles determined from these time cross-section cases were as follows: (1) 3-day resolution - 168, (2) 12-hour resolution - 60, (3) 4-hour resolution - 18, and (4) all cases - 246.

Three-day resolution. -- The two cases with 3-day resolution (that is, Cape Kennedy, March 1, 1964 - February 27, 1965; Fort Churchill, October 1, 1964 - February 13, 1965) were analyzed with the basic data and techniques described earlier. The interpolated temperatures at 10 mb and below were obtained at the designated times from analyzed surface pressure and constant pressure charts. Interpolated temperatures between 30-60 km were obtained at 2.5 km vertical intervals from the rocketsonde data which were plotted and analyzed on continuous time cross section charts for the entire period covered by each case.

The general features of spatial and temporal variability shown by the Cape Kennedy and Fort Churchill time cross sections are quite comparable. Since the Cape Kennedy cross section covers an entire year, its reproduction here would entail an extremely long series of 37 separate cross-sectional panels covering ten days each. For this reason, only the shorter Fort Churchill cross section, covering 13 cross-sectional panels, will be presented here for illustrative purposes.

Figure 15 presents the Fort Churchill time cross section for 30-60 km which was prepared for the entire case study period from 1200 GMT October 1, 1964 to 1200 GMT February 13, 1965. Some of the more significant aspects of temperature variability within this region will now be discussed.

Several periods of pronounced cooling and warming appear on the Fort Churchill time cross section, interspersed between periods of relative thermal stability at all levels. Particular note should be taken of the following periods of dynamic thermal change: (1) from November 27 to December 4, a general cooling of 15-30°C occurred throughout the entire 30-60 km region, (2) from December 16 to December 23, a general warming of 10-60°C took place over the entire height range, with the maximum warming centered near 43 km, and (3) from February 27 to March 5, a general warming of 15-35°C occurred over the entire altitude interval. Such periods of pronounced stratospheric cooling and warming, which occur over a typical period of several days, are common features of high latitude stations during the arctic winter.

The amount of analytical detail in Figure 15 depends upon the frequency of rocketsonde observations. For example, during the period December 9-16, four soundings were made at the Fort Churchill station. As a consequence, the isotherm analysis with respect to the time axis of the chart contained smaller-scale features which could not possibly be specified for other situations where the frequency of rocketsonde observations was of the order of several days or, as in some cases, a few weeks. To some extent, therefore, there is an uneven effect introduced into the atmospheric profiles derived from the analyzed time cross sections, resulting from the fact that the observational sampling times were randomly interspersed within periods when the thermal conditions might or might not be rapidly varying. Nevertheless,

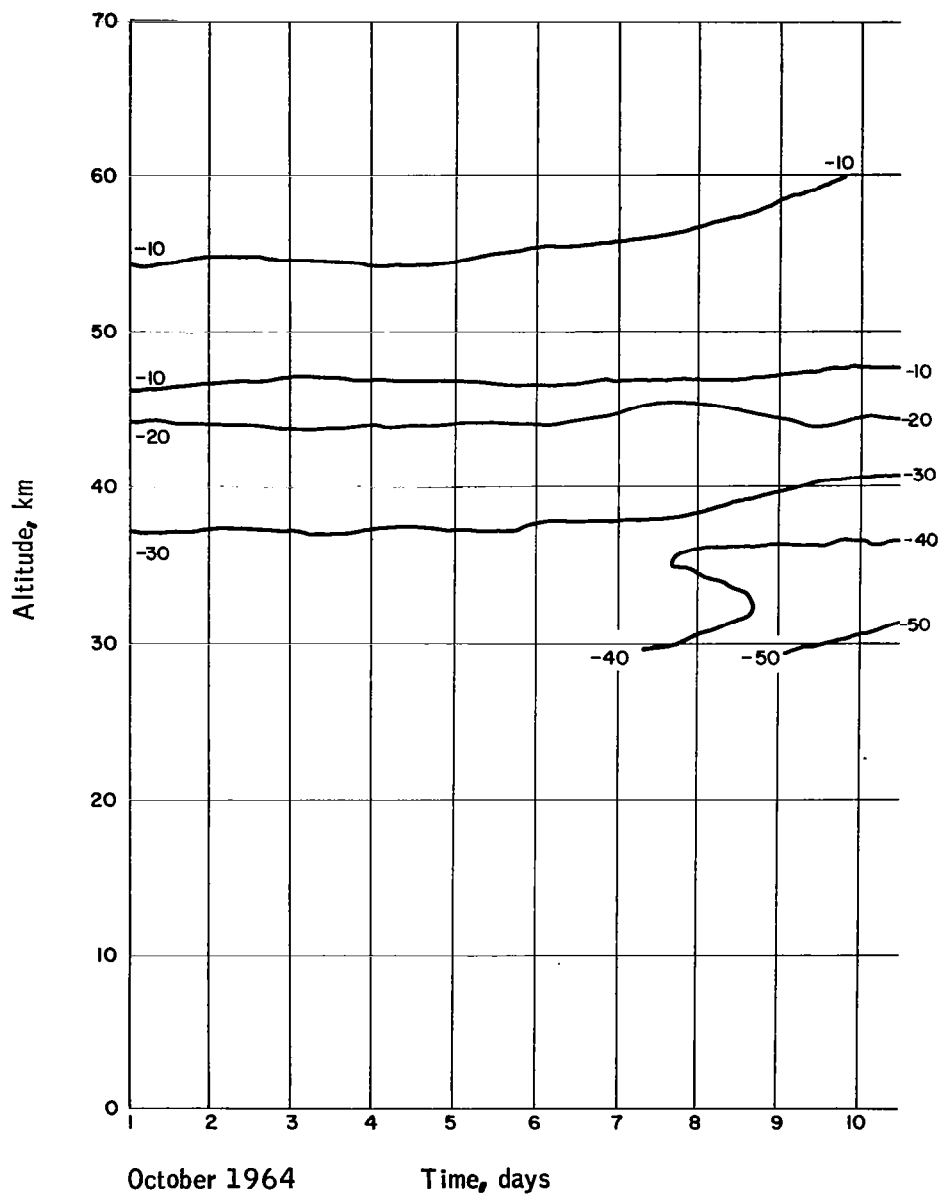


Figure 15. Fort Churchill Time Height Cross Section at 30-60 km  
From 1 October 1964 to 13 February 1965

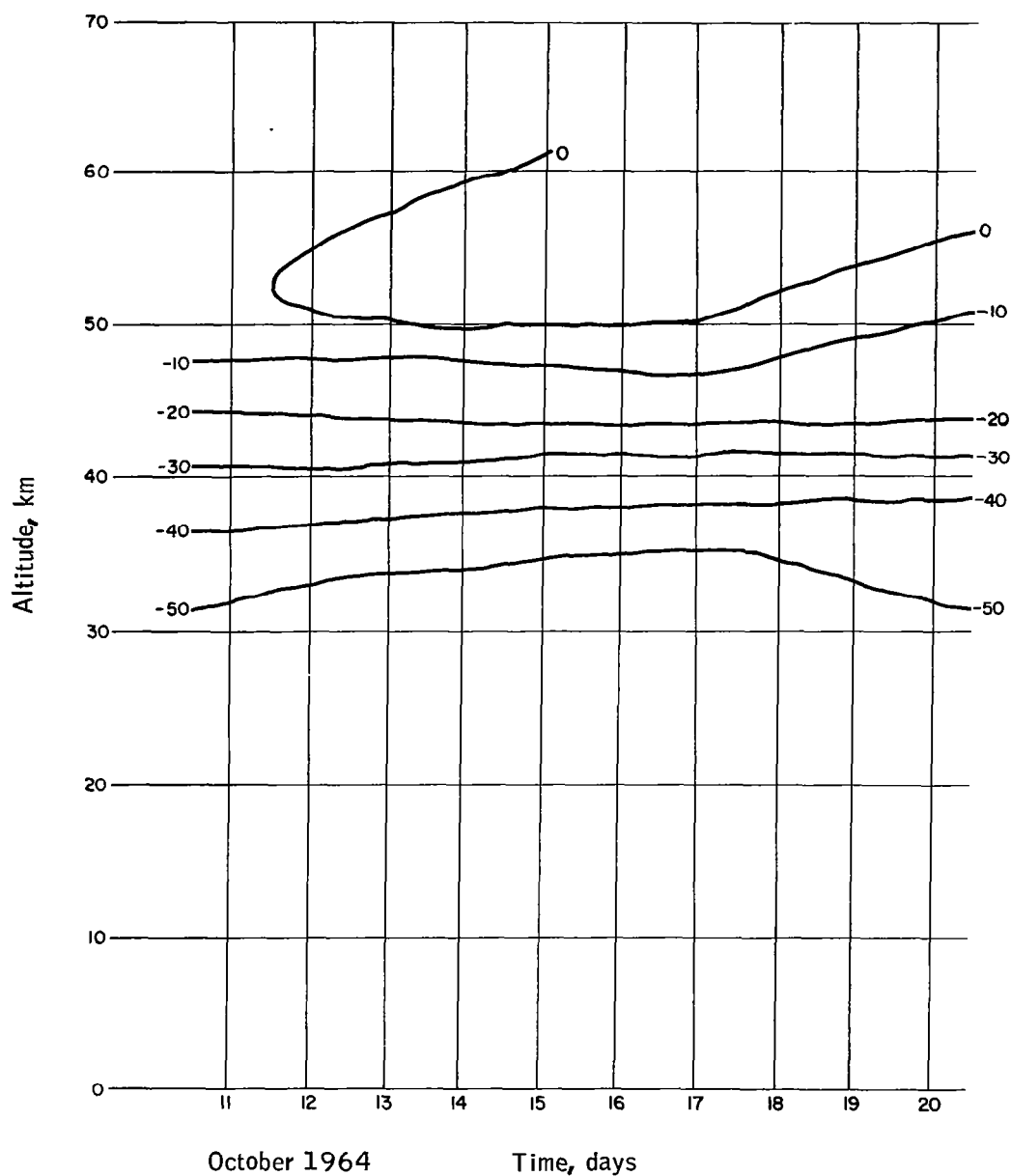


Figure 15. Fort Churchill Time Height Cross Section at 30-60 km  
From 1 October 1964 to 13 February 1965 - Continued

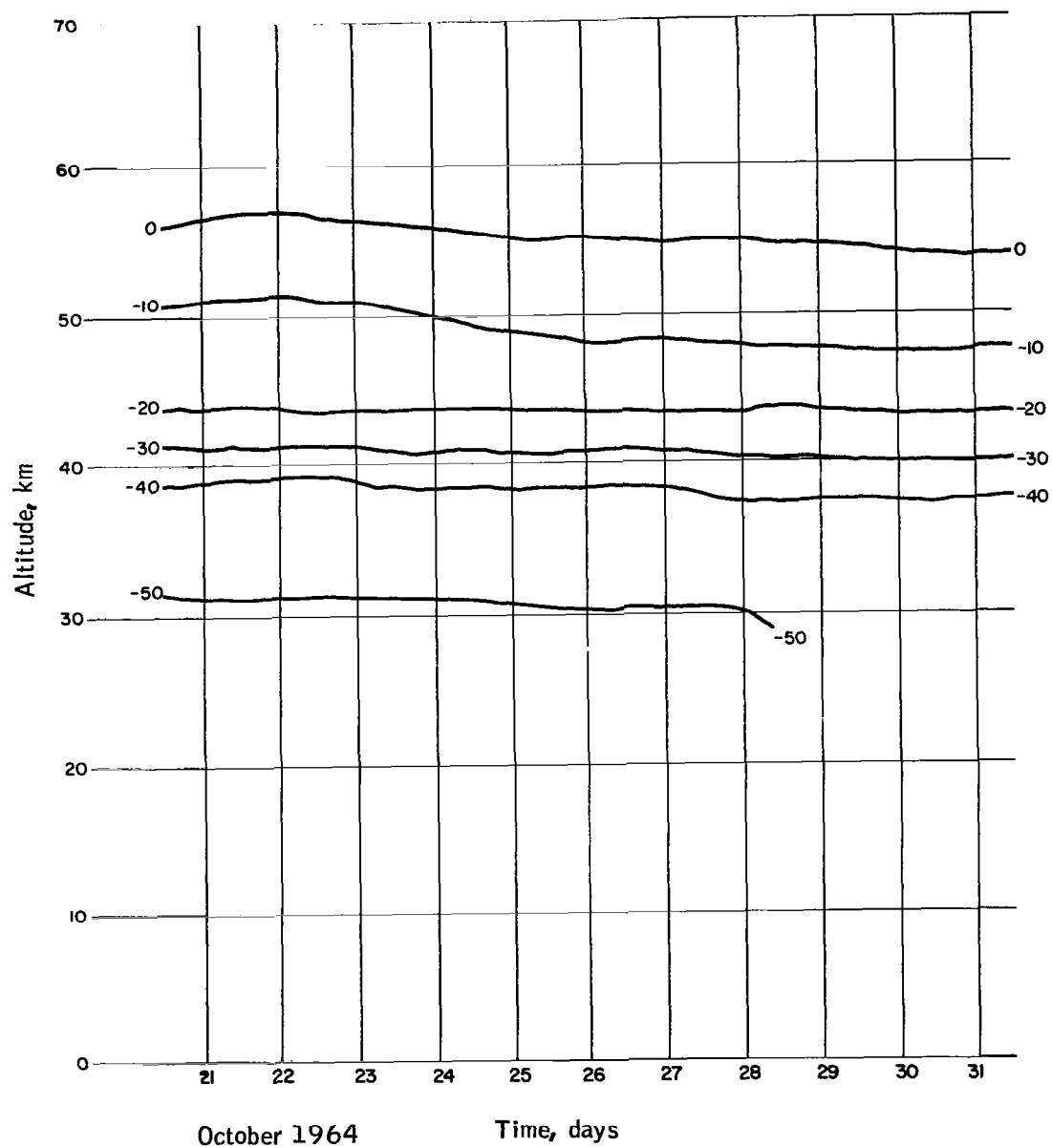


Figure 15. Fort Churchill Time Height Cross Section at 30-60 km  
From 1 October 1964 to 13 February 1965 - Continued

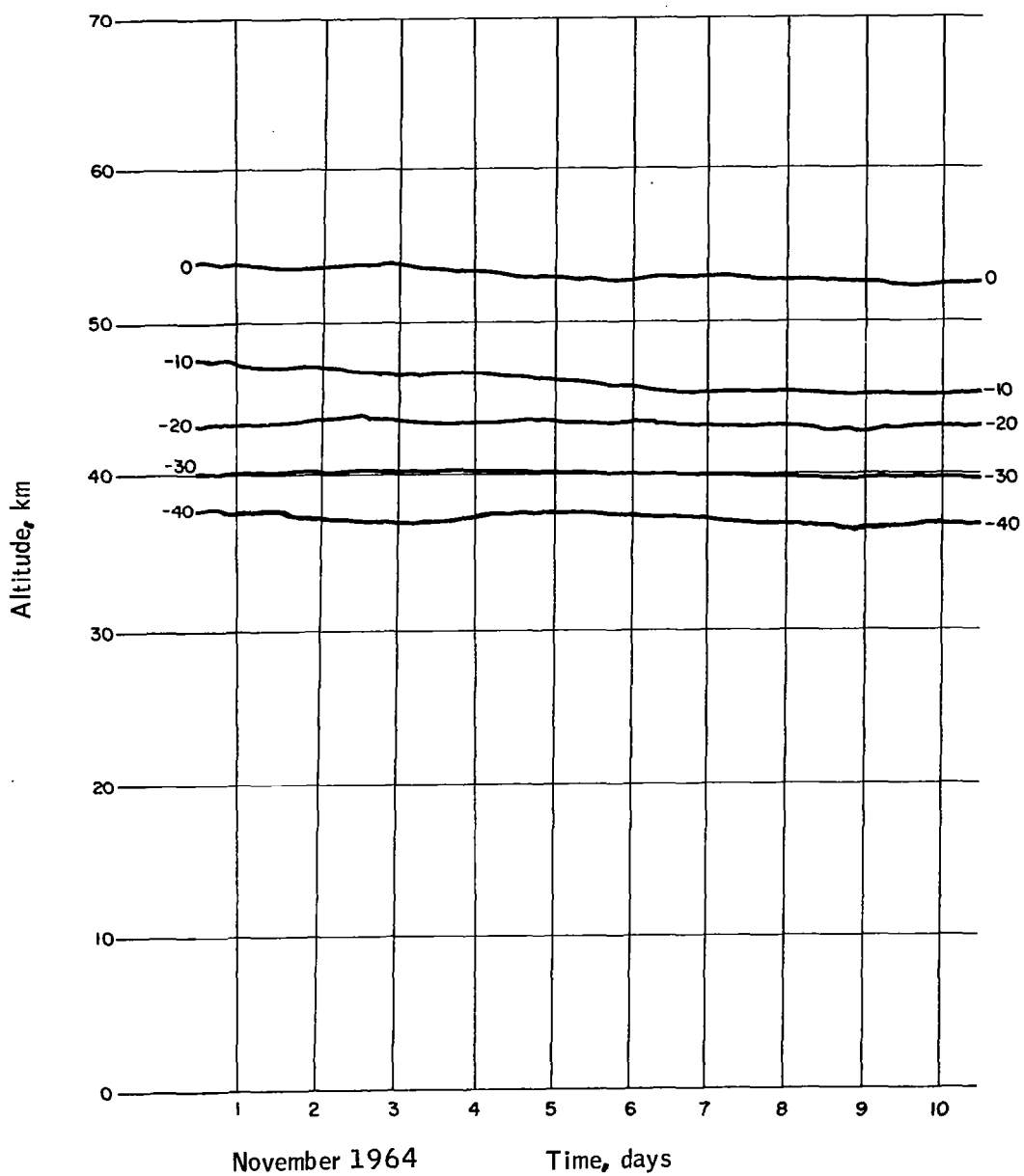


Figure 15. Fort Churchill Time Height Cross Section at 30-60 km  
From 1 October 1964 to 13 February 1965 - Continued

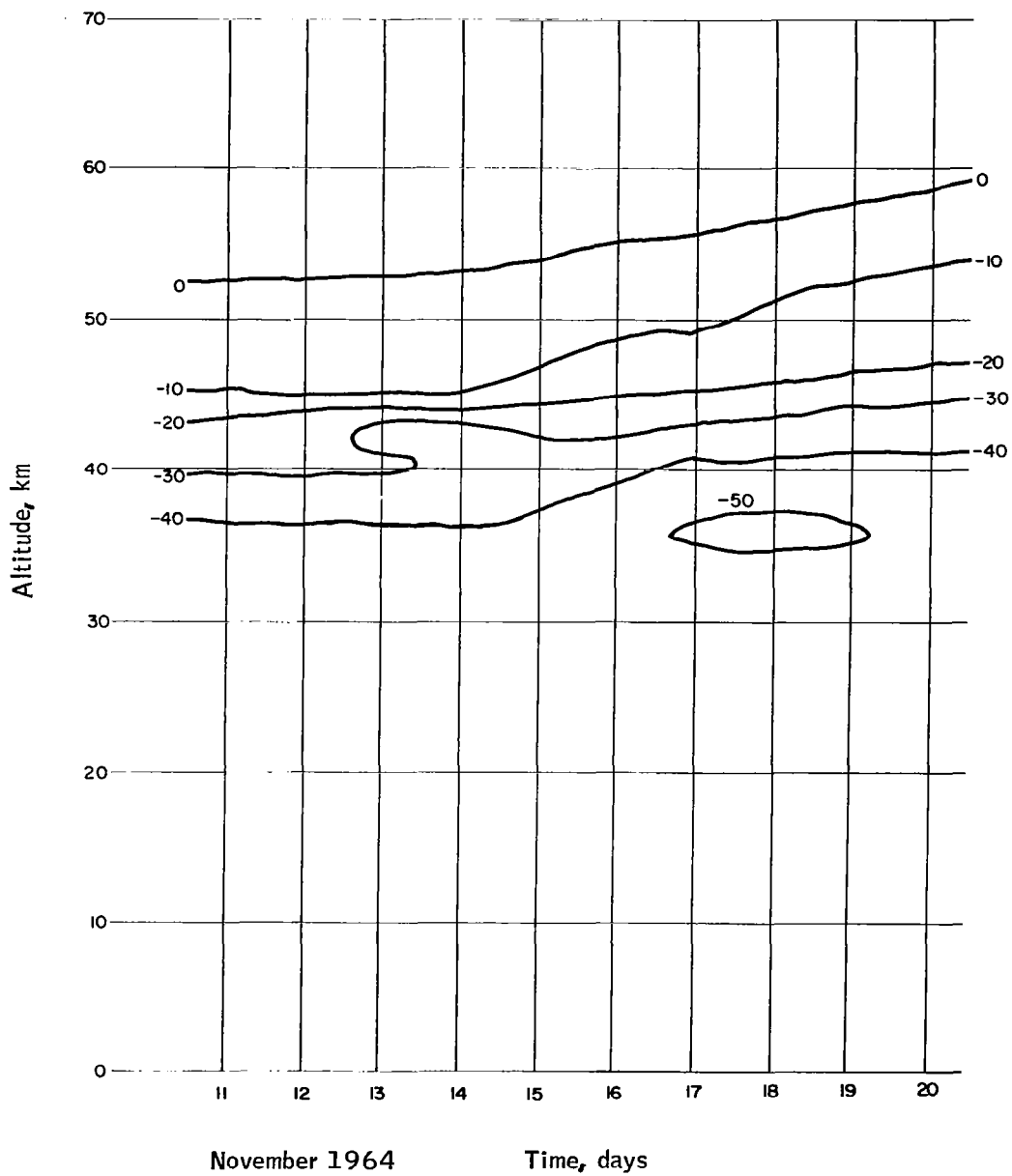


Figure 15. Fort Churchill Time Height Cross Section at 30-60 km  
From 1 October 1964 to 13 February 1965 - Continued

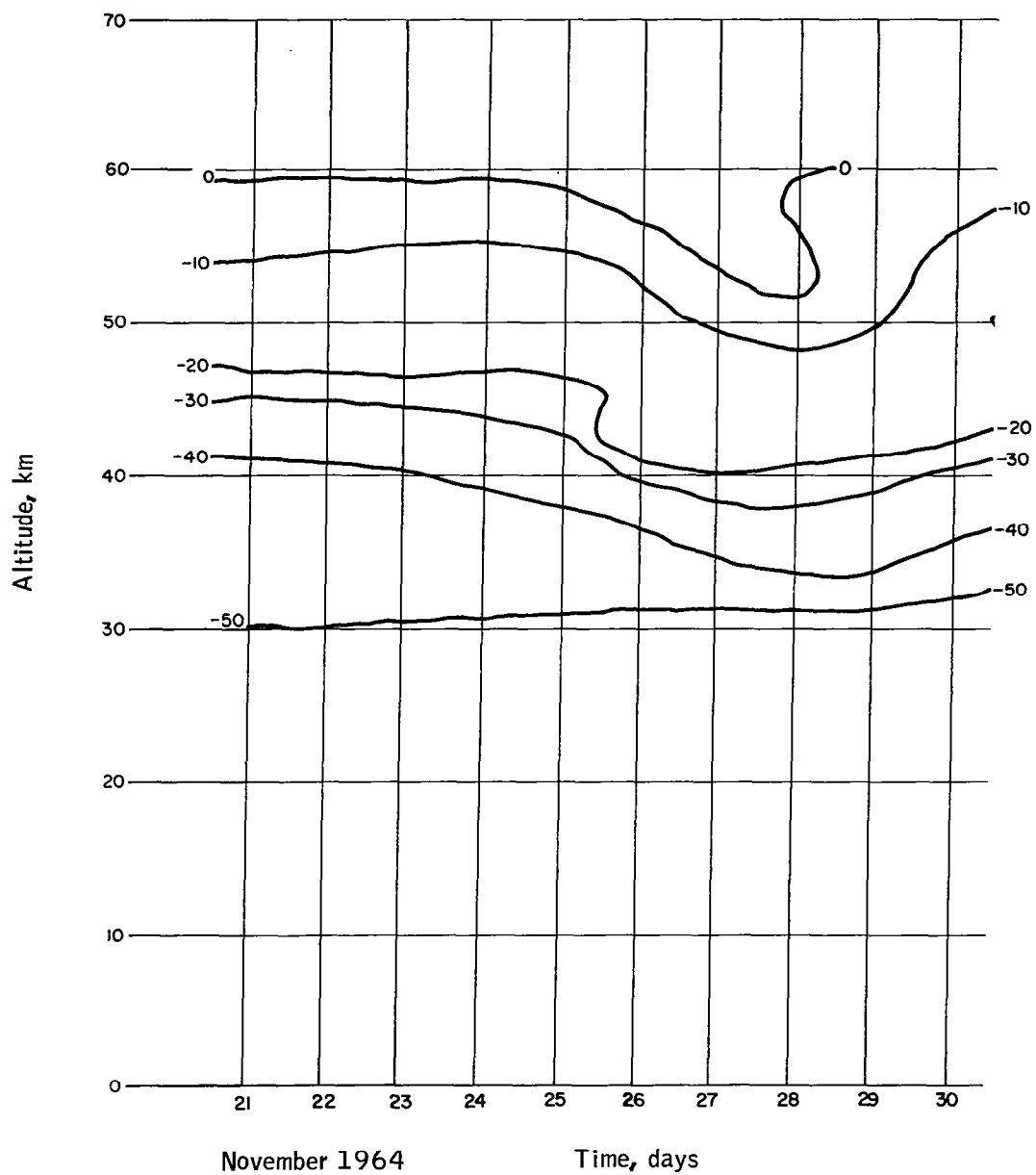


Figure 15. Fort Churchill Time Height Cross Section at 30-60 km  
From 1 October 1964 to 13 February 1965 - Continued

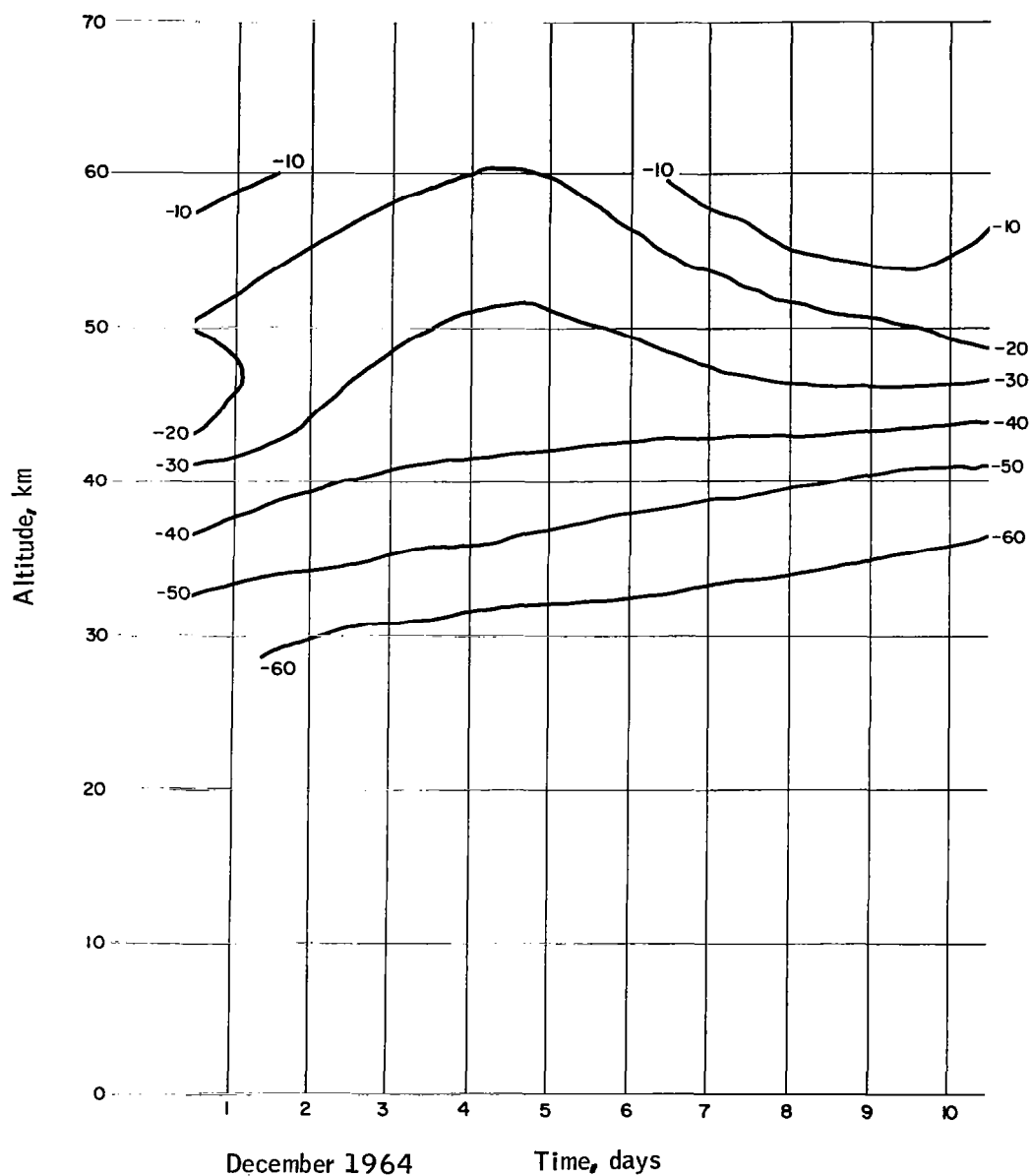


Figure 15. Fort Churchill Time Height Cross Section at 30-60 km  
From 1 October 1964 to 13 February 1965 - Continued

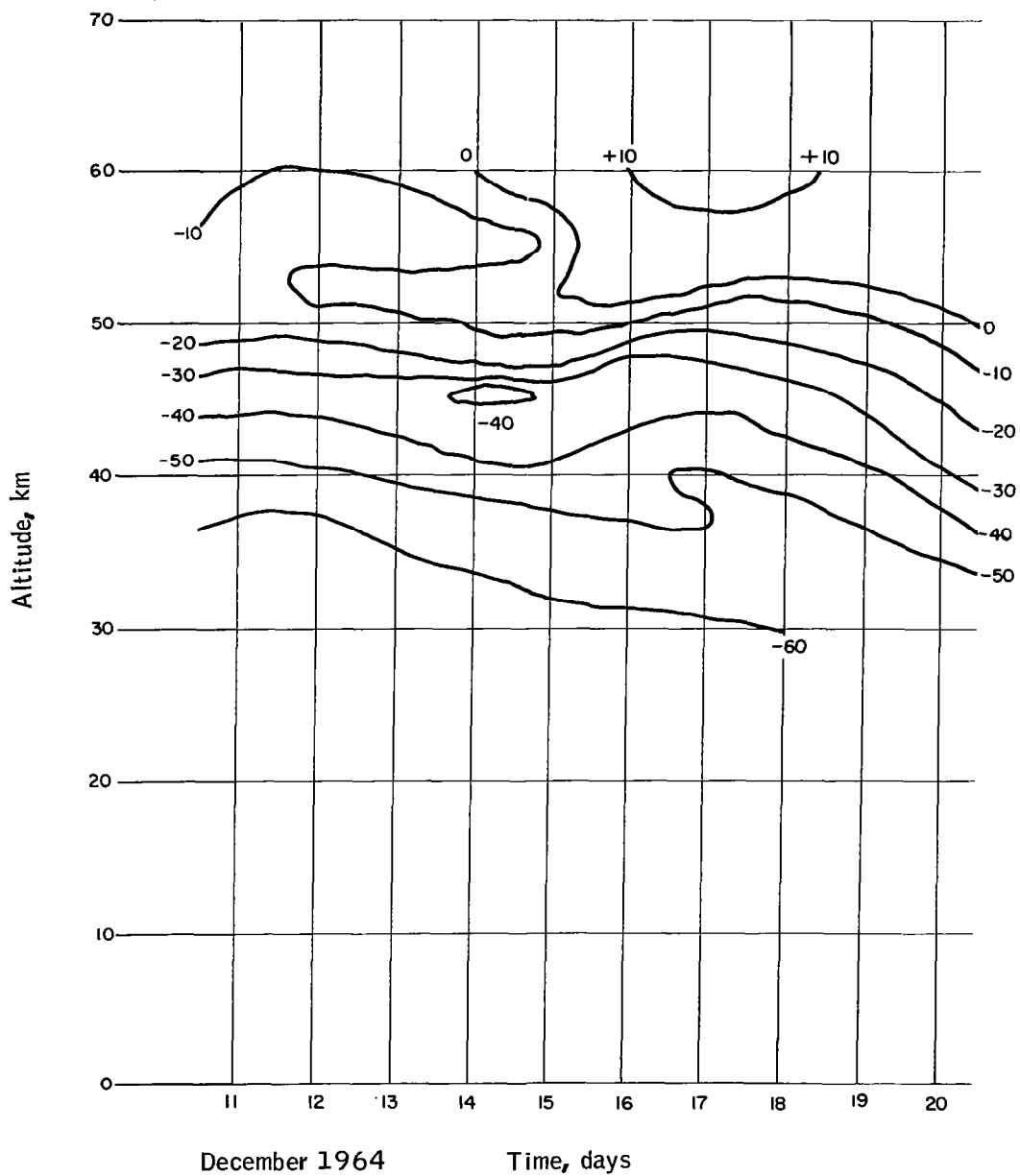


Figure 15. Fort Churchill Time Height Cross Section at 30-60 km  
From 1 October 1964 to 13 February 1965

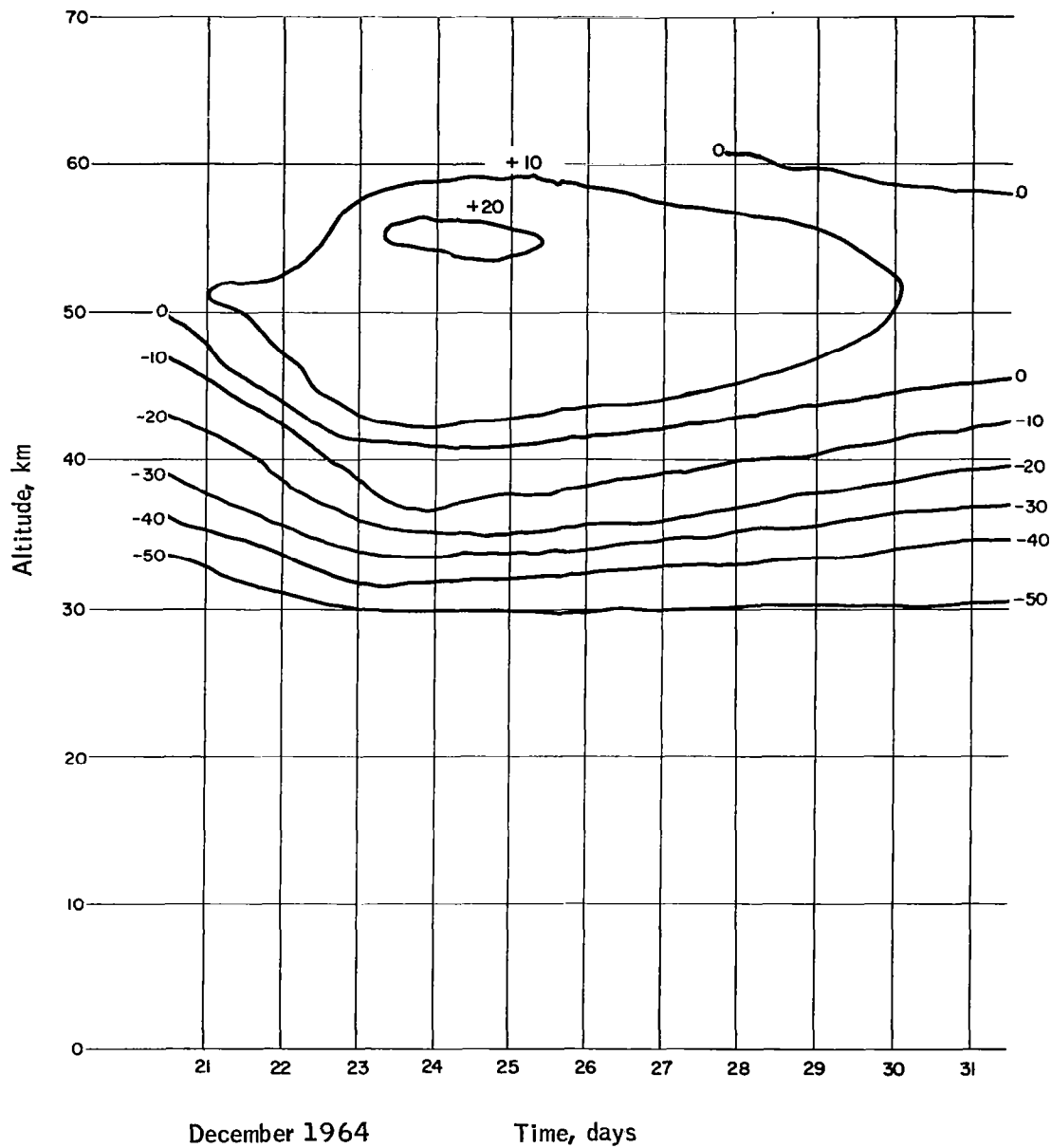


Figure 15. Fort Churchill Time Height Cross Section at 30-60 km  
From 1 October 1964 to 13 February 1965 - Continued

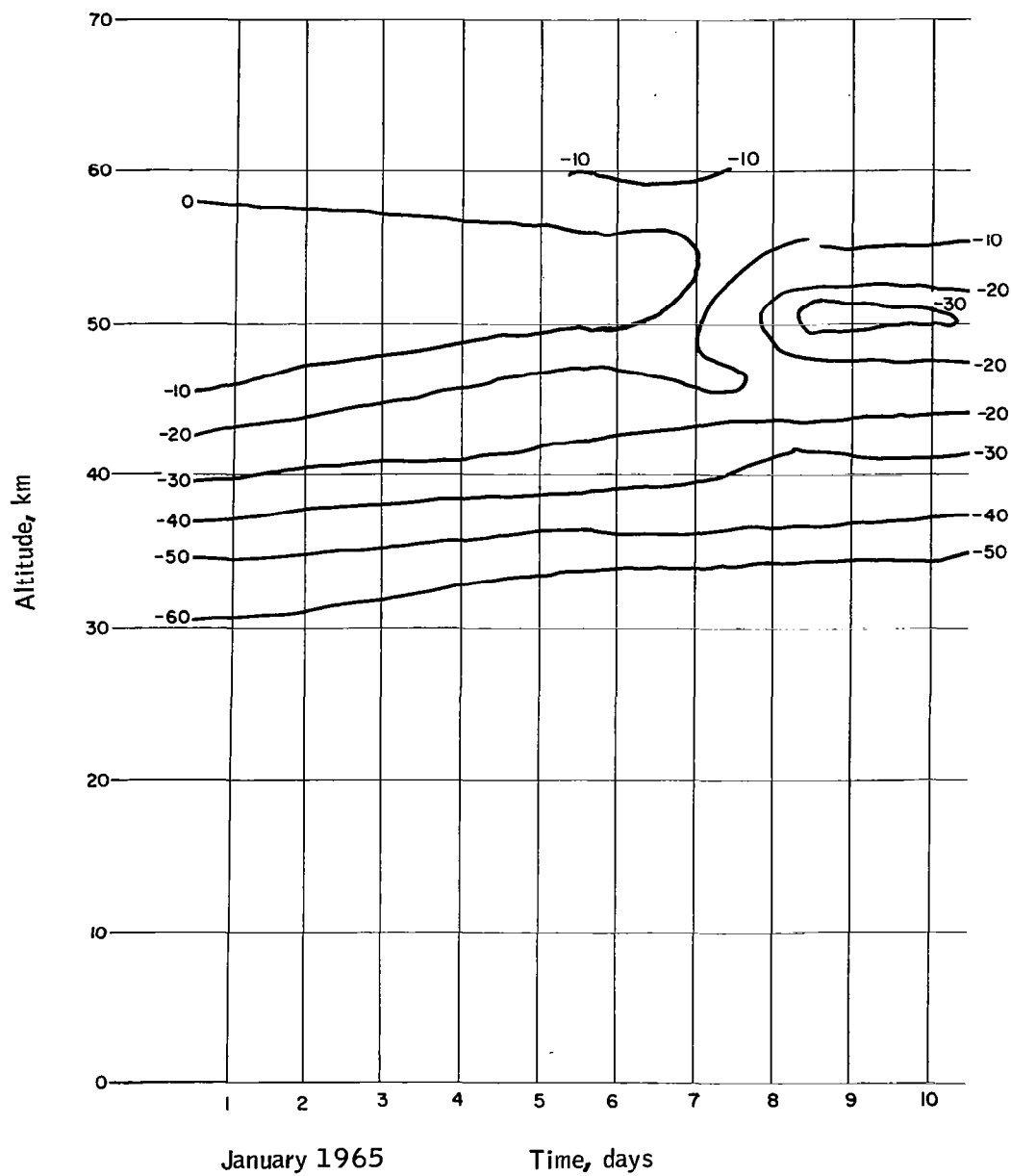


Figure 15. Fort Churchill Time Height Cross Section at 30-60 km  
From 1 October 1964 to 13 February 1965 - Continued

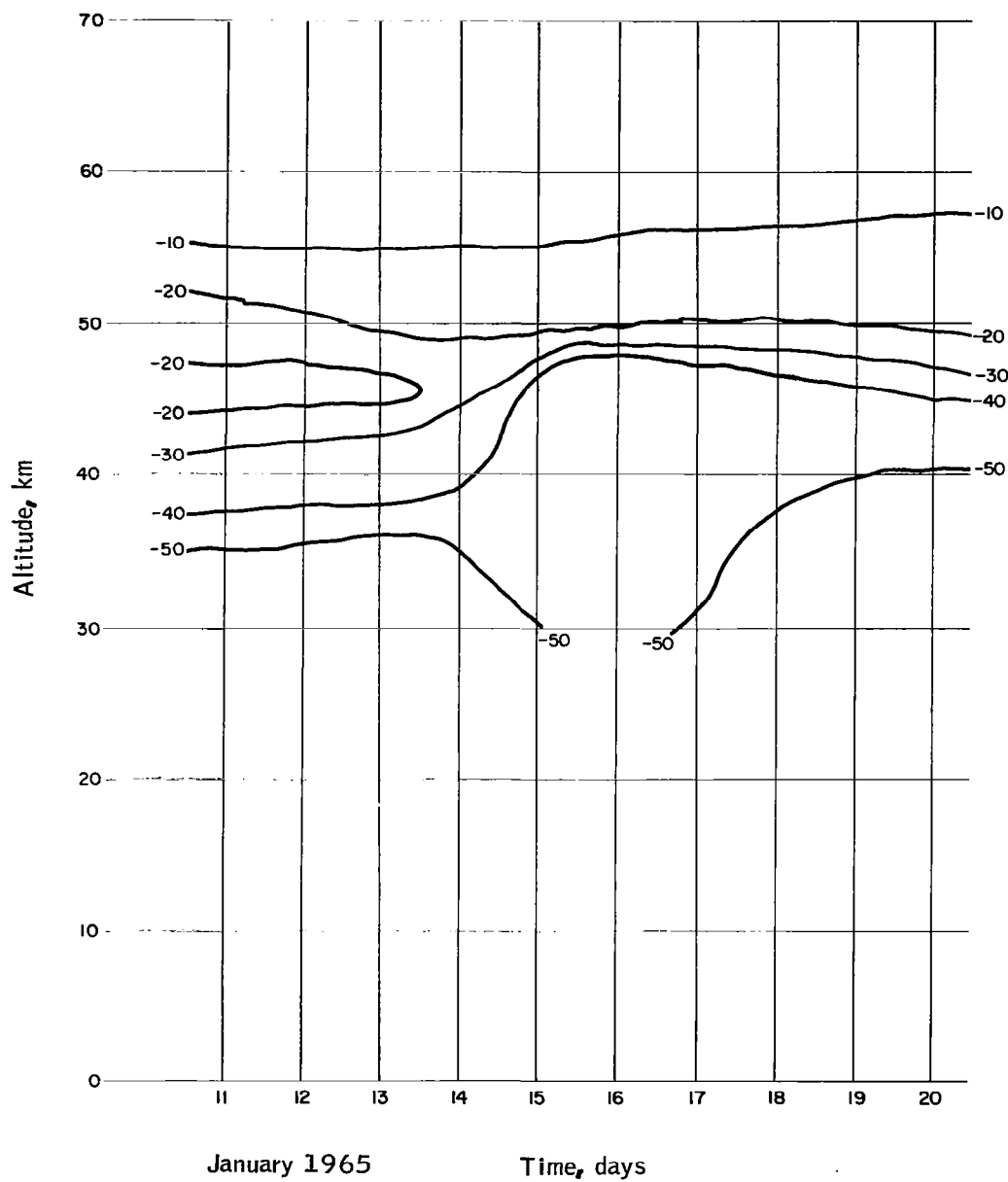


Figure 15. Fort Churchill Time Height Cross Section at 30-60 km  
From 1 October 1964 to 13 February 1965 - Continued

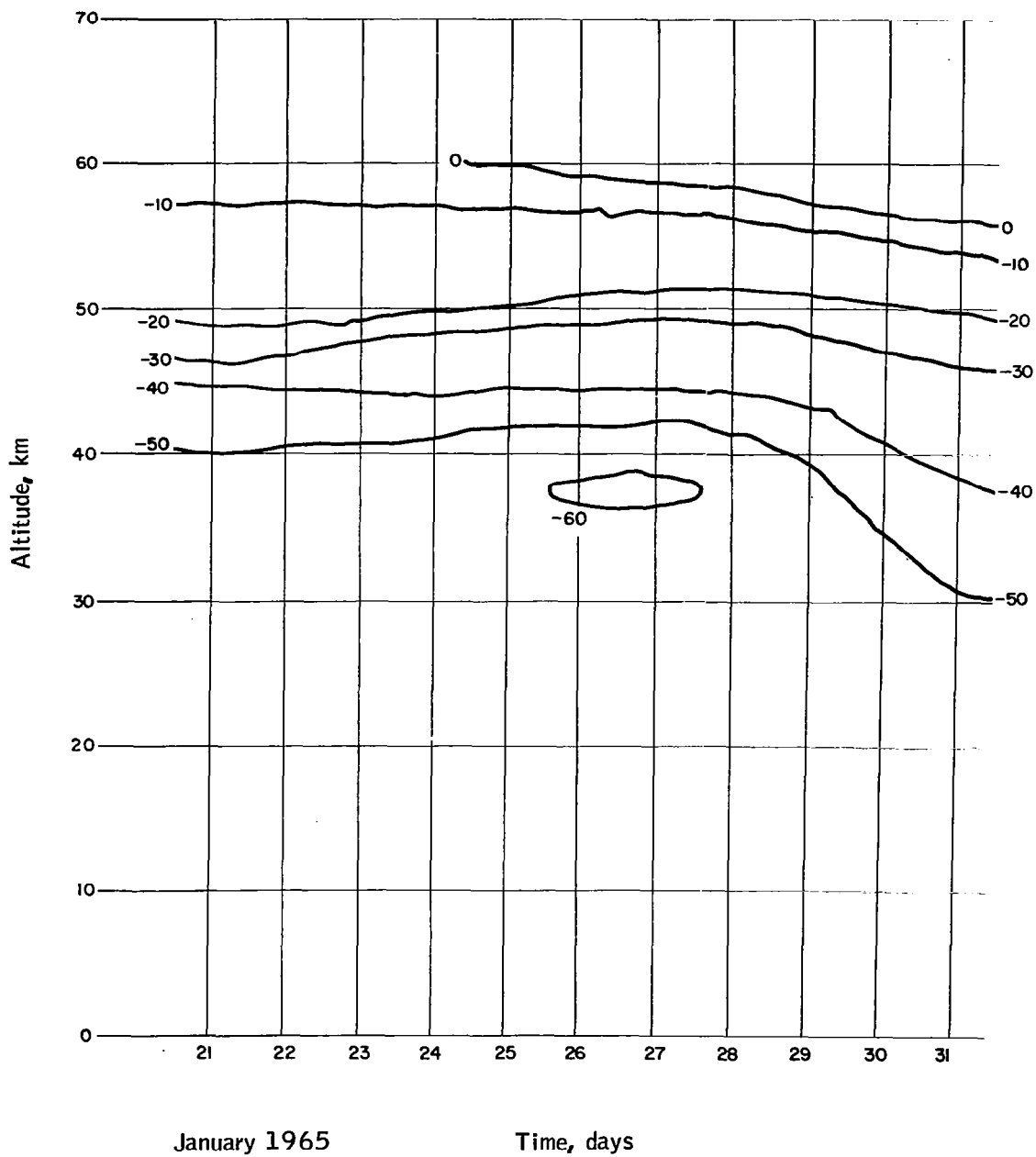


Figure 15. Fort Churchill Time Height Cross Section at 30-60 km  
From 1 October 1964 to 13 February 1965 - Continued

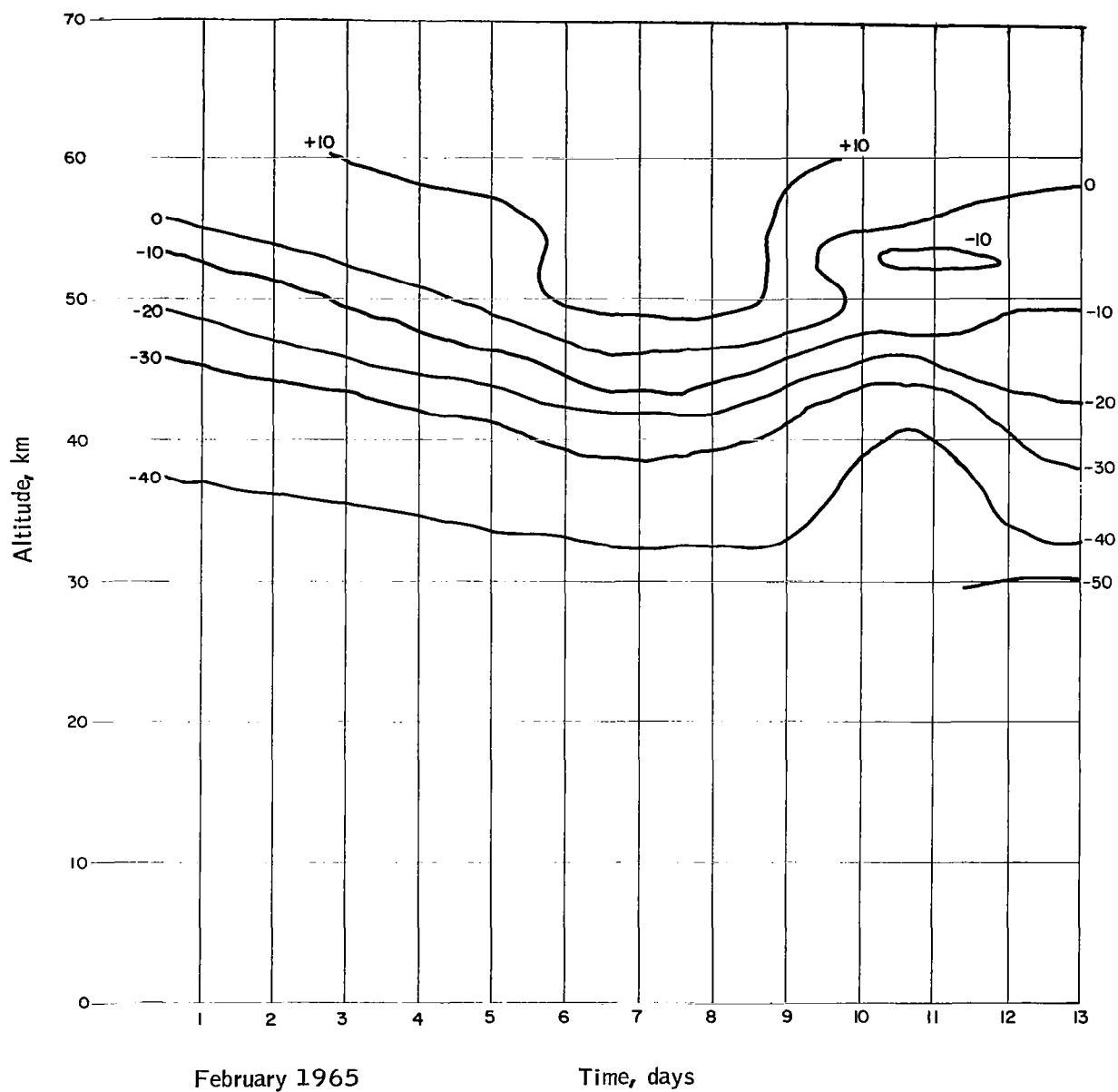


Figure 15. Fort Churchill Time Height Cross Section at 30-60 km  
From 1 October 1964 to 13 February 1965 - Concluded

the profiles derived at 3-day intervals from a series of observations over a period of several months should contain, if not all, at least a sufficiently large number of the more significant thermal profiles which occurred to be generally representative.

A total of 168 interpolated profiles were determined for the two time cross sections with 3-day resolution and the profile data tabulated on IBM cards.

Twelve-hour resolution. -- The four selected cases with 12-hour resolution (that is, Cape Kennedy, May 21-28, 1964; White Sands Missile Range, November 18-25, 1964; Cape Kennedy, December 7-10, 1964; Cape Kennedy, February 8-17, 1965) were analyzed in a manner similar to that used for the 3-day resolution cases. However, the greater observational frequency of rocketsonde observations naturally permitted a finer-scale analysis to be made of the thermal pattern between 30-60 km. In order to illustrate the temperature variability within the 30-60 km layer, three of the actual time cross sections will be presented and discussed below.

Figure 16 presents the time cross section for the May 21-28 Cape Kennedy case. In general, the isotherm pattern shows very little change during the first few days followed by some significant variations during the latter part of the week.

Fairly marked cooling is indicated by the 0830 GMT sounding on 25 May. However, some, if not all, of this cooling is likely due to the time of day in which the sounding was taken (0330 local time). Beyers and Miers (refs. 8 and 9) in a study of diurnal temperature changes at White Sands found that minimum temperatures occur near 0400 to 0600 MST and maximum temperatures occur around 1400 MST. These times correspond very closely to the times of occurrence of minimum and maximum temperatures at the surface. They found that the diurnal temperature range was 15 to 20°C between 55 and 60 km and decreased to approximately 5°C at 30 km. At the present time, it is frequently a matter of opinion as to whether changes in successive temperature observations represent true variations or merely random errors.

By comparing the 0830 GMT (near the time of diurnal minimum) sounding on 25 May with next one at 0045 GMT (about 4 hours after the expected maximum) on 26 May one can see that the temperature difference is greatest above 40 km; very little difference occurs below 35 km, where one expects the diurnal temperature wave to be small. This same effect is also noted when one compares this 0830 GMT sounding with the sounding taken at 1630 GMT on the 26th. Thus, there would appear to be some evidence that the 0830 sounding is relatively cold largely due to its coincidence in time with the expected diurnal temperature minimum rather than any significant change in large-scale atmospheric conditions.

The cooling which occurred at the very end of the week is undoubtedly due to a large-scale temperature change. Evidence for this is that the final sounding at 2100 GMT is taken near the time of expected maximum and the fact that substantial cooling occurred at 30 km as well as the upper levels. This final sounding occurs fairly close to the time of the expected maximum and hence the large-scale cooling could be even more pronounced than shown here.

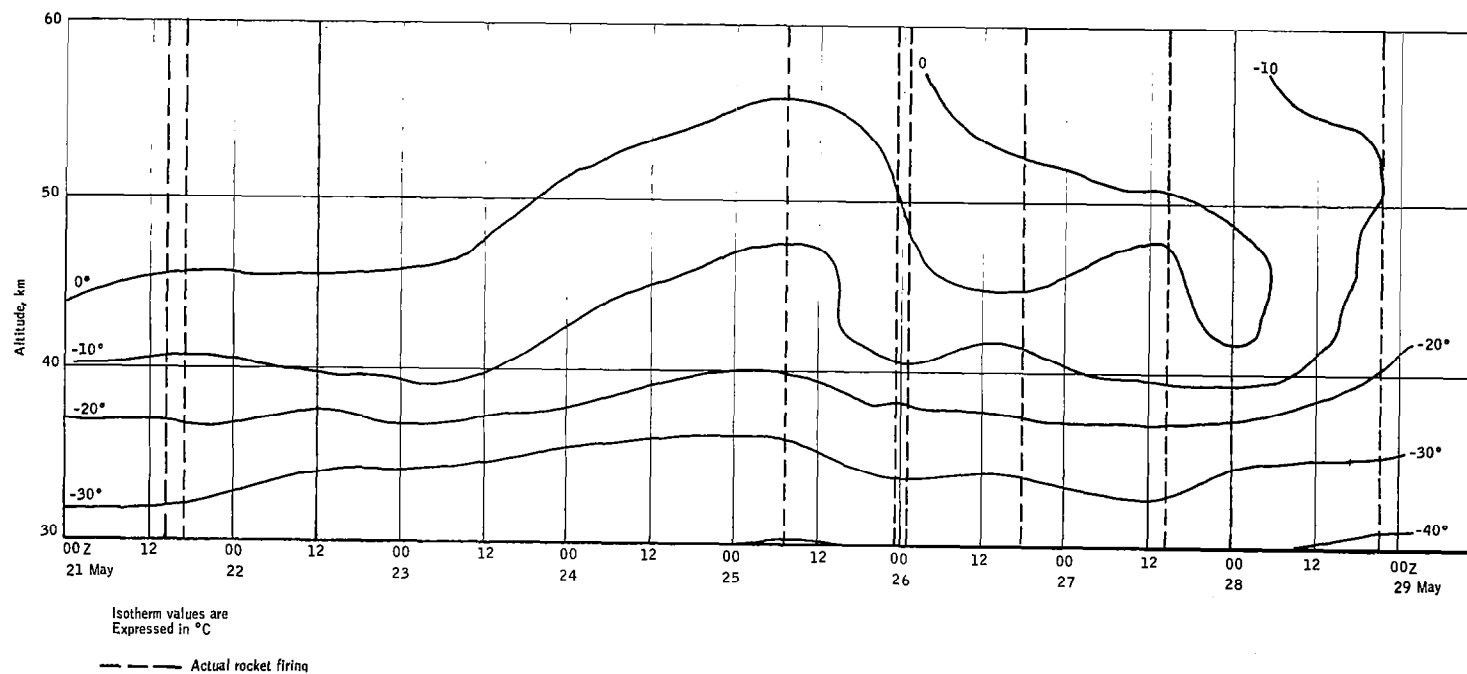


Figure 16. Cape Kennedy Time Height Cross Section From  
21-28 May 1964

Thus, some real cooling probably occurred toward the end of this week. However, the cooling during the middle of the week was likely due to the sounding being taken near the time of the diurnal minimum temperature. Thus, proper interpretation of day-to-day changes requires knowledge of the local time of the sounding in order to properly account for diurnal temperature changes.

Figure 17 presents the time cross section for the November 18-25 WSMR case. The most interesting feature is the abrupt, short-period warming between 48-60 km which occurred between 2100 and 2300 GMT on November 21, as revealed by successive soundings. Warming as great as  $17^{\circ}\text{C}$  occurred within this layer. Equally dramatic is the sudden cooling which subsequently occurred from 2300 GMT to 1100 GMT on November 22. If the 2300 GMT sounding can be taken as reliable in the layer above 48 km, the data would suggest that this region of the atmosphere is one where relatively large temperature changes can occur within short time periods. The most probable explanation for such rapid temperature changes is that they are caused by vertical motions in the vicinity of the strato-pause. Further extensive study is required, however, to determine whether such temperature changes are real and to define a causal mechanism. The validity of this kind of rapid temperature change is supported by the work of Beyer and Mier (refs. 8 and 9), who observed temperature changes as great as  $12^{\circ}\text{C}$  occurring within a 2-hour period.

Figure 18 shows the time cross section for the February 8-17 Cape Kennedy case. The isotherm patterns indicate that relatively small temperature changes occurred below 40 km throughout the 10-day period. The 40-50 km region was quite active, however, with frequent and rather abrupt temperature changes. From February 8-9 warming occurred above 45 km, with 24-hour temperature increases as high as  $17^{\circ}\text{C}$  observed near 50 km. From February 9-11, a cooling took place between 45-50 km, with a maximum temperature decrease of  $-15^{\circ}\text{C}$  observed near 50 km. From February 11-12, localized warming occurred, centered at 45 km where a  $14^{\circ}\text{C}$  temperature increase was observed. From February 12-13, widespread cooling occurred over the entire 30-50 km layer, with a maximum decrease of  $-28^{\circ}\text{C}$  near 45 km. This was followed by a general warming trend, which occurred from February 13-14 between 45-50 km, where a maximum  $18^{\circ}\text{C}$  change was observed near 45 km, and from February 13-15 between 35-45 km, where a maximum change of  $17^{\circ}\text{C}$  was observed near 42 km. A succession of minor cooling and warming trends featured the remainder of the period covered by the cross section, except between 50-55 km, where cooling of over  $10^{\circ}\text{C}$  was observed late on the day of February 15, and was followed by  $10^{\circ}\text{C}$  warming through 1500 GMT on February 17.

Based upon the data provided by the four selected time cross section cases with 12-hour resolution, a total of 60 interpolated profiles were determined. The profile data were then tabulated on IBM cards, using the format to be described in this section.

Four-hour resolution. -- The one time cross section analysis performed on a 4-hour resolution basis was based upon observational data for White Sands Missile Range during the period from 0000 GMT February 7, 1964 to 2000 GMT February 9, 1964. The analytical methods were generally similar to those used in the other time cross section studies; however, in the 30-60 km layer the required temperature values were interpolated at 2.5 km vertical increments from the analysis of this series of rocketsonde data previously published by Beyers and Miers (refs. 8 and 9).

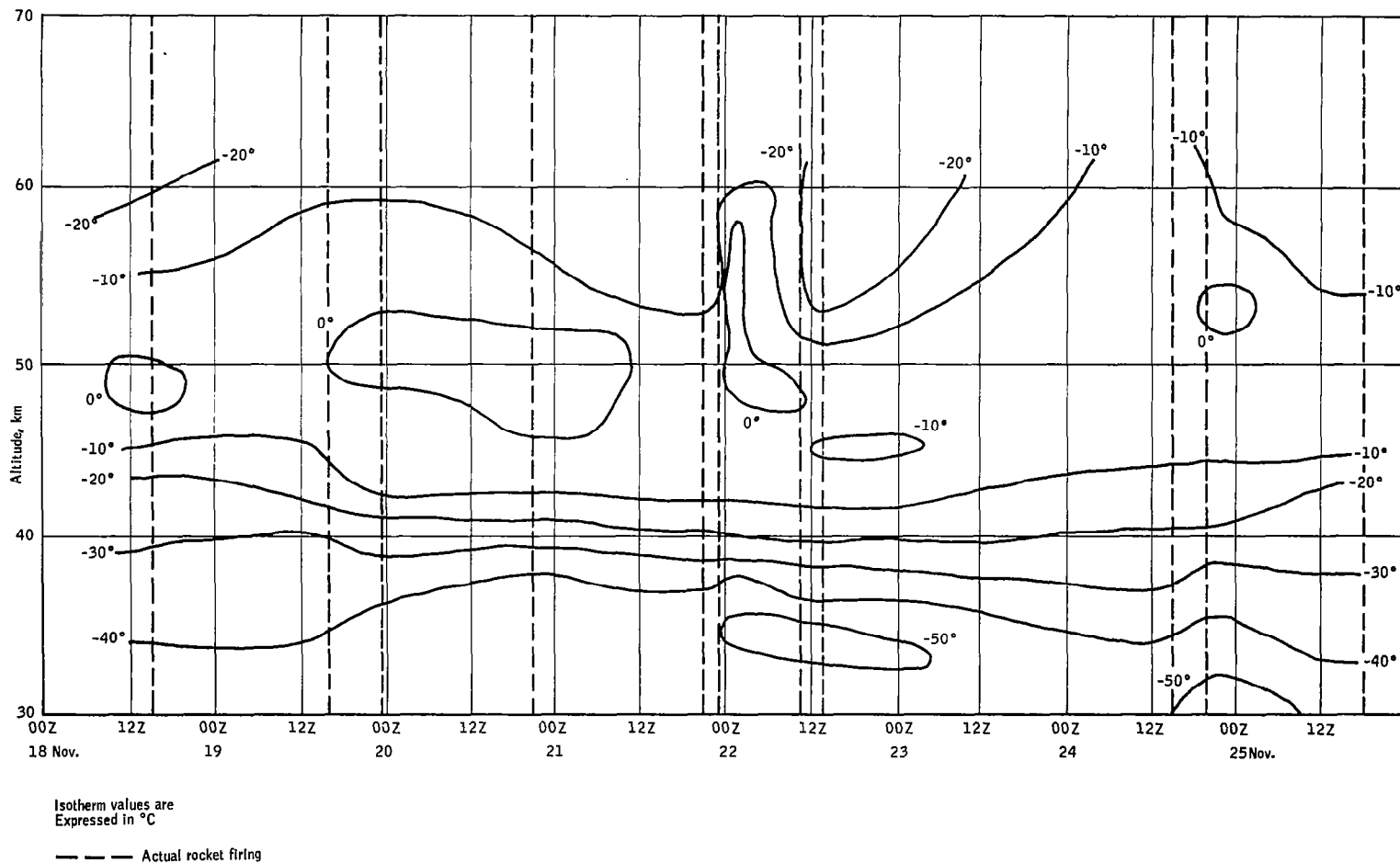


Figure 17. White Sands Time Height Cross-Section From  
18-25 November 1964

Figure 18. Cape Kennedy Time Height Cross Section From  
8-17 February 1965

Figure 19 is a time-height cross section taken from Beyers and Miers (ref. 9). The solid vertical lines on this figure indicate when the soundings were taken. Isotherms in the right half of the figure are dashed because of the relatively few soundings taken on February 8th and 9th. The authors concluded from their analysis that the diurnal temperature change may be as high as 15-20°C at 50 km, decreasing to near 5°C at 30 km. Also significant temperature changes can occur in very short time periods as shown by the temperature oscillations at 45 km, i. e., between the 2000 and 2222 sounding on 7 February at 12°C warming took place, and by 0013 (or less than 2 hours later) the temperature had dropped 12°C. Thus, these closely spaced soundings indicate that temperature changes may be abrupt and sharp in the upper atmosphere. Diurnal temperature changes in the vicinity of the stratopause would appear to be comparable to those occurring at the surface of the Earth.

The 4-hour resolution case considered above was used to determine 18 interpolated profiles (a description of tabulation format will be reported in this section).

### Stratospheric Warming Time Series

The stratospheric warming case was based upon Fort Churchill observations over the period March 1-31, 1965. A time resolution of 24 hours was used, based upon the observational frequency of reported rocketsonde data. These data, although relatively sparse during the early half of the period, are sufficiently dense during the latter half to delineate the major features of the stratospheric warming which reached its maximum intensity on March 23. The vertical interval used for temperature interpolation between 30-60 km was 2.5 km, or the same as that used for the space and time cross section cases previously described.

The radiosonde data for mandatory levels at and below 10 mb were plotted at 24-hour intervals. Most of these data were taken from actual radiosonde observations reported in the Northern Hemisphere Data Tabulations. However, a number of observations did not reach the 10 mb level and, more infrequently, the 30 and 50 mb levels. In such cases, the temperatures and heights were estimated from analyzed maps obtained on microfilm from NWRC, Asheville.

Figure 20 presents the time cross section analysis for Fort Churchill during March 1965. The temperatures are plotted in °C and are analyzed every 10°C. The stratospheric warming phenomenon is clearly marked by the closed -20°C isotherm centered at 25 km on March 23. A maximum warming of 33°C is indicated at 25 km over the period from 2255 GMT March 19 to 2126 GMT March 23. Also worthy of note is the subsequent cooling which occurred at 25 km - a net decrease of 42°C over the period ending at 1830 GMT March 30.

The implications of such large and rapidly occurring temperature changes in the stratosphere upon the temperature profile, the associated radiance profile

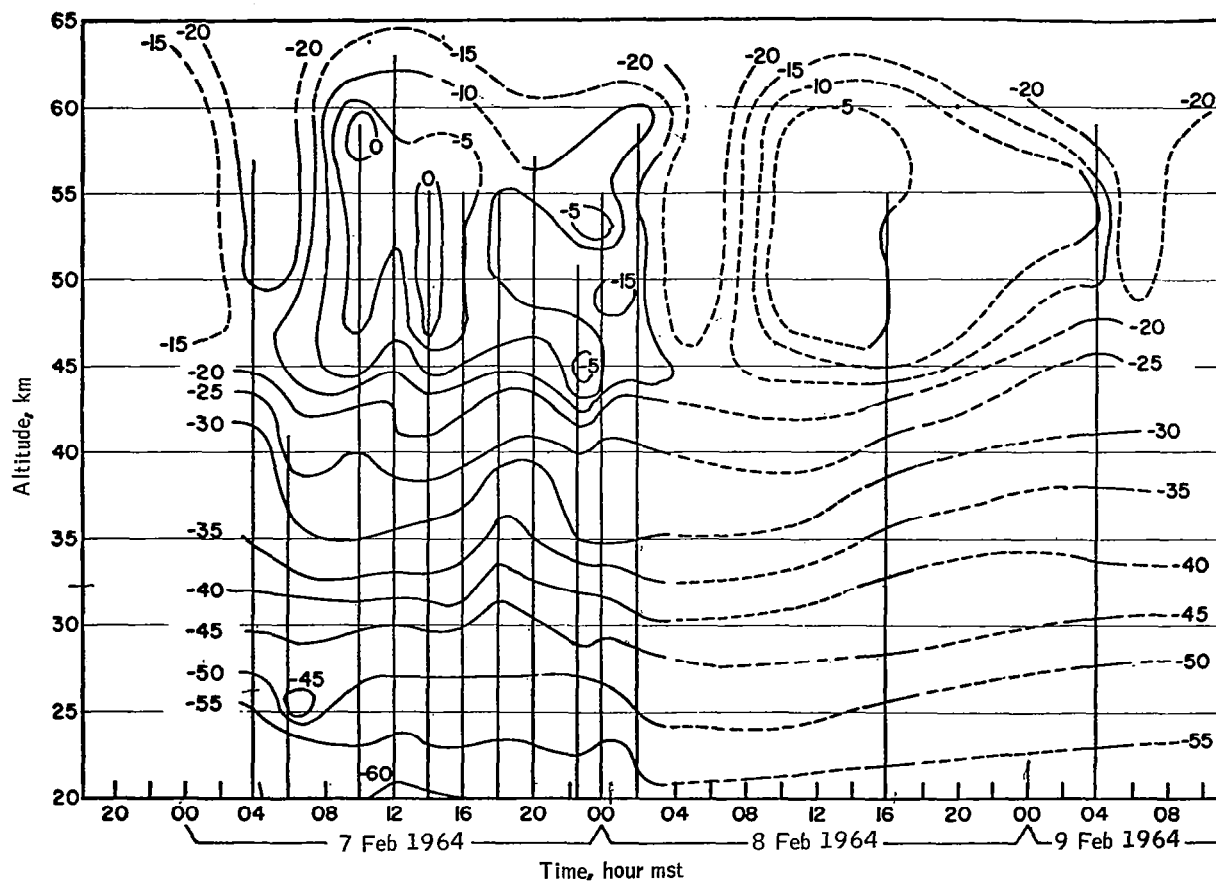
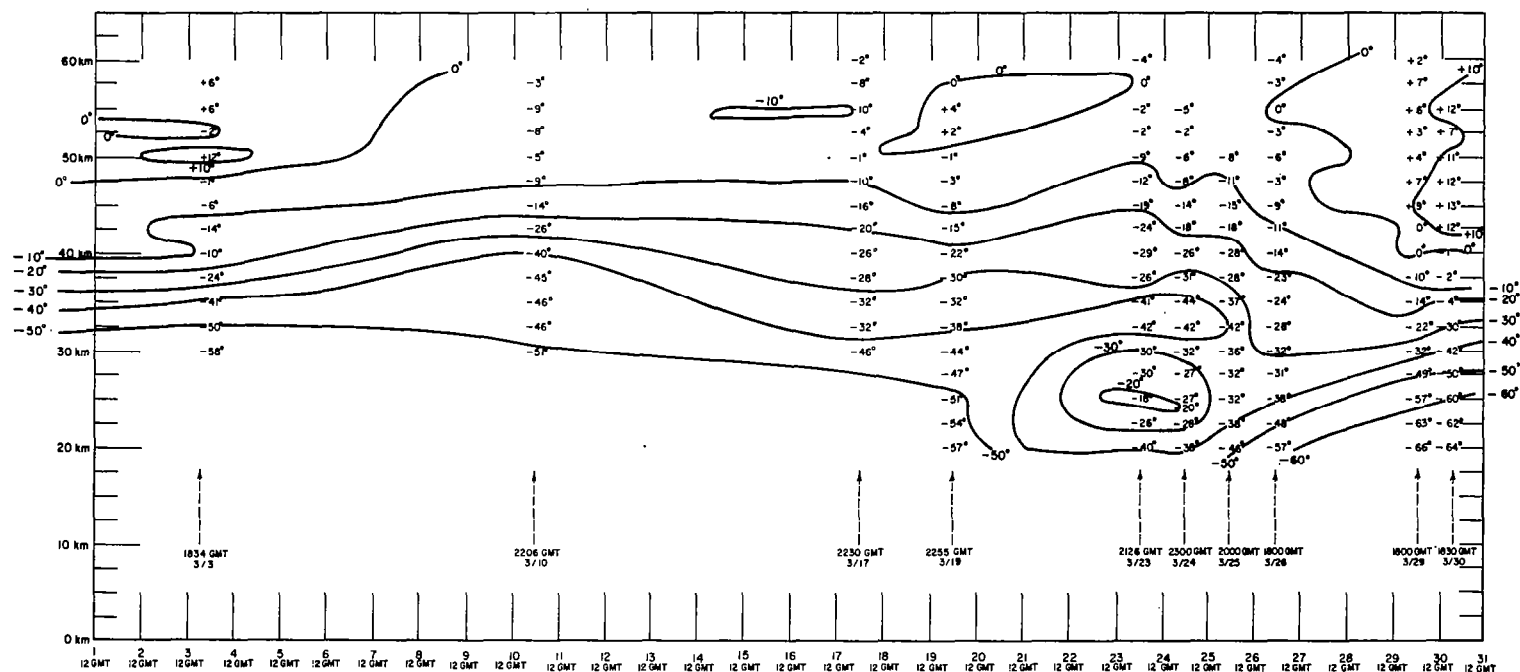


Figure 19. White Sands Missile Range Time Height Cross-Section of Temperature (°C) From 7-9 February 1964



Isotherms are expressed in  $^{\circ}\text{C}$

Figure 20. Time Cross Section at Fort Churchill During March, 1965

and horizon definition are fairly obvious. Fortunately, the stratospheric warming phenomenon is related to the breakdown of the strong polar vortex, generally occurring in late winter, so that it may be possible by means of time-lag correlation analysis to develop a sufficiently reliable method for predicting the occurrence and severity of stratospheric warming over the polar regions.

The series of 31 profiles interpolated from this one stratospheric warming case represents a significant beginning in studying this relatively infrequent but, nonetheless, important aspect of atmospheric variability. Since stratospheric warming is not a localized phenomenon but extends over a large geographical region and spreads on a time-phased basis from locale to locale and level to level, the perturbatory effects of stratospheric warming upon radiance profiles and horizon determination in the polar regions can be expected to persist over periods of several days. Recent extensions of MRN and the achievement of more frequent and reliable rocketsonde (and radiosonde) observations does offer the hope, however, that a rapidly improving body of atmospheric sounding data can eventually be used to define and to predict the stratospheric warming phenomenon. It would be a mistake, at this time, to emphasize the importance of the stratospheric warming phenomenon upon the overall objectives of this program, since, when viewed on a yearly basis, this phenomenon only occurs some 2 percent of the time and is fairly well confined to the polar regions.

### Climatological Cases

The climatological data available for use in this study was presented earlier in this section; discussion was directed toward the selection of climatological cases. Here, the process by which the data body of interpolated profiles was actually determined is discussed.

Figure 21 shows the distribution of 50 grid points which was used in determining the climatological profiles. The standard deviation of temperature for these points is also shown. In a broad sense, this distribution is similar to that used for the synoptic profiles (Figure 8), covering North America and a portion of the adjacent oceans. Table 15 lists the latitude and longitude for each climatological grid point. Since interpolated climatological profiles were determined for each of the four seasons, a total of 200 profiles were thus obtained.

The process by which the climatological data were analyzed is as follows. First, the mean temperatures and standard deviations of temperature in the 30-52 km layer for each season, as computed for several MRN stations by Quiroz, et al., (ref. 3) were plotted and analyzed on separate charts at 3 km intervals. Then, the values for each parameter were interpolated for each grid point in the same fashion as were the temperatures and heights for the synoptic cases. Occasionally, a steep mean lapse rate (which never violated the adiabatic laws) existed between the top of the Quiroz data (52 km) and the base of the latitude means (54 km) supplied by Cole and Kantor (ref. 7). Since these lapse rates may not be truly as steep as indicated, some caution should be exercised in interpreting profile data in the 52-54 km layer.

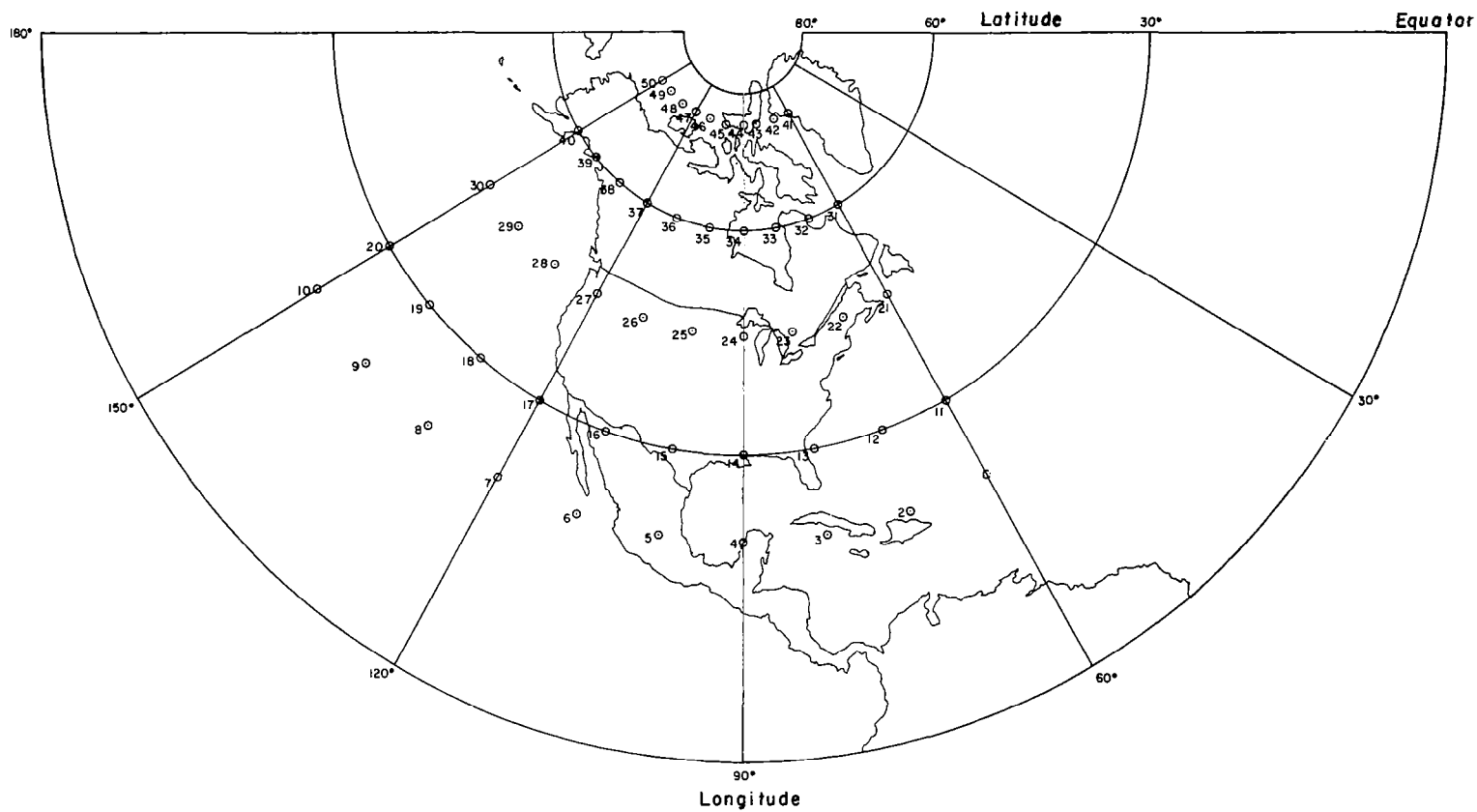


Figure 21. Location of the 50 Interpolated Climatological Soundings for Each Season

TABLE 15.- LATITUDE AND LONGITUDE OF CLIMATOLOGICAL  
GRID POINTS

Grid point reference number	Latitude, °N	Longitude, °W	Grid point reference number	Latitude, °N	Longitude, °W
1	20	60	26	45	110
2	20	70	27	45	120
3	20	80	28	45	130
4	20	90	29	45	140
5	20	100	30	45	150
6	20	110	31	60	60
7	20	120	32	60	70
8	20	130	33	60	80
9	20	140	34	60	90
10	20	150	35	60	100
11	30	60	36	60	110
12	30	70	37	60	120
13	30	80	38	60	130
14	30	90	39	60	140
15	30	100	40	60	150
16	30	110	41	75	60
17	30	120	42	75	70
18	30	130	43	75	80
19	30	140	44	75	90
20	30	150	45	75	100
21	45	60	46	75	110
22	45	70	47	75	120
23	45	80	48	75	130
24	45	90	49	75	140
25	45	100	50	75	150

Some of the climatological temperature data had to be interpolated or estimated above 52 km (above 46 km for the summer season at 75°N) since real climatological data are not available. The means for the spring and fall seasons at 20°N were interpolated from the winter and summer means. At 45°N in the spring and fall the means were interpolated from the 30°N and 60°N means for the same seasons. Since there were no temperature means available for 75°N, these means were estimated as follows. First, the latitude means for 60°N and 75°N were computed at the highest level of data provided by Quiroz, et al., (ref.3) for each season (that is, 52 km for winter, spring and fall; 64 km for summer). Then, the difference in these computed means was subtracted for the appropriate season from the 60°N climatological soundings provided by Cole and Kantor (ref.7) and Kantor and Cole (ref.5). The resulting climatological soundings have the same shape as the 60°N soundings but have been shifted according to the difference in computed latitude means at 60°N and 75°N.

It should be obvious, from the above discussion, that some degree of resourceful improvisation was necessary to complete the climatological profiles over the required 0-90 km range. Nevertheless, these profiles, based as they are upon all available processed climatological data, can be reasonably regarded as representative of the seasonal variations which occur over a large portion of the Northern Hemisphere. Obviously, important refinements will occur over the next few years as the climatological data base continues to expand, but the broad features of the climatological profiles should remain relatively constant.

### PROFILE DATA CODING AND CONVERSION

The interpolated temperature sounding data were coded for the 1039 profiles determined from the synoptic, space cross section, time cross section, stratospheric warming and climatological cases.

#### Formats Used

Two different formats were used, one for the real time sounding data and the other for the climatological sounding information. A detailed explanation of the two formats is given in Table 16. It should be noted that the stratospheric warming time series has been included in this table as a subcategory of the time cross section cases.

#### Computer Checking Operation

To assist in the use of the temperature data for all the profiles, a computer check was performed on the computer input cards. This check consisted of the following operations:

- (1) A check of the consistency of the identification information.
- (2) A check of the card format to see whether the data were punched in the appropriate columns on the cards.

TABLE 16.- TEMPERATURE PROFILE IDENTIFICATION FORMAT

Format No. 1 - Synoptic Studies, Space and Time Cross Sections

An eight number identification system was used to specify each of the temperature profiles. The first two numbers specify the type of study, the second two the study profile case, and the last four code an individual profile. For ease in identification and grouping of data, the total format system is:

Type of Study

1. 01 - synoptic
2. 02 - space cross sections
3. 03 - time cross sections

Study Cases

1. Synoptic
  - a. 01 - April 8, 1964
  - b. 02 - June 3, 1964
  - c. 03 - August 12, 1964
  - d. 04 - October 21, 1964
  - e. 05 - November 13, 1964
  - f. 06 - December 9, 1964
  - g. 07 - January 20, 1965
  - h. 08 - February 10, 1965
2. Space Cross Sections (WSMR to Antigua)
  - a. 01 - October 28, 1964
  - b. 02 - February 24, 1965
3. Time Cross Sections
  - a. 01 - Cape Kennedy (March 1964 - February 1965)
  - b. 02 - Fort Churchill (October 1964 - Mid-February 1965)
  - c. 03 - Cape Kennedy (May 21, 1964 - May 28, 1964)
  - d. 04 - WSMR (November 18, 1964 - November 25, 1964)
  - e. 05 - Cape Kennedy (December 7, 1964 - December 10, 1964)
  - f. 06 - Cape Kennedy (February 8, 1965 - February 17, 1965)
  - g. 07 - WSMR (February 7, 1964 - February 9, 1964)
  - h. 08 - Fort Churchill - Stratospheric warming (March 1965)

TABLE 16.- TEMPERATURE PROFILE IDENTIFICATION FORMAT-C ontinued

## Sounding Number

## 1. Synoptic - Location and Code for Each Sounding

1. 0001 - 63.75°N, 165°W	29. 0029 - 71.25°N, 90°W
2. 0002 - 52.5 °N, 165°W	30. 0030 - 67.5 °N, 90°W
3. 0003 - 75 °N, 150°W	31. 0031 - 63.75°N, 90°W
4. 0004 - 60 °N, 150°W	32. 0032 - 56.25°N, 90°W
5. 0005 - 45 °N, 150°W	33. 0033 - 52.5 °N, 90°W
6. 0006 - 30 °N, 150°W	34. 0034 - 48.75°N, 90°W
7. 0007 - 52.5 °N, 135°W	35. 0035 - 45 °N, 90°W
8. 0008 - 37.5 °N, 135°W	36. 0036 - 41.25°N, 90°W
9. 0009 - 26.25°N, 135°W	37. 0037 - 37.5 °N, 90°W
10. 0010 - 75 °N, 120°W	38. 0038 - 33.75°N, 90°W
11. 0011 - 67.5 °N, 120°W	39. 0039 - 30 °N, 90°W
12. 0012 - 60 °N, 120°W	40. 0040 - 26.25°N, 90°W
13. 0013 - 45 °N, 120°W	41. 0041 - 22.5 °N, 90°W
14. 0014 - 37.5 °N, 120°W	42. 0042 - 18.75°N, 90°W
15. 0015 - 30 °N, 120°W	43. 0043 - 15 °N, 90°W
16. 0016 - 15 °N, 120°W	44. 0044 - 11.25°N, 90°W
17. 0017 - 63.75°N, 105°W	45. 0045 - 7.5 °N, 90°W
18. 0018 - 56.75°N, 105°W	46. 0046 - 3.75°N, 90°W
19. 0019 - 48.75°N, 105°W	47. 0047 - 0°, 90°W
20. 0020 - 41.25°N, 105°W	48. 0048 - 56.25°N, 75°W
21. 0021 - 33.75°N, 105°W	49. 0049 - 48.75°N, 75°W
22. 0022 - 26.25°N, 105°W	50. 0050 - 41.25°N, 75°W
23. 0023 - 22.5 °N, 105°W	51. 0051 - 33.75°N, 75°W
24. 0024 - 90 °N	52. 0052 - 26.25°N, 75°W
25. 0025 - 86.25°N, 90°W	53. 0053 - 75 °N, 60°W
26. 0026 - 82.5 °N, 90°W	54. 0054 - 67.5 °N, 60°W
27. 0027 - 78.75°N, 90°W	55. 0055 - 60 °N, 60°W
28. 0028 - 75 °N, 90°W	56. 0056 - 45 °N, 60°W

TABLE 16.- TEMPERATURE PROFILE IDENTIFICATION FORMAT - Continued

## 2. Space Cross Sections - WSMR to Antigua - Location and Code for Each Sounding

1. 0001 - 32.4°N, 106.5°W	29. 0029 - 28.8°N, 80.5°W
2. 0002 - 32.4°N, 105.5°W	30. 0030 - 28.5°N, 79.7°W
3. 0003 - 32.4°N, 104.5°W	31. 0031 - 28.2°N, 78.9°W
4. 0004 - 32.4°N, 103.6°W	32. 0032 - 27.9°N, 78.1°W
5. 0005 - 32.4°N, 102.6°W	33. 0033 - 27.5°N, 77.4°W
6. 0006 - 32.4°N, 101.6°W	34. 0034 - 27.1°N, 76.7°W
7. 0007 - 32.4°N, 100.7°W	35. 0035 - 26.8°N, 75.9°W
8. 0008 - 32.3°N, 99.7°W	36. 0036 - 26.4°N, 75.2°W
9. 0009 - 32.2°N, 98.7°W	37. 0037 - 26.0°N, 74.4°W
10. 0010 - 32.1°N, 97.8°W	38. 0038 - 25.6°N, 73.7°W
11. 0011 - 32.0°N, 96.8°W	39. 0039 - 25.2°N, 73.0°W
12. 0012 - 31.9°N, 95.8°W	40. 0040 - 24.7°N, 72.3°W
13. 0013 - 31.8°N, 94.9°W	41. 0041 - 24.3°N, 71.6°W
14. 0014 - 31.6°N, 93.9°W	42. 0042 - 23.9°N, 70.9°W
15. 0015 - 31.5°N, 92.9°W	43. 0043 - 23.5°N, 70.2°W
16. 0016 - 31.4°N, 92.0°W	44. 0044 - 23.1°N, 69.6°W
17. 0017 - 31.2°N, 91.1°W	45. 0045 - 22.7°N, 68.9°W
18. 0018 - 31.0°N, 90.2°W	46. 0046 - 22.3°N, 68.3°W
19. 0019 - 30.9°N, 89.3°W	47. 0047 - 21.8°N, 67.7°W
20. 0020 - 30.7°N, 88.4°W	48. 0048 - 21.3°N, 67.1°W
21. 0021 - 30.5°N, 87.5°W	49. 0049 - 20.8°N, 66.5°W
22. 0022 - 30.3°N, 86.6°W	50. 0050 - 20.4°N, 65.9°W
23. 0023 - 30.1°N, 85.7°W	51. 0051 - 19.9°N, 65.3°W
24. 0024 - 29.9°N, 84.9°W	52. 0052 - 19.5°N, 64.7°W
25. 0025 - 29.7°N, 84.0°W	53. 0053 - 19.0°N, 64.1°W
26. 0026 - 29.5°N, 83.1°W	54. 0054 - 18.6°N, 63.5°W
27. 0027 - 29.2°N, 82.2°W	55. 0055 - 18.1°N, 62.9°W
28. 0028 - 29.0°N, 81.4°W	56. 0056 - 17.7°N, 62.3°W
	57. 0057 - 17.2°N, 61.8°W

TABLE 16.- TEMPERATURE PROFILE IDENTIFICATION FORMAT- Continued

3. Time Cross Sections

- a. Case 1 - Cape Kennedy Cross Section - Soundings begin at 1200 GMT March 1, 1964 with 3 day resolution with the last sounding at 1200 GMT February 27, 1965.
- b. Case 2 - Fort Churchill Cross Section - Soundings begin at 1200 GMT October 1, 1964 with 3 day resolution with the last sounding at 1200 GMT February 13, 1965.
- c. Case 3 - Cape Kennedy Cross Section - Soundings begin at 0000 GMT May 21, 1964 with 12 hour resolution with the last sounding at 1200 GMT May 28, 1964.
- d. Case 4 - White Sands Cross Section - Soundings begin at 0000 GMT November 18, 1964 with 12 hour resolution with the last sounding at 1200 GMT November 25, 1964.
- e. Case 5 - Cape Kennedy Cross Section - Soundings begin at 0000 GMT December 7, 1964 with 12 hour resolution with the last sounding at 1200 GMT December 10, 1964.
- f. Case 6 - Cape Kennedy Cross Section - Soundings begin at 0000 GMT February 8, 1965 with 12 hour resolution with the last sounding at 1200 GMT February 17, 1965.
- g. Case 7 - White Sands Cross Section - Soundings begin at 0000 GMT February 7, 1964 with 4 hour resolution with the last sounding at 2000 GMT February 9, 1964.
- h. Case 8 - Fort Churchill Cross Section - Soundings begin at 1200 GMT March 1, 1965 with 24 hour resolution with the last sounding at 1200 GMT March 31, 1965.

Format No. 2 - Climatology

Study Cases

1. 01 - January
2. 02 - April
3. 03 - July
4. 04 - October

TABLE 16.- TEMPERATURE PROFILE IDENTIFICATION FORMAT - Concluded

Sounding Number - Location and Code	
1. 0001 - 20°N, 60°W	26. 0026 - 45°N, 110°W
2. 0002 - 20°N, 70°W	27. 0027 - 45°N, 120°W
3. 0003 - 20°N, 80°W	28. 0028 - 45°N, 130°W
4. 0004 - 20°N, 90°W	29. 0029 - 45°N, 140°W
5. 0005 - 20°N, 100°W	30. 0030 - 45°N, 150°W
6. 0006 - 20°N, 110°W	31. 0031 - 60°N, 60°W
7. 0007 - 20°N, 120°W	32. 0032 - 60°N, 70°W
8. 0008 - 20°N, 130°W	33. 0033 - 60°N, 80°W
9. 0009 - 20°N, 140°W	34. 0034 - 60°N, 90°W
10. 0010 - 20°N, 150°W	35. 0035 - 60°N, 100°W
11. 0011 - 30°N, 60°W	36. 0036 - 60°N, 110°W
12. 0012 - 30°N, 70°W	37. 0037 - 60°N, 120°W
13. 0013 - 30°N, 80°W	38. 0038 - 60°N, 130°W
14. 0014 - 30°N, 90°W	39. 0039 - 60°N, 140°W
15. 0015 - 30°N, 100°W	40. 0040 - 60°N, 150°W
16. 0016 - 30°N, 110°W	41. 0041 - 75°N, 60°W
17. 0017 - 30°N, 120°W	42. 0042 - 75°N, 70°W
18. 0018 - 30°N, 130°W	43. 0043 - 75°N, 80°W
19. 0019 - 30°N, 140°W	44. 0044 - 75°N, 90°W
20. 0020 - 30°N, 150°W	45. 0045 - 75°N, 100°W
21. 0021 - 45°N, 60°W	46. 0046 - 75°N, 110°W
22. 0022 - 45°N, 70°W	47. 0047 - 75°N, 120°W
23. 0023 - 45°N, 80°W	48. 0048 - 75°N, 130°W
24. 0024 - 45°N, 90°W	49. 0049 - 75°N, 140°W
25. 0025 - 45°N, 100°W	50. 0050 - 75°N, 150°W

- (3) A check of the computed heights versus the reported heights utilizing the hydrostatic equation for the mandatory levels between 850 and 10 mb.
- (4) A check to test the lapse rates between successive levels above 30 km.

Essentially, the hydrostatic equation was used to compute the vertical thickness between successive pressure levels. This computed thickness was compared to the difference between the tabulated heights already on the cards, respectively, for each layer. If the difference between the computed thickness and the thickness derived from the tabulated heights exceeded 2.5 percent times the standard atmospheric height interval for the same pressure levels, a possible error was indicated on the output of the computer program.

All of the 1039 atmospheric profiles were subjected to the hydrostatic equation check. The output of the computer program indicated that about 15 percent of the levels checked exceeded the 2.5 percent limit. All of these possible errors were screened individually, and about half of them were obvious tabulating or card punching errors which were then corrected. The remaining 7 percent or so were interpreted to be reasonable data in view of the approximations assumed in the hydrostatic equation check.

Unfortunately the hydrostatic equation cannot be used as a test for levels above 30 km since the pressure at each level is not known. It would seem that the next best test would be a check of the temperature lapse rate between successive levels. Such a test of the data was implemented in a computer program. If the temperature increase or decrease with height exceeded a rate of  $\pm 10^{\circ}\text{C}$  per km, a possible error was indicated in the output of the program. The temperature decrease of  $10^{\circ}\text{C}$  per km is the dry adiabatic lapse rate while the temperature increase of  $10^{\circ}\text{C}$  per km was chosen as a case of extreme inversion. There was only one instance in the whole body of data (an inversion case) where the computed lapse rate failed the test, and the data still seemed realistic relative to adjacent temperature levels. Otherwise, all other levels met the lapse rate test criteria.

#### Conversion of Data to Local Time

All times given for data in this report are in terms of Greenwich Mean Time (GMT). Knowledge of the local time is desirable, however especially in the consideration of diurnal effects. Table 17 lists the time correction factors for converting the time base from GMT to local standard time (LST).

#### Conversion of Temperature Profile Data

The interpolated sounding data for the 1039 profiles, as outlined earlier in this section, are not in the required form for computing the radiance profiles. The computation of the radiance profiles is based upon a series of 67 atmospheric shells, ranging in thickness from 0.5 km at the base to 1.5 km at the top of the 0.90 km layer.

It was necessary, therefore, to develop a computer program for converting the interpolated sounding data into a format which provided the temperature and pressure at each altitude required for the selected number of atmospheric shells. This program basically performed linear interpolation on the temperature data from 0-90 km, linear interpolation of the pressure data from 0-30 km and extrapolation of pressure data from 30-90 km, based upon the hydrostatic equation (which relates the vertical change of pressure within an interval of height to the mean temperature).

TABLE 17.- CORRECTION FACTORS FOR CONVERSION TO LOCAL TIME

Synoptic Cases		Codes 0101-0108
Time for all dates and stations = 1200 GMT. The following corrections give LST at these stations (56 soundings according to list):		
Sounding no.	Time correction	
1-2	GMT - 11	
3-6	GMT - 10	
7-9	GMT - 9	
10-16	GMT - 8	
17-21, 23	GMT - 7	
22, 24-46	GMT - 6	
47-52	GMT - 5	
53-56	GMT - 4	

TABLE 17.- CORRECTION FACTORS FOR CONVERSION  
TO LOCAL TIME - Continued

Cross sections from WSMR to Antigua. Time for all soundings = 1200 GMT. The following corrections give LST at the 57 soundings along the great circle path from WSMR to Antigua (inclusive). Codes 0201-0202			
Sounding no.	Time correction	Sounding no.	Time correction
1	GMT - 7	29	GMT - 5
2	GMT - 7	30	GMT - 5
3	GMT - 7	31	GMT - 5
4	GMT - 7	32	GMT - 5
5	GMT - 6	33	GMT - 5
6	GMT - 6	34	GMT - 5
7	GMT - 6	35	GMT - 5
8	GMT - 6	36	GMT - 5
9	GMT - 6	37	GMT - 5
10	GMT - 6	38	GMT - 5
11	GMT - 6	39	GMT - 5
12	GMT - 6	40	GMT - 5
13	GMT - 6	41	GMT - 5
14	GMT - 6	42	GMT - 5
15	GMT - 6	43	GMT - 5
16	GMT - 6	44	GMT - 5
17	GMT - 6	45	GMT - 5
18	GMT - 6	46	GMT - 5
19	GMT - 6	47	GMT - 5
20	GMT - 6	48	GMT - 4
21	GMT - 6	49	GMT - 4
22	GMT - 6	50	GMT - 4
23	GMT - 6	51	GMT - 4
24	GMT - 6	52	GMT - 4
25	GMT - 6	53	GMT - 4
26	GMT - 6	54	GMT - 4
27	GMT - 5	55	GMT - 4
28	GMT - 5	56	GMT - 4

TABLE 17.- CORRECTION FACTORS FOR CONVERSION TO LOCAL TIME-  
Concluded

Time studies	Codes 0301-0308
<p>A. Year study Cape Kennedy 1200 GMT 3/1/64 - 1200 GMT 2/27/65 Time correction: GMT - 5</p>	
<p>B. 4-1/2 Month study Fort Churchill 1200 GMT 10/1/64 - 1200 GMT 2/13/65 Time correction: GMT - 6</p>	
<p>C. Twelve-hour studies (all beginning at 0000 GMT)</p>	
Beginning:	Time correction:
5/21/64	GMT-5 (Cape Kennedy)
11/18/64	GMT-7 (WSMR)
12/7/64	GMT-5 (Cape Kennedy)
2/8/65	GMT-5 (Cape Kennedy)
<p>D. Four-hour study (beginning 2/7/64 1200 GMT)</p>	
WSMR	Time correction: GMT-7
<p>E. Stratospheric warming (beginning 3/1/65 1200 GMT)</p>	
Fort Churchill	Time correction: GMT-6

The results obtained from the computer program were stored on magnetic tape and can be printed for direct inspection via a printer-plotter routine. A sample output from this routine is shown in Figure 22.

## ACCURACY OF TEMPERATURE/PRESSURE PROFILES

The overall accuracy of the sounding profiles derived from this study is a function of the actual reported data and of the various techniques employed in analyzing and handling the data. Due to the relative sparseness of rocket-sonde data it is at times difficult to separate the effect of error from that of natural atmospheric variability, either in time at a particular location or in space at a particular time. When a variety of analytical treatments are superimposed upon the basic body of observed data, the problem of determining the overall resultant error in derived parameters on a quantitative basis becomes even more difficult. Nevertheless, it is possible by means of reasoning and judgment to arrive at useful estimates of the overall error. The remainder of this section will be devoted, therefore, to a discussion of the various individual error effects and to a final estimation of overall error in the derived sounding profiles.

### Observation Errors

Radiosonde. -- Belmont, Peterson and Shen (ref.10), in their recent review of meteorological rocket data, have also summarized current knowledge regarding radiosonde observation errors. Table 18 is an excerpt from this report which presents references to previous studies regarding the component errors and overall errors in temperature and pressure. According to this table, the standard temperature error for U.S. radiosonde instruments has been rather clearly established as approximately  $\pm 1^{\circ}\text{C}$  in the troposphere, gradually increasing to an approximate value of  $\pm 2^{\circ}\text{C}$  near 100 000 ft.

According to the definitive study of radiosonde error made by the Air Weather Service (ref. 10), there are two principal components to the error in the height of pressure surfaces: (1) the height error which corresponds to the pressure error in the aneroid unit, and (2) the error in the height of pressure surface which results from the integrated error in successive thickness calculations based upon the use of the hydrostatic equation. The latter error component is predominantly caused by the error in determining the mean virtual temperature of each calculated layer; only a negligible error effect is produced by the mean error in the measurement of pressure. Table 19 presents estimates made by Air Weather Service of the pressure height errors associated with radiosonde aneroid elements commonly used during and before 1955. These figures are still regarded as valid for the standard aneroids still in use; however, where improved hypsometers are used between 50 to 4mb, a significant decrease in the pressure height error can result. For example, Table 19 shows a standard deviation of approximately 1000 meters in the height of the 10 mb surface, whereas Conover (ref. 15) gives a corresponding value of 600 meters when the improved hypsometer is used.

Profile Id = 01010051

T	P	Z	T	P	Z	T	P	Z	T	P	Z
195.0	0.2337E-02	90.0	244.0	0.1461E 00	64.5	266.0	0.3440E 01	39.0	211.3	0.1602E 03	13.6
195.0	0.3019E-02	88.5	252.0	0.1789E 00	63.0	263.4	0.4167E 01	37.5	216.0	0.2000E 03	12.2
195.0	0.3901E-02	87.0	259.0	0.2179E 00	61.5	261.0	0.5057E 01	36.0	222.3	0.2293E 03	11.3
195.0	0.5040E-02	85.5	266.0	0.2640E 00	60.0	253.5	0.6160E 01	34.5	228.6	0.2628E 03	10.4
195.0	0.6513E-02	84.0	270.0	0.3186E 00	58.5	246.0	0.7550E 01	33.0	235.0	0.3000E 03	9.5
195.0	0.8418E-02	82.5	274.0	0.3835E 00	57.0	239.9	0.9674E 01	32.0	242.3	0.3548E 03	8.3
195.0	0.1088E-01	81.0	276.0	0.4607E 00	55.5	234.0	0.1000E 02	31.0	249.6	0.4222E 03	7.0
196.0	0.1406E-01	79.5	278.0	0.5528E 00	54.0	227.9	0.1432E 02	28.5	257.0	0.5000E 03	5.8
197.0	0.1814E-01	78.0	279.5	0.6626E 00	52.5	221.0	0.2062E 02	26.1	264.3	0.5595E 03	4.9
200.5	0.2334E-01	76.5	281.0	0.7935E 00	51.0	216.0	0.3000E 02	23.7	271.6	0.6268E 03	4.0
204.0	0.2991E-01	75.0	280.4	0.9499E 00	49.5	214.3	0.3561E 02	22.6	279.0	0.7000E 03	3.1
209.0	0.3813E-01	73.5	280.0	0.1138E 01	48.0	212.6	0.4217E 02	21.6	282.3	0.7469E 03	2.5
214.0	0.4834E-01	72.0	277.9	0.1354E 01	46.5	211.0	0.5000E 02	20.5	285.6	0.7971E 03	2.0
219.0	0.6096E-01	70.5	276.0	0.1637E 01	45.0	207.9	0.6320E 02	19.1	289.0	0.8500E 03	1.5
224.0	0.7648E-01	69.0	275.4	0.1967E 01	43.5	204.9	0.7936E 02	17.8	289.6	0.9021E 03	1.0
230.0	0.9544E-01	67.5	275.0	0.2365E 01	42.0	202.0	0.1000E 03	16.4	290.3	0.9573E 03	0.5
236.0	0.1184E-00	66.0	270.5	0.2848E 01	40.5	206.6	0.1277E 03	15.0	290.9	0.1016E 04	0.0

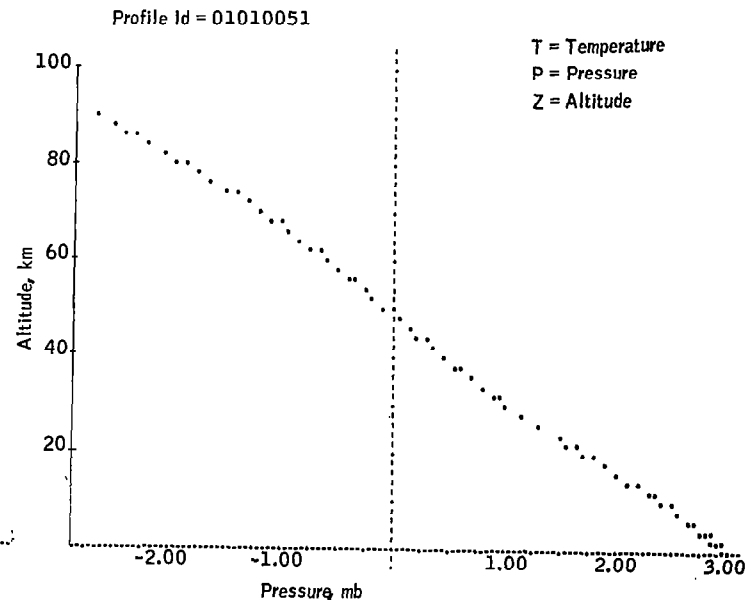
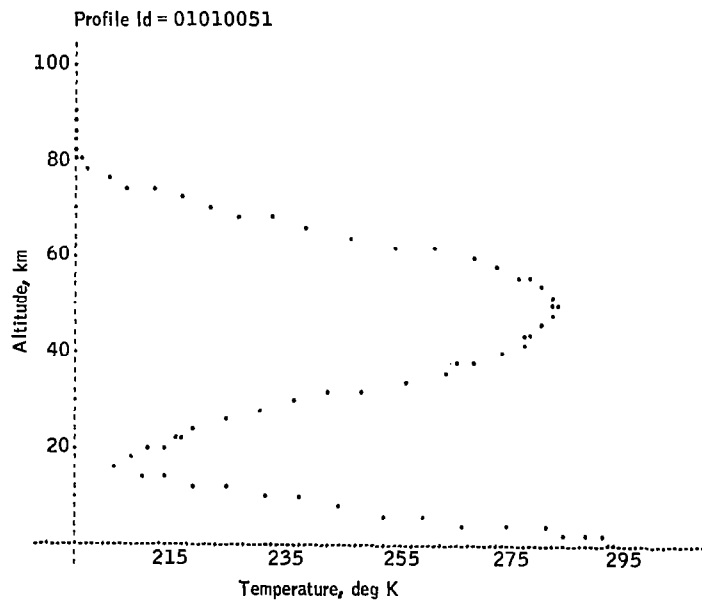


Figure 22. Temperature and Pressure Profiles Taken From the Body of Synoptic Case Data for 8 April 1964, 33.75°N, 75°W

TABLE 18.- ERRORS IN RADIOSONDE TEMPERATURE AND PRESSURE DATA

[ref. 10]

Parameter	Component errors in sensor, tracking, processing, etc.	Overall errors
Temperature	<p>Errors due to solar radiation, instrument radiation, lag, calibration and recording. Rad. error 3° C. to 30 km, 10° C. at 45 km (a).</p> <p>RMS temperature error due to sensing is 1° C. to 10 mb (b).</p> <p>RMS temperature error due to pressure error increases from 0.2° C. at 700 mb to 1.7° C. at 10 mb (c).</p>	<p>Standard error <math>\pm 1^\circ</math> C. below 30 km (e). External thermistor 2° C. at 25 km, smaller below and larger above. Duct type has larger errors in stratosphere (f).</p> <p>Standard temperature error of <math>\pm 1^\circ</math> C. to 60 000 ft. and somewhat greater at higher altitudes (g).</p> <p>Total temperature error increases from <math>\sim 1^\circ</math> C. at 700 mb to 2° C. at 10 mb (b). Temperature error <math>\pm 0.7^\circ</math> C.</p>
Pressure	<p>Aneroid cell -- subject to hysteresis and lag at high altitudes.</p> <p>Hypsometer: full range: 1060 to 40 mb; high altitude: 70 to 4 mb. Uses AN/AMT 12 or 15 modulator. In practice used from 50 to 4 mb (d).</p>	<p><math>\pm 1</math> mb at low pressure. At 10 mb, 1 mb = 600 m. At 2 mb, 1 mb = 1500 m. (d).</p> <p><math>\pm 0.3\%</math> of true pressure, 1060 to 40 mb. <math>\pm 0.7\%</math> pf true pressure, 70 to 4 mb. (k)</p>

a From ref. 11

b From ref. 12

d From ref. 15

e From ref. 51

f From ref. 13

g From ref. 14

k From ref. 16

TABLE 19.- PRESSURE HEIGHT ERRORS OF RADIOSONDE  
[ref. 14]

Pressure, mb	Error in height of pressure surface, $\sigma_H$ , ft	Corresponding pressure error, ft (a)	Standard deviation of true height, $\sigma_Z$ , ft
700	34	111	116
500	67	144	159
300	119	219	250
200	161	315	354
100	229	418	477
50	291	630	694
25	355	1257	1306
10	456	3140	3173

<sup>a</sup> 3 mb up to and including 200 mb; 2 mb at 100 mb, and 1.5 mb above.

Rocketsonde. -- Table 20 presents a summary of estimated errors in rocketsonde temperature and density data. As noted by the authors, it is not absolutely certain whether these values represent standard errors, probable errors or two-standard deviation errors (since precise definition of statistical error terms is, as a rule, lacking in much of the published literature). In the case of Wagner, et al. (ref. 19), the estimate of  $\pm 2^{\circ}\text{C}$  for temperature error to 60 km was taken by Belmont, et al., (ref. 10) to represent the standard error; the estimate of temperature error within  $\pm 2^{\circ}\text{C}$  below 45 km and within  $\pm 5^{\circ}\text{C}$  to 56 km (ref. 10) was taken to represent approximately the two-standard deviation error, or the range within which some 95 percent of a population of normally distributed standard errors would occur. The estimate by Beyers, et al. (ref. 17) of  $\pm 2^{\circ}\text{C}$  for uncorrected temperature data to 57-60 km was regarded as a standard error; similarly, their estimate of  $\pm 0.5^{\circ}\text{C}$  for corrected temperature data was taken to represent a standard error. The estimate of approximately  $1^{\circ}\text{C}$  error in temperature measurements to 50 km (ref. 24) was regarded as a standard error; this estimate, it should be noted, applies to perfectly aluminized thermistor beads, otherwise the error is larger, although probably not exceeding  $5^{\circ}\text{C}$ .

By way of summarizing the information in Table 20, the standard error in rocketsonde temperature measurements is approximately  $\pm 1^{\circ}\text{C}$  in the 30-45 km range, increasing to a value of  $\pm 2^{\circ}\text{C}$  near 60 km. These values apply to uncorrected temperature data obtained under average conditions. Beyers, et al., (ref. 17) have shown that appreciable error reduction can be achieved by applying appropriate corrections. It should also be mentioned in passing that the temperature error increases very rapidly above 60 km.

Certain problem areas regarding temperature measurement are still not completely resolved in regard to self-heating, solar radiation, fall velocity and instrumental time constant. In addition, Wagner, et al., (ref. 19) have pointed out that very large temperature errors may occasionally result from a calibration shift due to nose cone heating during rocket ascent. Large systematic errors of this type in rocketsonde temperature measurements can be corrected, however, if parallel radiosonde temperature data are available. At some MRN stations the current practice is to correct the rocketsonde temperature profile to agree with the overlapping portion of the radiosonde temperature profile, whenever such data are available.

Since temperature measurements are made with different types of rocket sounding systems throughout the MRN, various correction techniques are used in the attempt to produce a set of consistent corrected data. Most of the correcting that is done is performed at the various MRN launching sites and other corrections are performed by the U.S. Army Electronic Research and Development Activity at White Sands Missile Range (WSMR), New Mexico. One of the most frequently used systems of temperature measurement is the Deltasonde employed by WSMR, Fort Greeley, Alaska, and Point Mugu, California. Wagner (ref. 25) has developed corrections for data acquired by the Deltasonde. The Wagner (ref. 25) correction takes into account effects of compressional or frictional heating, lead wire length and heat conduction through the leads to the thermistor varying time constant, internal heating and dissipation, solar radiation and the effective infrared radiation temperature below the thermistor. Application of this correction system to the MRN

TABLE 20.- ERRORS IN M/R TEMPERATURE AND DENSITY DATA  
[ref. 10]

Type of system	Errors	Special remarks
Parachute (8 ft and 15 ft diam)	<p>The temperature error at 50 km is <math>\sim 1^\circ \text{C}</math> with a perfectly aluminized bead thermistor, otherwise higher but not <math>&gt; 5^\circ \text{C}</math>. (a)</p> <p>Error of <math>\pm 0.5^\circ \text{C}</math> for corrected temperature data to 57-60 km and <math>\pm 0.5^\circ \text{C}</math> for corrected data (b)</p> <p>Temperature error is within <math>\pm 2^\circ \text{C}</math> below 45 km and within <math>\pm 5^\circ \text{C}</math> to 56 km (c)</p> <p>Temperature error is <math>\pm 2^\circ \text{C}</math> to 60 km (d)</p> <p>Occasionally large temperature errors may result from a calibration shift due to nose cone heating during rocket ascent (d)</p> <p>Density data derived from rocketsonde temperature measurements have a probable error of 2% and are all accurate to within 5% (e)</p> <p>RMS error in density is 3% at 60 km and about 2% at lower levels, assuming no vertical winds (f)</p>	<p>Strange spikes on the temperature traces have been noted; these may be due to heat flow from thin support wires. The major problem areas, however, involve self-heating, solar radiation, fall velocity and time constant.</p>
"ROBIN"	<p>Density values are accurate to within <math>\pm 3\%</math> for an assumed "normal" wind of 1 mps (g)</p>	<p>Density computation from ROBIN critically depends upon the drag coefficient and this in turn upon the state of inflation of the balloon sphere.</p>
Balloon	<p>Neglect of vertical motion may significantly affect calculated density values. A vertical wind <math>\sim 0.5</math>-1.5 mps causes <math>\sim 2\%</math> density error and a vertical wind <math>\sim 2</math>-8 mps produces a <math>\sim 10\%</math> density error in the altitude range of 40-60 km. (h)</p>	<p>Smoothing is another vital area as shown by Engler's detailed studies.</p>
Sphere	<p>ROBIN density data appears suitable for climatological studies (g)</p>	

a From ref. 25  
b From ref. 17  
c From ref. 18  
d From ref. 19

e From ref. 20  
f From ref. 21  
g From ref. 22  
h From ref. 23

temperature data gathered at WSMR and Fort Greeley, Alaska was begun in January 1964. Published Point Mugu data were not corrected in 1964. As a result, GCA, on the basis of information furnished by Texas Western College (Neary, 1966), applied the appropriate corrections to the 1964 Point Mugu data. All other corrections to the 1964 MRN published data were assumed to have been performed by the contributors for the temperature measuring devices other than the Deltasonde. In 1965, all data collection and reduction were accomplished by each contributor to the MRN network. All published 1965 Point Mugu data were corrected by the Wagner method.

Compatibility of rocketsonde and rawinsonde temperature measurements. -- The following excerpt from Belmont, et al., (ref.10) discusses the topic of data compatibility:

The basic differences in R/W<sup>(a)</sup> and M/R<sup>(b)</sup> temperature measurements may be viewed as relatively minor compared to those associated with wind measurements. The sensor and telemetry units are essentially the same for R/W and M/R temperature observations. Nevertheless, there are some differences which arise in connection with dissimilar exposure conditions and vertical rate of movement.

There are a variety of published opinions regarding the basic compatibility of R/W and M/R temperature measurements. One report (ref.26) is somewhat critical of the type of qualitative comparison which is usually made between overlapping of short-gapped data samples. This report states: 'Many investigations have attempted to justify the accuracy of the temperature profiles they obtained by the excellence with which their data "tied into" the radiosonde data. This agreement, however, does not demonstrate that the higher altitude data is accurate'.

Another report by the USAF 4th Weather Group (ref.27), which provides meteorological support at Cape Kennedy, views the matter of temperature compatibility somewhat pragmatically: 'No hard and fast rules are established for setting the maximum allowable difference between the rocketsonde and rawinsonde temperatures -- however, since we are providing both rawinsonde data and rocketsonde data for support purposes, we can't tolerate wide differences in the data. Until definite proof is provided to the contrary, the rawinsonde data are assumed to be correct and the rocketsonde data must be adjusted to within reasonable limits.' However, a more recent paper by Quinlan, Crutcher, and Smith reviews this assumption, and states that: 'this assumption may not be valid when the time and space differences between the two are considered'.

---

a R/W - radiosonde

b M/R - meteorological rocket

These authors have made the most extensive statistical study of R/W - M/R temperature differences, based upon 27 pairs of observations taken between 80-100 000 ft at Cape Kennedy from May 1960 to February 1963. Their conclusions were that: 'In the 80 000 to 100 000 ft region the rocketsondes yield slightly warmer temperature than those of the radiosonde with significant differences at the 95 000 and 100 000 ft levels'. The level of significance, in this case, was the 95 percent probability level. No effort was made in that study to determine the extent of instrumental and observational errors or to eliminate their effects.

Finger, et al., (ref. 28) have compared a sample of overlapping rocketsonde and rawinsonde temperatures at Fort Churchill during November 1960. They conclude the following: 'At the beginning of the period there is considerable difference, throughout the area of overlap, between reported rawinsonde temperatures and those measured during the single rocketsonde observation. During the middle of the period, however, the compatibility appears to be good with differences of 5°C or less -- the deviations again increase as rawinsonde temperatures remain relatively cold.....'

### Errors in Analysis

Effects of reduced data coverage. -- The effective analysis of reported on constant level charts and cross-sections depends upon good data coverage. However, in analyzing a series of charts based upon rocketsonde data, the coverage is characteristically uneven from chart to chart. Two studies were performed, therefore, to assess the effect which reduced data coverage would have upon the analyst's ability to draw accurate isotherms.

Analysis of constant height charts: To study errors of analysis in the 30-60 km region, an experiment was performed in which three sets of isotherm analyses were made for the same 42 km chart; one based upon data for eight stations and the others based upon data for two different sets of three stations each. The 9 December 1964 synoptic case was selected for this experiment since it contained seven stations reporting temperature and wind and one station (Wallops Island) reporting only wind.

Table 21 contains a listing of the stations used for the three analytical error study cases. Case 2 contains the least information with two stations reporting wind and temperature and one reporting only wind; in addition, it does not contain any information in the polar regions since the Fort Churchill report was eliminated. Case 3 contains slightly more information with three stations reporting both wind and temperatures; however, it contains no information on the east coast of the United States since the wind observation at Wallops Island was eliminated. In order to avoid any biasing effects from the analyst's memory of the all-data case, the analyses of Cases 2 and 3 were performed prior to the analysis of Case 1.

TABLE 21.- STATIONS USED FOR STUDY CASES OF ANALYTICAL ERROR

Case 1 (All Data)	Case 2	Case 3
Antigua	Grand Turk	Antigua
Cape Kennedy	White Sands	Fort Churchill
Grand Turk	Wallops Island	White Sands
San Salvatore		
Fort Churchill		
White Sands		
Wallops Island (wind only)		
Point Mugu		

Figure 23 shows the 42 km isotherm analysis based upon all the data. This analysis is used as the "correct" analysis from which to measure deviations for the other cases. The plotted arrows on this figure point in the direction of the thermal wind and the speed of the thermal wind (computed from the wind shear between 40.5 and 43.5 km) is plotted at the head of the arrow.

The thermal analysis on Figure 23 shows a cold area over the central part of North America extending southward to the Gulf States. The western Atlantic region immediately off the east coast is relatively warm as shown by the north-south orientation of the isotherms. This basic north-south orientation of the isotherms in eastern North America is largely determined from the southerly thermal winds at Wallops Island and Fort Churchill.

Figure 24 shows the analysis which was made at 42 km for Case 2 (three stations with only two temperature reports). This chart contains about the least amount of information from which an analysis is feasible. On this chart, the temperatures are still analysed as cold over the central part of North America and warm off the east coast. These conclusions are largely based upon the thermal winds at White Sands and Wallops Island: White Sands has a north-westerly thermal wind indicating colder temperatures to the northeast, and Wallops Island has a southerly thermal wind indicating colder temperatures to the west. Although the thermal patterns on Figures 23 and 24 generally agree, it may be noted in this limited-data case that the isotherms in the western United States are analyzed in a more northwesterly direction than those for the complete-data case. In the latter case, as shown on Figure 23, the westerly thermal wind at Point Mugu flattens the isotherms into more of an east-west orientation. Furthermore, as a result of limited data the amplitude of the thermal pattern on Figure 24 is exaggerated in comparison to that shown on Figure 23.

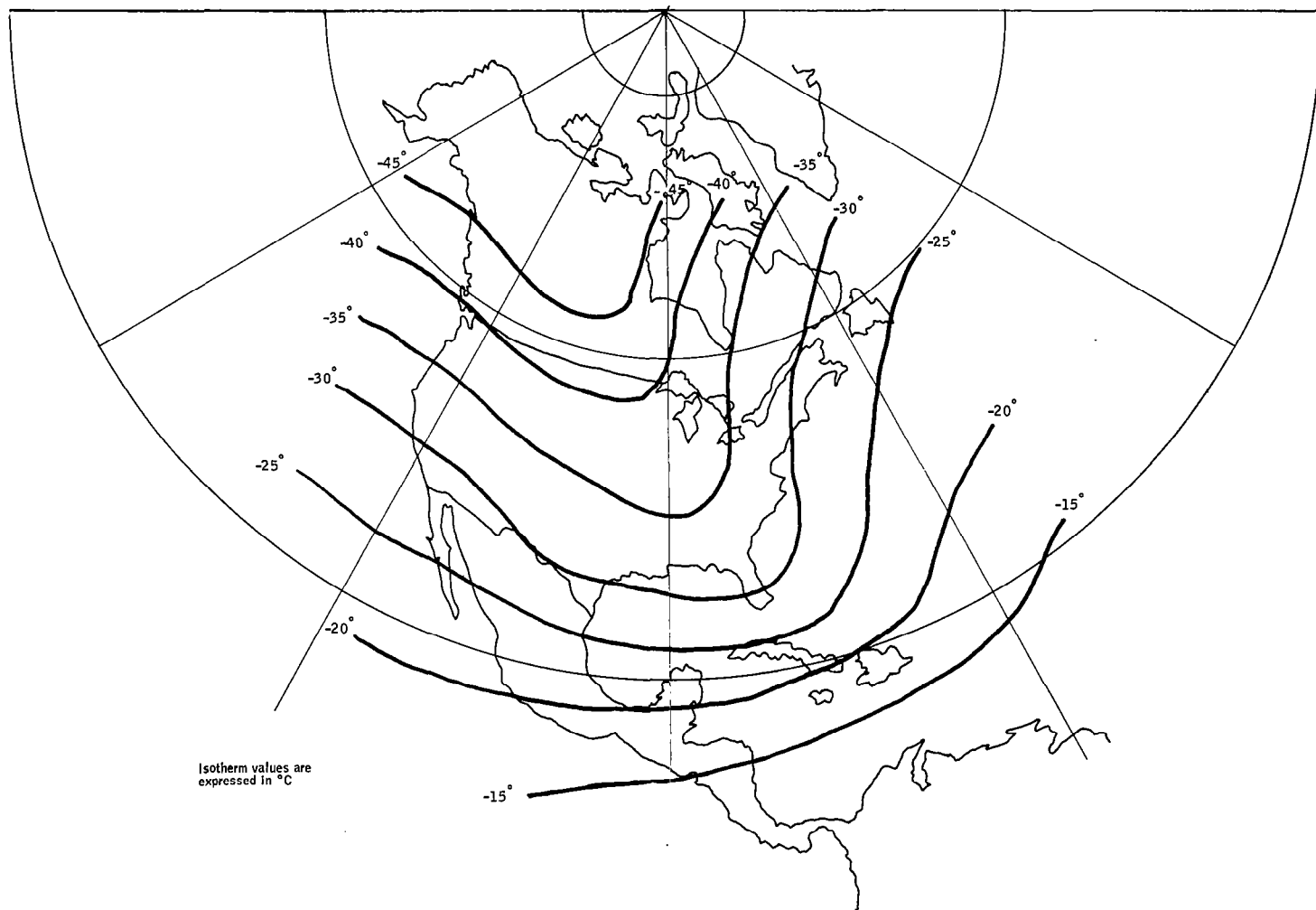


Figure 23. Isotherm Analysis at 42 km on 9 December 1964 for Case 1

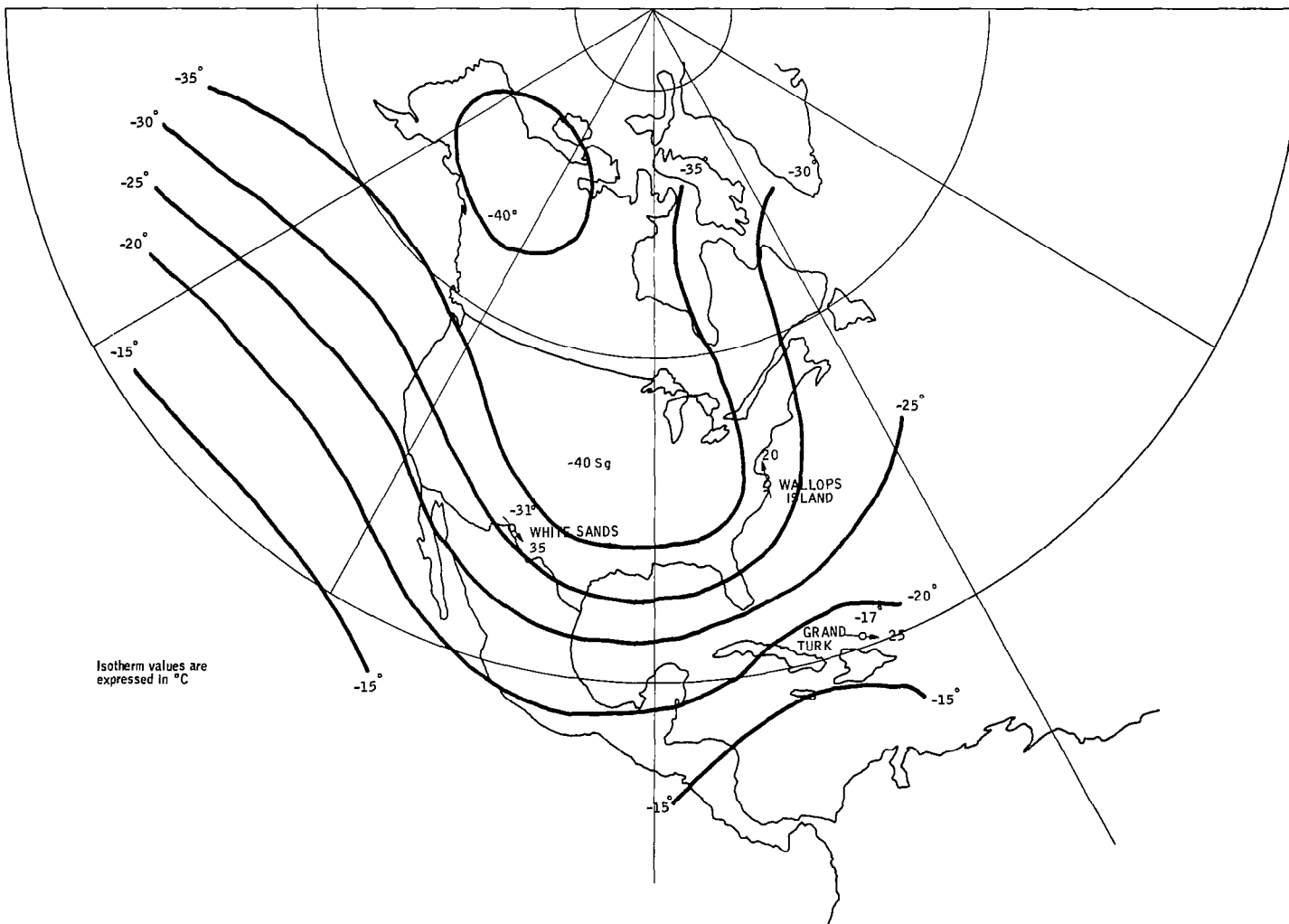


Figure 24. Isotherm Analysis at 42 km on 9 December 1964 for Case 2

Figure 25 shows the analysis of Case 3, where all three stations reported temperature. It should be noted that the axis of coldest air on this chart lies further west of the position analyzed for Case 2 on Figure 24. This difference in the analysis is due in large part to the inclusion of Fort Churchill data and the exclusion of Wallops Island data on Figure 25. The thermal winds at White Sands and Fort Churchill on Figure 25, in the absence of any other data, strongly suggest that the cold axis is located along a north-south line separating the two stations. However, on Figure 24, the inclusion of Wallops Island data with its straight southerly thermal wind serves to pull the cold axis to a more easterly position. This latter position of the cold axis more closely corresponds to the position shown on Figure 23, based upon the complete data sample.

The above analysis not only illustrates the uncertainties of analyzing constant level charts with limited data but also points how powerful and important the thermal wind technique is in supplementing basic temperature reports. The thermal winds are invaluable for determining the direction and spacing of the isotherms, whereas the temperature reports determine their magnitude.

In order to evaluate quantitatively the analytical deviations between the complete-data case and the degraded-data cases, two separate temperature-difference charts were prepared, as shown in Figures 26 and 27.

Figure 26 shows the difference in analyzed temperatures between Cases 1 and 2. The temperature differences (which may be regarded as errors of a kind) tend to be least in the triangle of information where interpolation alone was used, and increase to more than 10 degrees at the edges of the analyzed areas where extrapolation was used exclusively. This overall result is, of course, not unexpected but it does provide a helpful quantitative estimate.

Similarly, Figure 27 shows the differences between Cases 1 and 3. Once again, the temperature differences (or errors) are generally less within the triangle of information and the largest errors of analysis tend to occur on the boundaries where extrapolation is used exclusively. The maximum errors in this instance also exceed 10° C.

The inclusion of Fort Churchill data in Case 3 served to reduce the errors over northern Hudson Bay to nearly zero (Figure 27), whereas analytical errors in excess of 5°C were measured over this same region in Case 2. Correspondingly, the exclusion of Wallops Island data in Case 3 served to increase the temperature error on the east coast of the United States to nearly 5° C, whereas essentially no error was measured over this region in Case 2, where this station data was included.

The effect of inclusion or exclusion of temperature data from relatively nearby stations can be illustrated by comparing the analytical errors in the vicinity of Grand Turk and Antigua in Figures 26 and 27. In the latter figure, the error at Grand Turk is + 5° C, when this station's data is excluded, whereas it is nearly zero when this report is included, as shown in Figure 26. On the other hand, the analytical error in the vicinity of Antigua, with data excluded, is nearly 9° C, as shown on Figure 26, whereas, the error is nearly zero when Antigua data is included, as shown on Figure 27.

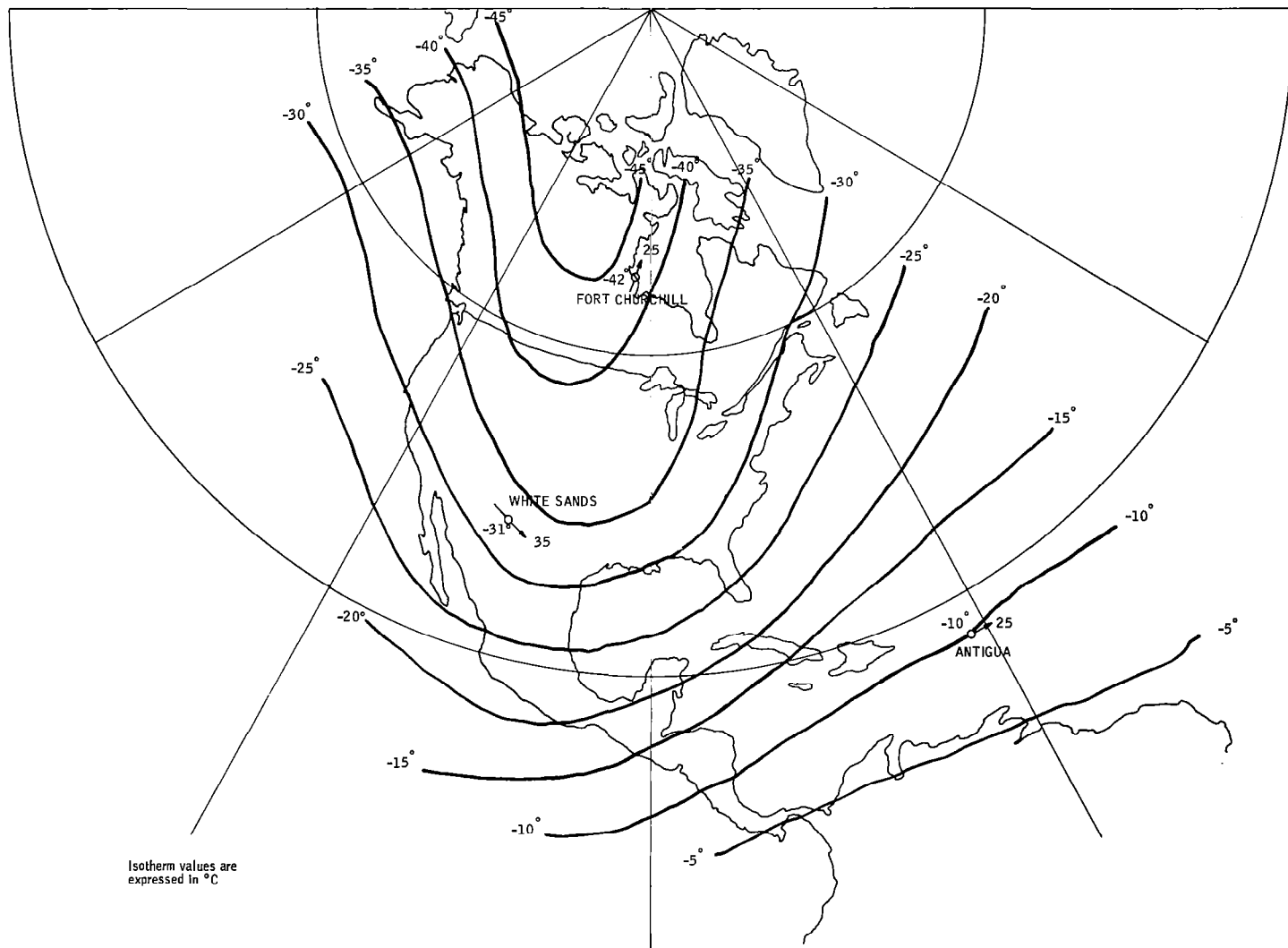


Figure 25. Isotherm Analysis at 42 km on 9 December 1964 for Case 3

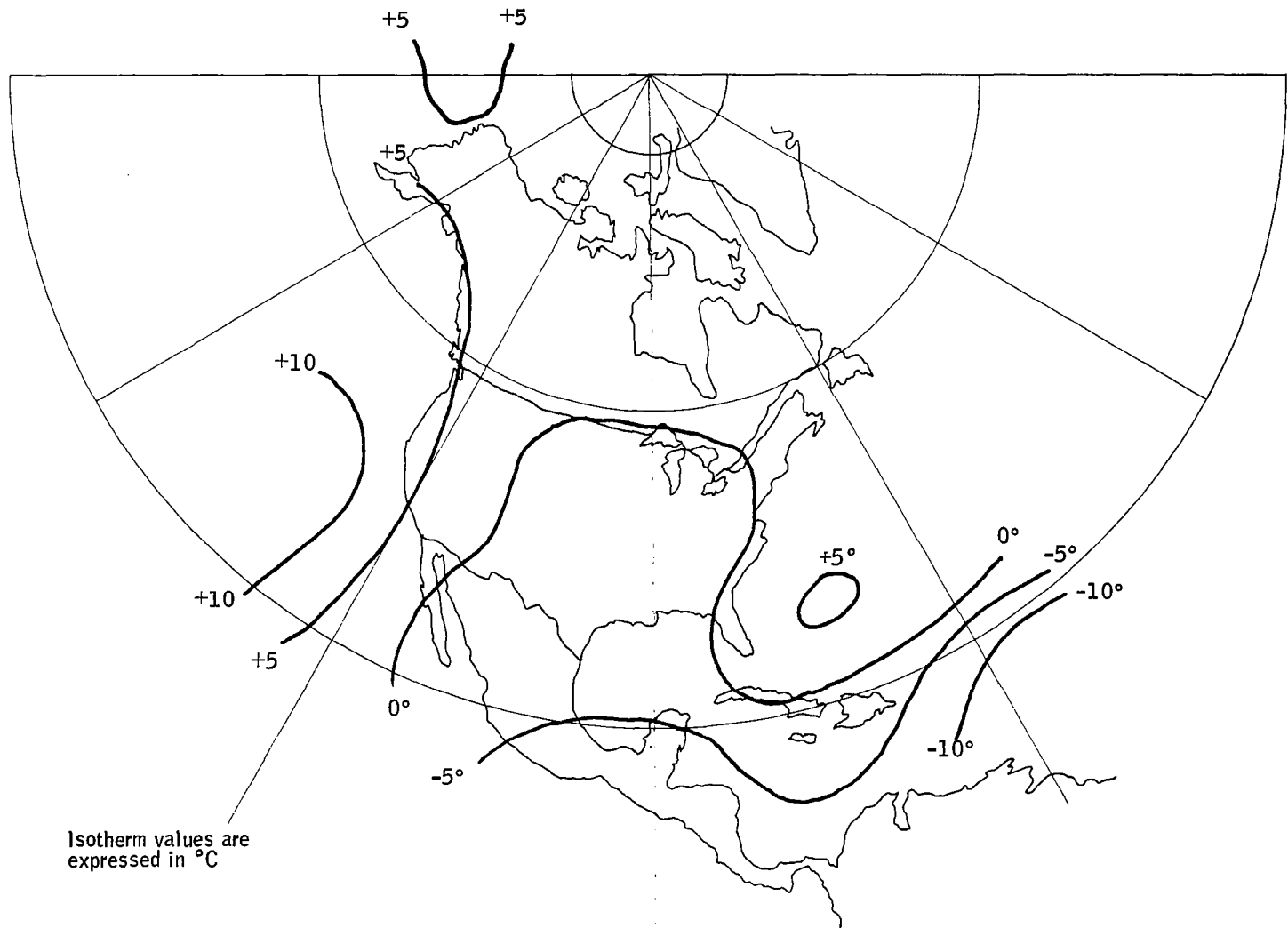


Figure 26. Temperature Analysis Error: Case 1 and Case 2

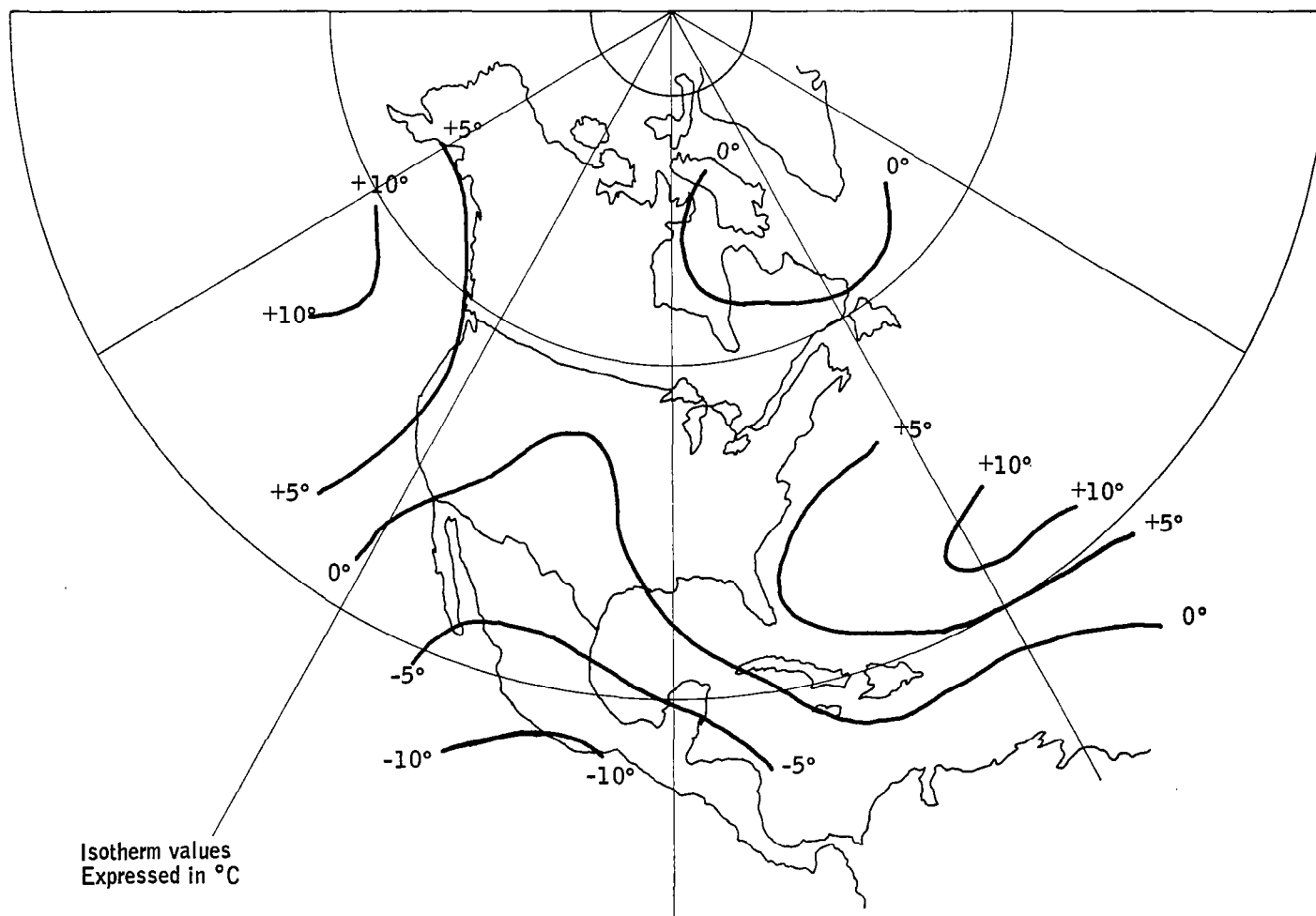


Figure 27. Temperature Analysis Error: Case 1 and Case 3

Thus, the analytical errors have been shown in these illustrative studies at 42 km to increase as the distance from an observation increases and to be greatest in areas outside the polygon which connects the data points. Errors in excess of 10° C are likely at distances greater than 400 to 500 miles from the perimeter of this polygon. Inside the data polygon, the temperature errors are less than 5° C and are generally not expected to exceed 3° C.

**Analysis of time cross sections:** Another important consideration in this study is the error in analysis which results from inaccurate interpolation between successive sounding data at the same station. A case was selected for study, therefore, where relatively frequent observations were available, and where the analytical error could thus be determined for test cases where a portion of the available data were purposely eliminated. Figure 28 shows two sets of isotherms drawn from rocketsonde data at Cape Kennedy on 11 and 12 February 1965. The solid lines show the isotherm analysis based upon all sounding data; the dashed lines represent the analysis made with the 1600 and 1700 GMT sounding data eliminated. Vertical lines indicate where soundings are taken.

The implications of data elimination (simulating the case where intermediate sounding data are unavailable) are significant. If one were interested in interpolating the temperature value at 42 km for 1200 GMT on 12 February, the value obtained from the all-data analysis is + 2° C; the comparable value for the reduced-data analysis is -5° C, for a net difference of -7° C. Undoubtedly, some of this temperature difference can be attributed to observational error, but most of it probably represents short-period variability in the thermal structure.

Effects of subjective interpretation. -- Another important source of analytical error is the subjective interpretation which is made of the data field by the individual analyst. The more sparse the data, the more leeway there is for individual interpretation. In order to test this difference for an instance where relatively dense rocketsonde data were available, Case 1, the all-data case at 42 km previously described earlier in this section was used (see Figure 23). The same data were independently analyzed by two experienced meteorologists to determine the isotherm distribution at this level.

Figure 29 presents the calculated differences between the two independent isotherm analyses. The differences are shown to exceed 5° C on the edge of the station network, but over the center of the network the differences are no more than 2-3° C. The effect of subjective interpretation by different analysts is thus comparable in magnitude to the effect produced by reduced data coverage, as previously discussed in this section. Thus, the differences are greatest outside the network of reporting stations and least inside the network; and increase with increasing distance from a reporting station.

Extrapolation errors. -- The 60-90 km temperature extrapolation technique described earlier in this section involves considerable error, even though it must be necessarily used for want of anything better. The scatter diagram of points used in developing this technique (Figure 5) provides a basis for estimating the extreme error in extrapolated temperatures. The

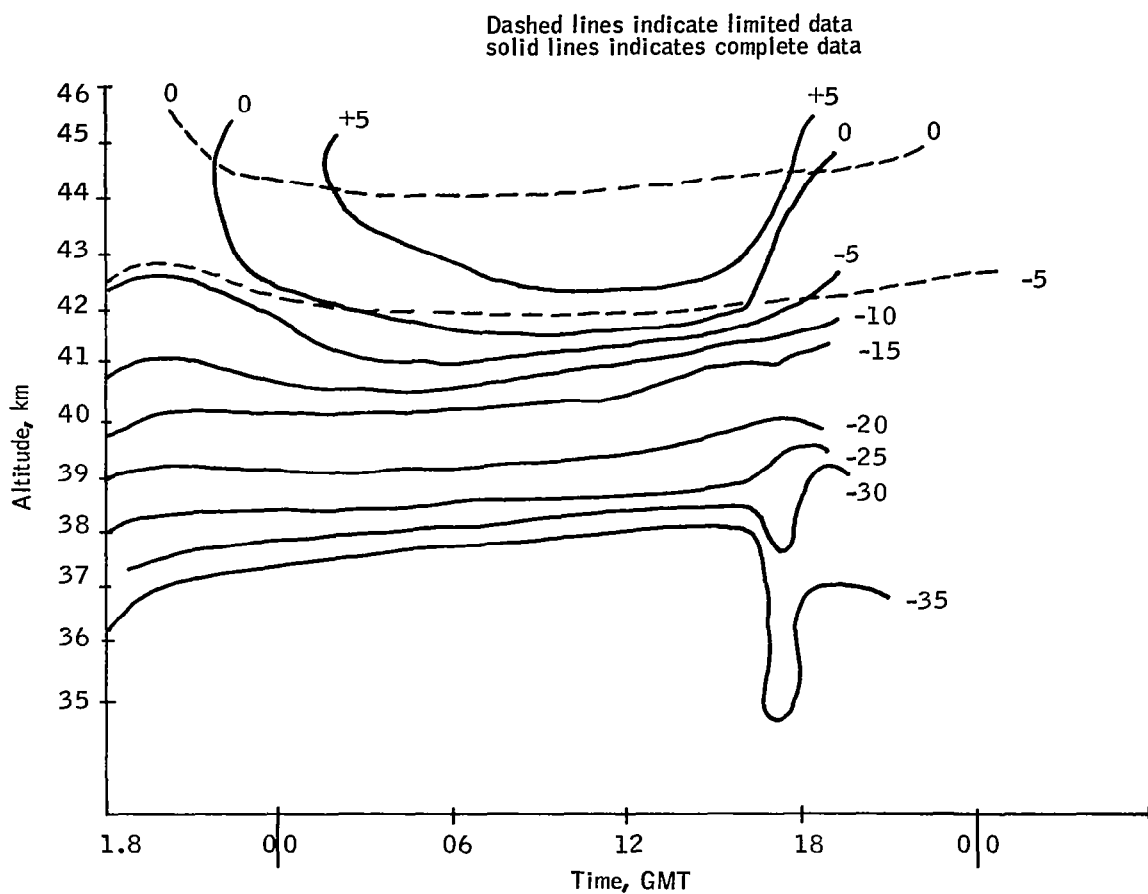


Figure 28. Cape Kennedy Time Height Cross Section

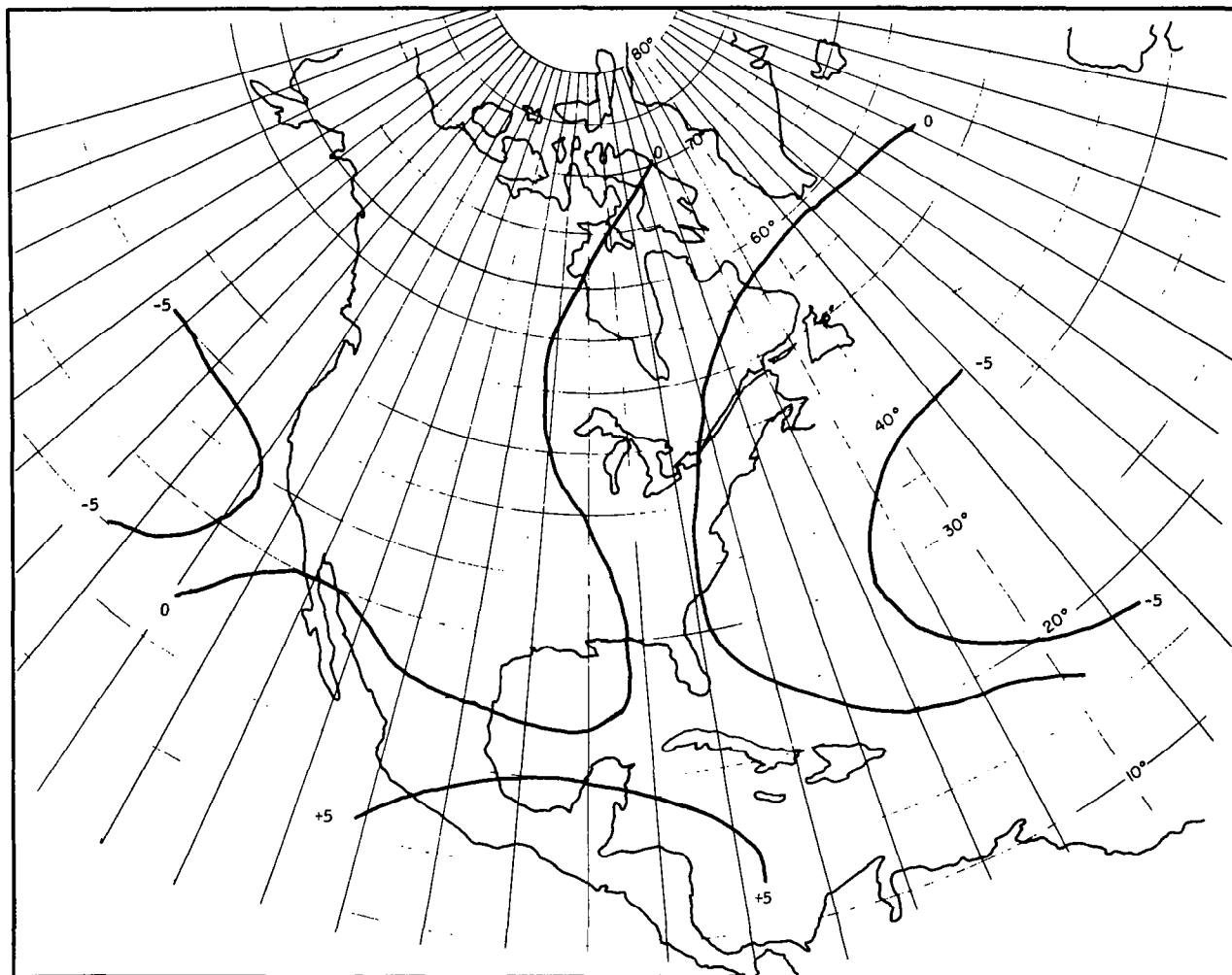


Figure 29. Difference Between Analyst A and Analyst B for Isotherm Analysis at 42 km on 9 December 1964

point scatter indicates that the extreme error of temperature estimation within the 60-90 km layer is  $\pm 20^{\circ}\text{C}$  in summer and  $\pm 30^{\circ}\text{C}$  in winter. (The term "extreme error" as used here may be taken to represent an approximate value of three times the error standard deviation; although the standard error of estimate may be directly computed from the scatter points or estimated from the range, this approach was not adopted here because such a value could possibly be misleading without a detailed justification of the statistical assumptions involved).

The higher estimate of temperature error for winter is reflected by the lower linear correlation coefficient of 0.47, as compared to the corresponding summer value of 0.62. Thus, extrapolated winter-time temperatures in the 60-90 km layer are considerably less accurate.

### Errors in Data Handling and Tabulation

Errors resulting from data handling and tabulation were essentially eliminated by the computer checking operating described in this section. The hydrostatic equation check and the temperature lapse rate check were particularly effective in spotting possible errors; these were then closely examined to determine whether values had been misread from a chart, erroneously transcribed or mis-tabulated on the punch cards.

### Overall Uncertainties in Derived Profile Data

The overall uncertainties in estimating temperatures from radiosonde data up to the 10 mb level are estimated to be small, generally less than  $\pm 5^{\circ}\text{C}$  over land areas. Over ocean areas, due to the relative sparseness of radiosonde reports, the temperature error may infrequently exceed  $\pm 5^{\circ}\text{C}$ .

The errors in estimation of temperatures in the 30-60 km layer are expected to be generally larger than at lower levels (i. e., from  $5-10^{\circ}\text{C}$ ) due to the relatively sparse coverage of the MRN network and the greater observation errors. Figure 30 shows a chart of the synoptic case grid area containing a delineation of three data confidence zones. These zones represent three levels of relative confidence which can be placed in temperatures estimated from MRN measurements. In deriving this chart, a confidence factor was assigned to each grid point regarding the relative degree of accuracy in estimating the temperature. Those points nearest rocketsonde stations received the highest confidence rating ( No. 1) whereas those points well outside the rocketsonde network were given the lowest confidence rating ( No. 3). The assignment of confidence factors in this chart is based upon data reporting from all North American, Bahaman and Caribbean Stations. Obviously, the distribution of confidence factors for a particular case would significantly vary whenever any of the MRN stations fail to report.

Between 60-90 km the extreme error in temperature estimation is some  $\pm 20^{\circ}\text{C}$  in summer and  $\pm 30^{\circ}\text{C}$  in winter. These values best apply to the middle of this layer; the vertical variation of error in extrapolated temperatures could not be determined due to the small sample available for deriving the extrapolation.

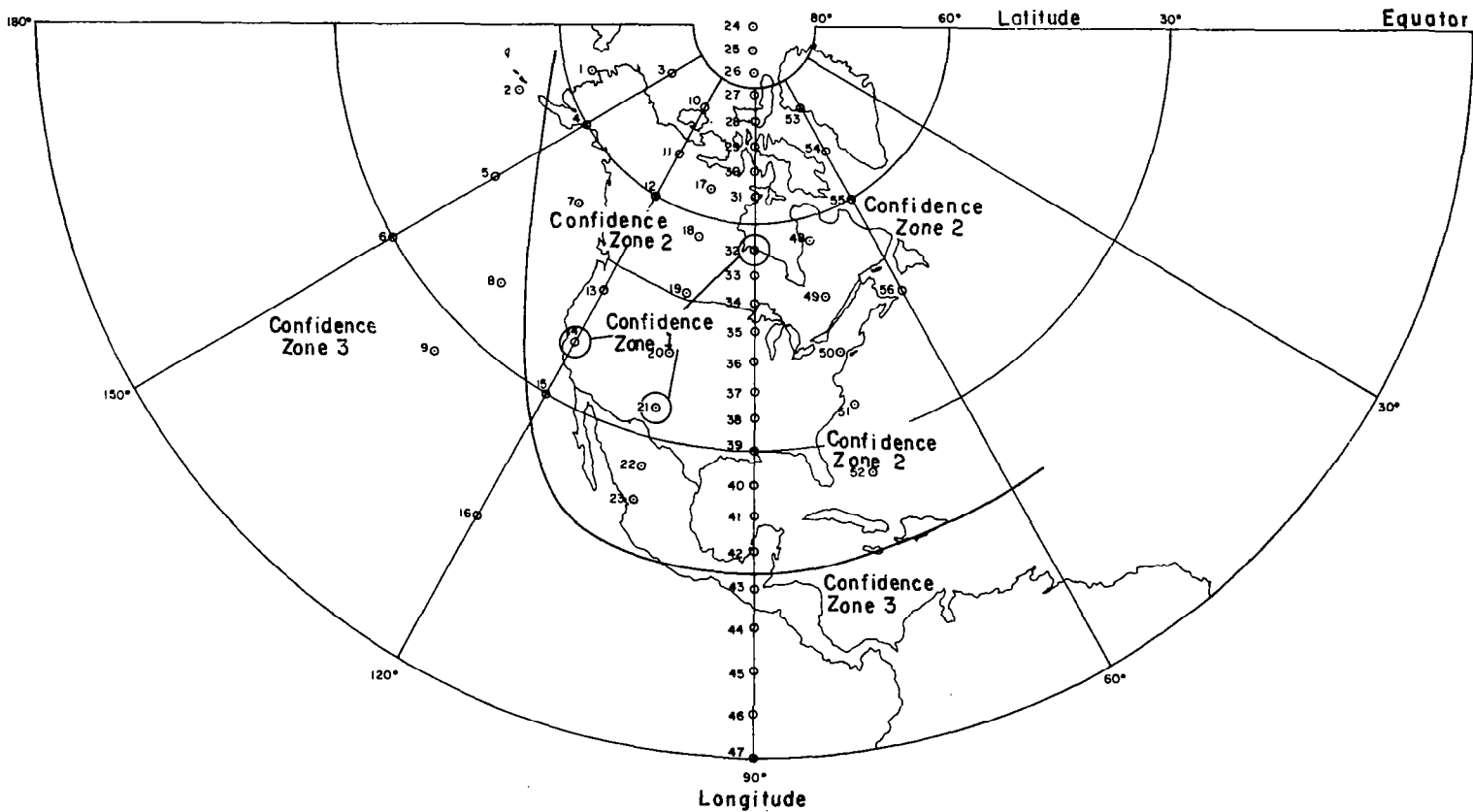


Figure 30. Chart Showing the Three Confidence Zones for the Estimate of Temperature From the MRN Measurements Based on all MRN Stations Giving Data

## VARIABILITY OF CARBON DIOXIDE CONCENTRATION

The concentration of atmospheric carbon dioxide is of considerable importance to the horizon locator problem. When scanning the horizon with a satellite mounted detector, sensitive to radiation in the 14 to 16 $\mu$  CO<sub>2</sub> band, the measured radiance emitted by the atmosphere is intimately related to the concentration of carbon dioxide. Also, the observed horizon radiance profile would be affected by large variations in the concentration of carbon dioxide. Therefore, it is important to review our present knowledge of the concentration of atmospheric carbon dioxide and its variation with time and space.

It is equally important to avoid a fragmented approach which merely considers the variability of CO<sub>2</sub> in the upper troposphere, the stratosphere and the lower mesosphere (where the more important effects upon horizon radiance profiles are produced) without providing a complete basis of understanding the entire process of variability, which begins with the exchange of CO<sub>2</sub> between the atmosphere and the biosphere near the earth's surface. Thus, a comprehensive study approach was adopted to outline the entire process by which CO<sub>2</sub> variations arise and are propagated throughout the atmosphere. The ultimate objective of this study was, of course, to determine the specific aspects of average CO<sub>2</sub> concentration and variability which relate to the problem of reliably determining the horizon from radiance profile measurements.

In the following discussion, available observations of the variations of carbon dioxide are reviewed in terms of diurnal variations, monthly and yearly variations, latitudinal variations and variations with height in the atmosphere. Based on these observations, a standard vertical profile of carbon dioxide concentration between the surface and 90 km is presented. Briefly, observations indicate that the average concentration of carbon dioxide is about 0.0314 percent by volume, that is, 314 parts per million (ppm); that, above a height of one kilometer, the average deviations about the mean concentration is, at all levels, less than  $\pm 3$  percent; and that the concentration generally decreases slightly with height in the atmosphere. These results provide the basis for calculating the effects of CO<sub>2</sub> concentration and variability upon the horizon radiance profiles which are discussed later in the report.

### DIURNAL VARIATIONS

The diurnal variations of the concentration of CO<sub>2</sub> in the atmosphere are due to exchange of CO<sub>2</sub> between the atmosphere and the biosphere. In particular,

vegetation plays a major role in this exchange. The  $\text{CO}_2$  exchange of plants depends on the time of day because plant photosynthesis involves assimilation and respiration processes which depend on the amount of sunlight, water, and  $\text{CO}_2$ . The concentration of  $\text{CO}_2$  near vegetation has a maximum near dawn and a minimum near noon (ref. 29). Observations indicate that the range of variation depends upon the type of vegetation. At a height eight meters above a forest, the diurnal variation is about 38 ppm, about 12 percent of the lowest concentration of  $\text{CO}_2$ , 320 ppm (ref. 29). At 1.5 meters above a wheat field the diurnal variation is about 130 ppm which is about 33 percent of the lowest concentration of  $\text{CO}_2$ , 320 ppm (refs. 30, 31, and 32). It should be mentioned that the above measurements are taken a few meters above the vegetation. Because of different mixing processes, the concentration inside of the vegetation can be 20 to 50 ppm higher, while the concentration far above the vegetation would be the same as that of the free atmosphere. Figure 31 illustrates the diurnal variation of  $\text{CO}_2$  at different heights above vegetation. The ordinate is concentration in ppm and the abscissa is the time of day in hours.

Little information in the literature is available on the diurnal variation of the  $\text{CO}_2$  concentration above vegetation of heights from 100 m to the free atmosphere. Qualitatively, one would expect strong vertical mixing during the daytime, owing to the steeper temperature lapse rate, which would lead to a  $\text{CO}_2$  concentration larger than the mean value. During the night, the converse would be true. A temperature inversion would tend to restrict the vertical exchange leading to smaller concentrations of  $\text{CO}_2$ . No theoretical treatment of this problem is presently available.

Observations of the diurnal variation of atmospheric  $\text{CO}_2$  for different months at Mauna Loa Observatory in Hawaii are shown in Figures 32 and 33. The observatory is located 30 km away from any vegetation, but is under the influence of a sea breeze circulation during the afternoon, which is correlated with the observed minimum concentration at this time.

The average daily changes, in general, have a pattern similar to that of Figure 33. That is, the maximum and minimum concentrations in a day are found during the forenoon and afternoon, respectively. However, the nocturnal bursts, a general increase in concentration after sunset, are less regular than the dip in the afternoon. The general trend of daily extremes shifts slightly to later times from September to March. The largest range is found in September and the smallest range is found in February. The annual average of the diurnal variation of atmospheric  $\text{CO}_2$  at Mauna Loa is shown in Figure 34.

The nocturnal burst is related to the south wind, by which the volcanic  $\text{CO}_2$  is brought to the station by down-slope winds from the summit of the mountains. The afternoon dip is mainly due to the sea breeze circulation effect in which  $\text{CO}_2$  is taken up by the vegetation on the lower slope before reaching the observing station.

### ANNUAL VARIATIONS

The monthly and yearly variations of the daily maximum and minimum  $\text{CO}_2$  concentrations in the open air close to the top of a vegetation unit were

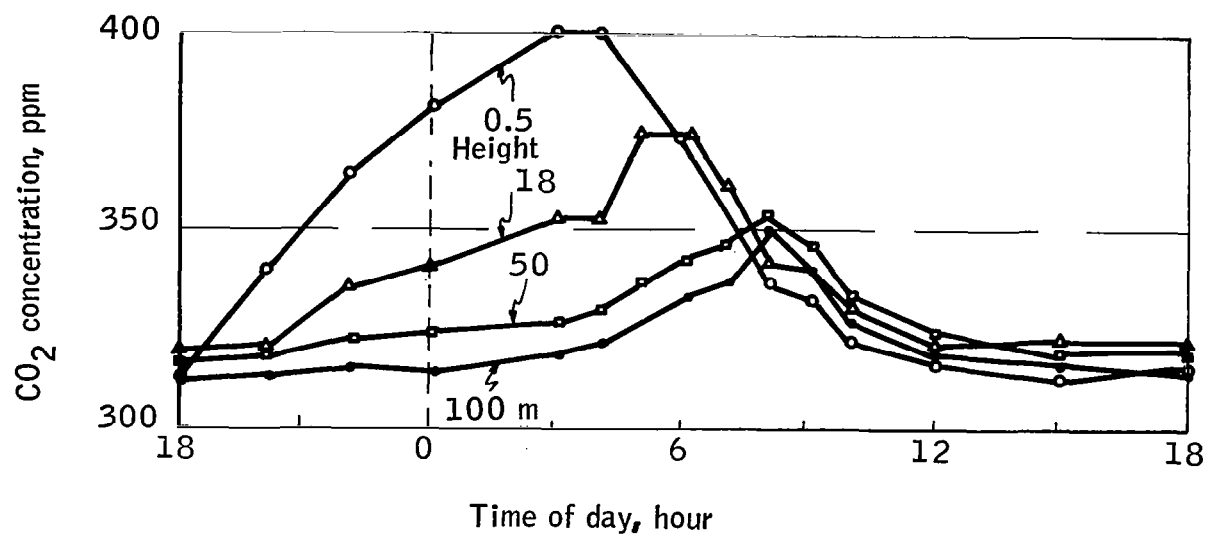


Figure 31. Average Daily Variation of CO<sub>2</sub> Concentration at Different Heights Above Vegetation

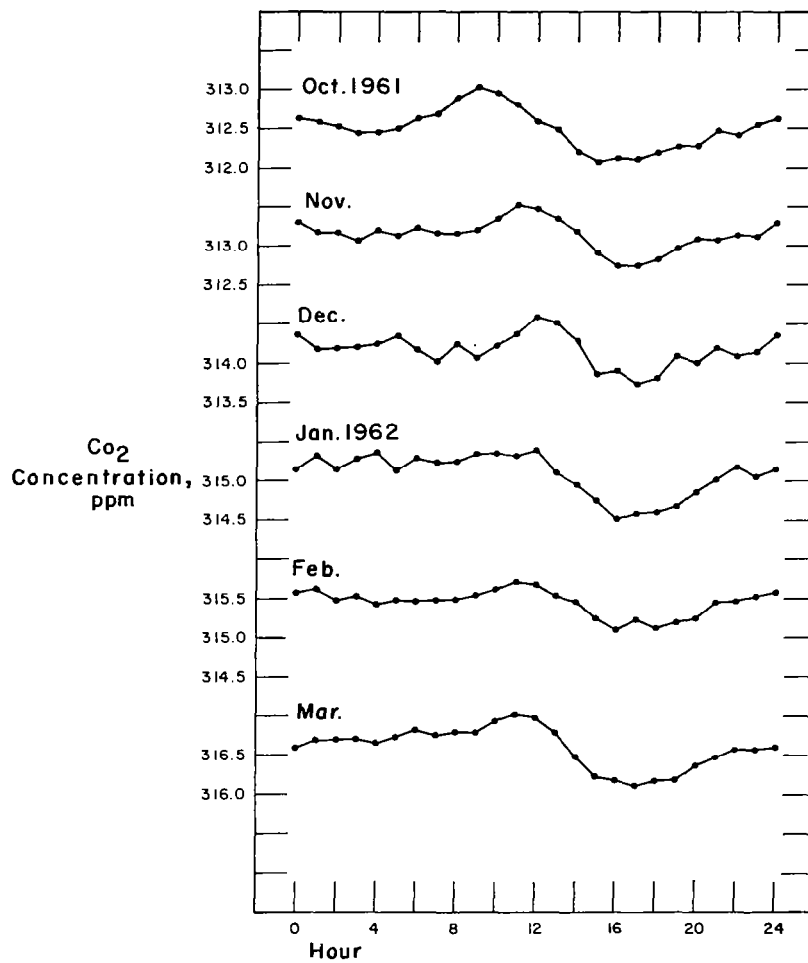


Figure 32. Diurnal Variation of Atmospheric CO<sub>2</sub> at Mauna Loa Observatory in Hawaii

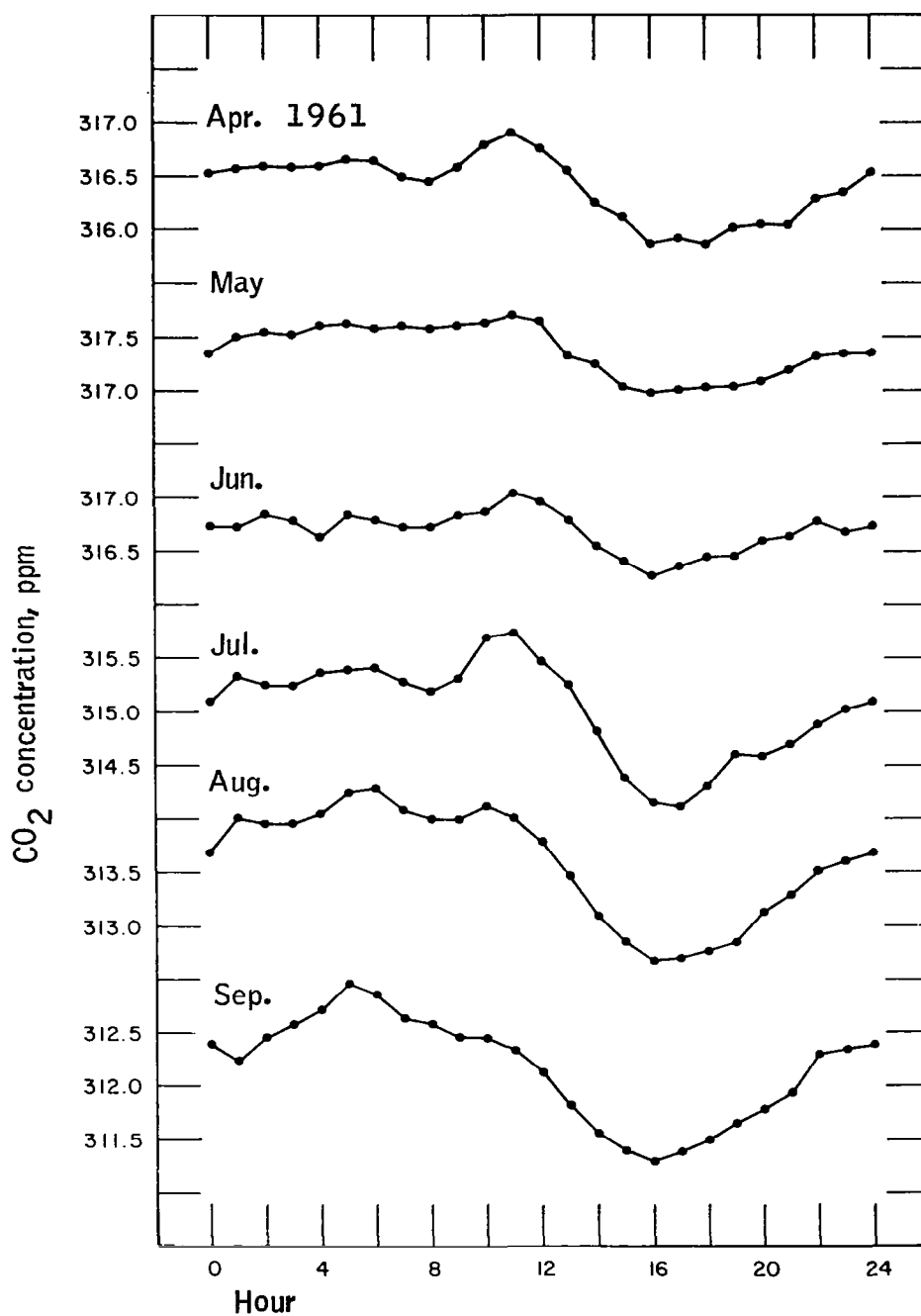


Figure 33. Diurnal Variation of Atmospheric CO<sub>2</sub> at Mauna Loa Observatory in Hawaii

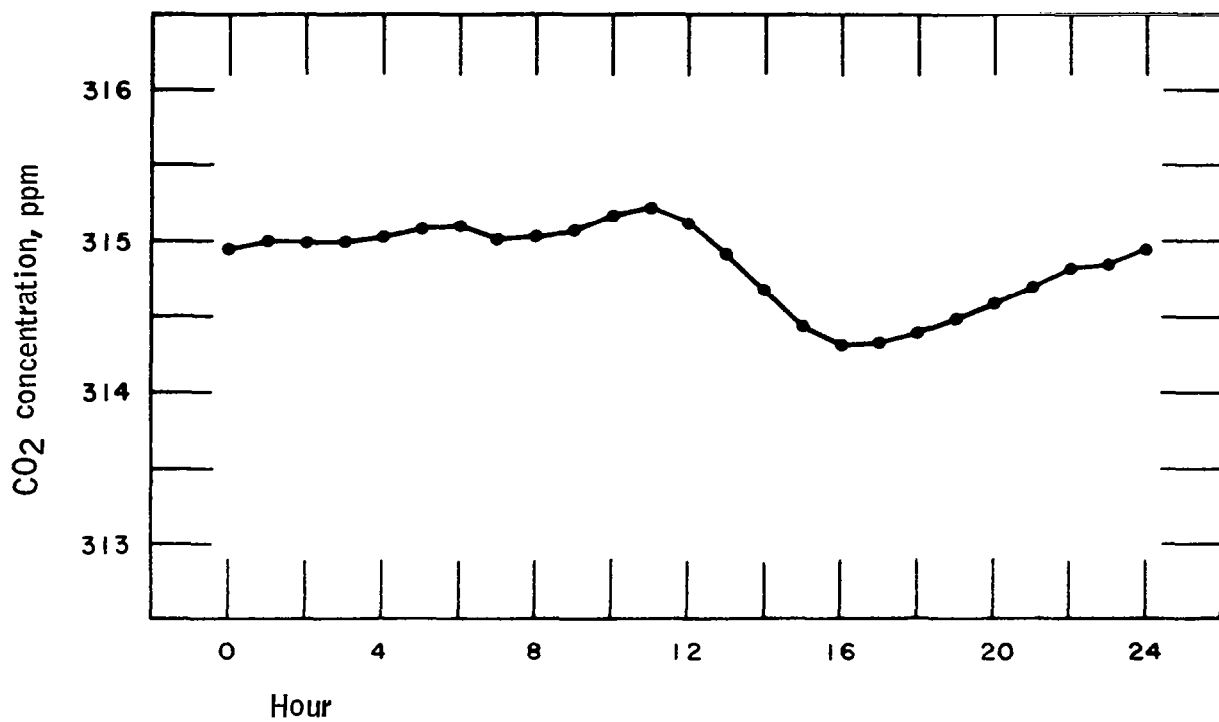


Figure 34. Annual Average Diurnal Course of Atmospheric CO<sub>2</sub> at Mauna Loa Observatory

measured and analyzed by Huber (refs. 32 and 33) and are shown in Figure 35. The extreme maximum is about 440 ppm in July and the extreme minimum is about 300 ppm in November. The peak of the monthly average of the maximum is at about August, and the lowest value of the monthly average of the minimum is in July.

The daily average concentration of atmospheric CO<sub>2</sub> at Mauna Loa Observatory in the course of 1963 is shown in Figure 36. Values are shown by unconnected points. If no value was determined on a given day, a point appears below the main plot as a reading aid. Vertical lines denote days in which nocturnal bursts occurred within a 24-hour period commencing 12 hours before the calendar day. The approximate intensity of the maximum burst is indicated by the length of the line: shortest lines denote 0 to 5 ppm; medium-length lines, 5 to 10 ppm; and longest lines, 10 to 15 ppm. Shaded areas represent periods when the analyzer was shut down for 48 hours or more. The monthly average versus time for the period between 1958 and 1963 is shown in Figure 37. Note that the time cycle is interrupted after April and September. The crosses indicate monthly averages of maximums, the circles indicate monthly averages of minimums. The upper thin line connects extreme maximums and lower thin line connects extreme minimums. These observations also show that the annual maximums and minimums of the CO<sub>2</sub> concentration occur in May, and September-October, respectively. Based on these results, the rate of yearly increase of atmospheric CO<sub>2</sub> at the Observatory, presumably due to world wide combustion of fossil fuels, is about 0.68 ppm per year. The data collected from aircraft observations at 700 mb during 1960 and 1961 near Mauna Loa Observatory are compared with surface observations in Figure 38. The phase and magnitude at the 700 mb level during 1960 and 1961, in general, reveal the same characteristics as the observations at the surface.

The month to month variations of CO<sub>2</sub> concentration in the free atmosphere over the Northern Hemisphere were collected and analyzed by Bolin and Keeling (ref. 35). For illustration, these variations are shown in Figures 39 and 40. The maximum CO<sub>2</sub> concentration is detected in May and the minimum CO<sub>2</sub> concentration is detected in September. The monthly range at lower latitudes is smaller than the range at higher latitudes. The average range is about 7 ppm.

### LATITUDINAL VARIATIONS

The variation with latitude of the annual average concentration of CO<sub>2</sub> is shown in Figure 41. Several features stand out. The highest values occur at equatorial latitudes, the lowest values at the poles. This is attributed to a net release of CO<sub>2</sub> from the oceans to the atmosphere at low latitudes. The Northern Hemisphere values are greater than the Southern Hemisphere values. This is due to the greater industrialization and attendant release of CO<sub>2</sub> into the atmosphere by fossil fuel combustion. A secondary maximum at 500 mb at middle latitudes of the Northern Hemisphere is probably the result of a concentration of industrialization at these latitudes. The total CO<sub>2</sub> range is only about 2 ppm - from 313 ppm at the South Pole to 315 ppm at the equator.

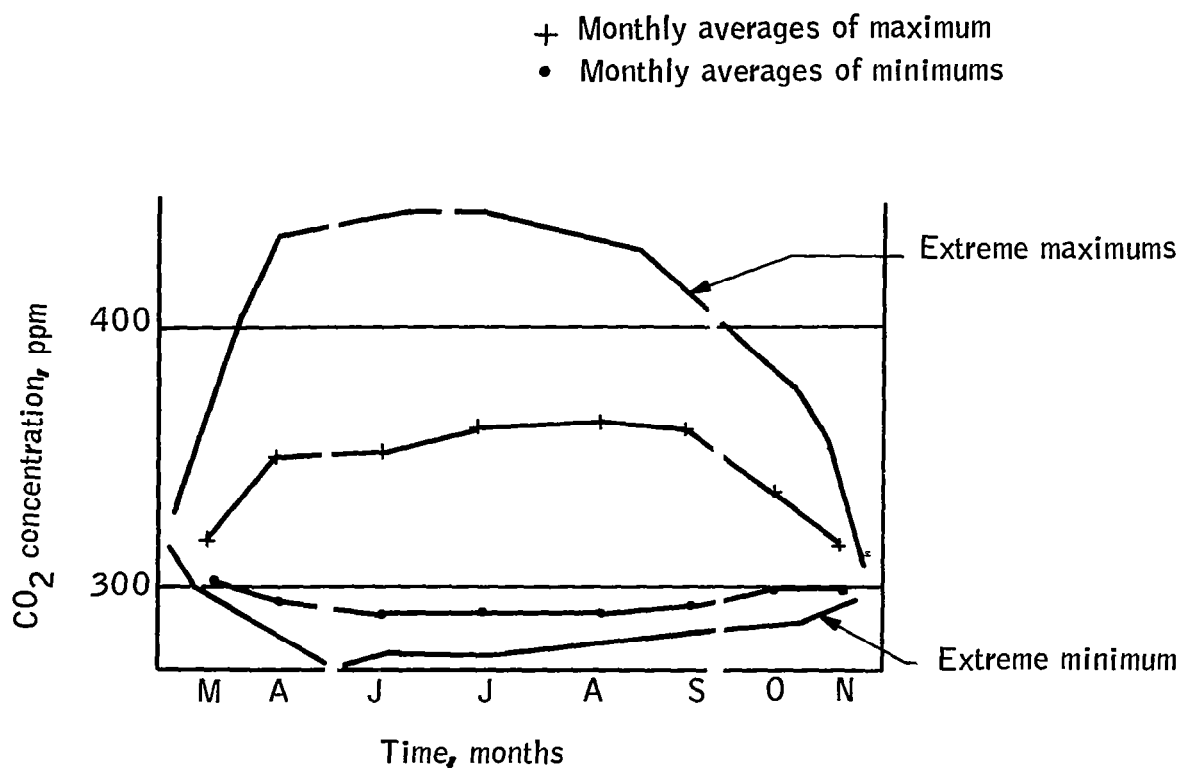


Figure 35. Year Variation of Daily Maximums and Minimums of The CO<sub>2</sub> Concentration 18 Meters Above a Crop Field

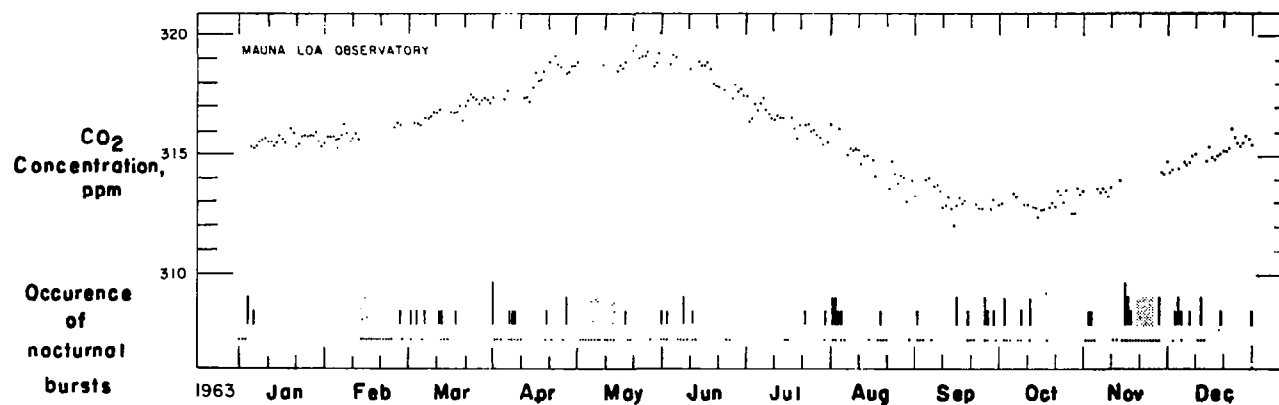


Figure 36. Daily Average Concentration of Atmospheric CO<sub>2</sub> at Mauna Loa Observatory for 1963

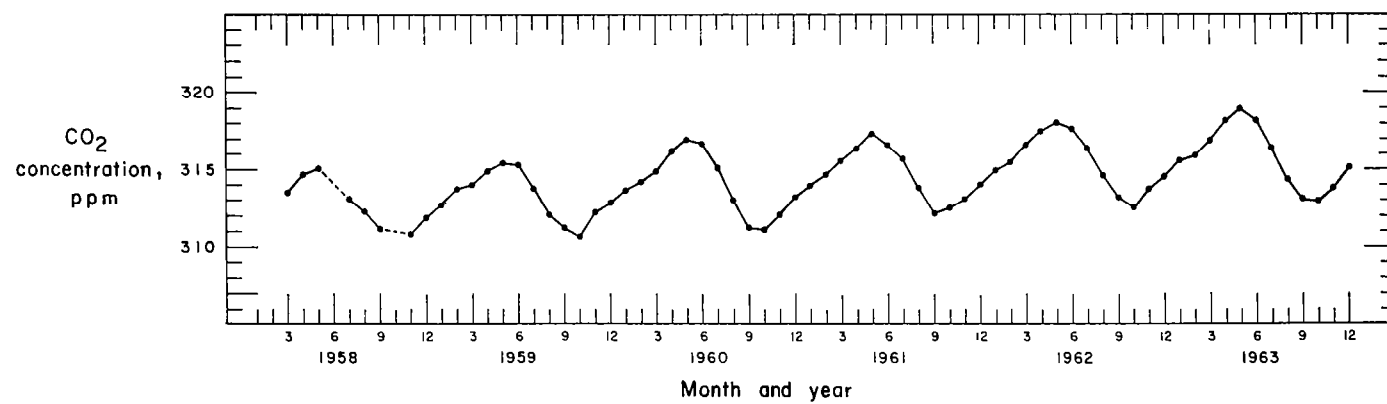


Figure 37. Monthly Average Concentration of Atmospheric CO<sub>2</sub> at Mauna Loa Observatory versus Time

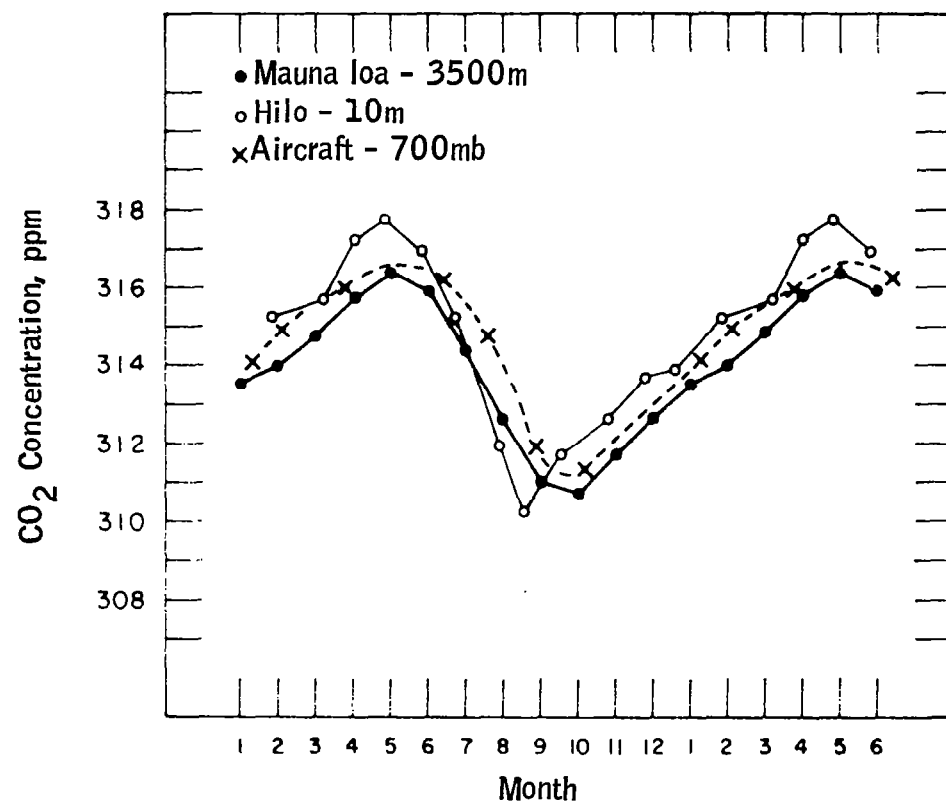


Figure 38. CO<sub>2</sub> Concentration at 700 mb Level Near Hawaii

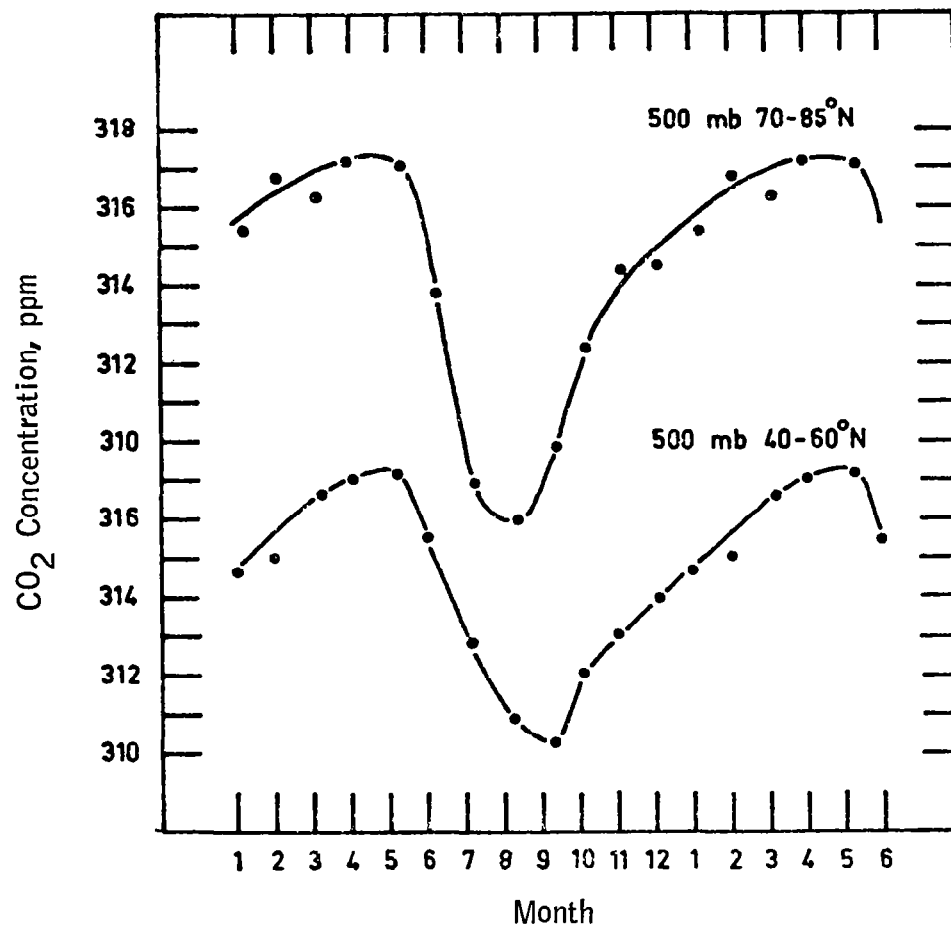


Figure 39. Concentration of Atmospheric CO<sub>2</sub> at 500 mb Level and Latitudes Between 40 and 60°N and Between 70 and 85°N as Functions of the Month of the Year

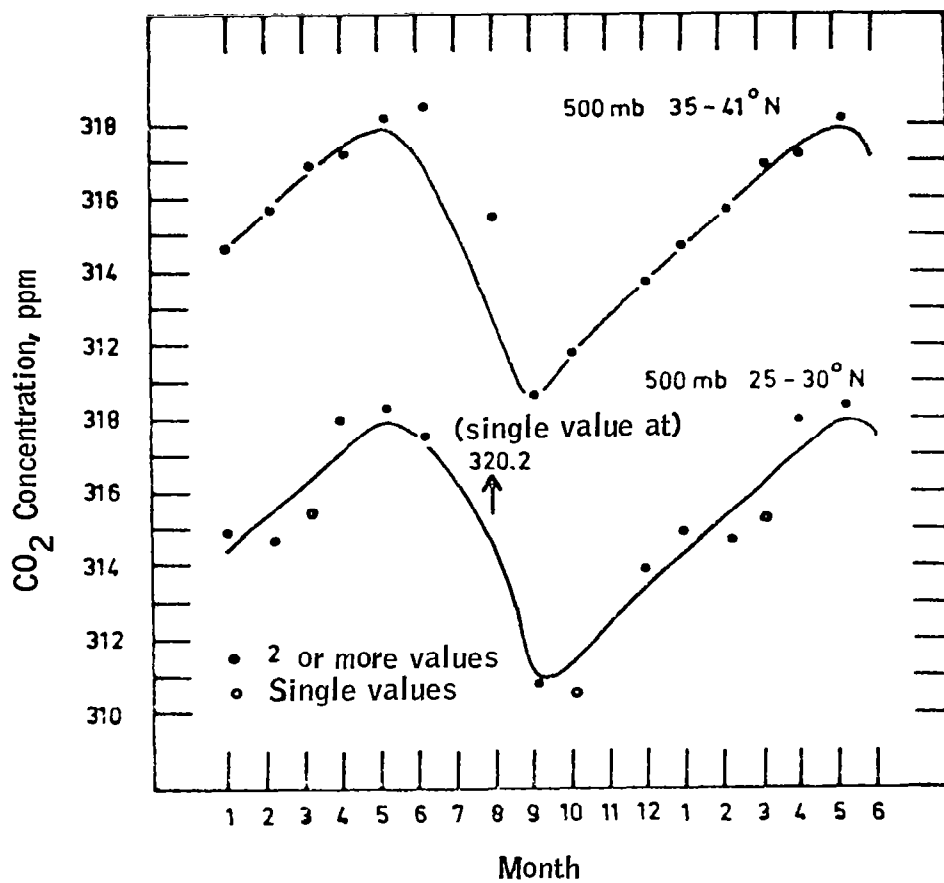


Figure 40. Concentration of Atmospheric CO<sub>2</sub> at 500 mb Level and Latitudes Between 25 and 30°N and Between 35 and 41°N as Functions of the Month of the Year

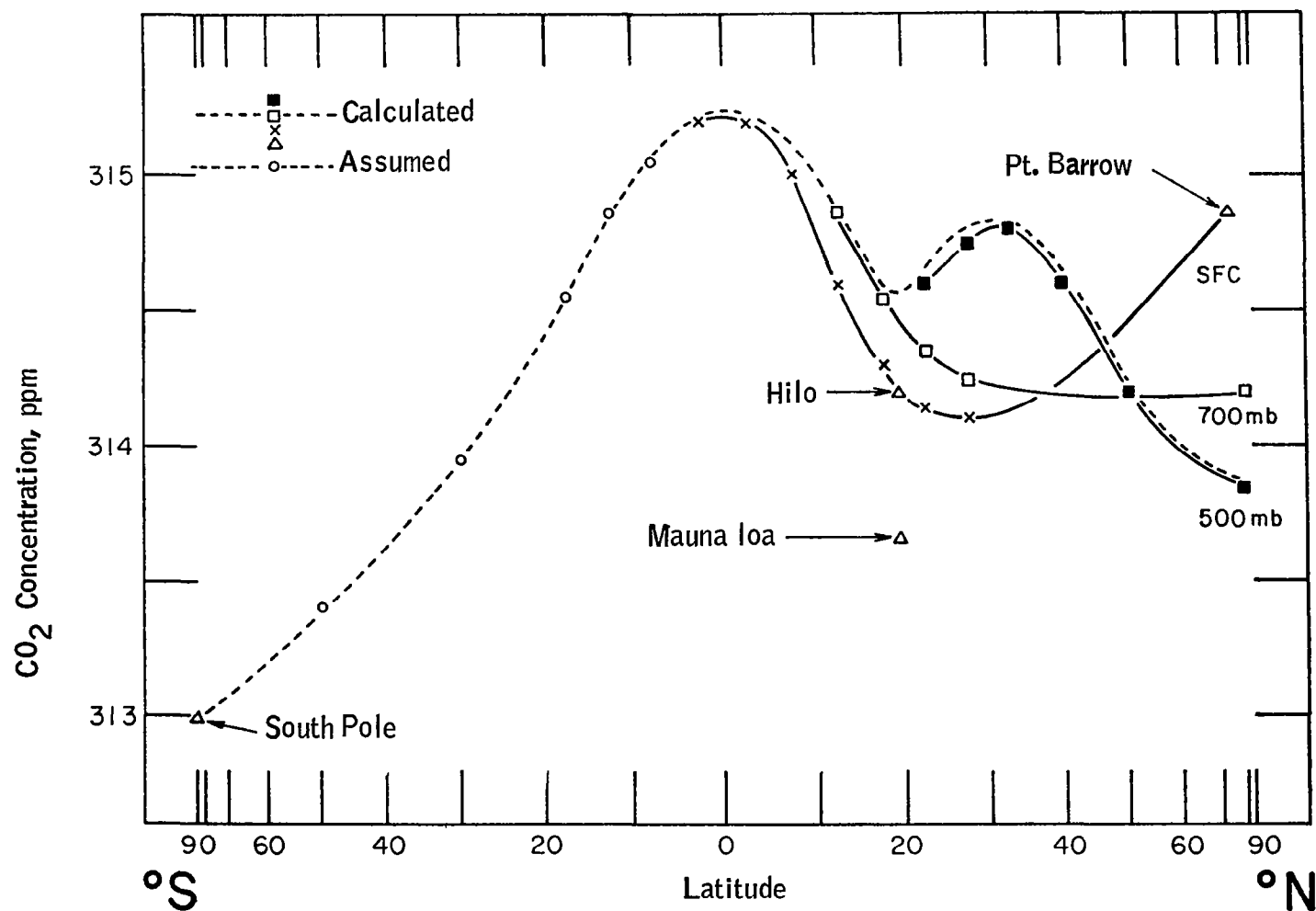


Figure 41. Annual Average Concentration of Atmospheric CO<sub>2</sub> as a Function of Latitude at the Surface, at 700 mb and at 500 mb

The variation of CO<sub>2</sub> concentration with latitude and month of the year is shown in Table 22. The annual average concentration of atmospheric CO<sub>2</sub> as a function of latitude at the surface, at 700 mb, and at 500 mb is shown by the symbols X, open square, and solid square, respectively; plotted points from 5° to 85°S are shown by open circles and are assumed values. These data are based upon CO<sub>2</sub> observations at 500 mb and 700 mb for the Northern Hemisphere and near the surface for the Southern Hemisphere. The seasonal variation increases with latitude from a range of about 1 ppm at the South Pole to about 9 ppm at high latitudes of the Northern Hemisphere. This latitudinal variation of annual range of CO<sub>2</sub> concentration is due to the large amounts of land vegetation in the Northern Hemisphere. In the Northern Hemisphere the maximum CO<sub>2</sub> concentration generally occurs in late spring and the minimum concentration generally occurs in late summer and early fall.

Since it is located far from industrial and vegetated areas, the South Pole is an excellent place to measure CO<sub>2</sub> concentrations for the purpose of deducing the long term atmospheric CO<sub>2</sub> increase due to combustion of fossil fuels on a world wide scale. Table 23 shows the results of CO<sub>2</sub> concentrations at the South Pole during the years 1958, 1960, 1961, 1962, and 1963. These data indicate that the mean atmospheric CO<sub>2</sub> concentration is rising at a rate of 0.68 ppm per year.

### VERTICAL VARIATIONS

The overall vertical variations of CO<sub>2</sub> concentration is small except near the Earth's surface. From Figure 31 we notice that the maximum CO<sub>2</sub> concentration near the vegetation surface is about 400 ppm, and the corresponding CO<sub>2</sub> concentration at 100 m is only 330 ppm, the maximum difference being about 70 ppm. One may speculate as to the cause of this difference that in the morning after the convection currents are established, there is a steady vertical transfer of CO<sub>2</sub> from the surface to higher elevations. This transfer diminishes and reaches a nearly steady-state condition in the afternoon, and results in a uniform CO<sub>2</sub> concentration with height. These results are believed to represent the vertical CO<sub>2</sub> variations for the planetary boundary layer in a vegetation area.

Observations of the vertical variation of CO<sub>2</sub> concentration for other areas are available in the limited regions of the Earth, such as Scandinavia. These measurements are usually taken from either aircraft (refs. 35, 37, 38, and 39) or constant level balloons (ref. 40).

The annual average value of CO<sub>2</sub> concentration in Scandinavia from 0 to 3 km is shown in Table 24. It can be seen that the CO<sub>2</sub> concentration near the surface is about 318 ppm, and the concentration decreases sharply to 314 at 0.4 to 0.6 km. From this level up, the change is rather small.

According to Bischof (ref. 39), the effects of the surface variation of the CO<sub>2</sub> concentration can extend up to tropopause. The temperature inversion at the tropopause tends to suppress any further vertical mixing. These observations

TABLE 22.- SMOOTHED AVERAGE VALUES OF THE CO<sub>2</sub> CONCENTRATION  
ppm , BY LATITUDE AND MONTH  
[ref. 35]

	Jan.	Feb.	March	April	May	June	July	Aug.	Sept.	Oct.	Nov.	Dec.	Average
78.0°N	315.7	316.4	316.9	317.2	317.2	315.5	309.9	308.0	308.8	311.8	313.7	315.0	313.85
50.0°N	314.8	315.7	316.5	317.1	317.3	315.5	313.0	311.2	310.3	311.9	313.0	313.9	314.2
40.0°N	314.6	315.6	316.5	317.3	317.9	317.1	315.2	312.6	310.6	311.7	312.7	313.7	314.6
32.5°N	314.5	315.4	316.3	317.3	318.0	317.6	316.0	313.7	310.9	311.5	312.6	315.6	314.8
27.5°N	314.4	315.3	316.1	317.1	317.9	317.5	316.3	314.3	311.1	311.4	312.5	313.5	314.8
22.5°N	314.2	315.1	315.9	316.6	317.2	317.0	316.4	314.8	311.5	311.3	312.3	313.3	314.65
17.5°N	314.1	314.9	315.6	316.2	316.7	316.6	316.3	315.1	312.3	311.3	312.2	313.2	314.55
12.5°N	314.3	314.8	315.4	315.9	316.3	316.4	316.2	315.4	313.7	312.9	313.2	313.8	314.85
7.5°N	314.6	315.0	315.4	315.8	316.1	316.3	316.1	315.5	314.5	313.9	313.8	314.2	315.1
2.5°N	314.8	315.1	315.4	315.7	316.0	316.2	316.0	315.6	315.0	314.3	314.0	314.4	315.2
2.5°S	314.8	315.1	315.35	315.6	315.85	316.05	316.0	315.6	315.0	314.3	314.1	314.4	315.2
7.5°S	314.6	314.9	315.15	315.4	315.65	315.9	315.9	315.6	314.9	314.3	314.1	314.3	315.05
12.5°S	314.3	314.6	314.85	315.1	315.4	315.7	315.8	315.55	314.8	314.2	314.0	314.1	314.85
17.5°S	313.8	314.1	314.4	314.8	315.2	315.6	315.7	315.5	314.8	313.7	313.5	313.6	314.55
30.0°S	312.7	312.6	312.8	313.9	314.7	315.2	315.4	315.4	314.8	313.8	313.1	312.8	313.95
50.0°S	312.7	312.3	312.0	312.8	313.6	314.0	314.3	314.5	314.3	313.9	313.5	313.1	313.4
90.0°S	313.0	312.6	312.4	312.4	312.5	312.8	313.2	313.4	313.5	313.6	313.5	313.3	313.0
Average	313.37	314.67	315.11	315.66	316.09	315.94	315.16	314.22	312.49	312.43	312.28	313.89	314.51

TABLE 23.- MONTHLY AVERAGE CONCENTRATION OF ATMOSPHERIC  
CARBON DIOXIDE AT LITTLE AMERICA IN 1960 THROUGH 1963  
[ref. 36]

1958			1960		1961		1962		1963	
Month	No. of days	Concentration, ppm	No. of days	Concentration, ppm	No. of days	Concentration, ppm	No. of days	Concentration, ppm	No. of days	Concentration, ppm
January	7	310.86					11	314.70	31	315.23
February	27	310.77					27	314.48	28	314.97
March	31	311.05					30	314.26	29	314.57
April	30	311.35					30	314.31	18	315.31
May	30	211.68	4	313.40	13	313.56	28	314.36	30	315.64
June	30	311.86	30	313.08	30	313.56	20	314.48	25	315.58
July	31	311.92	10	313.56	31	313.64	28	314.48	28	315.60
August	30	312.61	18	313.53	23	314.03	31	314.80	24	315.64
September	28	312.90			19	314.34	28	315.21	22	315.74
October	29	312.81			18	314.96	29	316.01	16	316.30
November	3	312.25			30	315.07	16	316.23		
December					30	314.89	31	315.71		
Annual mean		311.82		313.39		314.26		314.92		315.46

TABLE 24.- MEASUREMENTS OF CO<sub>2</sub> CONCENTRATION IN  
SCANDINAVIA FROM 0 to 3 km  
[ref. 37]

Height, km	Number of measurements	Lower and upper limit of concentration CO <sub>2</sub> , ppm	Average of all values, ppm
0 -0.2	51	306-340	318
0.2-0.4	31	300-329	316
0.4-0.6	19	305-327	314
0.6-0.8	10	304-325	314
0.8-1.0	13	305-322	315
1.0-1.2	12	309-320	313
1.2-1.4	5	309-318	312
1.4-1.6	12	309-321	316
1.6-1.8	9	308-319	312
1.8-2.0	4	307-319	315
2.0-2.2	7	308-320	314
2.2-2.4	--	---	---
2.4-2.6	3	310-319	315
2.6-2.8	4	310-317	312
2.8-3.0	6	308-320	315
1.0-3.0	62	307-321	314

from jet aircraft at a 10 km level indicate that the concentration in the stratosphere is about 4 ppm lower than the same height in the troposphere. It is important to mention that the observations are made in different locations on a flight path between Los Angeles and Scandinavia. Thus, the CO<sub>2</sub> concentration is about 314-315 ppm in the upper troposphere and about 310-311 ppm in the lower stratosphere. Also, because of the lack of convection and vertical mixing in the stratosphere, the time variation of the CO<sub>2</sub> concentration in the stratosphere will be less than in the troposphere.

Between 15 and 30 km, observations of the CO<sub>2</sub> concentration were made from constant altitude balloons, and the results were analyzed by Hagemann, Gray, Jr., Machta and Turkevich (ref. 40). They conclude that the CO<sub>2</sub> concentration is about 312, 310, 313, and 310 ppm for the levels 15.5, 20.0, 24.8, and 28.0 km, respectively. The standard error of a single observation is about 0.5 to 1.0 percent. The average value for all cases is about 311 ppm with an average deviation of less than one percent and a range of  $\pm 2$  percent.

No measured CO<sub>2</sub> concentrations are available above 30 km. One would expect the concentration at higher elevations to be about the same as the value observed at 20 km.

Another aspect of the problem is the possible dissociation of the CO<sub>2</sub> molecule by ultraviolet radiation at 1600 Å. Bates and Witherspoon (ref. 41) have considered this problem theoretically. Their calculations indicate that the lifetime of the CO<sub>2</sub> molecule is extremely long at 90 km, which suggests that dissociation effects are not important at this level. Above 90 km, the probability of dissociation increases with height. On the basis of these findings, the possible dissociation of the CO<sub>2</sub> molecule can be neglected in the horizon radiance problem.

#### STANDARD PROFILE OF MEAN CO<sub>2</sub> CONCENTRATION AND VARIATION

Based on the results in the preceeding subsections, a standard atmosphere profile of CO<sub>2</sub> concentration has been constructed and is shown in Figure 42. The CO<sub>2</sub> concentration decreases somewhat from the surface up to 1 km level. The vertical variation in the troposphere and stratosphere are relatively small. Near the tropopause, which we assume is at 10 km, there is another small decrease of CO<sub>2</sub> concentration.

If we assume that the value of the CO<sub>2</sub> concentration at 5 km, 314 ppm, is representative of the average for the whole atmosphere, then the concentration at 0.1 km is about 2.2 percent higher than the average and the concentration at 30 km is about 1.0 percent lower than the average. A reasonable estimate of the average vertical variation of the CO<sub>2</sub> concentration about the mean value is about  $\pm 1$  percent.

Estimates of the average deviation of CO<sub>2</sub> concentration about the mean values are also indicated in Figure 42. The average deviations in the stratosphere

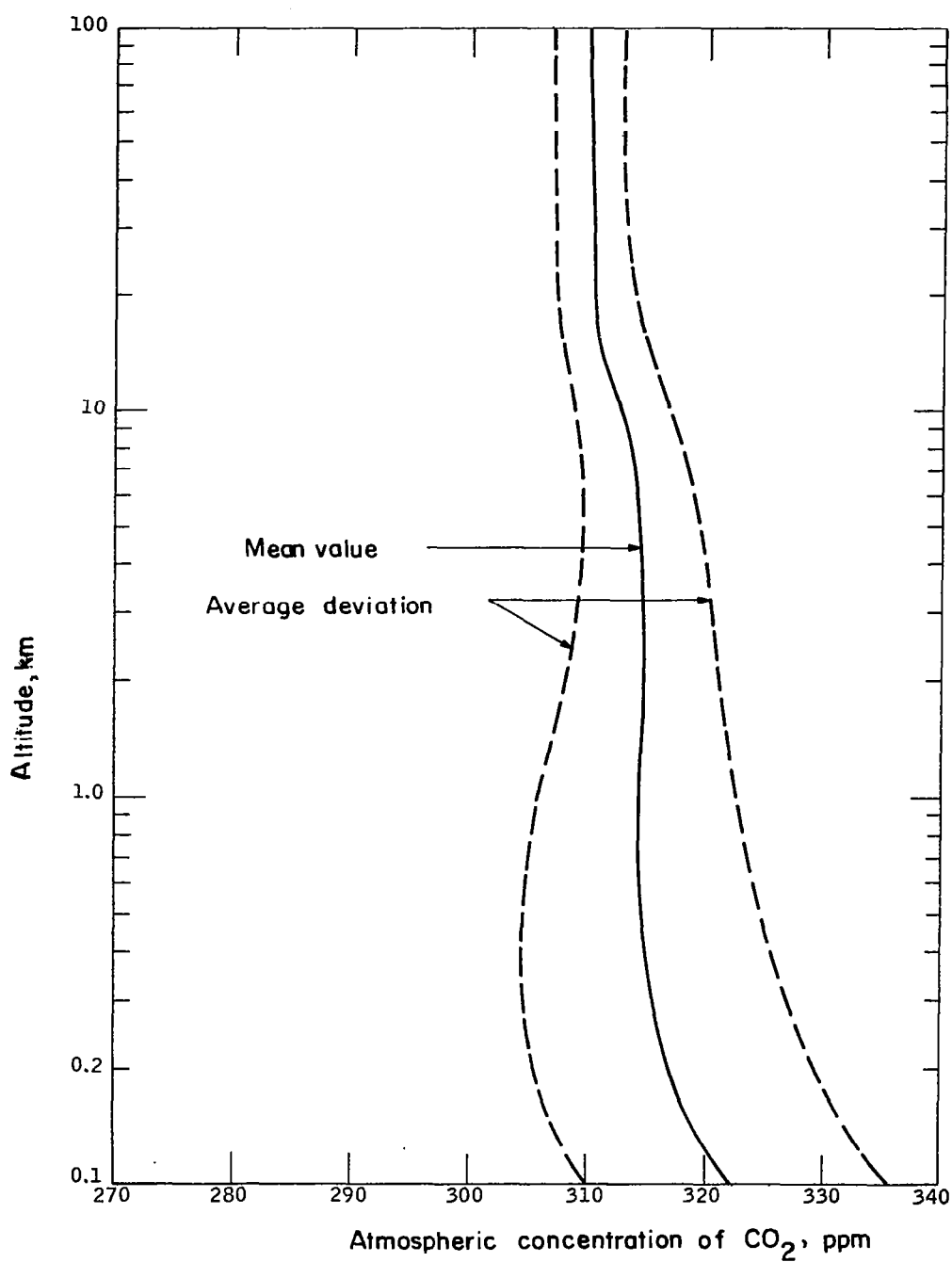


Figure 42. Estimated Mean CO<sub>2</sub> Concentration and Average Deviation of CO<sub>2</sub> Concentration as a Function of Height

are based upon the observations of Hagemann, et al., (ref. 40). The average deviations for the troposphere are based upon a gross interpretation of the values presented in previous sections of this report. Above a height of 1 km, the average deviation of CO<sub>2</sub> concentration is less than  $\pm 3$  percent.

## CLOUD CHARACTERISTICS AND FREQUENCIES OF OCCURRENCE

The objective of this portion of the study is to provide a body of background information relating to cloud characteristics and frequencies of occurrence. This information serves as the basis for evaluating the effects which cloudiness may produce upon the reliable determination of horizon radiance profiles. These effects will be discussed in Effects of Temperature, CO<sub>2</sub> Concentration and Clouds Upon Horizon Radiance Profiles section; the discussion here will cover (1) radar observations of cloud tops, (2) climatological frequencies of cloud occurrence, (3) cloud observations from meteorological satellites, and (4) suggested approach for further cloud studies.

The highest clouds occur in severe thunderstorm situations in mid-latitudes, in the intertropical convergence zone in the tropics, and in the heavy monsoon cloud buildups over Southeast Asia. De (ref. 42) observed a thunderstorm on radar at Calcutta which extended to 22 to 23 km height during the pre-monsoon season of 1958. Arnold (ref. 43) reported radar clouds at 23 km in Texas during the spring of 1960. Clouds in a severe thunderstorm situation at Minneapolis, Minnesota on 10 July 1966 were observed by a WSR-57 radar to be present at 21 km. Several times during the summer of 1966 thunderstorm clouds were observed above 80 000 feet at Minneapolis. Vonnegut and Moore (ref. 44) estimated the maximum cloud top of the Worcester, Massachusetts tornado of 1953 to extend to 20 km. Since the visual cloud top usually exceeds the radar cloud top by approximately one kilometer (refs. 45 and 46), these radar cloud heights must be adjusted accordingly.

It must be emphasized that the above reports of extreme cloud heights are isolated cases; they merely indicate what is possible on a local basis in exception situations, but do not represent necessarily frequent or widespread occurrences. In cases where the cloud tops are unusually high, they penetrate the tropopause by 6 km or more. At these times the tropopause is probably weak and ill-defined; in fact, the existence of a tropopause at all may be questionable within a very high cloud mass.

The cases cited above represent some extreme values of cloud heights reported in the literature and are by no means representative of the usual occurrence. However, De (ref. 45) has examined frequencies of clouds above 10 km at Dum Dum Airport, Calcutta, between March-June 1961. (May and June represent the beginning months of the summer monsoon at this location). During these four months, 188 instances of cloud tops above 10 km were observed. The specific monthly occurrences were: March, 29; April, 10; May, 61; June, 88.

The increase in high cloud top occurrences during May and June undoubtedly reflects the increased monsoon activity. Tiros III window measurements reported by Rasool (ref. 47) indicated very low temperatures over East Pakistan in the period 1 July through September 1961 thus implying a heavy cloud cover of high vertical extent due to monsoon activity. (A quasipermanent

cloud over Central Africa also was indicated from Tiros III measurements; this is no doubt associated with convective activity in the intertropical convergence zone).

Solomon (ref. 48) has prepared a study of the frequency of cloud occurrences of various amounts within 5000 foot sections of the atmosphere. Figures 43 and 44 show the percentage frequency of 6/10 through 10/10 cloud cover at altitudes greater than 9 km in January and July, respectively. During both winter and summer the frequency of cloudiness above 9 km is shown not to exceed 10-20 percent over the predominant portion of the Northern Hemisphere. The frequency does markedly increase during summer in two general areas: (1) the region including Central America, the Caribbean, and Southeastern United States, and (2) the region including Southeast Asia, Indonesia and the Philippines. The effects of the summer Asiatic monsoon are very pronounced over India and the Bay of Bengal, where extensive high cloudiness occurs more than 80 percent of the time, as compared to wintertime values of less than 10 percent.

It is apparent, therefore, from Figures 43 and 44, that there are significant geographical and seasonal variations in the percentage of high cloud cover above 9 km.

As noted earlier in this section, Tiros III window measurements have been used to deduce high cloud cover from the observation of very low temperatures over certain areas. The Nimbus I and II satellites also provided powerful tools for studies of cloud top heights from black body temperature measurements in the atmospheric window.

According to radiometric measurements in the window region, Nimbus I showed, on one occasion, a cloud top at 16 km in the intertropical convergence zone, based upon a cloud top temperature of 190°K, (ref. 49) and a sea surface temperature in the same region of 293°K, as shown by the radiometric data. Window measurements of Hurricane Gladys made from Nimbus I showed that cloud tops in the spiral bands were at 14 km; clouds of lesser vertical extent were observed between the spiral bands.

Nimbus II, launched on 15 May 1966, provided, in addition to 800-line vidicon cloud pictures, radiometric data in the window region (10-11 microns) and in the CO<sub>2</sub> absorption band (14-16 microns), measured by the Medium Resolution Infrared Radiometer (MRIR). The presence of clouds can be determined from the CO<sub>2</sub> channel data and the cloud top heights from the window channel data (the heights are calculated on the basis of radiometric temperature measurements in the window channel and the temperature-height profile determined from radiosonde data).

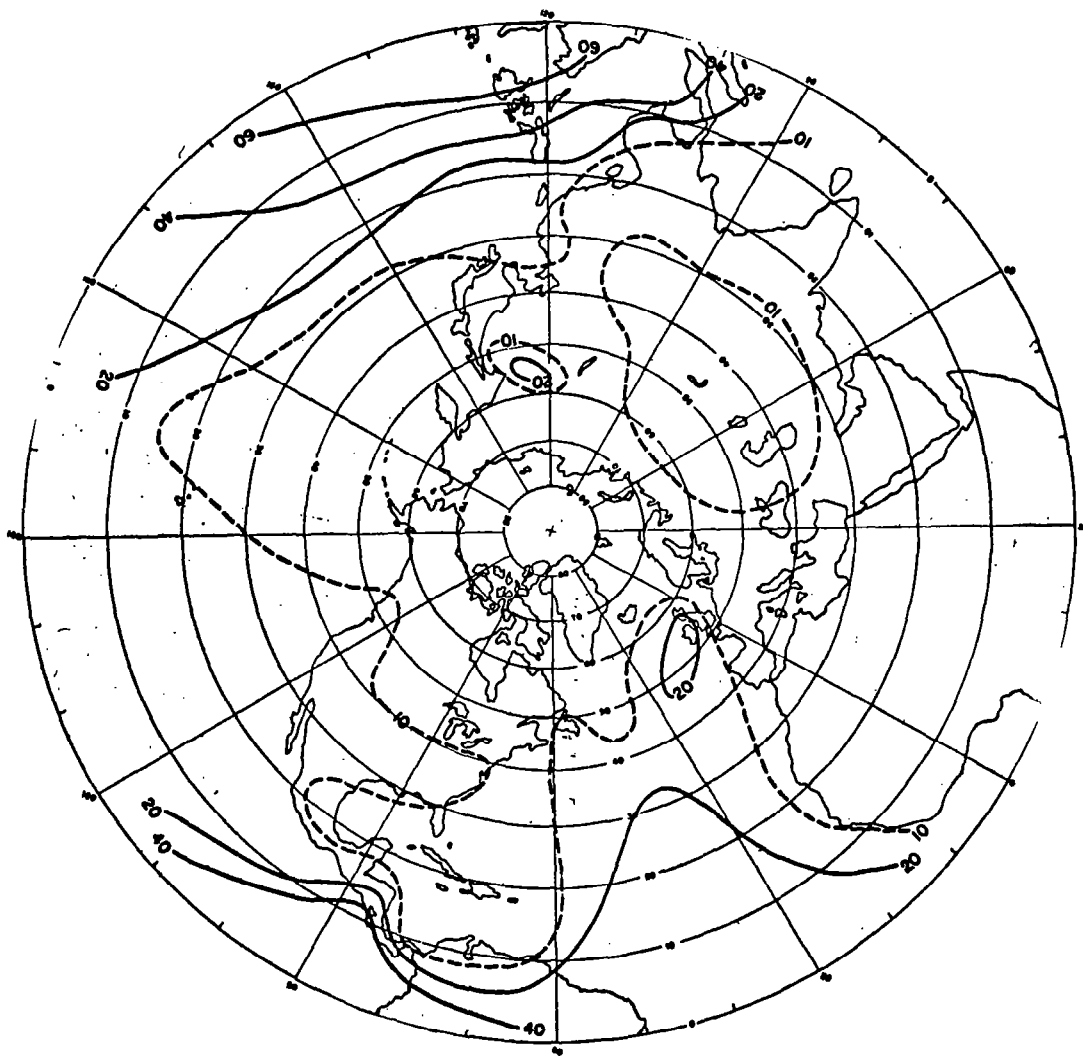


Figure 43. Percentage Frequency of 6/10 Through 10/10 Cloud Cover - Greater Than 9 km, January

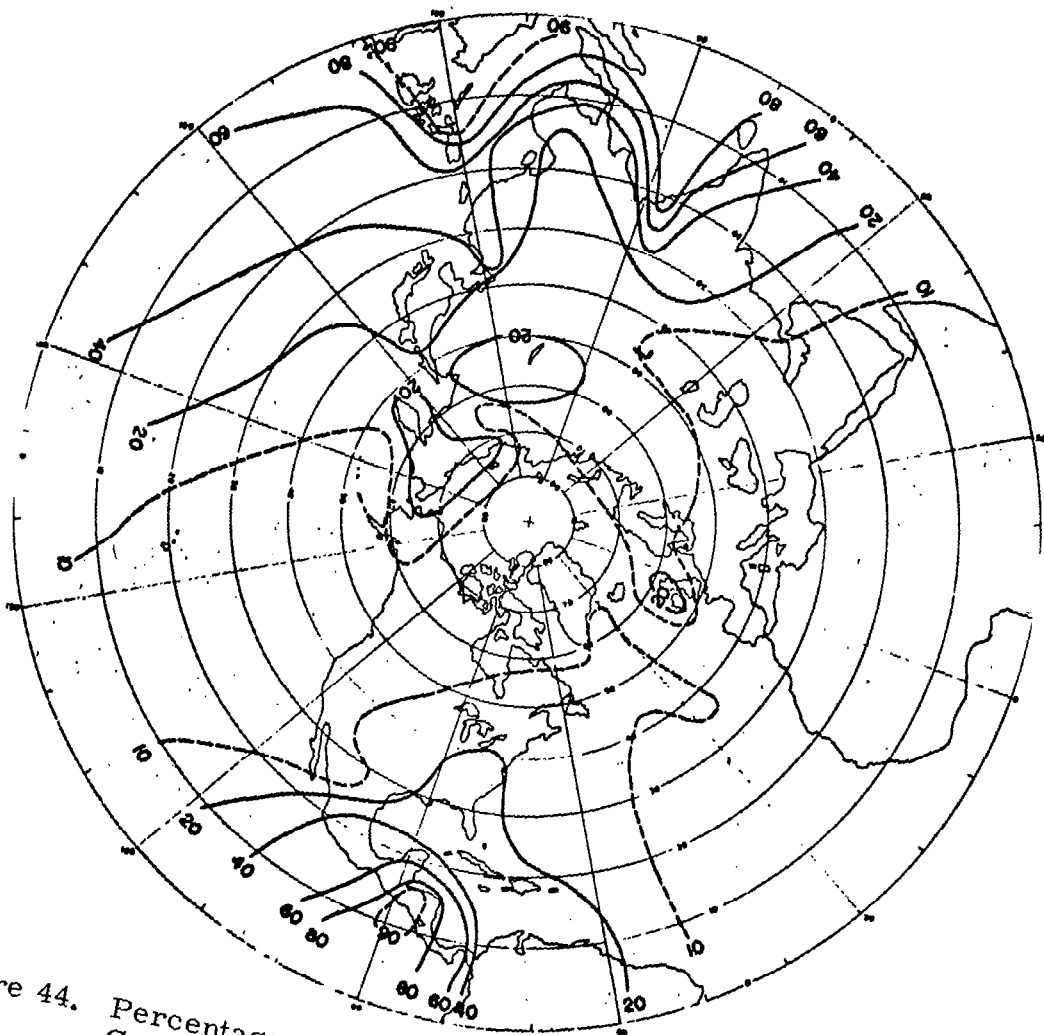


Figure 44. Percentage Frequency of 6/10 Through 10/10 Cloud Cover - Greater Than 9 km, July

Figure 45 is a pictorial representation of a sample of MRIR 14-16 micron channel data taken from Nimbus II on 19 May 1966. The pictorial representation is in the form of a strip approximately 1250 miles wide extending from pole to pole. Latitude and longitude lines are superimposed at 10 degree intervals to permit rapid location of areas of interest. For pictorial representation of the 14-16 micron channel the gray scale is selected so that low radiance is shown on the white end of the scale and high radiance at the black end. Hence clouds, which are colder than the earth's surface, appear white, and the whiter the clouds, the higher and denser they are presumed to be. Of special interest in Figure 45 is the cloud area at 3°S and 103°E over the island of Sumatra. This cloud, which shows up clearly on the CO<sub>2</sub> and window channels, is an excellent example of high cloud buildups in the equatorial region. (Actual radiosonde data were not available at the time of this study to provide temperature-height profile data for estimating the cloud height from the cloud-top radiometric temperature, but on the basis of the radiometric cloud top temperature of 198°K and the temperature-height profile for the mean tropic atmosphere, the cloud top height is estimated to be at about 15km).

Figure 46 shows the record of the channel 2 (10-11 micron) and channel 3 (14-16 micron) output associated with this high cloud area over Sumatra. On this graph, higher values of voltage indicate lower values of radiance. The cloud top temperature of 198°, based upon channel 2 window measurements for the encircled high cloud area, represents a 13° C drop in black body temperature and corresponds to a 24 percent reduction in radiance. However, since this cloud is in the nadir portion of the radiometer scan, less reduction in radiance would be expected for a cloud on the horizon, depending upon the nadir angle (see the next section for information regarding the radiance reduction produced by clouds as a function of cloud top height and nadir angle). The Brush chart record also indicates that there are some lower and warmer clouds present on either side of the high cloud, but their effects on the 14-16 micron channel are negligible, as can be seen by the relative flatness of the trace on either side of the encircled high cloud area.

Analysis of previous synoptic studies of cloud height and coverage has shown that Nimbus data has significant advantages in terms of (1) providing wide geographic distribution, and (2) including many different kinds of weather situations within one integrated body of data. Previous cloud studies have suffered from the fact that pilot reports of cloud tops are sporadic, and for high clouds above 10 km are even more infrequent. In addition, radar reports of cloud tops are only available on a local, limited basis. Previous cloud studies have not been able, therefore, to provide reliable information on the areal extent or distribution of high clouds on a global basis.

In order to provide a comprehensive and systematic analysis of global cloud characteristics, available Nimbus data could be analyzed in the following manner:

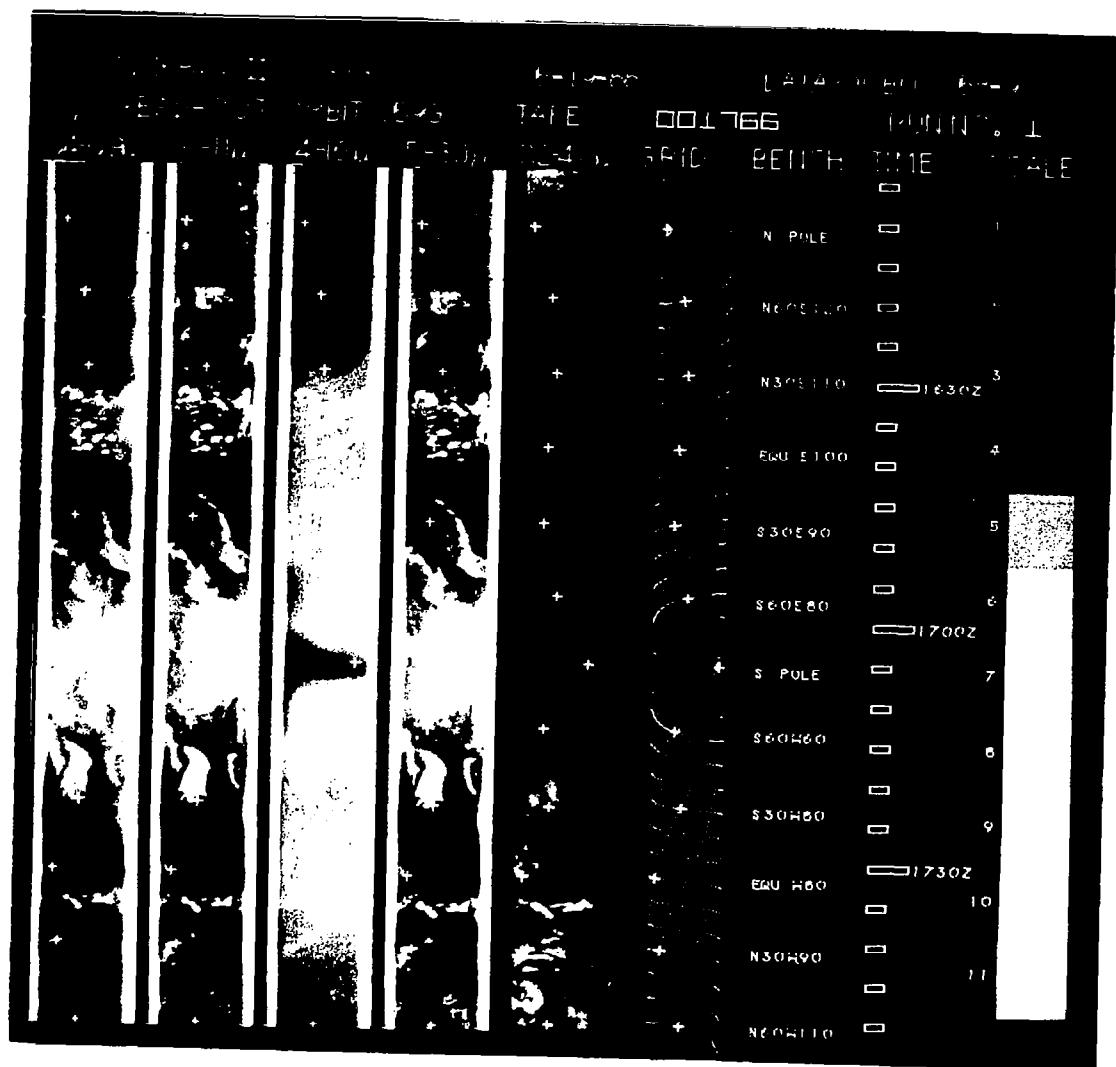


Figure 45. Pictorial Presentation NIMBUS II MRIR Orbit 59

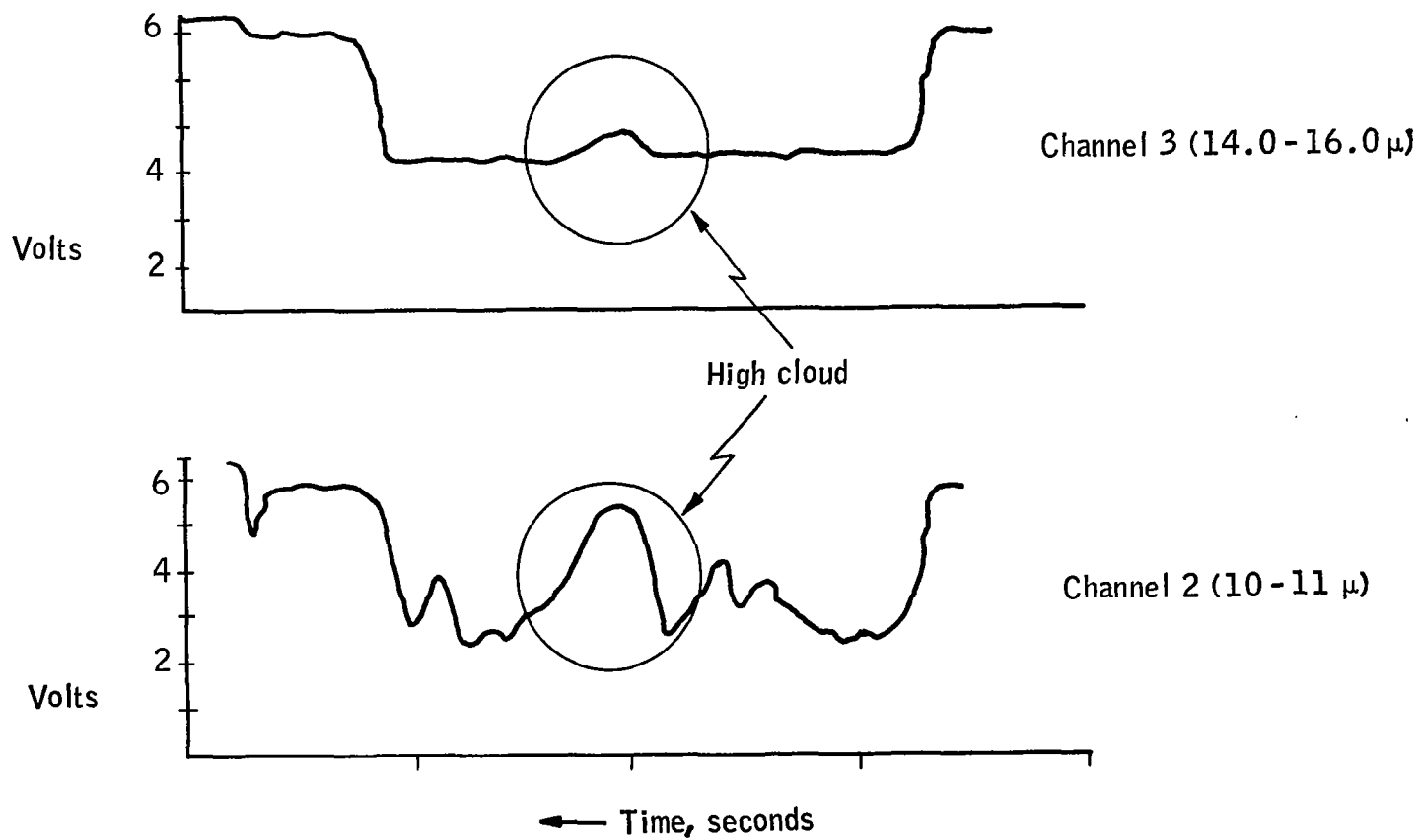


Figure 46. Brush Record of Channel 2 and 3 of Nimbus II on 19 May 1966 at 1639 GMT

- (1) The 14-16 micron CO<sub>2</sub> channel data could be studied in relation to the 10-11 micron window channel data to sort out those cases where cloud contamination is occurring in the CO<sub>2</sub> channel.
- (2) The magnitude of the temperature perturbation could be determined, i.e., the amount by which the black body temperature is reduced due to the presence of clouds.
- (3) The geographical dimensions of the region disturbed in the 14-16 channel could be determined.
- (4) The cloud occurrence could be related to the associated synoptic situation. Examples of such situations are intertropical convergence zones, frontal zones, easterly waves, squall lines, isolated air-mass thunderstorms, etc.
- (5) The heights and temperatures of the clouds affecting the 14-16 micron channel could be determined from radiometric and supporting radiosonde data.
- (6) The synoptic situations in (4) could be studied in terms of the temperature/pressure and horizon radiance profiles as determined from radiosonde and rocketsonde data.

By means of the approach outlined above, it would be possible not only to develop an excellent body of high cloud statistics but to tie this information in very closely to parameters which directly relate to the horizon definition problem. Thus, statistics on cloud tops associated with various synoptic situations could be obtained on a global basis, and the analysis of this information with profile data for select cases would permit the determination of the cloud effect. However, as will be subsequently shown in the next section, parametric studies of high cloud effects upon the horizon radiance profile suggest that the effects are relatively small; thus, the primary justification for the above study approach would appear to be one of basic scientific interest rather than any basic requirements for support of the Horizon Definition Study.

# EFFECTS OF TEMPERATURE, CO<sub>2</sub> CONCENTRATION AND CLOUDS UPON HORIZON RADIANCE PROFILES

## TEMPERATURE EFFECTS

The discussion here will be directed toward a qualitative explanation of the general effects that the vertical temperature structure has upon the radiance profile. The concern here will be with obvious broadscale features of the interpolated temperature profiles as they relate to general features of the horizon profiles computed from the vertical sounding data.

For purposes of general illustration, climatological cases were selected for the months of January and July at latitudes 20°N and 75°N. (These cases cover winter and summer conditions at tropical and arctic locations). Figure 47 shows the interpolated temperature profiles from a 0 - 90 km for these latitudes during January.

As compared to the 75°N profile, the 20°N profile (1) is considerably warmer from 0-13 km, (2) features a lower and colder tropopause at 16 km, (3) is considerably warmer from 22-60, with a lower stratopause at 46 km, and (4) is increasingly colder over the 60-90 km range.

Figure 48 presents the corresponding horizon profiles (over the spectral interval of 615-715 cm<sup>-1</sup>) for January at 20°N and 75°N, plotted in terms of radiance versus tangent height. The obvious feature in this figure is the large displacement in the two profile curves at 20°N, the radiance is higher for all values of tangent height, with a marked difference of 1.6 W/m<sup>2</sup>-sr at a tangent height of 23 km.

The basic question, now, is to relate significant differences in the temperature profiles shown in Figure 47 with differences in the horizon profiles shown in Figure 48. A general relationship cannot be clearly established without some brief consideration of weighting functions for CO<sub>2</sub> transmittance in the 615-715 cm<sup>-1</sup> spectral range. These weighting functions determine the relative contribution which is made by each atmospheric layer to the overall radiance measured within a given spectral range from outside the earth's atmosphere; that is, the increase in radiance associated with increase in temperature is moderated by the influence of the weighting functions. Thus, in attempting to explain the higher radiance level at 20°N relative to that at 75°N, in terms of warmer temperature profile, due account must be taken of the weighting functions.

Figure 49 presents a curve of the average weighting function in the 615-715 cm<sup>-1</sup> spectral range for zero tangent height. For the purposes of general illustration, this curve has been selected from a family of curves determined for the entire range of tangent heights from -30 to +90 km. The curves for other tangent heights exhibit considerable variation, but the weighting function

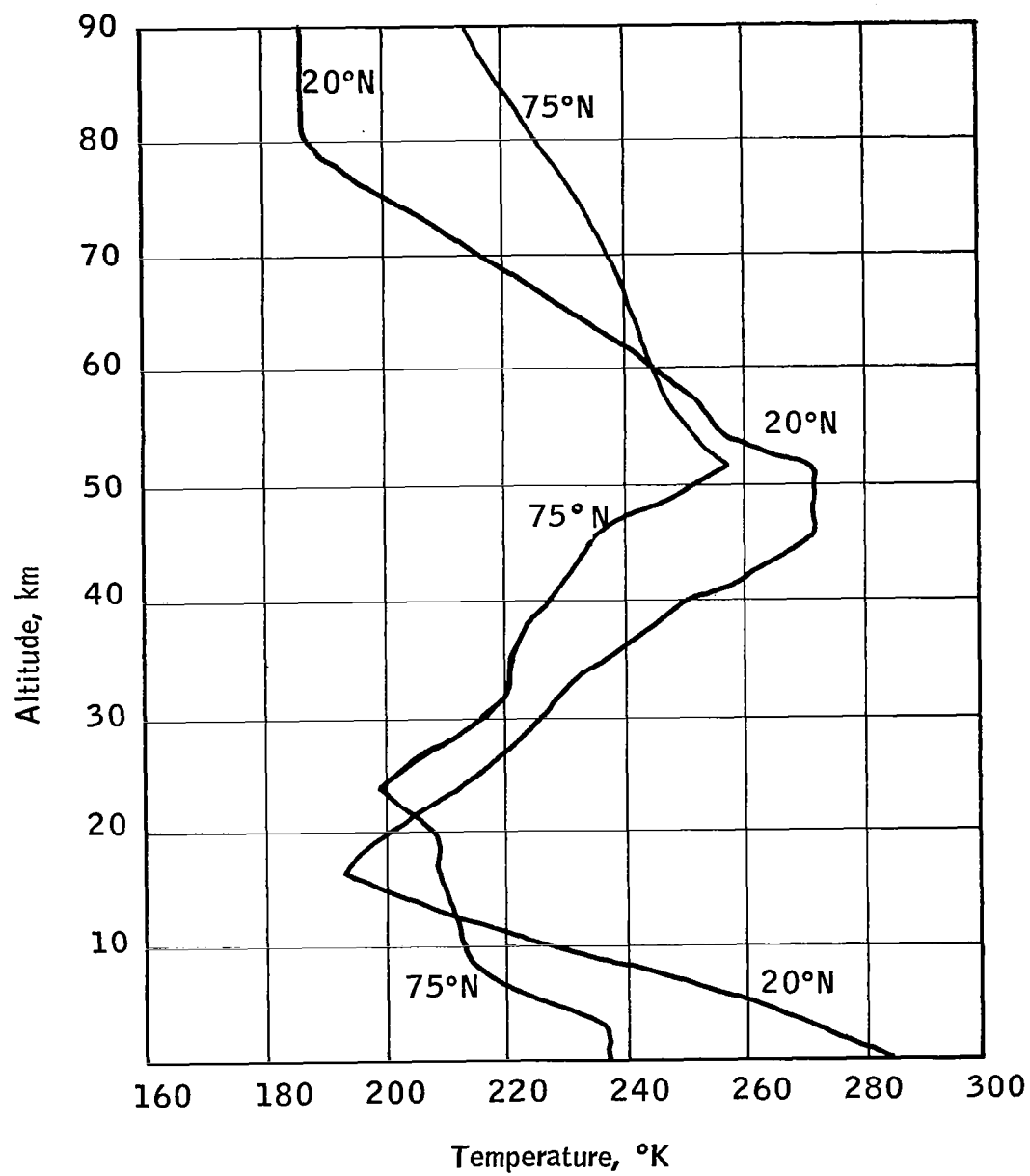


Figure 47. Mean Temperature Profiles at Latitudes 20°N and 75°N and Longitude 90°W, January

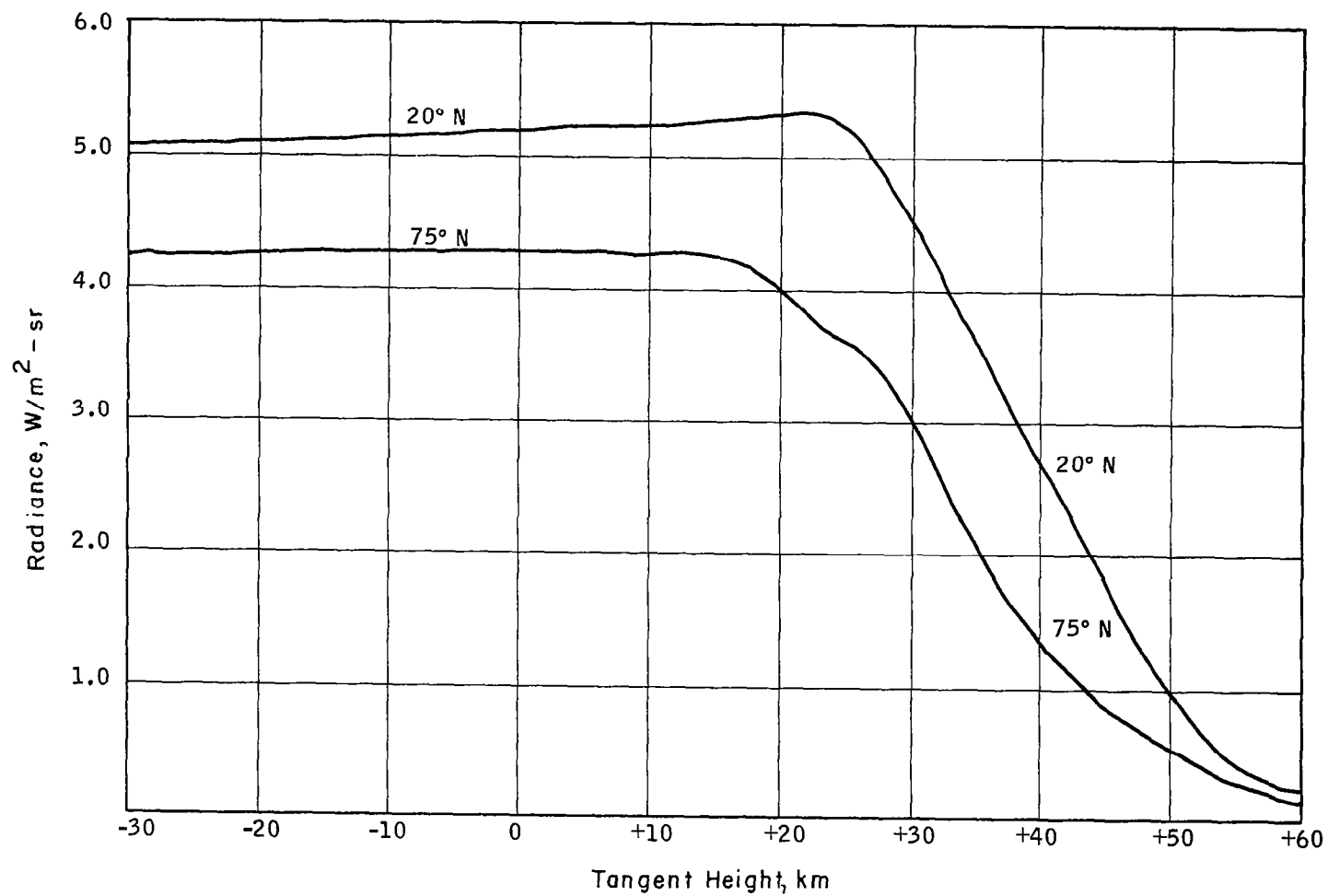


Figure 48. Fifteen Micron CO<sub>2</sub> Horizon Profiles Spectral Interval  
615 - 715 cm<sup>-1</sup>, at Latitudes 20°N and 75°N and Longitude  
90°W, January

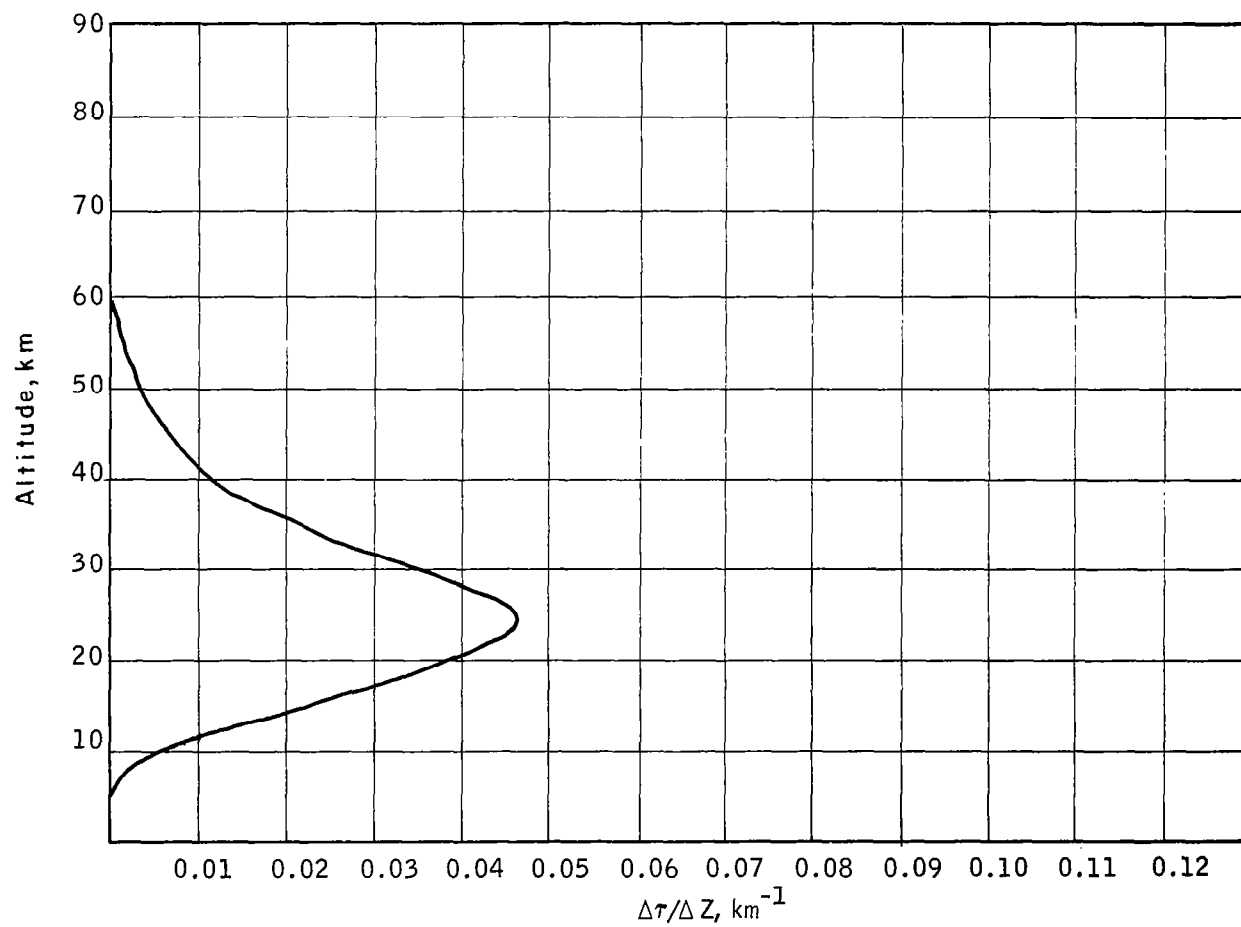


Figure 49. Average Weighting Function for Zero Tangent Height in the 615-715  $\text{cm}^{-1}$  Spectral Range

at zero tangent heights is representative for the purposes of discussion. The curve presented in Figure 49 shows that the maximum relative contribution made by temperature effects occurs between 20-30 km; below 10 km and above 50 km the relative contributions are small.

In this light, a re-examination of Figure 47 serves to readily explain the higher radiance level at 20°N, relative to that at 75°N. Between the 20-30 km, the 20°N temperature profile is warmer, and although this profile is relatively cooler in the vicinity of 15-20 km, the effect of this is more than offset by the relative warmth between 30-60 km. From 60-90 km, the 20°N temperature profile is significantly cooler than the 75°N profile, but the effect of this difference, as reflected in the horizon radiance profiles, is relatively small.

Figures 50 and 51 present a comparable set of temperature and horizon profiles at 20°N and 75°N for the month of July. It may be noted on Figure 50 that the 75°N temperature profile, overall, is considerably warmer than the 20°N profile as a result of continuous summertime heating over the polar region; the mean temperature difference is some 10-40°C warmer over the altitude interval from 10-75 km. Of particular note is the extreme temperature difference in the two profiles in the vicinity of 15-20 km. The effect of this large difference in the monthly temperature profiles is clearly reflected in the horizon profiles shown in Figure 51; the radiance at 75°N is approximately 1.4-1.7 W/m<sup>2</sup>-sr higher than at 20°N over the tangent height ranges from -30 to +20 km and is also higher over the remaining range of tangent height values.

An even more comprehensive view of the relationship between temperature and horizon profiles can be gained by plotting each set of four profiles together on a separate graph. Figure 52 shows all four temperature profiles; Figure 53, all four horizon profiles. On the former graph, it may be noted that the progression of increasingly warmer profiles over most of the stratosphere (from approximately 15-50 km) follows the following order: (1) 75°N in winter, (2) 20°N in winter, (3) 20°N in summer, and (4) 75°N in summer. Correspondingly, on Figure 53, the progression of higher-value radiance profiles follows the same order. It may be noted on the latter figure that the horizon profiles at 20°N in the tropics are relatively constant from winter to summer, whereas the horizon profiles at 75°N exhibit a large seasonal variation. The temperature profiles shown in Figure 52 clearly show the same kind of winter-summer differences at both latitudes.

The temperature sensitivity of horizon radiance profiles can also be examined parametrically by (1) selecting a sample horizon profile, (2) applying a constant plus and minus correction to the associated temperature profile, and (3) computing the corresponding radiance profiles. Figure 54, based upon one of the profiles derived for the synoptic cases, illustrates the effect produced by applying a temperature correction of ±5°C over the entire altitude range of 0-90 km. The effect upon the

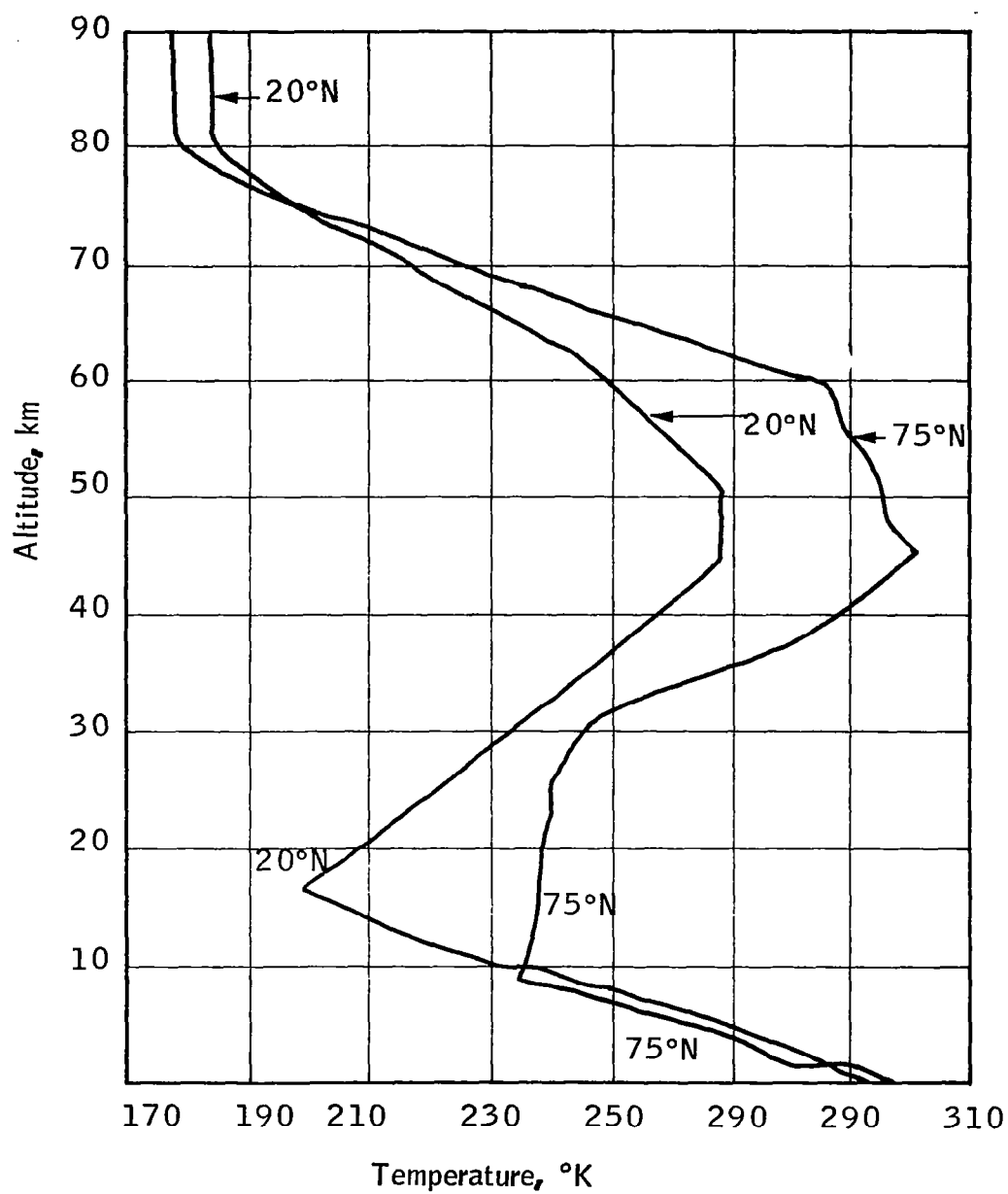


Figure 50. Mean Temperature Profiles at Latitudes 20°N and 75°N and Longitude 90°W, July

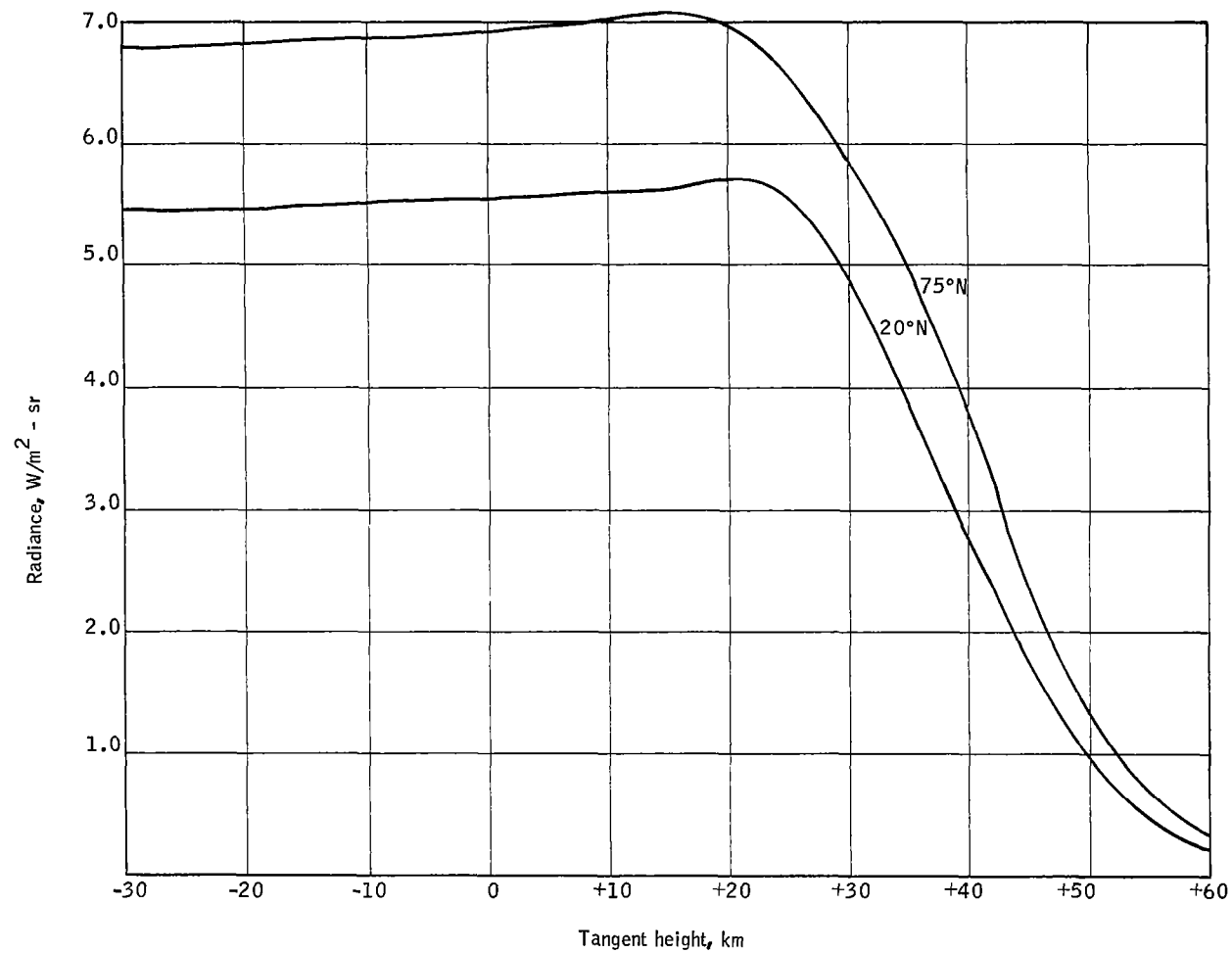


Figure 51. Fifteen Micron CO<sub>2</sub> Horizon Profiles Spectral Interval  
615 - 715 cm<sup>-1</sup>, at Latitudes 20°N and 75°N and Longitude  
90°W, July

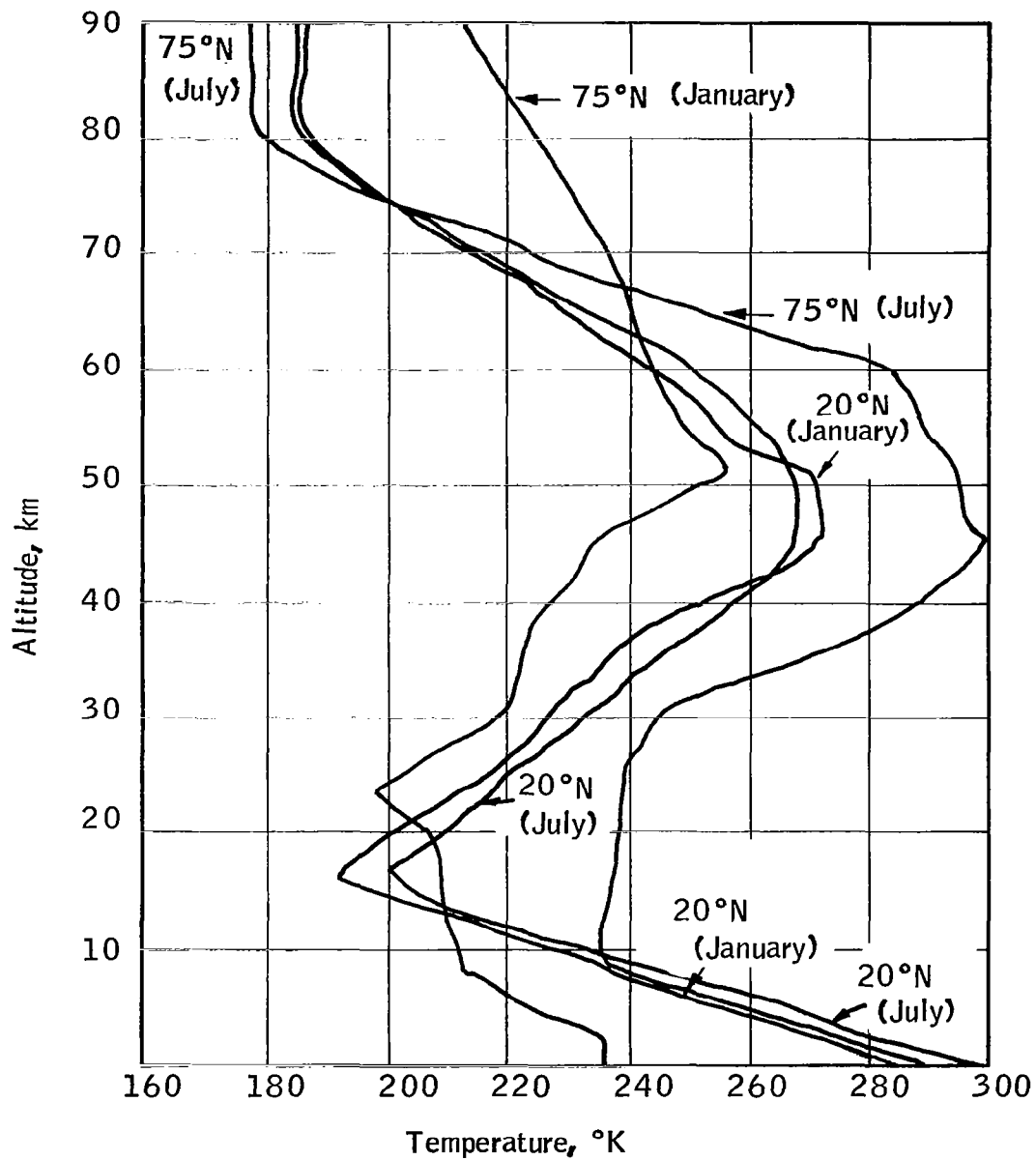


Figure 52. Temperature Profiles at Latitudes 20°N and 75°N, January and July

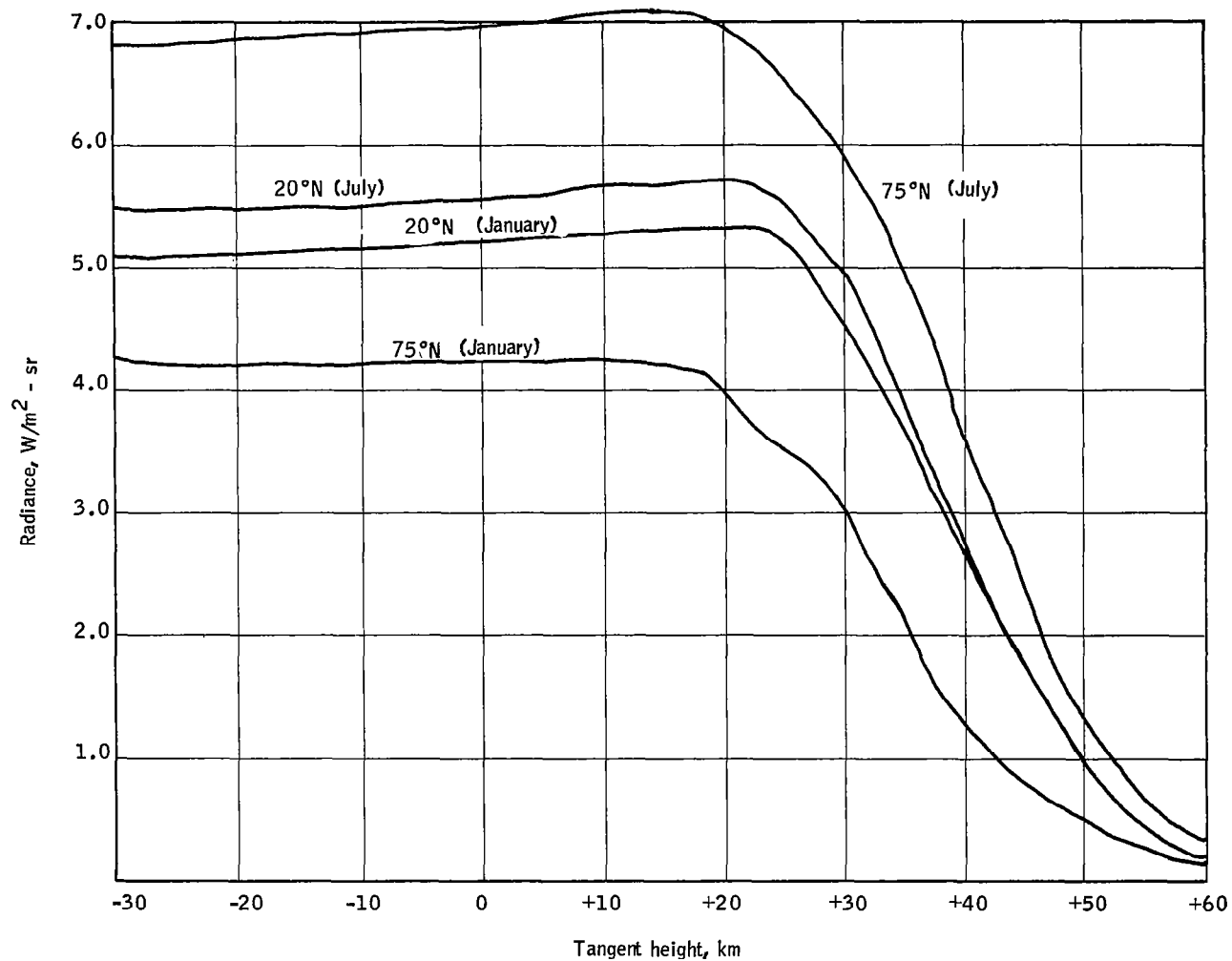


Figure 53. Fifteen Micron  $CO_2$  Horizon Profile Spectral Interval  $615 - 715 \text{ cm}^{-1}$ , at Latitudes  $20^\circ N$  and  $75^\circ N$ , January

Temperature sensitivity of horizon radiance profiles:

Spectral range:  $615 - 715 \text{ cm}^{-1}$   
Date: April 8, 1964  
Location:  $33.75^\circ \text{ N}, 105^\circ \text{ W}$   
Code number: 01010021

A temperature correction of  $\pm 5^\circ \text{C}$  was applied at each altitude. Curve #2 results from a  $+5^\circ \text{C}$  shift of the temperature profile, curve #3 from a  $-5^\circ$  shift.

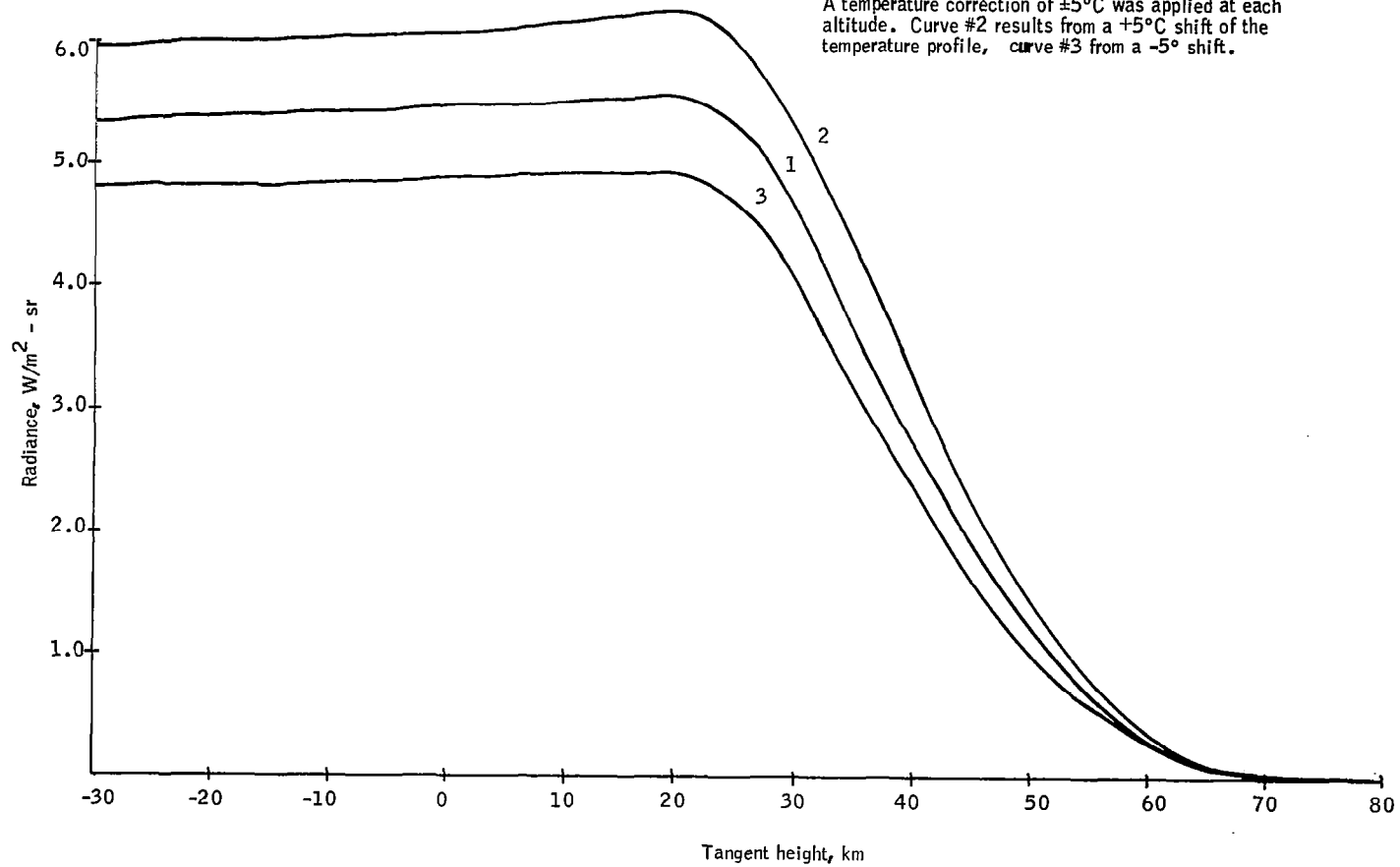


Figure 54. Temperature Sensitivity of Horizon Radiance Profiles

radiance values is to produce a relatively constant correction of  $\pm 11$  percent over the tangent height range of -30 to 10 km, and an increasing degree of percentage correction from  $\pm 11$  percent to  $\pm 20$  percent over the range from 10 to 60 km tangent height (beyond this value of tangent height the radiance values are extremely small).

### CARBON DIOXIDE EFFECTS

To investigate the effects of CO<sub>2</sub> variation on horizon radiance profiles observed in the 615-715 cm<sup>-1</sup> spectral region, a series of studies were performed in which radiance profiles were computed for various assumed vertical profiles of CO<sub>2</sub> concentration. First, a comparison was made between radiance profiles computed on the basis of (1) the mean CO<sub>2</sub> concentration profile shown earlier as Figure 42, (2) an assumed average concentration of 314 ppm throughout the 0-90 km layer. No detectable differences between the two radiance profiles could be observed. Next, a series of CO<sub>2</sub> concentration profiles, based upon  $\pm 2$  percent,  $\pm 10$  percent, and  $\pm 20$  percent variations from the mean profile shown in Figure 42, were used to compute the corresponding horizon radiance profiles. (Variations as large as  $\pm 10$  percent and  $\pm 20$  percent were shown in the CO<sub>2</sub> variation study to be beyond the realm of likelihood but were selected for illustrative purposes). No detectable differences could be observed in the horizon profiles computed for the  $\pm 2$  percent variation case. The calculated radiance profiles for the  $\pm 10$  percent and  $\pm 20$  percent cases are shown in Figures 55 and 56. It is obvious from these figures that the effects of such large (and completely unlikely) variations in CO<sub>2</sub> concentration are insignificant.

In view of the above results, a standard CO<sub>2</sub> concentration of 314 ppm throughout the entire 0-90 km layer was used as an explicit factor in the mathematical model, and no further attention was directed toward CO<sub>2</sub> variability as an implicit factor.

### CLOUD EFFECTS

Clouds may affect 15 micron horizon sensors in two ways: (1) by acting as cold radiation sources, and (2) by cutting out the CO<sub>2</sub> radiation emitted from below cloud top level. Both these factors serve to reduce the radiance measured from a satellite. Higher and, hence, colder clouds (i.e., colder up to the tropopause temperature minimum) have the greatest effect in terms of radiance reduction.

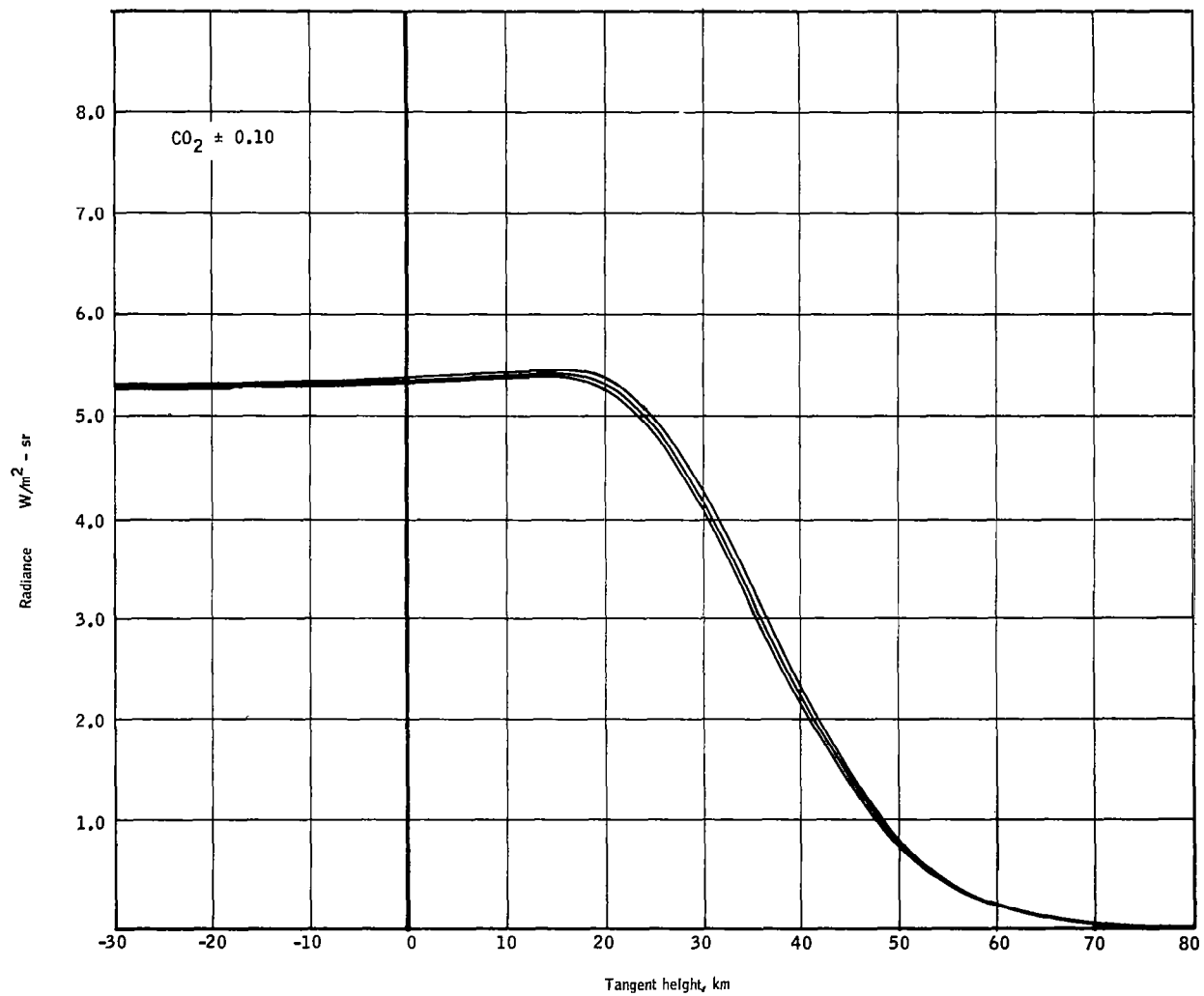


Figure 55.  $\text{CO}_2$  Concentration Effect,  $\pm 10$  Percent

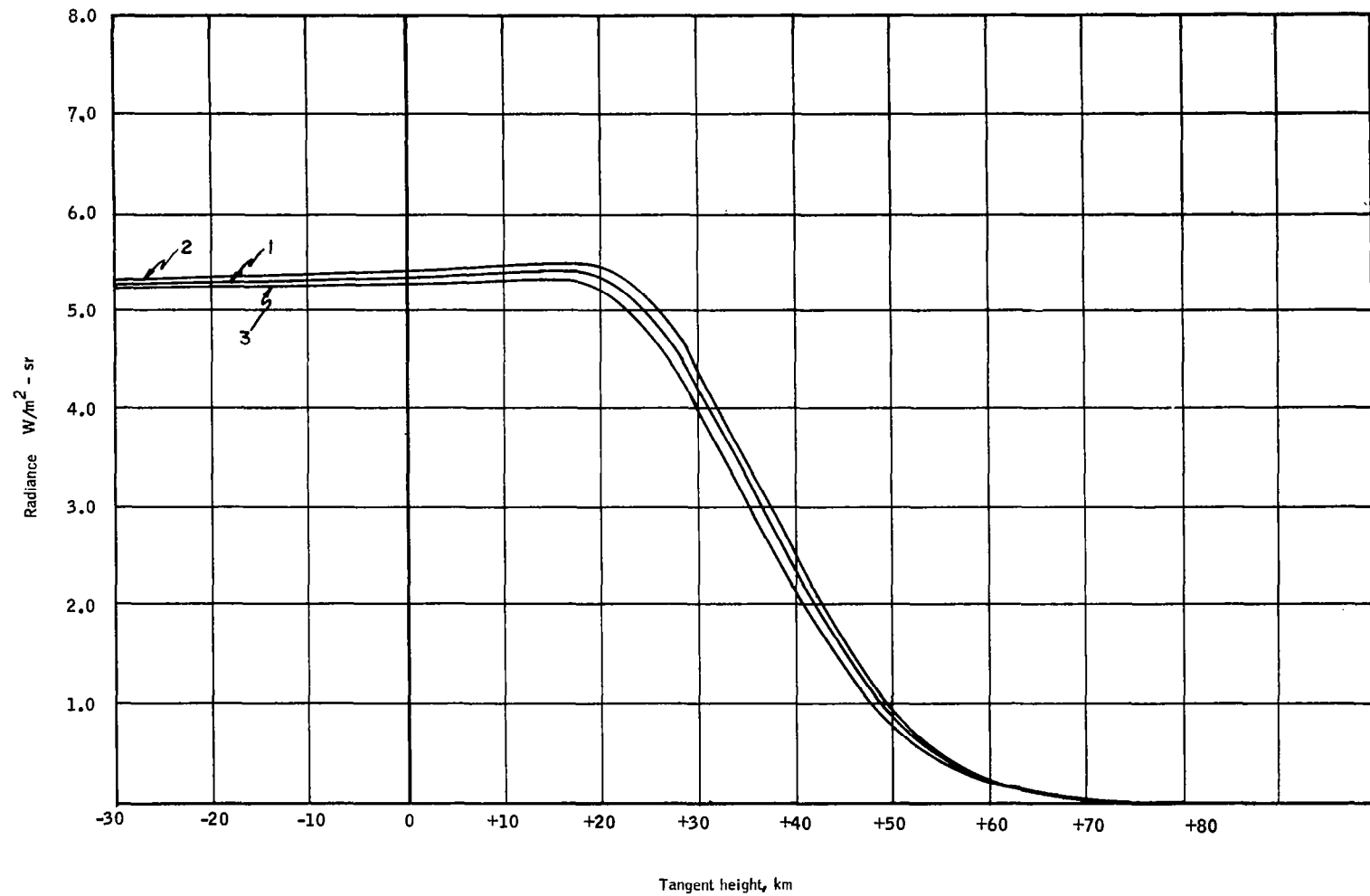


Figure 56.  $CO_2$  Concentration Effect,  $\pm 20$  Percent

The possible effects of clouds upon horizon sensors is illustrated by the problems encountered by the OGO II satellite. According to Technology Week (ref. 50), as OGO II passed over dense cloud formations, the horizon sensor at low nadir angles mistook them for cold space radiation and locked upon them. However, as will be shown below, the severity of cloud effects depends upon the nadir angle; effects which are significant in the disc region at low nadir angles rapidly diminish in importance for higher nadir angles in the limb region.

To determine the effects of clouds on radiance profiles as a function of nadir angles, a parametric study was carried out for six sample cases, based upon climatological profiles for January and July at 20°, 45° and 75°N. Here, for illustrative purposes, the January case at 20°N is described below.

Figure 57 shows, for this case, a series of curves which show radiance as a function of cloud top height for various select values of tangent height. Curves 2-9 cover the tangent height range from -30 to +20 km; curve 1, for -6370 km tangent height, or zero nadir angle, is provided for reference purposes. Radiance values for zero cloud top height represent the "no cloud effect" condition against which to evaluate the effects of clouds at various altitudes. The significance of cloud effects at zero nadir angle is obvious from this figure; at higher angles, or tangent heights, cloud effects are relatively less significant. Curves 1-7 indicate that the decrease in radiance is most pronounced at 16 km cloud height for tangent heights through 12 km; this radiance dip does not appear on curves 8-9 for tangent heights at 16 and 20 km.

Figure 58 shows the percentage deviation from "no cloud effect" radiance level as a function of nadir angle for select values of cloud top altitudes. A dashed reference line has been included on this figure at the nadir angle value of 71.8° corresponding to -30 km tangent height. The family of curves indicate two important points: (1) that cloud effects upon radiance decrease with increasing nadir angle, and (2) that the 16 km cloud top altitude is the most significant level, below and above which lesser percentage deviations in radiance level occur due to cloud effects. At small nadir angles, the decrease in radiance for 16-20 km clouds may exceed 20 percent; however, for nadir angles above 71.8° (or tangent heights above -30 km), the percentage deviations in radiance level do not exceed five percent.

Figure 59 shows a comparison of radiance profiles in January at 20°N for the 16 km cloud and no-cloud conditions. The cloud effect gradually decreases from five to zero percent over the tangent height range from -30 to +20 km; at tangent heights above 20 km (including the tangent height of peak radiance near 22 km), there is no cloud effect at all.

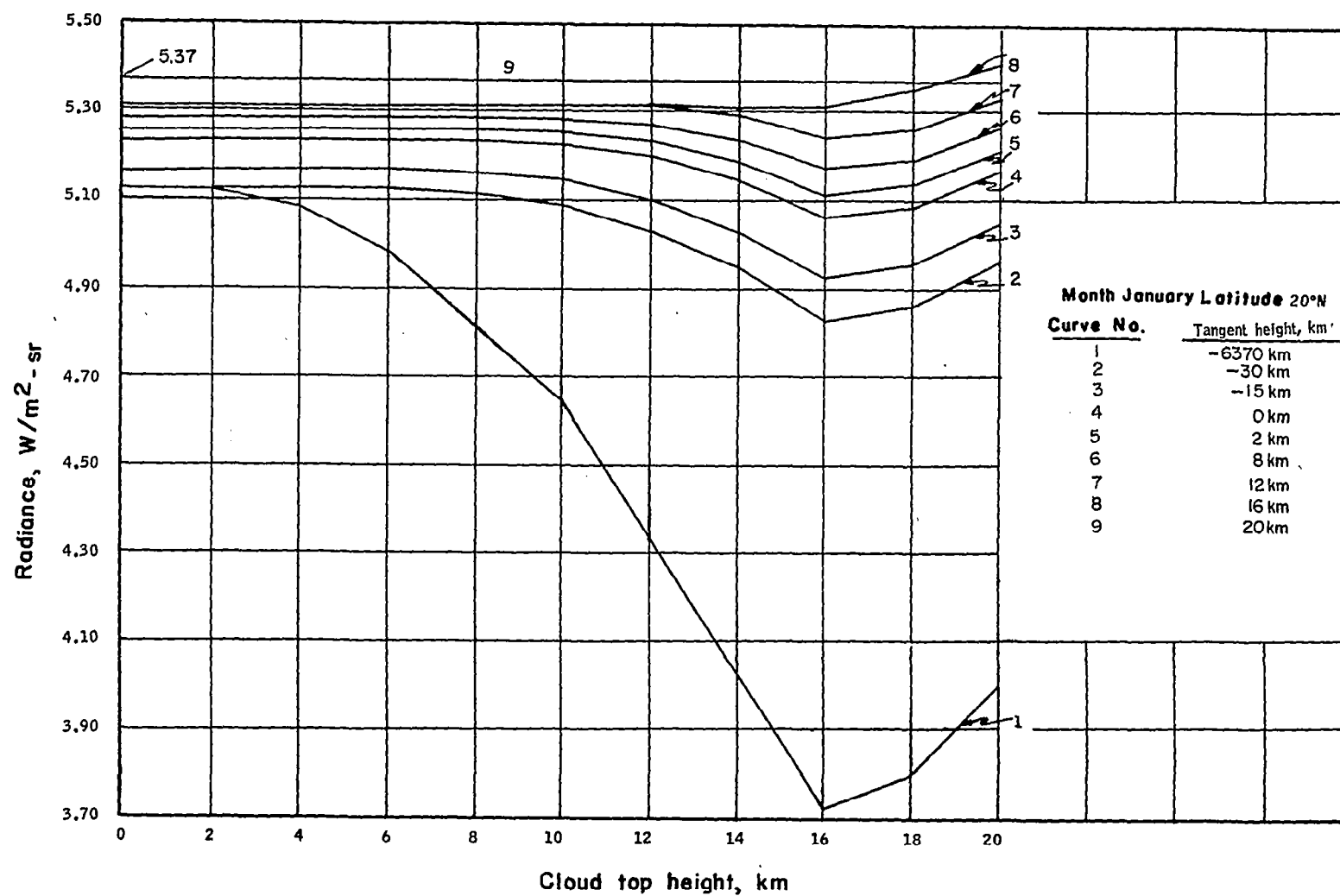


Figure 57. Cloud Effects on the 15 Micron Horizon Profile,  $615-715 \text{ cm}^{-1}$ , 20°N, January

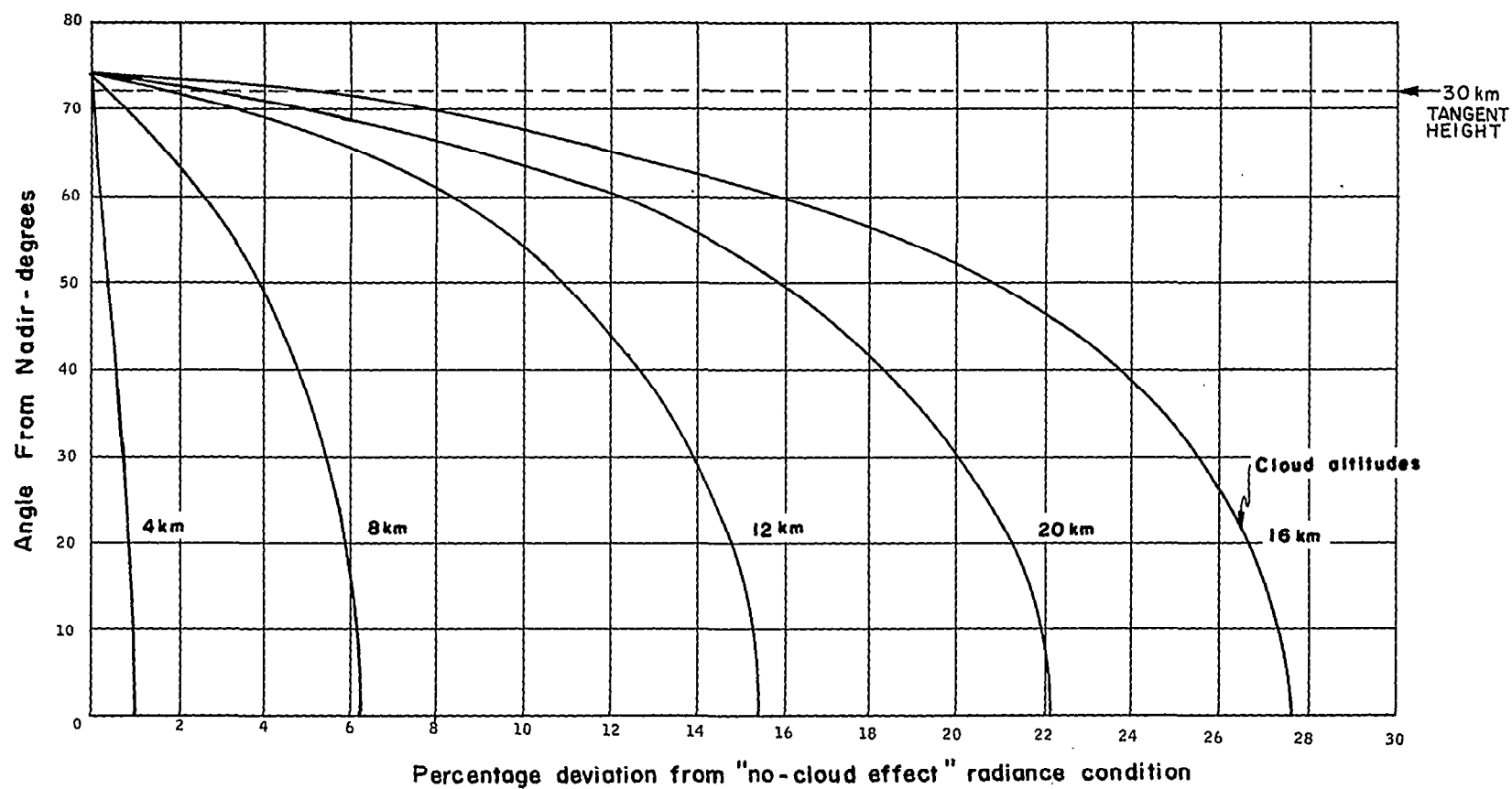


Figure 58. Percentage Deviation from No-Cloud Effect Radiance Level  
As a Function of Nadir Angle, 20°N, January

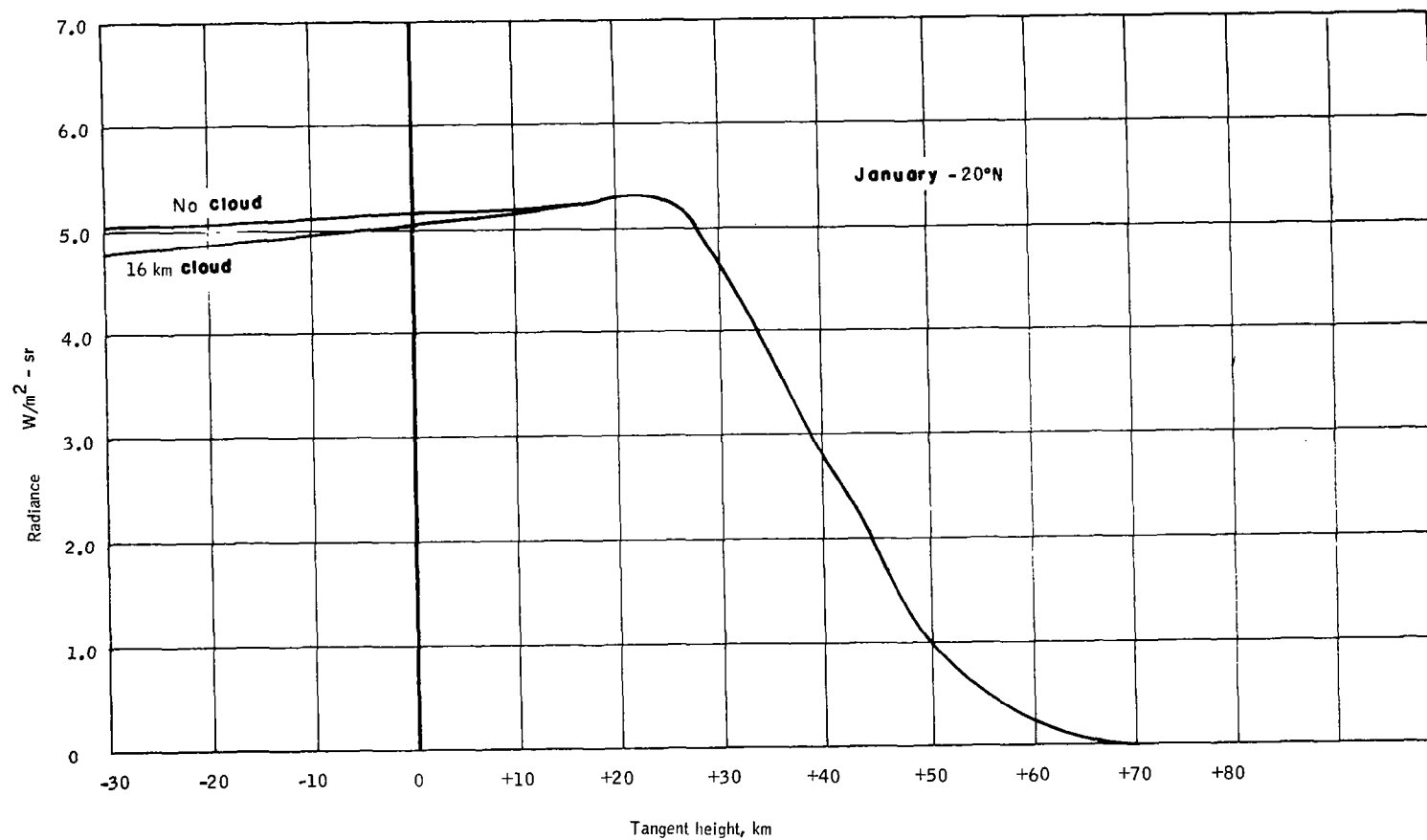


Figure 59. Comparison of 16 km-Cloud and No-Cloud Radiance Profiles, 20°N, January

## PROFILE IDENTIFIERS

A classification scheme of profile identifiers was developed to identify significant features of each sounding profile as well as the circumstantial conditions of time, location, topography, circulation regime, and data coverage which apply to each profile.

To describe the purposes for which the profile identifiers are to be used, it is necessary to briefly review the general methodology by which accurate horizon definition is to be achieved. First, the horizon sensing instrument will provide the raw data from which the radiance profile can be computed as a function of tangent height. Then, by the use of locators, certain processing operations will be performed upon the computed profile data (e.g., integration of total radiance, measurement of profile slope or inflection points), to yield a number which represents the indicated altitude. However, each indicated altitude, as it is furnished for each horizon radiance profile by the locator processor, is a function of several implicit factors, including latitude, longitude, date, local time, surface topology and various meteorological conditions. The effects of implicit factors which represent systematic variations can be largely removed, however, by applying suitable corrections to the values of indicated altitude. These effects can be evaluated on a statistical basis, and, on the basis of correlations established for each implicit factor, corrections can then be applied to the horizon profile measurements.

The profile identifiers serve to define, on a specific basis, the implicit factors which merit investigation to determine how their effects can be statistically removed to correct the altitude values as indicated by the locators.

Two classifications of identifiers were selected for this study: primary identifiers and reserve identifiers. Primary identifiers are those that were considered in this study for statistical analysis by the Time Series Analyser. These identifiers are the ones which are believed to be most closely related to the temperature and horizon profiles and are therefore expected to be most highly correlated with various locators.

Reserve identifiers are those which are proposed for use in future analyses, or for sorting purposes. These identifiers have not been used for statistical studies using the Time Series Analyser.

### PRIMARY IDENTIFIERS

Table 25 presents a listing of the twelve primary identifiers. The first four identifiers are concerned with location and time; their importance is directly related to how the temperature structure varies spatially and temporally.

TABLE 25.- PRIMARY IDENTIFIERS

1. Latitude
2. Longitude
3. Date
4. Local time (day, night, polar day, polar night)
5. Topographic regime
  - 0) Sea
  - 1) Land < 0.5 km
  - 2) Land 0.5 - 1.5 km
  - 3) Land 1.5 - 2.5 km (Note: no profiles were determined at locations whose elevations exceed 2.5 km)
6. Temperature at 10 mb
7. Temperature at tropopause
8. Temperature at stratopause
9. Lapse rate from 500 mb to tropopause
10. Lapse rate from tropopause to 10 mb
11. Lapse rate 10 mb to stratopause base
12. Circulation regime -- location relative to profile

To determine daytime and nighttime periods for primary identifier 4 it is necessary to compute local sunset and sunrise times. It is a simpler matter to compute sunrise and sunset times than it is to provide a table lookup for their determination. The computational procedure outlined below neglects refraction, which is constant for a standard atmosphere; also, in computing the solar declination, the eccentricity of the Earth's orbit is neglected since this effect is negligible.

Sunrise time, SR, and sunset time, SS, can be expressed as follows:

$$SR = 1200 - \frac{T}{15^\circ} \quad (4)$$

$$SS = 1200 + \frac{T}{15^\circ} \quad (5)$$

T is the angle in degrees through which the Earth turns between sunrise and noon (or noon and sunset) and is computed from this expression:

$$\cos (T) = -\tan (L) \tan (d) \quad (6)$$

where L is the latitude and d is the solar declination. The declination is computed by assuming a sinusoidal variation, as follows:

$$d = 23^\circ 27' \cos \left( \frac{n}{365} \times 2 \pi \right) \quad (7)$$

where n is the day number, based upon day "zero" occurring at the summer solstice.

The above procedure also provides a means of determining polar day and polar night. When the value of the right side of Equation (6) is greater than one, polar day or night exists. This condition occurs at high latitudes within the Arctic and Antarctic circles, and at high declinations. The equation, of course, breaks down completely at either pole where  $\tan L$  becomes infinite.

It may be noted that  $\tan d$  is negative in the period between 21 September and 21 March and positive during the other half of the year. Therefore, the decision as to whether polar day and night exists is based upon the application of the following criteria to Equation (6):

Polar night:  $\cos T > +1.0$

Polar day:  $\cos T < -1.0$

Primary identifiers 6 through 11 are concerned with the vertical temperature distribution; the selected temperature and lapse rate identifiers refer to key points and regions in the atmosphere. Figure 60 shows a typical temperature

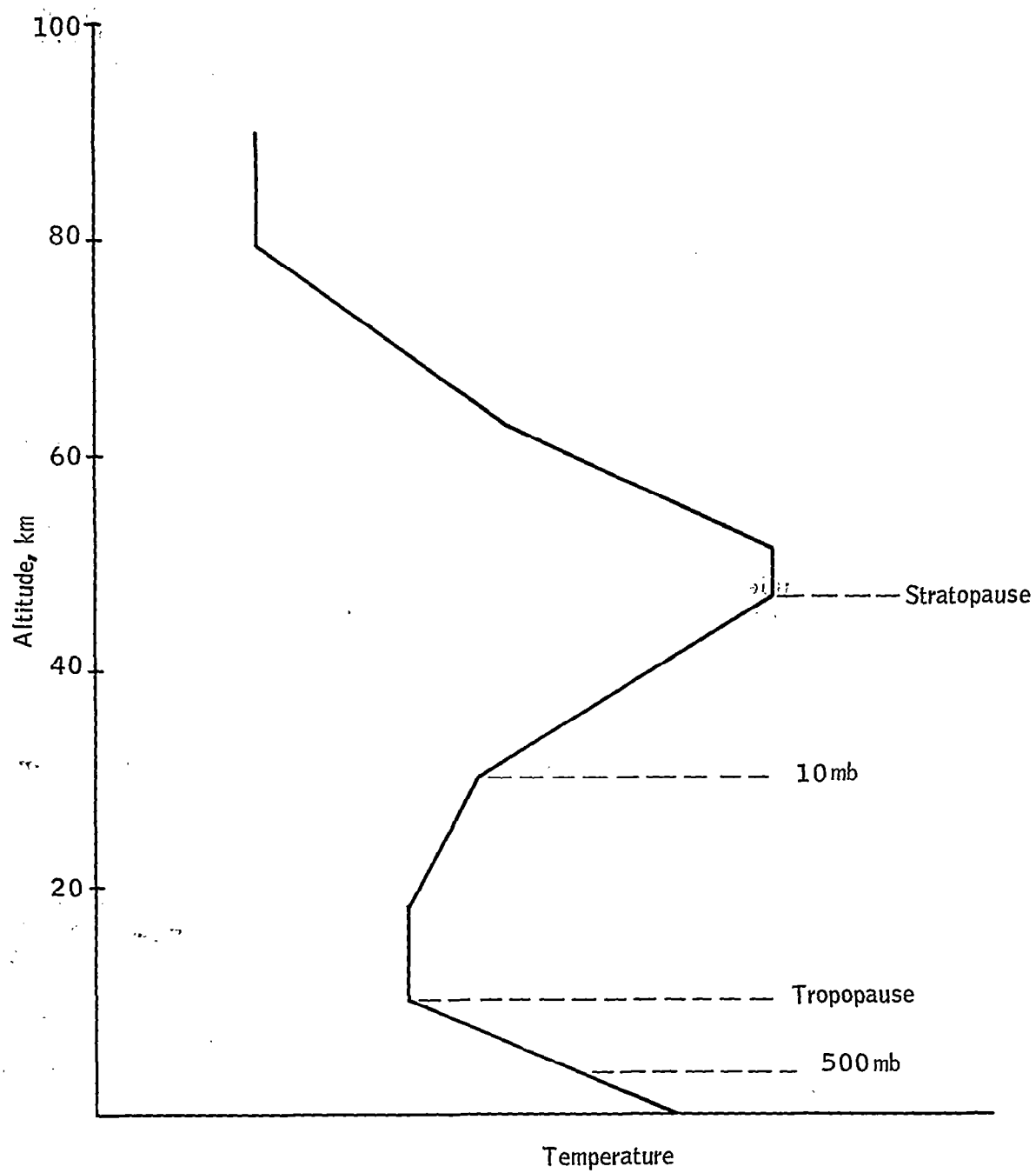


Figure 60. Typical Temperature Distribution with Height

structure up to 90 km, including the significant levels used in defining the temperature identifiers. These temperature identifiers, in general, serve to define the temperature structure quite well between the 500 mb level and the stratopause.

In the use of identifiers 7, 9 and 10, it should be noted that an important problem arises when selecting the tropopause level in polar regions in winter, due to the common presence of very cold air in the 20 to 30 km region. Figure 61 is a mean temperature profile for January at 60°N. and 60°W. The actual tropopause occurs at the first break in lapse rate at 8.4 km, where the temperature is 219°K. This condition is about what one normally expects for the polar tropopause. However, a more significant temperature break occurs at 24.2 km, where the temperature is 205°K. The dashed line represents the temperature profile that results from the choice of the actual polar tropopause as primary identifier 7 (tropopause temperature). It can be seen that this provides a rather poor representation by identifiers 9 and 10 of the actual temperature lapse rates. A much better representation of the temperature profile is given by the dash-dot line, which results from the choice of the tropopause identifier at the base of the higher level temperature inversion.

Figure 62 is an actual temperature profile at Fort Churchill, observed on 9 February 1965 at 1200 GMT. Here again, the best choice for the tropopause is the higher level temperature discontinuity; when the actual tropopause is selected, the temperature profile in the region from 15 to 28 km is poorly represented. This region is most important in radiance calculations whereas the region below 15 km, although it is better represented by using the actual tropopause, is less important to radiance calculations.

It cannot be stated, however, as a general rule, that the temperature profile is best represented in polar regions by using the higher level temperature break. Figure 63 shows an exception. Here, the temperature profile is best represented by using the actual tropopause. The reason for this is that this upper cold region in this case extends to the 10 mb level. Thus, the lapse rate from 500 mb to the tropopause (identifier 9) and the lapse rate from the tropopause to 10 mb (identifier 10) are well represented when the actual tropopause is selected.

In view of the above discussion, general ground rules for the proper choice of tropopause, which yields the best representation of the temperature profile, were determined: (1) When the base of the inversion associated with the high cold region is near or above the 10 mb level, select the actual lower polar tropopause. (2) When the base of the higher inversion is below 10 mb, and especially when this inversion base is below 25 km and the inversion is quite strong, the higher level should definitely be selected as the tropopause identifier.

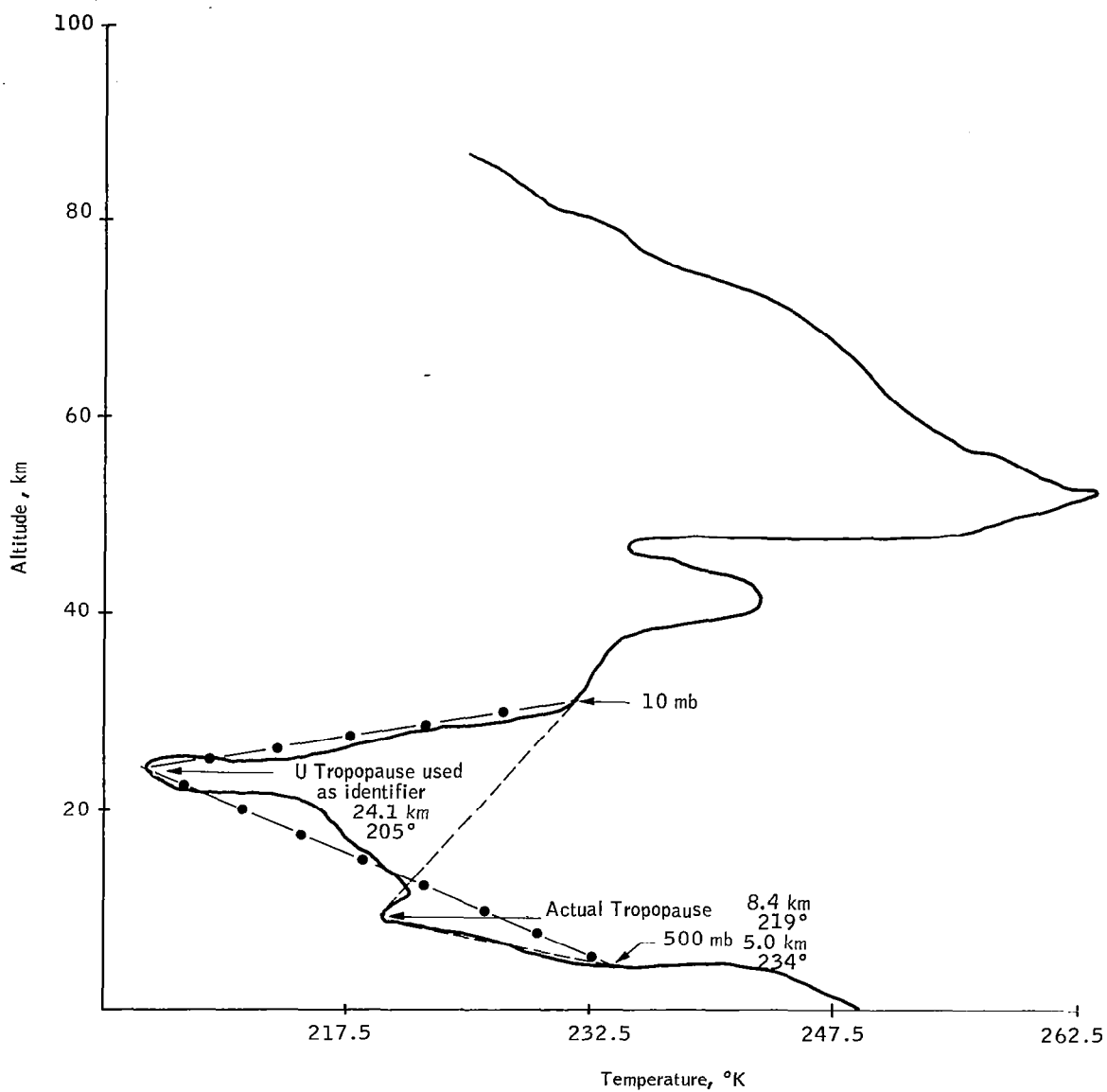


Figure 61. Mean Temperature in January at 60°N, and 60°W.

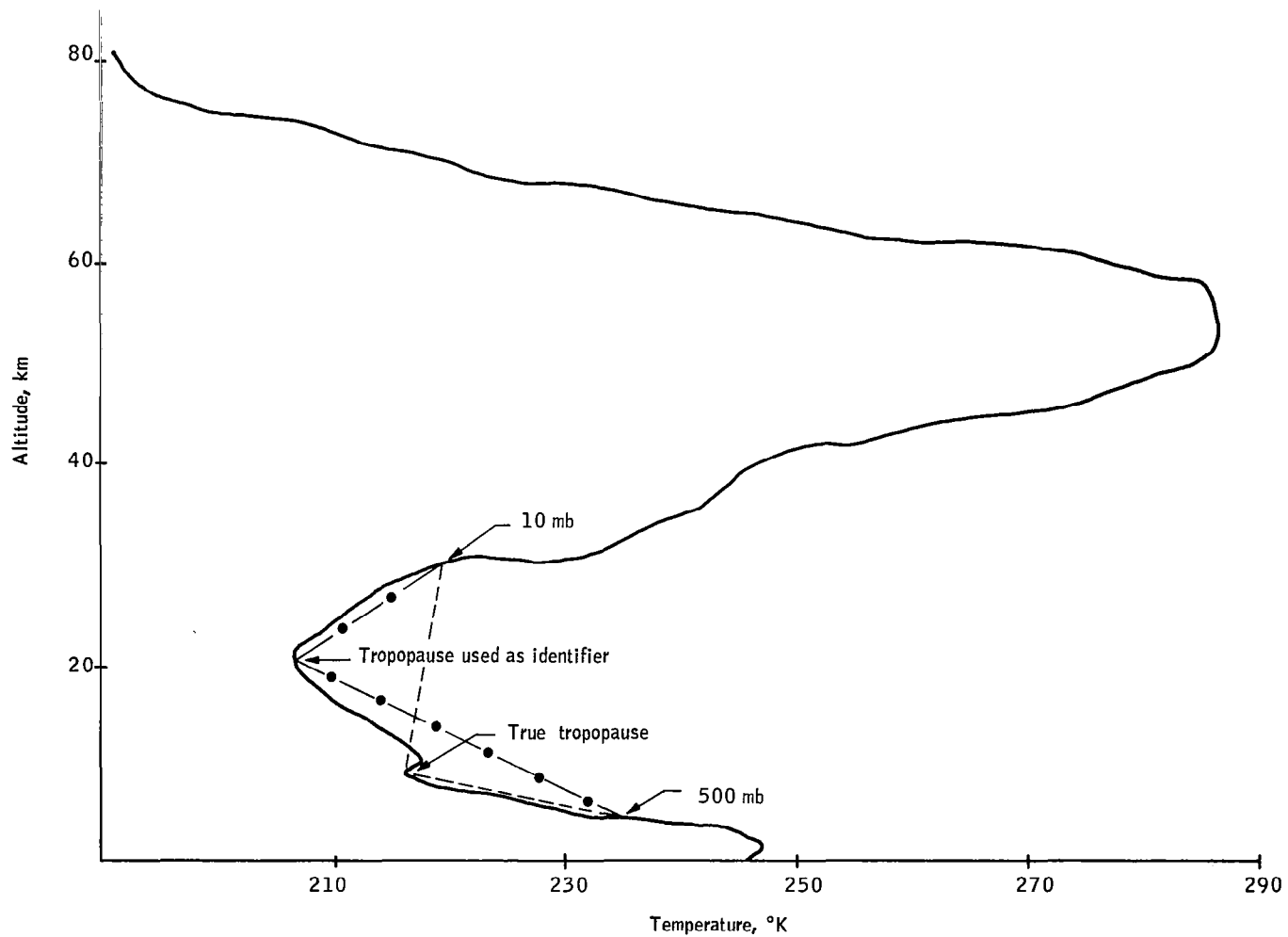


Figure 62. Temperature Profile at Fort Churchill on 9 February 1965, 1200 GMT

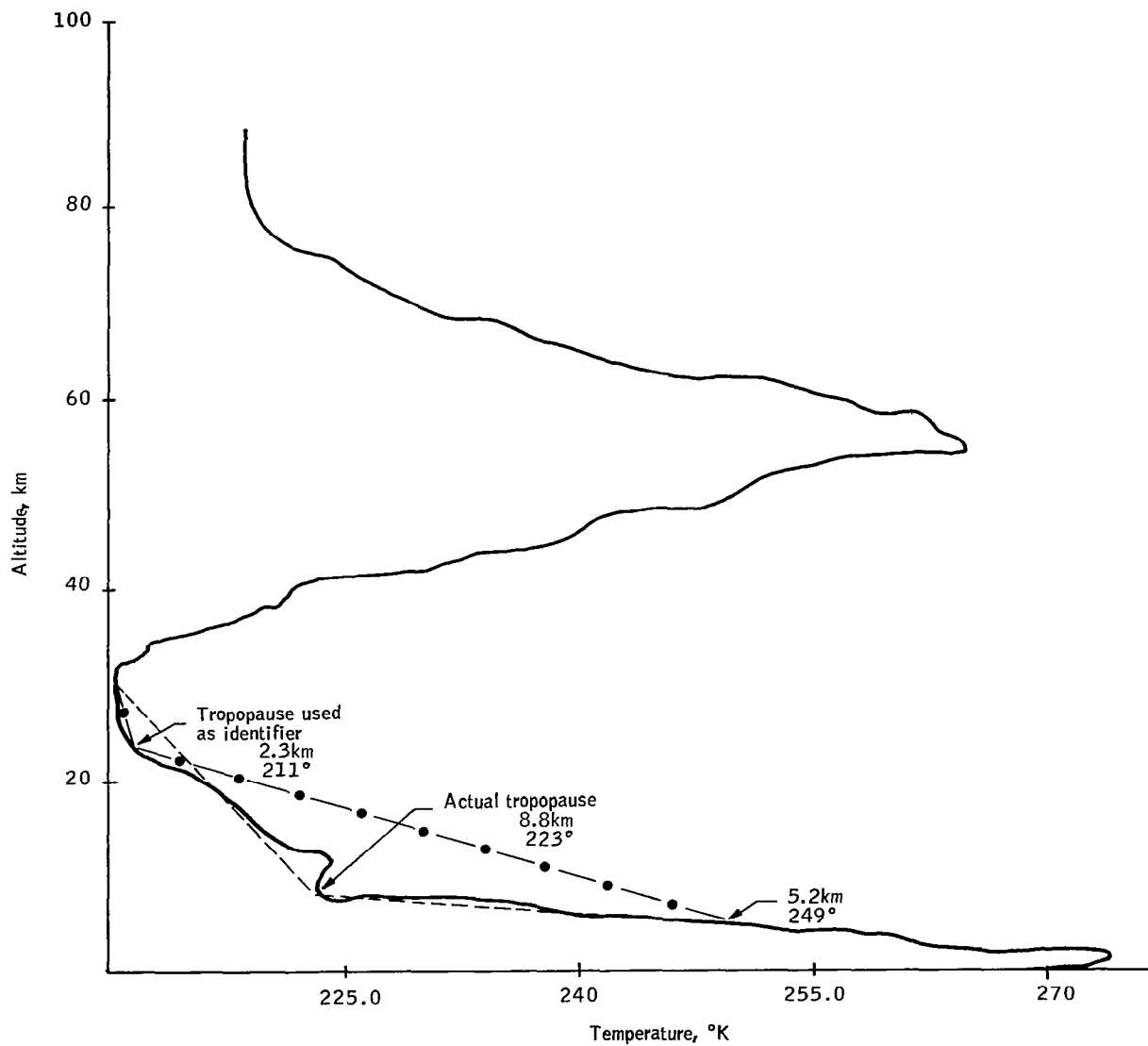


Figure 63. Temperature Profile at Fort Churchill on 12 December 1964, 1200 GMT

In selecting the identifiers for the temperature profiles, the above rules were applied in deciding whether to use the actual low polar tropopause or the high cold temperature inversion. In other words, the choice of tropopause identifier was governed by whichever one best approximated the actual temperature profile.

Circulation identifier number 12 provides an indication of the dominant feature of the 200 mb circulation believed to have an important influence on the temperature profile. The dominant features which were considered are troughs, ridges and jet streams. For the profile to be considered to be under the influence of a ridge or trough, the curvature of the height contours had to be anticyclonic or cyclonic, respectively. To be considered under the influence of the jet stream, the wind speed at the designated location had to exceed a value of three-fourths the maximum jet speed. The coding scheme devised for the circulation identifier was as follows:

- 0 = No feature
- 1 = Jet
  - + = Cyclonic side; - = Anticyclonic side
- 2 = Trough
  - + = Downstream (ahead); - = Upstream (behind)
- 3 = Ridge
  - + = Downstream (ahead); - = Upstream (behind)
- 4 = Jet and trough
  - + = Cyclonic side of jet; - = Anticyclonic side
- 5 = Jet and ridge
  - + = Cyclonic side of jet; - = Anticyclonic side

#### RESERVE IDENTIFIERS

Table 26 provides a list of the eight reserve identifiers. Reserve identifier 1 is an identification number. Reserve identifier 2 refers not to the calendar seasons, but to the meteorological seasons defined as follows:

Winter:	1 December - 28 February
Spring:	1 March - 31 May
Summer:	1 June - 31 August
Fall:	1 September - 30 November

TABLE 26.- RESERVE IDENTIFIERS

1.	Number of the atmospheric profile
2.	Season (spring, summer, fall, winter, Arctic summer, Arctic winter)
3.	Atmospheric anomaly index
	a. Aleutian anticyclone
	b. Hurricane
	c. Stratospheric warming
4.	Mesopause temperature when real data is available
5.	10 mb height
6.	Tropopause height
7.	Stratopause height
8.	Confidence factor
	a. Real data
	b. Interpolated
	c. Extrapolated

Arctic summer and Arctic winter are defined as the time periods during which polar day and polar night exist, respectively.

The atmospheric anomaly index (reserve identifier 3) specifies certain meteorological conditions that may affect the radiance profile. For example, the Aleutian Anticyclone appeared to be quite strongly developed at the time of the 13 November 1965 synoptic case. No hurricanes were in evidence during the selected times for the eight synoptic cases or space cross sections. However, the Cape Kennedy time series data were taken in the vicinity of hurricanes for the 27-28 August 1964 and 14-15 October 1964 cases. The stratospheric warming case, which occurred in March 1965, was discussed previously.

Auxiliary identifier 4 (mesopause temperature when real data is available) is applicable only to cases such as the 30 GCA profiles that were used in developing the extrapolation procedure. These were the only profiles where real data were available at the mesopause level.

Auxiliary identifiers 5 through 7 refer to the heights of the key points in the sounding. These identifiers provide a necessary supplement to the temperature identifiers at these points.

The confidence factor (identifier 8) gives an idea of the relative expected accuracy of the data. Real data, of course, has the highest confidence since the accuracy is only limited by instrumentation and observational procedures. Interpolated points are those which occur within the polygon circumscribing the available rocket sounding data. Extrapolated points are those which occur outside the polygon of rocket station data coverage.

## CONCLUSIONS AND RECOMMENDATIONS

### TEMPERATURE PROFILE ANALYSIS

Upper air sounding observations from radiosondes and rocketsondes were available in sufficient quantity to generate a representative body of synthesized temperature profiles over North America. Due to significant limitations in present-day data coverage, a global series of interpolated profiles could not be determined at this time. In addition, time resolutions of less than four hours were not obtainable from any currently available series of sounding data.

Various analytical techniques were successfully used with real-time observational data and climatological data summaries to determine relatively accurate representations of temperature profiles over the 0-90 km altitude range of interest. The accuracy of interpolated temperature profiles varies with altitude. From 0-30 km, the accuracy is approximately 2-3°C. From 30-60 km, the estimated accuracy is within 5°C for interpolation between reported temperature values and may exceed 10°C for interpolation at boundary points outside the area of data coverage. Between 60-90 km, where extrapolation techniques must necessarily be used, the extreme error in temperature estimation is approximated as  $\pm 20^{\circ}\text{C}$  in summer and  $\pm 30^{\circ}\text{C}$  in winter.

The synthesized temperature profiles provide a representative sampling of; (1) large-scale synoptic variability over a one-year period, (2) small-scale spatial variability at 100-km intervals along a 5600 km-long-cross-section of the atmosphere, (3) small-scale temporal variability at time resolutions of three days, 12 hours and four hours, (4) temporal variability at a northern-latitude station during a select case of pronounced stratospheric warming, (5) large-scale climatological variability on a seasonal basis.

The profile cases which were examined during this study represent only a beginning. Continuing improvements in the Meteorological Rocket Network are being made in terms of equipment, operational procedures and more frequent observations. It is recommended, therefore, that additional profile cases be selected in the near future from this new data as it becomes available to provide an independent check of the results obtained during this study.

It is further recommended that impetus and support be directed toward special series of rocketsonde observations (performed on a concurrent basis with special series of radiosonde observations) which would be aimed at obtaining a more consistent, more accurate and more complete body of basic data from which to study spatial and temporal variations in the sounding and radiance profiles. Particular attention should be directed

toward special series of rocketsonde observations during stratospheric warming situations to examine in detail variations in the temperature and radiance profiles. During periods where peak warming (or subsequent cooling) is occurring, rocketsonde observations should be performed as frequently as possible.

Special series of rocketsonde observations are also recommended which are specifically directed toward the detailed study of natural variability and error effects. At the present time, it is frequently a matter of opinion as to whether changes in successive temperature observations represent true variations or merely random errors. The problem of diurnal variability in temperature is of particular relevance to the horizon definition problem; the preliminary studies performed in Part I suggest that diurnal variability may be of importance, but available data cannot provide a definitive answer.

### ANALYSIS OF CARBON DIOXIDE VARIABILITY

The study results provide evidence that the average vertical variation of CO<sub>2</sub> concentration about the mean profile is approximately  $\pm 1$  percent between 0-90 km. If the value of CO<sub>2</sub> concentration at 5 km (i.e., 314 ppm) is taken as representative of the average throughout the entire 0-90 km range, then the average deviation of CO<sub>2</sub> concentration about this uniform mean value is no more than  $\pm 3$  percent.

### CLOUD ANALYSIS

Clouds can occur at altitude levels to approximately 20 km. Severe thunderstorms, the Asiatic monsoon and the intertropical convergence zone produce the highest clouds. As a rule, very high clouds are not representative of general conditions, but are relatively isolated buildups. In the case of thunderstorm cells, the very high buildups have relatively short lifetimes.

The available climatological summaries on frequencies of 6/10 to 10/10 cloud cover above 9 km indicate significant geographical and seasonal variations. Over the predominant portion of the Northern Hemisphere, the cloud frequencies do not exceed 10-20 percent in winter and summer. However, cloud frequencies in summer above 9 km markedly increase in certain areas to values in excess of 80 percent.

Additional studies of high cloud frequencies are definitely recommended, based upon meteorological satellite observations and concurrent radiosonde observations. In particular, cloud frequencies near 16 km are especially needed, since clouds at this level have the greatest effect on radiance determination in the 15 micron CO<sub>2</sub> absorption band. Nimbus I

and II data are available which would permit the frequency and height of high clouds to be determined on a global basis and to be correlated with associated meteorological conditions.

### EFFECTS OF TEMPERATURE, CO<sub>2</sub> AND CLOUD VARIATIONS ON RADIANCE PROFILES

Sample computations of the radiance profile sensitivity to temperature, CO<sub>2</sub> and cloud variations clearly indicate the relative importance of temperature. For example, a temperature profile correction of  $\pm 5^{\circ}\text{C}$  over the entire 0-90 km altitude range was shown (for a typical case) to produce a radiance profile correction of at least  $\pm 11$  percent over the -30 to +90 km tangent height interval. As shown earlier, the uncertainty in interpolated temperatures is the order of 5 to  $10^{\circ}\text{C}$  at altitudes between 30-60 km, as a result of rocketsonde errors and large-scale interpolation and extrapolation from relatively sparse measurements. Thus, the effect of temperature uncertainties upon radiance profile determination can be significant.

The effect of CO<sub>2</sub> variability upon radiance profiles is clearly shown to be negligible. Sensitivity analyses of radiance profiles based upon  $\pm 2$  percent and  $\pm 10$  percent variations in the CO<sub>2</sub> concentration show an insignificant effect. Since a  $\pm 3$  percent variation is shown by this study to be a representative value between 0-90 km, it is concluded that CO<sub>2</sub> variability may be safely neglected.

The effects of clouds upon radiance profiles strongly depend upon the nadir angle. For nadir angles above  $71.8^{\circ}$  (corresponding to tangent heights greater than -30 km), the percentage deviations in radiance do not exceed five percent, for a typical case. The reduction in radiance due to cloud effect is shown to decrease from five to zero percent over the -30 to +20 km tangent height range; at higher tangent heights, there is no cloud effect at all. The results also indicate that the 16 km cloud top altitude is the most significant level, below and above which lesser percentage deviations in radiance levels occur due to cloud effects.

### PROFILE IDENTIFIER CLASSIFICATION

An effective classification scheme, based upon select profile identifiers, has been developed for describing each profile in terms of the many implicit factors related to profile variability (i.e., temperature and height of significant points in the sounding; associated large-scale atmospheric conditions; circumstantial factors such as location, date, time, and topography).

Certain problems in applying the classification scheme were observed in those cases where a complicated tropopause structure exists such that a choice must be made between a lower level (the "true" tropopause, according to standard definition) and a higher level temperature inversion. These problems were resolved, however, by establishing a set of guidelines; thus, the classification scheme, as it is applied to temperatures, heights and lapse rates, provides the best fit to the actual temperature profile.

## REFERENCES

1. Panel on International Meteorological Cooperation: The Feasibility of a Global Observation and Analysis Experiment. National Academy of Sciences - National Research Council, Publication 1290, 1966.
2. Meteorological Working Group; Inter-Range Instrumentation Group; and Range Commanders Council: Data Report - Meteorological Rocket Network Firings. Vol. XLIII, Document 109-62, August 1965.
3. Quiroz, R. S.; Lambert, J. K.; and Dutton, J. A.: Upper Stratosphere Density and Temperature Variability Determined from Meteorological Rocket Network Results, 1960-1962. Air Weather Service Technical Report 175, 1963.
4. Panofsky, H. A.: Introduction to Dynamic Meteorology. University Park, Pa., 1958.
5. Kantor, A. J.; and Cole, A. E.: Monthly Atmospheric Structure, Surface to 80 Kilometers. J. of Applied Meteorology, Vol. 4, No. 2, April 1965, pp. 228-237.
6. Minzner, R. A.: Studies of Atmospheres and Structures and Variability of Earth's Atmosphere. GCA Corp. Quarterly Progress Report, November 1965.
7. Cole, A. E.; and Kantor, A. J.: Air Force Interim Supplemental Atmospheres to 90 Kilometers. Air Force Surveys in Geophysics No. 153, AFCRL-63-936, 1963.
8. Beyers, N. J.; and Miers, B. T.: Diurnal Temperature Change in the Atmosphere between 30 and 60 km over White Sands Missile Range. U.S. Army Electronics Research and Development Activity, ERDA-284, 1965.

9. Beyers, N. J.; and Miers, B. T.: Diurnal Temperature Change between 30 and 60 km Over White Sands Missile Range. J. of Atmospheric Sciences, Vol. 22, May 1965, pp. 262-266.
10. Belmont, A.; Peterson, R.; and Shen, N.: Evaluation of Meteorological Rocket Data. NASA CR-138, 1964
11. Shaw, J. H.: Numerical Evaluation of Radiation Errors of Radiosonde Temperature Element ML419 at Altitude up to 150,000 ft. Technical Report 3, Dept. of Physics and Astronomy, Ohio State University, 1959.
12. Lenhard, R. W.: Meteorological Accuracies in Missile Testing. J. Meteorology, Vol. 16, 1959, pp. 447-453.
13. Teweles, S.; and Finger, F. G.: Reduction of Diurnal Variation in the Reported Temperatures and Heights of Stratospheric Constant-Pressure Surfaces. J. Meteorology, Vol. 17, 1960, pp. 177-194.
14. USAF Air Weather Service: Accuracies of Radiosonde Data. Technical Report AWS TR 105-133 (ASTIA No. AD 758631), 1955.
15. Conover, W.: Radiosonde Modulator using a Hypsometer. American Meteorological Society, Vol. 42, 1961, pp. 249-251.
16. Sapoff, M.; Geosey, J.; and Ellern, F.: Development of a Hypsometer for a Constant Level Balloon System. Victory Engineering Corp. Final Report Part I, 1958.
17. Beyers, N. J.; Thiele, O. W.; and Wagner, N. K.: Performance Characteristics of Meteorological Rocket Wind and Temperature Sensors. U.S. Army Electronics Research and Development Activity, Missile Meteorology Division, ASTIA No. AD 286254, 1962.
18. Wagner, N. K.: Theoretical Time Constant and Radiation Error of a Rocketsonde Thermistor. J. Meteorology, Vol. 18, 1961, pp. 606-614.

19. Wagner, N. K.; Haragan, D. R.; Jehn, K. H.; and Gerhardt, J. R.: Wind and Temperature in the Atmosphere between 30 and 80 Kilometers. Fourth Quarterly Technical Report, Electrical Engineering Research Lab., University of Texas, 1961.
20. Thiele, O. W.: Mesospheric Density Variability Based on Recent Meteorological Rocket Measurements. J. of Applied Meteorology, Vol. 2, 1963, pp. 649-654.
21. Leviton, R.; and Wright, J. B.: Accuracy of Density from the Robin Falling Sphere. GRD Research Notes No. 73, AFCRL-1095, 1961.
22. Engler, N. A.: Method of Determining Wind, Density, Pressure, and Temperature from the Robin Falling Balloon. Paper presented at the AIAA/AMS Conference on Stratosphere-Mesosphere Structure, (El Paso, Texas), Nov. 19-21, 1963.
23. Kern, L. C.; and Rapp, R. R.: The Effect of Vertical Air Motion on Atmospheric Density Determination from "Robin" Flights. Rand Corp. RM 3687PR (ASTIA No. 409533), 1963.
24. aufm Kampe, H. J.; and Lowenthal, M.: Review of U.S. Meteorological Rocket Network Activities and Results. Proceedings of the First International Symposium on Rocket and Satellite Meteorology, Washington, D.C., April 23-25, 1962, North Holland Publishing Co. (Amsterdam), 1963, pp. 15-33.
25. Wagner, N. K.: Theoretical Accuracy of a Meteorological Rocketsonde Thermistor. J. of Applied Meteorology, Vol. 3, No. 4, August 1964, pp. 461-469.
26. Wright Instruments, Inc.: A Survey for Naval Ordnance Laboratory of High Altitude Atmospheric Temperature Sensors and Associated Problems. Final Report, 1961.
27. USAF 4th Weather Group: Meteorological Rocket Operations on the Atlantic Missile Range. Pamphlet 105-7-3 (ASTIA No. 283549), 1962.

28. Finger, F. G.; Teweles, S.; and Mason, R. B.: Synoptic Analysis Based on Meteorological Rocketsonde Data. J. of Geophysical Research, Vol. 68, No. 5, March 1, 1963, pp. 1377-1399.
29. Lieth, H.: The Role of Vegetation in the Carbon-Dioxide Center of the Atmosphere. J. of Geophysical Research, Vol. 68, 1963, pp. 3887-3898.
30. Huber, B.: Der Einfluss Der Vegetation Auf Die Schwankungen Des CO<sub>2</sub> Gehaltes Der Atmosphere. Arch., Meteorol., Geophys., Broklimato., Vol. 4, 1952a, pp. 154-167.
31. Huber, B.: Uber Die Vertikal Reichweite Vegetationsbedingter Tageschwankungen in CO<sub>2</sub> Gehaltder Atmosphere. Vorstwiss, Zentr., Vol. 71, 1952b, pp. 372-380.
32. Huber, B.: Die CO<sub>2</sub> Konpensation in Pflangeng Esellschaften. Encyclopedia of Plant Physiology, Vol. 512, 1960, pp. 339-348.
33. Huber, B.; and Pommer, D.: Zur Frage Eines Jahrezeithichen Ganges im CO<sub>2</sub> - Gehalt Der Atmosphere. Angew. Botan., Vol. 28, 1954, pp. 53-62.
34. Pales, J.C.; and Keeling, C. D.: The Concentration of Atmospheric Carbon Dioxide in Hawaii. J. of Geophysical Research, Vol. 70, No. 24, December 1965, pp. 6053-6076.
35. Bolin, B.; and Keeling, C. D.: Large-Scale Mixing as Deduced from Seasonal and Meridional Variations of Carbon Dioxide. J. of Geophysical Research, Vol. 68, 1963, pp. 3899-3920.
36. Brown, C. W.; and Keeling, C. D.: The Concentration of Atmospheric Carbon Dioxide in Hawaii. J. of Geophysical Research, Vol. 70, No. 24, December 15, 1965, pp. 6077-6085.
37. Bischof, W.: Periodic Variations of the Atmospheric CO<sub>2</sub> Content in Scandinavia. Tellus, Vol. 12, 1960, pp. 212-226.

38. Bischof, W.: Variations in Concentration of Carbon Dioxide in the Free Atmosphere. *Tellus*, Vol. 14, No. 1, February 1962, pp. 87-90.
39. Bischof, W.: Carbon Dioxide Concentration in the Upper Troposphere and Low Stratosphere. *Tellus*, Vol. 17, No. 3, 1965, pp. 398-402.
40. Hagemann, F.; Gray, Jr., J.; Machta, L.; and Turkevich, A.: Stratospheric  $C_{14}$ ,  $CO_2$ , and Tritium. *Science*, Vol. 130, 1959 pp. 542-552.
41. Bates, D. R.; and Witherspoon, A. E.: The Photo Chemistry of Some Minor Constituents of the Earth's Atmosphere ( $CO_2$ ,  $CO$ ,  $CH_4$ ,  $H_2O$ ). *Royal Astronomical Society M. N.*, Vol. 112, 1952, pp. 101-124.
42. De, A. C.: An Unusually High Nor'wester Radar Cloud. *Indian Journal of Meteorology and Geophysics*, Vol. 10, No. 3, July 1959, pp. 359-360.
43. Arnold, J. E.: Conference on Severe Storms. AMS, Norman Okla., 1962.
44. Vonnegut, B.; and Moor, C. B.: Recent Advances Atmospheric Electricity. 1956, pp. 309-411.
45. De, A. C.: High Radar Clouds Above 10 km. *Indian Journal of Meteorology and Geophysics*, Vol. 14, No. 3, July 1963, pp. 327-330.
46. Saunders, P. M.; and Ronne, F. C.: A Comparison between the Height of Cumulus Clouds and the Height of Radar Echoes Received from Them. *J. of Applied Meteorology*, Vol. 1, September 1962, pp. 296-302.
47. Rasool, S. I.: Cloud Heights and Nighttime Cloud Cover from Tiros Radiation Data. *J. of Atmospheric Sciences*, Vol. 21, March 1964, pp. 152-156.

48. Soloman, I.: Estimated Frequencies of Specified Cloud Amounts Within Specified Ranges of Altitudes. Air Weather Service Technical Report 167, 1963.
49. Nordberg, W.: Geophysical Observations from Nimbus I. Science, Vol. 150, 1965, pp. 559-572.
50. Technology Week, June 13, 1960, p. 18.
51. Leviton, R.: Height errors in a rawin system. AF Surveys in Geophysics No. 60, Air Force Cambridge Research Center, 1954.